WHOI-99-04

Coastal Ocean Processes Symposium

a tribute to

William D. Grant

September 27 - September 30, 1998
Woods Hole Oceanographic Institution
Woods Hole, MA 02543 U.S.A.

May 1999

Technical Report

19991117 091

Coastal Ocean Processes Symposium:
A Tribute to William D. Grant

Woods Hole Oceanographic Institution
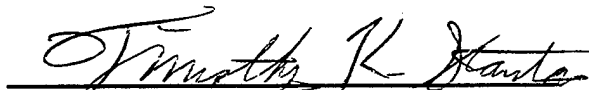Woods Hole, Massachusetts 02543

May 1999

Technical Report

Approved for Distribution:

Timothy K. Stanton, Chair

Department of Applied Ocean Physics and Engineering

Coastal Ocean Processes Symposium

a tribute to
William D. Grant

September 27 - September 30, 1998
Woods Hole Oceanographic Institution
Woods Hole, MA 02543
U.S.A.

This symposium is dedicated to Bill Grant. Together with Ole Madsen and Jim Smith, Bill started a new era in research on boundary layer flows and sediment transport, by articulating a set of fundamental physical processes and quantifying them in a simple yet realistic manner. He broadened the field by encouraging interaction among scientists in all oceanographic disciplines. Bill's insights, dedication and enthusiasm had an extraordinary impact on a generation of students, post-docs and scientists.

He led with an open heart.

Coastal Ocean Processes Symposium

a tribute to
William D. Grant

September 27 - September 30, 1998
Woods Hole Oceanographic Institution, Woods Hole, MA 02543

Sponsored by:
Office of Naval Research
Rinehart Coastal Research Center
United States Geological Survey
Woods Hole Oceanographic Institution

Location:
The symposium will be held in the Clark Building, rooms 507 and 509, at the Woods Hole Oceanographic Institution in Woods Hole, Massachusetts.

Registration:
In lieu of a registration fee, donations towards the William D. Grant Summer Student Fellowship Fund will be gratefully accepted.

Correspondence:
Any inquires regarding the Symposium should be directed to:

> Mrs. Gretchen McManamin
> Woods Hole Oceanographic Institution
> Crowell House, MS41
> Woods Hole, Massachusetts 02543-1138
> Email: gmcmanamin@whoi.edu
> Tel: 508/289-2292
> Fax: 508/457-2184

Organizing Committee:
Dr. Robert Beardsley, Woods Hole Oceanographic Institution
Dr. David Cacchione, Aubrey Consulting, Incorporated
Dr. W. Rockwell Geyer, Woods Hole Oceanographic Institution
Mrs. Gretchen McManamin, Woods Hole Oceanographic Institution
Dr. John Trowbridge, Woods Hole Oceanographic Institution

September 27 - September 30, 1998

Woods Hole Oceanographic Institution, Woods Hole, MA 0254

AGENDA

Sunday, September 27, 1998

11:30	3rd Annual Bill Grant Run Captain Kidd Restaurant to Rinehart Coastal Research Center
1:00	Welcome and Cookout

Monday, September 28, 1998

7:45-8:20	Registration and Coffee/Pastries
8:20	General Announcements - Dr. John Trowbridge, Woods Hole Oceanographic Institution
8:25	Welcome - Dr. James Luyten, Senior Associate Director and Director of Research, Woods Hole Oceanographic Institution
Session 1:	**Coastal Fluid Dynamics** Moderator: Dr. W. Rockwell Geyer, Woods Hole Oceanographic Institution
8:30-9:15	*Keynote Address - Dr. Ole Madsen,* Massachusetts Institute of Technology

9:15-9:45	Dr. Robert Beardsley, Woods Hole Oceanographic Institution
9:45-10:00	Break
10:00-10:30	Dr. John Allen, Oregon State University
10:30-11:00	Dr. Clinton Winant, Scripps Institution of Oceanography
11:00-12:00	Poster Session
12:00-1:15	Lunch
1:15-1:45	Dr. Robert Guza, Scripps Institution of Oceanography
1:45-2:15	Dr. Scott Glenn, Rutgers University
2:15-2:30	Break
2:30-3:00	Dr. Anthony Bowen, Dalhousie University
3:00-3:30	Dr. Steven Lentz, Woods Hole Oceanographic Institution
3:30-5:00	Posters (same as above) and Refreshments

POSTER EXHIBITORS - MONDAY, SEPTEMBER 28

Dr. William Boicourt, University of Maryland
Dr. Wendell Brown, University of New Hampshire
Dr. Cortis Cooper, Chevron, Incorporated
Dr. Glen Gawarkiewicz, Woods Hole Oceanographic Institution
Dr. Hans Graber, University of Miami
Dr. Robert Holman, Oregon State University
Dr. Harry Jenter, U.S. Geological Survey
Dr. Joseph Katz/Dr. Thomas Osborn, Johns Hopkins University
Dr. W. Kendall Melville, Scripps Institution of Oceanography
Dr. Marlene Noble, U.S. Geological Survey
Dr. Leslie Rosenfeld, Naval Postgraduate School
Dr. Eugene Terray, Woods Hole Oceanographic Institution
Dr. John Trowbridge, Woods Hole Oceanographic Institution

Tuesday, September 29, 1998

Session 2: **Sediment Transport**
Moderators: Dr. Steven McLean, University of California and
Dr. W. Kendall Melville, Scripps Institution of Oceanography

8:00 Coffee and Pastries

8:30-9:15 ***Keynote Address - Dr. James Smith,*** U.S. Geological Survey

9:15-9:45 Dr. David Cacchione, Aubrey Consulting, Incorporated

9:45-10:00 Break

10:00-10:30 Dr. Richard Sternberg, University of Washington

10:30-11:00 Dr. Yogesh Agrawal, Sequoia Scientific, Incorporated

11:00-12:00 Poster Sessions

12:00-1:15 Lunch

1:15-1:45 Dr. Lawrence Sanford, University of Maryland

1:45-2:15 Dr. Patricia Wiberg, University of Virginia

2:15-2:30 Break

2:30-3:00 Dr. John Sleath, Cambridge University

3:00-3:30 Dr. Christopher Paola, University of Minnesota

3:30-5:00 Posters (same as above) and Refreshments

6:15 Dinner - The Falmouth Yacht Club

POSTER EXHIBITORS - TUESDAY, SEPTEMBER 29

Dr. Michael Bruno, Stevens Institute of Technology
Dr. Bradford Butman/Dr. Richard Signell, U.S. Geological Survey
Dr. Thomas Gross, National Oceanographic & Atmospheric Administration
Ms. Courtney Harris, University of Virginia
Dr. Alexander Hay, Dalhousie University
Dr. Paul Hill, Dalhousie University
Dr. Gail Kineke, Boston College
Dr. James Lynch/Dr. James Irish, Woods Hole Oceanographic Institution
Dr. Steven McLean, University of California
Dr. Ashish Mehta, University of Florida
Dr. Jonathan Nelson, U.S. Geological Survey
Dr. Andrea Ogston, U.S. Geological Survey
Dr. L. Donelson Wright/Dr. Carl Friedrichs, Virginia Institution
of Marine Science

Wednesday, September 30, 1998

Session 3:	**Animal-Sediment-Flow Interactions**
	Moderator: Dr. Arthur Nowell, University of Washington
8:00	Coffee and Pastries
8:30-9:15	***Keynote Address - Dr. Cheryl Ann Butman***, Woods Hole Oceanographic Institution
9:15-9:45	Dr. Steven Monismith, Stanford University
9:45-10:00	Break
10:00-10:30	Dr. Gary Taghon, Rutgers University
10:30-11:00	Dr. Donald Rhoads, Science Applications International Corp.
11:00-12:00	Poster Sessions
12:00-1:30	Concluding Luncheon

POSTER EXHIBITORS - WEDNESDAY, SEPTEMBER 30

Dr. Jonathan Grant, Dalhousie University
Dr. Douglas Miller, University of Delaware
Dr. Lauren Mullineaux, Woods Hole Oceanographic Institution
Dr. Jeffrey Shimeta, Franklin and Marshall College
Dr. Paul Snelgrove, Memorial University of Newfoundland
Dr. David Thistle, Florida State University
Dr. Robert Whitlatch, University of Connecticut
Dr. Richard Zimmer, University of California

COASTAL OCEAN PROCESSES SYMPOSIUM
A Tribute to William D. Grant

LIST OF ABSTRACTS

Agrawal, Y.C. and H.C. Pottsmith. *Particle Transport in Bottom Boundary Layers: Size Distribution and Concentration, and Settling Velocity Distribution.*

Allen, J.S. *Model Studies of Upwelling Relaxation Events off Northern California.*

Werner, S.R. and R.C. Beardsley. *Observations and Modeling of the Tidal Bottom Boundary Layer on the Southern Flank of Georges Bank.*

Boicourt, W.C., L.J. Walstad, M. Roman, R. Hood, A. Valle-Levinson, C. Lascara, L. Heilman, and R. Burgett. *Convergences and Hydraulic Controls in Partially Mixed Estuaries.*

Bowen, A.J. and P. MacAulay. *Another Glimpse of the Wave Boundary Layer.*

Brown, W.S. and P. Mupparapu. *Winter Mixed Layer Evolution in the Gulf of Maine.*

Bruno, M.S. and K.L. Rankin. *Application of Simple Profile Evolution Concepts: Analysis of a Dynamic Shoreline.*

Butman, B. and R.P. Signell. *New Perspectives of the Sea Floor.*

Butman, C.A. *Organism-Flow-Sediment Interactions: An Eclectic Overview.*

Cacchione, D.A. *Internal Tides and Sedimentation on Continental Slopes.*

Cooper, C. *Ocean Currents Near the Congo River Outfall.*

Duda, T.F., C.R. Rehmann and J.R. Ledwell. *Mixing in a Bottom Layer Associated with The New England Shelf/Slope Water Front.*

Lee, G., C.T. Friedrichs, L.D. Wright, and C.E. Vincent. *Diffusion Versus Advection Dominated Suspension on the Inner Shelf Under Storm and Swell Conditions, Duck, N.C.*

Gawarkiewicz, G., R. Pickart, F. Bahr, and R. Beardsley. *Shelfbreak Frontal Structure during Spring, 1996: SeaSoar Observations from the ONR Shelfbreak PRIMER Experiment.*

Glenn, S. *Coastal Predictive Skill Experiments at the Long-term Ecosystem Observatory.*

Graber, H.C. *High-Frequency Radar Remote Sensing: A New Tool For Coastal Oceanography.*

Grant, J. and D. Adler. *Chlorophyll as a Tracer of Small-Scale Hydrodynamics on the Seabed: Preliminary Studies.*

Gross, T.F. *Control of Sediment Transport Reference Concentration by Flux Rate Boundary Conditions.*

Lentz, S., F. Feddersen, R.T. Guza, S. Elgar, and T.H.C. Herbers. *Alongshore Momentum Balances in Shallow Water.*

Harris, C. and P. Wiberg. *Suspended Sediment Flux and Sediment Redistribution on the Continental Shelf.*

Hay, A.E., C. Smyth, L. Zedel, and T. Mudge. *On Remotely Probing the Structure of the Bottom Boundary Layer Over an Evolving Seabed.*

Hill, P.S. and T.G. Milligan. *Suspicions about Settling Columns.*

Jenter, H.L. *Laboratory Experiments for Evaluating the Effects of Wind Forcing on Shallow Waters with Emergent Vegetation.*

Kineke, G.C. *High Concentration Suspensions in Coastal Sediment Transport: Observations from Field Investigations.*

Lentz, S. and J. Trowbridge. *Mean Current Profiles over the Northern California Shelf in Fall and Winter.*

Lynch, J., J. Irish, and P. Traykovski. *Some Thoughts on the Advancement of Acoustics Methods for Monitoring Sediment Transport Since 1986.*

Madsen, O.S. *Review, Modification and Extension of What the Grant-Madsen Model for Wave-Current Interaction Can Do For You.*

McLean, S.R. and J.M. Nelson. *The Role of Bedform-induced Spatial Acceleration in Determining Bedform Evolution.*

Jinchai, P. and A.J. Mehta. *An Examination of Mud Slurry Discharge Through Pipes.*

Melville, W.K. and M Ritter. *The Sound of the Surf.*

Miller, D.C. *What u_* Is It?*

Mullineaux, L.S., R. Dunn, S.W. Mills, H.L. Hunt and L.K. Gulmann. *Biological Influences on Transport of Postlarval Soft-Shell Clams (Mya arenaria).*

Nelson, J.M., R.L. Shreve, J. Fredsøe, M. Sumer, and C. Lodahl. *Bedload Transport in Oscillatory Flows at Intermediate Wave Reynolds Numbers.*

Noble, M.A. and S.R. Ramp. *Evidence for Offshore Veering of the Undercurrent over the Central California Coast.*

Ogston, A.S., D.A. Cacchione, R.W. Sternberg, and G.C. Kineke. *Mechanisms of Sediment Dispersal and the Influence of Floods on the Northern California Continental Shelf.*

Bertuccioli, L., P. Doron, J. Katz, and T. Osborn. *PIV Measurements of Turbulence and Flow Structure in the Bottom Boundary Layer.*

Paola, C., J.B. Swenson, and G. Parker. *Experimental and Theoretical Study of Shoreline Response to Changing Base Level.*

Rhoads, D.C., R. Ward, J. Aller, and R. Aller. *The Importance of Technology in Benthic Research and Monitoring; Looking Back to See Ahead.*

Rhoads, D.C., D. Carey and J. Scott. *REMOTS® UV-Imaging Spectrometer.*

Rosenfeld, L. and E. Kunze. *Internal Waves in Monterey Canyon.*

Sanford, L.P. and J.P.-Y. Maa. *A Unified Erosion Formulation for Cohesive Sediments.*

Shimeta, J. *Tidal Resuspension of Protists in Buzzards Bay; Alterations of Community Structure and Implications for Food-Web Dynamics.*

Sleath, J.F.A. *Plugs and Plumes.*

Snelgrove, P.V.R., J. Grant, and C.A. Pilditch. *Flume Experiments on Larval Settlement of the Soft-Shell Clam, Mya arenaria L.*

Sternberg, R.W., A.S. Ogston and D. Cacchione. *Modes of Sediment Dispersal on Continental Shelves: Time for a Reappraisal of Methods and Concepts?*

Taghon, G.L. and D.L. Linton. *Effect of Sediment Organic Content on Settlement and Growth of Capitella sp. I.*

Terray, E.A., R.L. Gordon and B.H. Brumley. *Measuring Waves and Currents with an Upward-Looking ADCP.*

Thistle, D. and L.A. Levin. *The Effect of Experimentally Increased Near-Bottom Flow on Metazoan Meiofauna at a Deep-Sea Site.*

Trowbridge, J. and G. Voulgaris. *Nearshore Estimates of Turbulent Reynolds Shear Stress.*

Wiberg, P. *Controls on the Volume and Distribution of Resuspended Fine Sediment on the Continental Shelf.*

Zimmer, R.K. *Chemical Mediation of Interactions Between Organisms and Their Environments.*

INTRODUCTION

On October 7, 1986, the oceanographic community was deeply saddened by the loss of Dr. William D. Grant to cancer just 10 days after his 40th birthday. During nine short years at the Woods Hole Oceanographic Institution after his Ph.D., Bill rose to the rank of Senior Scientist, attesting to his profound and lasting impact on the field. Bill specialized in theoretical, laboratory and field studies of benthic processes, especially interactions between boundary layer flow, sediment transport, and the benthos. His article on wave-current boundary layers (Grant and Madsen 1979) showed theoretically how the centimeters-thick boundary layer produced by surface gravity waves can have a marked effect on low-frequency currents through an apparent enhancement of bottom roughness. This article has generated an enormous literature addressing the detailed dynamics and implications of near-bottom wave-current interactions. Bill's article on bedform roughness (Grant and Madsen 1982) articulated a number of issues related to bottom roughness produced by the interaction of a fluid flow with an erodible boundary, and it similarly stimulated a large body of theoretical and experimental work. His review article on benthic boundary layers (Grant and Madsen 1986) has provided the conceptual foundation for a decade of research on shelf boundary layers and sediment transport. The list goes on, with a common thread of excellence and impact marking every article to which Bill contributed.

In addition to contributions documented in the scientific literature, Bill's energy, insight, enthusiasm, and generosity had an enormous effect on the people with whom he interacted, including students, post-docs, employees, colleagues, friends, and family. To his students, unfortunately few in number, he was unfailingly generous with his ideas, time and financial support. To his post-docs and colleagues he was an energetic, actively engaged scientific collaborator. To his employees he was a generous, patient, challenging boss. To his tennis opponents and running companions, he was a fierce but fair competitor. To his family he was a loving, supportive son, brother, husband, and father. To all who knew him, he was a little larger than life, and he has become even more so with the passage of time since his death.

In recognition of his remarkable influence, members of the coastal oceanographic scientific community and Bill's family gathered from September 27-30, 1998 in Woods Hole, Massachusetts for a symposium entitled "Coastal Ocean Processes: A Tribute to William D. Grant". The symposium brought together leading researchers in three of the areas to which Bill Grant contributed - Coastal Fluid Dynamics, Sediment Transport, and Animal-Sediment-Flow Interactions. The purpose of the symposium was to stimulate creative research by means of presentations and critical discussion of the latest ideas and results. The atmosphere was informal, with discussions lasting well into the evening hours. The symposium began on Sunday, September 27, 1998 with the third annual Bill Grant Run from the village of Woods Hole to WHOI's Quissett Campus, followed by a welcoming barbecue. The program also included a banquet on Tuesday evening and a farewell lunch on Wednesday. Scientific presentations began on Monday, September 28, with talks and posters focusing on the general area of Coastal Fluid Dynamics. Tuesday's presentations focused on Sediment Transport, and Wednesday morning was devoted to Animal-Sediment-Flow Interactions. The scientific content of the symposium is summarized in the series of extended abstracts that comprise this volume.

The symposium was, by all accounts, a resounding success. The presentations were stimulating, the discussion was open and extensive, old friendships were renewed, and new friendships were made. Most remarkable was the outpouring of admiration, remembrance, gratitude, and acknowledgment expressed by the participants for Bill Grant. Speaker after speaker, some of whom never met Bill, told of his impact on their lives and careers. At times, especially at the Tuesday evening banquet, a sense of personal and professional loss was palpable among the assembly. In the end, we were left with a sense of gratitude for having known Bill, with questions about what we have missed in his absence, and with a renewed dedication to the pursuit of excellence that he embodied.

This symposium would not have been possible without the dedicated work of many people and the support of several organizations. The organizing committee consisted of Drs. Robert Beardsley, David Cacchione, Rockwell Geyer, John Trowbridge, and Ms. Gretchen McManamin. John and Gretchen worked especially long and hard to make both the symposium and this volume a reality, and they deserve special thanks for their efforts. The Woods Hole Oceanographic Institution was an excellent host. The Rinehart Coastal Research Center at WHOI, the U.S. Geological Survey, and the Office of Naval Research made the symposium possible through their generous sponsorship. Finally, Bill Grant's family members are commended for their remarkable endurance as they sat through the scientific proceedings. We also thank them for their participation in this event, which evoked even more strongly Bill's spirit and legacy.

Larry Sanford and Scott Glenn, March, 1999

Particle Transport in Bottom Boundary Layers: Size Distribution and Concentration, and Settling Velocity Distribution

Yogesh C. Agrawal and H. C. Pottsmith
Sequoia Scientific, Inc., Mercer Is., Washington

The theory of sediment transport, in its most robust form requires knowledge of particle volumetric concentration and fall velocity, or size distribution and density. The theory of vertical diffusion of particles in boundary layers, first published by Rouse in 1937, predicted a strong dependence on particle size: as the square of particle diameter in the exponent of the vertical co-ordinate z! Thus, particle size is critically important in the physics of sediment dispersion. Yet, perhaps because this quantity is optimally reachable only optically, and optical engineers have largely ignored the needs of sediment transport, *in situ* particle size and settling velocity data are only now becoming available with our work. Prior work, carried out with optical transmissometers, or with simple scattering-based measures obtained with optics and acoustics, has produced a vast amount of the historical field data. These data should be considered semi-quantitative whenever size-distribution, against which instruments were calibrated, is not assuredly constant in nature. In the historical data, the error bounds on the measurement of concentration arising from changes in particle size distribution are, typically, unknown. Our work in measuring the 2 critical quantities in the title addresses this need.

First, for the sake of completeness, note that a single - parameter sensor measures the following:

$$P = \int n(a)\, \sigma\, (a, k, \rho..)\, da \qquad\qquad (i)$$

where P is a measured quantity (optical transmission or scattering; acoustic pressure), σ is an interaction cross-section of a particle of radius a, interacting with a wavelength defined by $k = 2\pi/\lambda$, and depending, at least, also on a physical property (e.g. mass density) of the particle ρ. When an optical transmissometer is used to measure suspended sediment concentration, σ is the 'extinction cross-section' of the particle; otherwise, whether for optical or acoustic backscatter, σ represents the integration of *the differential scattering cross-section* (cm^2/sr) of the particle over some, hopefully, defined geometry. Clearly, the measured quantity P in (i) sums over the range of sizes, weighted by the number distribution $n(a)$ [defined so that the number of particles in the size range a to $a+da$ is $n(a)da$]. In the integration in (i), the size information is clearly lost. Further, as is widely recognized, the cross-section parameter σ scales approximately with particle area in optics, and as a^6 for Rayleigh acoustics; thus neither system comes close to reporting true volumetric concentration of particles. The calibration procedures that are the norm are only applicable with the assumption of an unchanged field size distribution.

In this paper, we describe instruments that measure the size distribution C_n, and settling velocity distribution $w_{f,n}$. We also show field data that illustrate significant spatial and temporal variability of particle size distribution. The 2 systems in this paper are based on the principle commonly known as *laser diffraction*. The name derives from the

diffraction-like property of scattering at small angles from the original beam. The diffraction through apertures is the familiar Airy function. This function, *for small scattering angles*, quite nicely fits the full Mie theory, which is valid for scattering of light at arbitrary angles from particles of arbitrary size and (homogeneous) composition. Thus although the method was initially called laser diffraction because of the use of the Airy function to approximate the scattering model, it is now also known as multi-angle scattering or low-angle scattering. In fact, using the full Mie theory, and by observing scattering over the full range of angles (0-π), in a modified method called Reverse Fourier Scattering, particles of far smaller size than the wave-length of light are now measured.

a

b

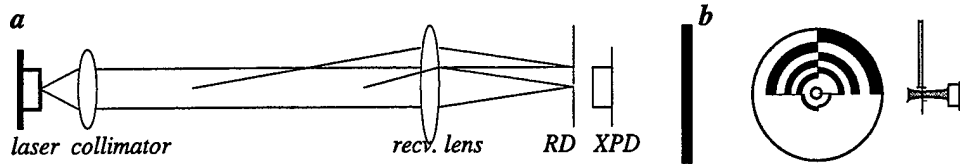*laser collimator*   *recv. lens*   *RD XPD*

Figure 1: The basic optics of a multi-angle instrument. In (a), a collimated laser beam illuminates particles in water. Ring detector (RD) shown in detail in (b) senses scattering. Also visible in (b) is an edge-on view of RD showing the transmissometer photo-diode (XPD) behind it.

When the scattering is sensed by azimuthally integrating ring-sensors, the scattering signature of size becomes obvious, Figure 1c. Ring detectors, placed in the focal plane of a receiving lens, represent logarithmically increasing scattering angles. The scattered optical power profile sensed by the rings per unit particle area (the term scattered *energy* is frequently used to denote integration over azimuth angles instead of time) is of nearly equal magnitude for all sizes. It exhibits a peak *at outer rings for small particles*, and vice versa. When a continuum of sizes is present, the observed optical power on the rings is a weighted sum of the particle area distribution: $N_A = n(a)a^2da$. Thus the scattered optical power distribution on the detector rings $\underline{E}$ is related to the scattering property kernel matrix K and the area distribution $\underline{N_A}$ through $\underline{E} = K . \underline{N_A}$ where K is the scattering kernel (constructed from Mie theory, with K_i a row, being the scattered energy distribution of particles of size class i). The observation $\underline{E}$ is inverted to obtain the area distribution, and thence the volume concentration in the various size classes. For more details, reference is suggested to Agrawal and Pottsmith(1998).
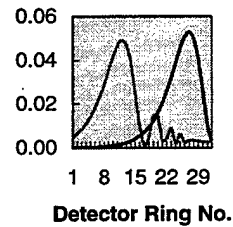
0.06
0.04
0.02
0.00

1 8 15 22 29

Detector Ring No.

Figure 1c: The signature of 2 sizes of particles on the ring detectors

For the measurement of settling velocity, a settling column is attached and the size distribution is observed at the bottom of the column as particles settle. Faster settling particles vanish from the observed size distribution earlier than slower ones. Thus the concentration history of each size class is used to estimate the settling velocity for that size class. For the measurement of the reference concentration, the same optics are employed, except with a miniature folded optical path. The 5 mm optical path (contrasted with 50 mm) permits a smaller sensing head, suitable for measurements near the seabed

4

without causing scour. This is the idea behind the MSCAT instrument (to be described elsewhere). The 3 instruments can be seen on a tripod Figure 2.

Field observations with the basic size-distribution sensing instrument LISST-100 reveal a rich variability of the natural size distribution of particles, both in time and in space. Figure 3a shows the optical transmission (upper trace). In the lower trace an estimate of surface gravity wave is obtained as follows: the 15-minute interval pressure samples are filtered to remove tide, and then smoothed (lower trace). The evolution of scattering distribution (right) is displayed at 2 day intervals over the ten day period of a broad surface wave event (second, broad event, lower trace). These data were acquired at 1m above bed, in the Coastal Mixing and Optics experiment, off Martha's Vineyard, Massachusetts in Fall 1996. There is clear evidence of large particles (energy at small angles) at some times and not at others. No evidence of the large particles was seen with another LISST instrument at 2m above bottom (not included here for brevity). This size change with height is striking.
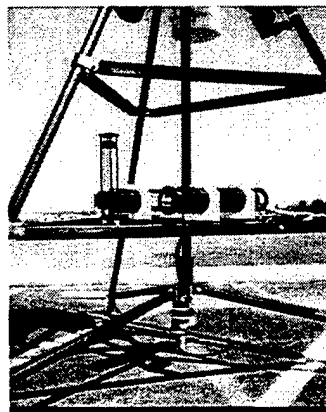

Figure 2: A field tripod shows the LISST-100 (top, slanted), LISST-ST and MSCAT instruments (sensor head at the bottom of center column).
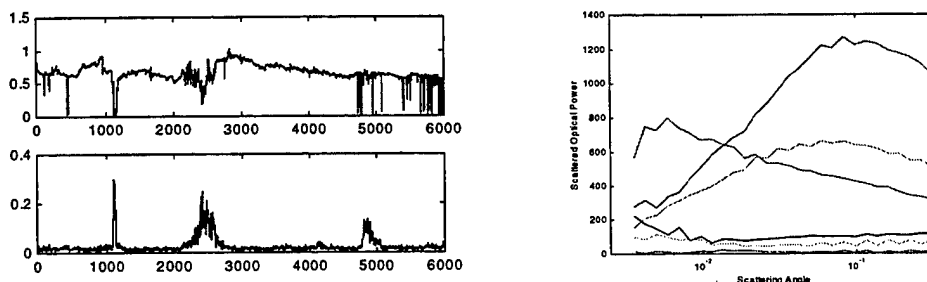

Figure 3: The optical transmission (left, upper) and 2-hour averaged rms pressure fluctuation (left lower). Pressure is shown uncalibrated . Right: angular scattering for the second major pressure event, records 2000-3000.

Examples of data for settling velocity measurements are displayed in Figure 4. After the settling column is closed and particles in a trapped water sample settle, the optical transmission monotonically returns to 1. The histories of concentration are constructed for 8 size classes only, as this is believed to be the limit of resolution in this observation of temporal concentration gradient. The histories are displayed from an *in-situ* settling experiment lasting 24 hours at LEO-15, off the New Jersey coast. The data were acquired in Fall 1997. The histories reveal that coarse particles disappear earlier than the finer fractions. By finding a single parameter – a settling velocity – that fits the concentration

history observed for each size class, the settling velocity variation with size of each class is estimated.
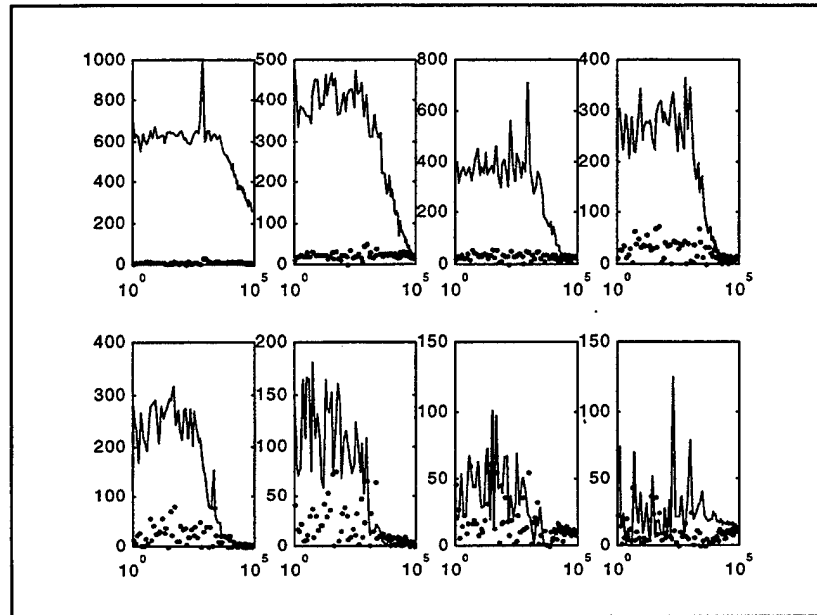

Figure 4: (From top left) Time history of concentration of 8 size classes in a settling column. The fine particles fall through the 30cm column slowly, vice versa. The dots represent noise in estimates of concentration. The data yielded settling velocities for 6 size classes. The size classes were centered at (left –right, top): 6.6, 11.8, 21.1, 37.5, 66.7, 118.6, 211 and 375 microns.

Again, details are omitted for brevity, but the data from LEO-15 suggest a relation between particle size (diameter in microns) and settling velocity, expressed in cm/sec, of the form:

$$w_f \sim 10^{-3.7} \, d^{1.1}.$$

Summary: New sensor systems reveal a rich diversity in temporal and spatial variation of size distribution of suspended particles. This is not surprising, it is only new in our ability to make the observations. Similarly, the size-resolved settling velocity distribution is also a new instrumental capability and it suggests that settling velocity at the LEO-15 site does not increase as particle diameter square, as constant density Stokes settling predicts, hinting at aggregation.

Reference:
Agrawal, Y.C., Pottsmith, 1998: Instruments for Particle Size and Settling Velocity Observations in Sediment Transport, Marine Geology (*in revision.*)

Model Studies of Upwelling Relaxation Events off Northern California

J. S. Allen
(Joint work with J. Gan)
College of Oceanic and Atmospheric Sciences
Oregon State University
Corvallis, OR 97331-5503

ABSTRACT

Time-dependent, three-dimensional circulation on the continental shelf off northern California in the region (37-40N) of the Coastal Ocean Dynamics Experiment (CODE) is studied using the Blumberg-Mellor, finite difference stratified, hydrostatic primitive equation model. A limited-area, high resolution curvilinear grid (approximately I km horizontal spacing, 30 vertical sigma levels) with realistic bottom topography and coastline is used. The grid extends 350 km alongshore and 150 km offshore and contains three open boundaries, where approximate open boundary conditions are implemented. The focus of the study is on the dynamics of observed upwelling relaxation events which involve the time-dependent development of northward currents on the inner shelf near the coast following the cessation of southward winds. A signature of these relaxation events in the CODE region is the advection near the coast of warm water from south of Point Reyes (38N) northward toward Point Arena (39N). Northward winds are typically not present and are not a necessary forcing mechanism for these events. Numerical experiments are conducted using forcing by spatially uniform winds with the time variability and direction of the observed winds at the CODE central line (38.6N) during April 1982. The model results are compared with moored current and temperature measurements from CODE. The model response includes a robust simulation of the April 1982 relaxation event with good qualitative agreement found between behavior of model and observed velocity and temperature fields. Analysis of the alongshore momentum balance shows that, after the abatement of southward winds, northward currents are forced by a northward pressure gradient. The northward alongshore pressure gradient is generated during the periods of southward winds by alongshore density gradients associated with topography-induced alongshore variability in upwelling intensity. Similar flow behavior is found in additional response experiments involving idealized wind relaxation scenarios. It appears that the dynamical processes involved in these upwelling relaxation events may be general features of the shelf flow field response to time-varying winds off the US West Coast.

OBSERVATIONS AND MODELING OF THE TIDAL BOTTOM BOUNDARY LAYER ON THE SOUTHERN FLANK OF GEORGES BANK

Sandra R. Werner
MIT/WHOI Joint Program in Oceanography
Cambridge, MA 02139

Robert C. Beardsley
Woods Hole Oceanographic Institution
Woods Hole, MA 02543

ABSTRACT: The vertical structure of the bottom boundary layer (BBL) is investigated in a shallow coastal region with strong semidiurnal tides. Moored temperature, salinity, and velocity data were taken from February-August 1995 near the 76-m isobath on the southern flank of Georges Bank. Measurements are presented for periods of weak and strong vertical stratification (Werner and Beardsley[a,b], submitted; hereafter WB[a] and WB[b]). From tidal current profiles representative of near-homogeneous winter conditions, we derive scale expressions for the BBL-thickness that are consistent with the logarithmic law of the wall. Numerical experiments show a simple turbulence closure model reproduces the observed velocity distribution closely when the water column is nearly unstratified. Results from the second order Mellor-Yamada level 2.5 turbulence closure model suggest the model underestimates the BBL-thickness in the presence of stratification, even for small buoyancy frequencies representative of winter.

INTRODUCTION

In many locations on the continental shelf, tidal currents are an important component of the near-shore circulation and account for significant turbulence production at the lower boundary. The thickness of the friction-induced BBL varies greatly with current strength, bottom roughness, and vertical stratification. For homogeneous conditions, Grant and Madsen (1986) derived scale expressions for the BBL-heights of steady planetary and rectilinear oscillating flows and showed that these expressions are in agreement with the logarithmic law of the wall. Based on our velocity measurements and bottom stress estimates, we investigate whether similar scaling applies to the case of a rotating tide.

Previous observations of rotating tidal flows indicate vertical stratification suppresses turbulent mixing, resulting in large current shear in and across the pycnocline (Maas and van Haren, 1987; Soulsby, 1990). To investigate the impacts of stratification on the BBL, we compare velocity measurements and bottom stress estimates representative of nearly homogeneous and strongly stratified conditions.

Numerical modeling studies frequently make use of second order turbulence closure schemes to compute the velocity and density distribution in the BBL. Here, we investigate the performance of the Mellor-Yamada level 2.5 model during periods of weak and strong stratification. Observations representative of winter are compared to predictions from a simple two-layer viscosity model designed for homogeneous conditions.

LOCATION

Georges Bank is a shallow submarine bank located off the east coast of the United States between the deeper Gulf of Maine and the continental slope. Over the southern flank and most of the bank-plateau, the semidiurnal M_2 tidal cur-

rents carry more than 90% of the kinetic energy. The interaction of the tidal flow with the rough bottom results in a turbulent shear flow, which keeps the crest of the bank well-mixed at all times. In summer, the competing effects of bottom friction-induced turbulence and increasing stratification manifest as a tidal mixing front (TMF), which surrounds the bank-plateau near the 60-m isobath. On the southern flank, the shelf-slope front (SSF) marks the transition from cooler, fresher shelf water to warmer, more saline slope water; its base is located near the 100-m isobath about 50 km south of the TMF.

MEASUREMENTS

As part of the U.S. GLOBEC/Georges Bank 1995 Stratification Study, moored current, temperature, and conductivity measurements were made on the southern flank of Georges Bank. Data were taken from February-August at a study site on the 76-m isobath, about 20 km south of the TMF and 30 km north of the SSF. Velocities were measured using eleven VMCMs between 6 and 71 m above the bottom. In addition, a bottom tripod was deployed from Feb.3-Apr.4 and Jul.11-Aug.23. The tripod was equiped with five acoustic travel time current meters (Benthic Acoustic Stress Sensors, herafter BASS, see Williams *et al.*, 1987) and eight thermistors between 0.2 and 6 m above the bottom.

All data presented in this study are hourly averaged, with exception of the half-hourly bottom tripod measurements. A more detailed description of the data set is given in WB[a].

BOTTOM FRICTION

Estimates of bottom friction velocity u_* and bottom roughness z_0 were obtained from instantaneous best-fit logarithmic profiles to acoustic travel time current meter data at 0.2, 0.6, 1.2, and 2.5 m above the bottom. From least-squares fits of u_*^2 to measured current speeds squared, we computed the quadratic drag coefficients at the BASS sensors and lowest VMCM located 6 m above the bottom. Histograms of bottom roughness peak at $O(1)$ mm. To derive one representative bottom roughness, we inverted the definition of the quadratic drag coefficient $c_D = \kappa / \left(\ln \left(z/z_0 \right) \right)^2$ using our c_D-estimates at the BASS sensors between 0.2-2.5 m above the bottom, and averaged the results.

Estimates of bottom friction velocity, drag coefficients, and bottom roughness are listed in Table 1 for Feb.12-Mar.26 (BASS 1) and Jul.12-Aug.14 (BASS 2). Characteristic values of these parameters are similar for both periods, indicating vertical stratification does not have a pronounced effect on bottom friction. This behaviour may be explained by the nearly well-mixed conditions immediately above the sea-floor; thermal stratification between 0.6 and 2.5 m above the bottom is less than $0.005°C$ for BASS 1, and less than 0.005 $(0.01)°C$ during 81 (95)% of the time during BASS 2. The lack of significant variations in drag coefficient from winter through summer suggests bottom stress may be estimated from the quadratic drag law at 6 m above the bottom when BASS measurements are not available.

THE BBL DURING NEAR-HOMOGENEOUS CONDITIONS

Time-mean temperature and salinity profiles representative of Feb.12-Mar.10 indicate the presence of a bottom mixed layer at $z < 30$ m above the bottom, followed by a weakly stratified interior with buoyancy frequencies squared $N^2 \approx 10^{-5}$ s^{-2}, and a surface mixed layer at $z > 65$ m above the bottom (Fig.1d).

Tidal decomposition of velocity measurements shows the M_2 current ellipse has an eccentricity $e \approx 0.64$, with the major axis oriented in the cross-bank direction.

Results are presented in rotating components (Soulsby, 1990) according to

$$u + i \cdot v = \left(\mathbf{R}^+ e^{i\sigma t} + \mathbf{R}^- e^{-i\sigma t} \right) \quad , \tag{1}$$

where u and v are the cross- and along-bank velocities, respectively, $\sigma = 1.41 \cdot 10^{-4}\,\mathrm{s}^{-2}$ is the frequency of the M_2 tide, and $\mathbf{R}^{\pm} = R^{\pm} e^{i\phi^{\pm}}$ are the counterclockwise (+) and clockwise (-) rotating components of the velocity vector. On Georges Bank, $R^- \approx 4 \cdot R^+$ results in clockwise rotation of the tidal currents (Fig.1a). Profiles of R^+, R^-, ϕ^+, and ϕ^-, show two boundary layers with relative thickness $\delta^-/\delta^+ \approx 5$ (Fig.1), where $\delta^+ \approx 12\,m$ and $\delta^- \approx 57\,m$ describe the counterclockwise and clockwise boundary layer, respectively. This result is supported by the veering of the stress vector away from the bottom (WB^a). The observed ratio $\delta^-/\delta^+ \approx 5$ suggests BBL-height scaling according to $\delta^{\pm} = c \cdot \kappa u_* / (\sigma \pm f)$, where $\kappa = 0.4$ is von Karman's constant, $u_* = 1.2\,\mathrm{cm\,s}^{-1}$ is the time-mean friction velocity, $f = 0.95 \cdot 10^{-4}\,\mathrm{s}^{-1}$ is the Coriolis parameter, and $c \approx 0.5$ is a proportionality constant. These scale expressions are in agreement with the logarithmic law of the wall, and are partially supported by earlier observations from Soulsby (1990).

THE BBL DURING STRONGLY STRATIFIED CONDITIONS

An example of the BBL during stratified conditions is presented for May 14-21. During this period, moored array measurements indicate warm and saline water was advected past the mooring, suggestive of an on-bank intrusion of the SSF. Maps of sea-surface temperature show the intrusion coincided with the presence of a Gulf Stream ring, which caused instabilities at the transition zone between the Shelf and Slope Waters. Cross-bank gradients in the BBL were strong during the SSF intrusion, resulting in the advection of colder, fresher, highly stratified water during ebb, and warmer, more saline, less stratified water during flood (WB^b). Time-mean buoyancy frequencies squared were about $N^2 = 0.2 \cdot 10^{-4}$ at 10 m above the bottom, and $N^2 = 1.3 \cdot 10^{-4}\,\mathrm{s}^{-2}$ near the surface (Fig.2d).

Tidal decomposition of VMCM measurements indicates stratification affects the counterclockwise rotating component $\mathbf{R}^+$ to a lesser degree than the clockwise rotating component $\mathbf{R}^-$. Vertical distributions of R^+ and $\Delta\phi^+$ are similar during near-homogeneous and strongly stratified conditions (Fig.2a,b). On the other hand, the clockwise component develops a maximum R^-_{Max} about 30 m above the bottom, and phase angles $\Delta\phi^-$ display strong veering toward the bottom during the SSF intrusion (Fig.2a,c). This behaviour reflects the different scales for the clockwise and counterclockwise boundary layers; with $\delta^-/\delta^+ \approx 5$ derived in the previous section, the clockwise boundary layer extends further into the stratified interior than the counterclockwise boundary layer. Based on the observations presented in Fig.2 together with their analysis of a bottom-trapped SSF intrusion in early May, WB^b concluded vertical stratification limits the thickness of the clockwise boundary layer, resulting in the observed maximum R^-_{Max} and pronounced veering $\Delta\phi^-$.

MODEL-DATA COMPARISON

Two one-dimensional models were run to investigate the effects of turbulent mixing on the velocity distribution. The models were forced with a tidal pressure gradient derived from the measurements (WB^a). The specified bottom roughness was 0.6 mm based on our BASS data analysis summarized in Table 1.

The first model is a simple two-layer viscosity model with a linear distribution in the lower layer and a constant value in the upper layer. Trowbridge and Madsen

(1984) showed a similar model performed well for homogeneous rectilinear flow in the absence of rotation. Model results vary depending on the height of the lower layer where the eddy viscosity $K = \kappa u_* z$. In the present case of a rotating tide, numerical results match the observations closely if the lower layer thickness is 5 m (Fig.1). Numerical friction velocities are 1.2 ± 0.2 cm s^{-1}, in good agreement with 1.2 ± 0.4 cm s^{-1} from BASS data analysis (Table 1).

The second model investigated here utilizes the Mellor-Yamada level 2.5 (MY2.5) turbulence closure (Mellor and Yamada, 1974, 1982). To evaluate the model performance for nearly homogeneous conditions, the model was run for $N^2 = 0$ and the N^2 distribution shown in Fig.1d. Vertical stratification was specified a priori as described in WB^a. Model results indicate the predicted phase veering $\Delta\phi^-$ is in better agreement with the observations if the effects of weak stratification are taken into consideration (WB^a). For $N^2 > 0$, the model predicts a region of zero shear and no turbulent momentum transfer at heights > 55 m above the bottom (Fig.1a). The transition from the turbulent BBL to the frictionless region above it is marked by a velocity maximum of the clockwise rotating component which is not supported by the observations. For strongly stratified conditions representative of the time-mean stratifiation from May 16-21, model velocities peak about 10 m below the observed maximum R_{Max}^- (Fig.2a). The predicted BBL-thickness is ≈ 26 m, followed by a frictionless free-stream at greater heights. Numerical results can be improved if vertical stratification varies on tidal time-scales as shown in Fig.2d. The reason for the improvement is that bottom friction-induced mixing is large at the end of flood when N^2 in the BBL is very small, resulting in a thicker time-averaged boundary layer than for the N^2 distribution representative of the time-mean (Fig.2a-c).

For both periods Feb.12-Mar.10 and May 16-21, bottom stress values from the MY2.5-model are within 6% of the estimates derived from best-fit logarithmic profiles to BASS data and the quadratic drag law at 6 m above the bottom.

CONCLUSIONS

1. From our analysis of bottom tripod data, we obtained estimates of friction velocity, quadratic drag coefficients, and bottom roughness that are almost identical for winter and summer. Thermal stratification below 2.5 m above the bottom is $< 0.01°$ C at least 95% of the time during both tripod deployments, corresponding to $N^2 = 0.5 - 0.7 \cdot 10^{-5}$ s^{-2} if salinity is assumed constant. The lack of significant variations in bottom friction parameters from winter through summer suggests near-bottom turbulence remains largely unaffected by vertical stratification.

2. Vertical profiles of the M_2 current and stress vectors indicate two distinct boundary layers describe the clockwise and counterclockwise rotating components. The relative thickness of these boundary layers is $\delta^-/\delta^+ \approx 5$, suggesting scale expressions $\delta^\pm = c \cdot \kappa u_*/(\sigma \pm f)$ that are in agreement with the logarithmic law of the wall ($c \approx 0.5, u_* = 1.2$ cm s^{-1}).

3. Strong stratification representative of a SSF intrusion limits the vertical extent to which bottom friction-induced turbulence can diffuse. As a result, velocity profiles develop a maximum in the lower water column which is accompanied by strong phase veering toward the bottom. The SSF intrusion particularly affects the clockwise rotating component, since the clockwise BBL extends far into the stratified interior.

4. A simple two-layer viscosity model reproduces the observed velocity structure closely when the water column is nearly unstratified.

5. Model predictions utilizing the Mellor-Yamada level 2.5 turblence closure scheme show marginal agreement with the observations. The model performance is limited by the underestimation of the BBL-thickness in the presence of stratification, even for small buoyancy frequencies representative of winter. Based on our model-data comparison, we conclude that the Mellor-Yamada level 2.5 model underpredicts turbulence production during stratified conditions, in agreement with results by Simpson et $al.$ (1996). Numerical solutions for strongly stratified conditions can be improved if tidal variations of N^2 are taken into consideration. Such variations allow for enhanced mixing during those times of the tidal cycle when stratification is smallest.

REFERENCES

Grant, W. D., and O. S. Madsen, The continental-shelf bottom boundary layer. *Annual Rev. Fluid Mech.*, **18**, 265–305, 1986.

Maas, L. R. M., and J. J. M. van Haren, Observations on the vertical structure of tidal and inertial currents in the central North Sea. *J. Marine Res.*, **45**, 293–318, 1987.

Mellor, G. L., and T. Yamada, A hierarchy of turbulence closure models for planetary boundary layers. *J. Atmos. Sc.*, **33**, 1791–1896, 1974.

Mellor, G. L., and T. Yamada, Development of a turbulence closure model for geophysical fluid problems. *Rev. Geophys. Space Physics*, **20**, 851–875, 1982.

Simpson, J. H., W. Crawford, T. P. Rippeth, A. R. Campbell and J.V.S. Cheok, The vertical structure of turbulent dissipation in shelf seas. *J. Physical Oceanogr.*, **26**, 1579–1590, 1996.

Soulsby, R. L., Tidal-current boundary layers. *The Sea*, **9**, 523–566, 1990.

Trowbridge, J., and O. S. Madsen, Turbulent wave boundary layers 1. Model formulation and first–order solution. *J. Geophys. Res.*, **89**, 7989–7997, 1984.

Williams, A. J., 3rd, J. S. Tochko, R.L. Koehler, W. D. Grant, T. F. Gross, and C.V.R. Dunn, Measurement of turbulence in the oceanic bottom boundary layer with an acoustic current meter array. *J. Atmos. Oceanic Techn.*, **4**, 312–327, 1987.

Werner, S.R., and R. C. Beardsely, The vertical structure of the tidal boundary layer on the southern flank of Georges Bank during near-homogeneous and weakly stratified conditions, submitted to *JGR*.

Werner, S.R., and R. C. Beardsely, The vertical structure of the tidal boundary layer on the southern flank of Georges Bank during strongly stratified conditions, submitted to *JGR*.

	u_* [cm s^{-1}]	z_o [mm]	c_d (1.2 m)	c_d (6 m)	r
Feb 12–Mar 26	1.2 ± 0.4	0.6	2.80 ± 0.01	1.74 ± 0.01	0.97 ± 0.03
Jul 12–Aug 14	1.1 ± 0.4	0.6	2.80 ± 0.01	1.68 ± 0.01	0.93 ± 0.07

Table 1: Bottom friction velocity, bottom roughness, and quadratic drag coefficients at 1.2 and 6 m above the bottom from BASS data analysis. The last column gives the linear correlation coefficient averaged over all instantaneous best-fit logarithmic profiles. Values following the $\pm$ are standard deviations from the mean.
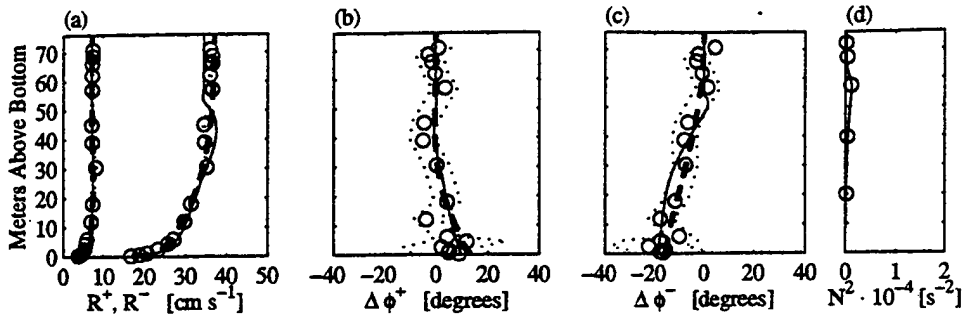
Fig.1: Profiles of the (a-c) M_2 rotating components and (d) time-mean buoyancy frequencies squared for the winter period Feb.12-Mar.10. Circles are observations, and dotted lines are data uncertainties. Shown are (a) magnitudes R^+ (smaller values) and R^- (larger values), and phase angles (b) $\Delta\phi^+$ and (c) $\Delta\phi^-$. Phase angles are given with respect to the phase of the near surface currents (averaged over the topmost five VMCMs). Also shown are model results from the (heavy dashed) two-layer viscosity model, and the (solid) MY2.5-model with the N^2 distribution indicated by the solid line in (d).

Fig.2: Same as Fig.1, but for the SSF intrusion May 16-21. Model results are from the MY2.5-model with (solid) N^2 specified according to the time-mean, and (heavy dashed) N^2 superimposed by tidal variations as shown in (d). Plusses and triangles in (d) are tidal variations inferred from observations.

15
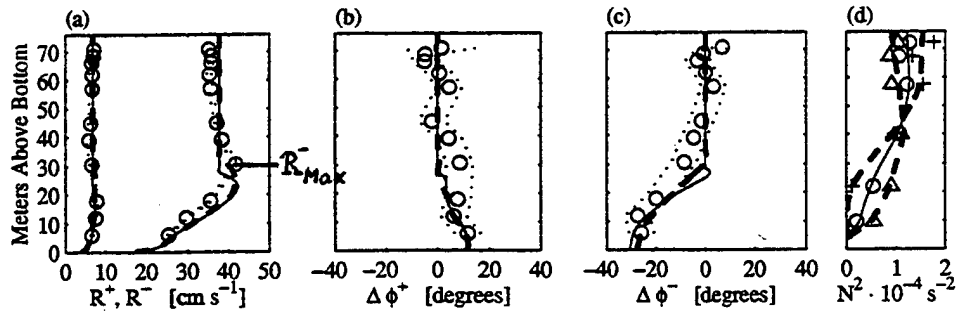
Convergences and Hydraulic Controls in Partially Mixed Estuaries

W. C. Boicourt, L. J. Walstad, M. Roman, R. Hood
Horn Point Laboratory, University of Maryland Center for Environmental Sciences

A. Valle-Levinson, C. Lascara, L. Heilman, and R. Burgett
Center for Coastal Physical Oceanography, Old Dominion University

Although the elevated primary production of estuaries appears to be the result of retention and recycling of nutrients, reasons for elevated secondary production have proved more elusive. An interdisciplinary study is underway in the Chesapeake Bay to test the hypothesis that pulsed inputs and circulation processes create localized ecosystems that enhance this trophic transfer. We are focusing on the role of the pycnocline, and on convergent structures such as turbidity maxima, fronts, residual eddies, and hydraulic controls, which concentrate both food and fish larvae.

These circulation features have inherently small space scales, yet the perspective for addressing the production balance is necessarily system-wide. For this reason, observational techniques must provide both spatial resolution and coverage. A combination of an undulating towed vehicle--the SCANFISH equipped with multiple sensors, including an Optical Plankton Counter-- and an underway sampler has been employed in conjunction with a Doppler velocity profiler, a split-beam acoustic mapper for fish, and moored instrumentation. From the outset, we have recognized that the attempt to estimate the relative roles of singularities versus the continuum in the trophic transfer process would be difficult on the basis of observations alone. An appeal to a variety of numerical techniques has been made to bolster this effort.

The approach toward deciphering the mechanisms of trophic transfer has been to use both Bay-wide surveys, and a dedicated focus on specific convergent features. In 1996, we addressed the turbidity maximum zone and have reported the results elsewhere. Fronts and hydraulic controls in the Chesapeake Bay entrance region were studied in 1997, and the primary hydraulic control in the central Bay, in 1998. Hydraulic controls have been observed at the sills of fjord estuaries (Farmer and Smith, 1980; Farmer and Denton, 1985), but laboratory and modeling studies in partially mixed estuaries (Stommel and Farmer, 1952, 1953; Chao and Paluszkiewicz, 1991) have been followed by field efforts. Previous observations provided evidence for tidally modulated fronts, and puzzling large excursions of the pycnocline in both the Bay entrance and central Bay regions. These excursions occurred near abrupt topographic transitions in both depth and width of the channels. Time-series transects over multiple tidal cycles were employed along with moored instrumentation to examine the details of these variations.

Preliminary results indicate hydraulic controls are active at the marked topographic features, but that hydraulic processes are also prevalent at subtler topographic transitions. In coastal-plain estuaries such as the Chesapeake Bay, these controls act as key internal sluicegates for both salt and fresh water transport. In addition, these circulation structures provide concentrating mechanisms for food and larval fish. Agreement with numerical

models is encouraging, especially because we anticipate accurate estimates of the biologically important vertical velocities.

References:

Chao, S.-Y., and T. Paluszkiewicz 1991. The hydraulics of density currents over estuarine sills. Journal of Geophysical Research 96, 7065-7076.

Farmer, D.M., and J.D. Smith 1980. Tidal interaction of stratified flow with a sill in Knight Inlet. Deep-Sea Research 27A, 239-254.

Farmer, D.M., and R.A. Denton 1985. Hydraulic control of flow over the sill in Observatory Inlet. Journal of Geophysical Research 90, 9051-9068.

Stommel, H., and H.G. Farmer, 1952. Abrupt changes in width in two layer open channel flow. Journal of Marine Research 11, 205-214.

Stommel, H., and H.G. Farmer, 1953. Control of salinity in an estuary by a transition. Journal of Marine Research 12, 13-20.

Another Glimpse of the Wave Boundary Layer

A.J. Bowen and P. MacAulay
Department of Oceanography, Dalhousie University
Halifax, NS B3H 4J1, Canada

The study of the bottom boundary layers associated with surface gravity waves, or a combination of waves and steady currents, has been a topic of very considerable interest over the last twenty-five years. The result is a very extensive literature, perhaps surprisingly extensive in view of the apparently well-posed nature of the problem. This is seen, for example, in the many models that have been proposed for the vertical structure of the eddy viscosity (time invariant), the model of Grant and Madsen (1979) being of particular relevance, and, representing one of several 'schools of thought' which have continued semi-independent existences in the USA, UK, Denmark and Australia throughout the further development of the field.

The problem in resolving the discrepancies between the various schools is the classical problem of modelling turbulence. At very low Reynolds Numbers the viscosity is effectively molecular, constant in space and time. Small scale experiments confirm the theoretical predictions of scales, phase lags, etc. for this case. For larger waves, the assumption of constant eddy viscosity breaks down, the predictions of boundary layer thickness are overestimates. To test more elaborate models, data is needed and most of the data comes from experiments in narrow flumes with regular waves and, necessarily, co-directional currents (with or against the waves). The use of regular waves of constant height and frequency, while apparently simplistic, offers very significant attractions. It is a simple situation to model being defined by a small number of parameters; the concepts of phase shifts between free stream flow and bottom stress, between bottom stress and initiation of sediment movement are clear and unambiguous; and because the wave motion is regular it can be subtracted from velocity measurements to leave 'the turbulence'.

However, such measurements show that the assumption of a constant eddy viscosity in time, is a poor representation of the real physics, although perhaps an adequate description of the boundary layer structure for some practical predictions. In reality, turbulence is clearly a function of the recent history of the flow and analytical and semi-analytical model (Trowbridge and Madsen, 1984; Davies, 1995) show that the time variability of the eddy viscosity introduces new physics that may produce major changes (even direction changes) in the vertical structure of the wave induced drift velocity and the sediment transport.

Equivalent measurements of the bottom boundary structure in the ocean are difficult to make, and therefore infrequent. Trowbridge and Agrawal (1995) provide 'glimpses' of a real wave boundary layer. However, the capability to make sophisticated measurements close to the seabed is improving notably, focusing attention on the question of what we expect to see, and what models provide the appropriate predictions.

In the nearshore zone, the range of possible phenomenology is substantial. In the surf zone itself, wave breaking provides a major complication in the turbulent energy

balance, but even outside the surf zone the system is very energetic, waves and currents of same order of magnitude, up to O(1 m/s), with the currents frequently at large angles to the wave direction. However, the bottom line may be in providing adequate models to describe the effects of the variability of the flow, waves, wave groups, shear waves, pulsing 'mean' currents.

To examine some of the possible dynamics k-ε models are being increasingly used to determine the turbulent field and allow the appropriate time lags for turbulent development and decay complex flow conditions (Hagatun and Eidsvik, 1986). For regular waves, such models generate time varying eddy viscosities similar to those proposed earlier and similar changes in the higher order behaviour of the boundary layer. But the extension to skewed waves, to irregular waves, to wave groups, or to rapidly changing flows, produces a whole suite of new behaviours reflecting the new frequencies and time lags that are introduced by the more complex inputs to a fundamentally non-linear system.

The results suggest that the physics associated with waves groups, for example, may lead to several interesting and potentially observable behaviours in the boundary layer.

- first, there are significantly different vertical structures in the total instantaneous velocity field which may be important in reinforcing the shear instabilities which can occur in wave boundary layers.

- second, regular wave groups contribute significantly to the mean mass transport as well as providing time variability to all the high order terms.

- terms relating to the bottom stress, sediment suspension, skew flux, and sediment transport all become time variant in complex ways. As all classical models suggest that sediment transport is a function of a high power of the current speed, it is clear that the 'proper' time averaging of these processes is important in deriving sensible predictions of sediment mobility and transport.

Grant, W. D., and O. S. Madsen, 1989. Combined wave and current interaction with a rough bottom. *J. Geophys. Res.*, *84*, 1797-1808.

Trowbridge, J., and O. S. Madsen, 1984. Turbulent wave boundary layers 2. Second-order theory and mass transport. *J. Geophys. Res.*, *89*, 7999-8007.

Davies, A. G., 1995. Effect of the unsteadiness of the suspended sediment flux in co-linear wave-current flow. *Cont. Shelf Res.*, *15*, 949-979.

Trowbridge, J. H., and Y. C. Agrawal, 1995. Glimpses of a wave boundary layer. *J. Geophys. Res.*, *100*, 20,729-20,743.

Hagatun, K., and K. J. Eidsvik, 1986. Oscillating turbulent boundary layers with suspended sediment. *J. Geophys. Res.*, 91, 13,045-13,055.

Winter Mixed Layer Evolution in the Gulf of Maine

Wendell S. Brown and Prashant Mupparapu

Ocean Process Analysis Laboratory
Institute of the Study of Earth, Oceans and Space
Department of Earth Sciences
University of New Hampshire, Durham 03824

Introduction: Winters in certain high latitude oceanic regions are marked with cold dry offshore winds which cool the surface waters so rapidly that an unstable situation develops. The resulting convection, coupled with wind mixing, leads to deep vertical mixing of the upper water column. The relative roles of these two processes in determining the depth of the winter mixed layer is the topic of this paper.

Convection-induced deepening of the winter mixed layer and water mass formation processes have been observed in several marginal seas such as the Gulf of Lions in the western Mediterranean Sea (Stommel, 1972; Schott and Leaman, 1991), Greenland Sea (Schott et al.,1993) and Labrador Sea (Clark and Gascard, 1983). These winter convection-induced water formation processes are organized on a hierarchy of scales (Gascard, 1981). The lateral spatial scales of the near-surface, density-induced plumes are of the order of the mixed layer depth (depending upon location, 10m to 1000m), with time scales ranging from a few hours to a day. These intermittent plumes occur within "chimney-scale" zones of homogeneous water ($\sim$ 50km), which are bordered by mesoscale (1-10km) eddies, with time scales of days. The plumes and the eddies apparently combine to homogenize the water column, forming the seasonally varying chimney-scale winter water masses. The commonly found intermediate water masses in these regions result from the sinking, spreading and eventual springtime isolation of some of the winter water mass. Although our nearby marginal sea - the Gulf of Maine (Figure 1)- is shallower than these other marginal sea regions, it's wintertime conditions mimic those of the other marginal seas. Observational evidence (Hopkins and Garfield,1979; Brown and Irish,1993) implicates the cold, offshore southeastward winter winds in the formation of convective plumes and Maine Intermediate Water (MIW).

This paper focuses on this atmospherically-induced mixing and winter water mass formation in the Wilkinson Basin - a western Gulf of Maine site where most MIW is found. Observations from 4 to 18 February 1987 and models are used to explain the (1) intermittent periods of mixed layer deepening in terms of atmospherically-induced convection and wind mixing and (2) how lateral advection combines with the different mixing mechanisms to create winter water. Because of its relative simplicity and reasonable performance in previous applications, we chose the Price, Weller and Pinkel (PWP, 1986) model for this study. The PWP mixed layer model improved upon previous one-dimensional mixed models by replacing the sharp jump at the base of the mixed layer with a transition layer controlled by a gradient Richardson number stability criteria. Wind stress and heat fluxes, estimated from operational measurements in and around the Gulf, were used to force the PWP model as well as the Lynch et al. (1992) three-dimensional diagnostic circulation model which was also used to estimate lateral advection during the period. The

moored observations in Wilkinson basin are used to assess the performance of the models.
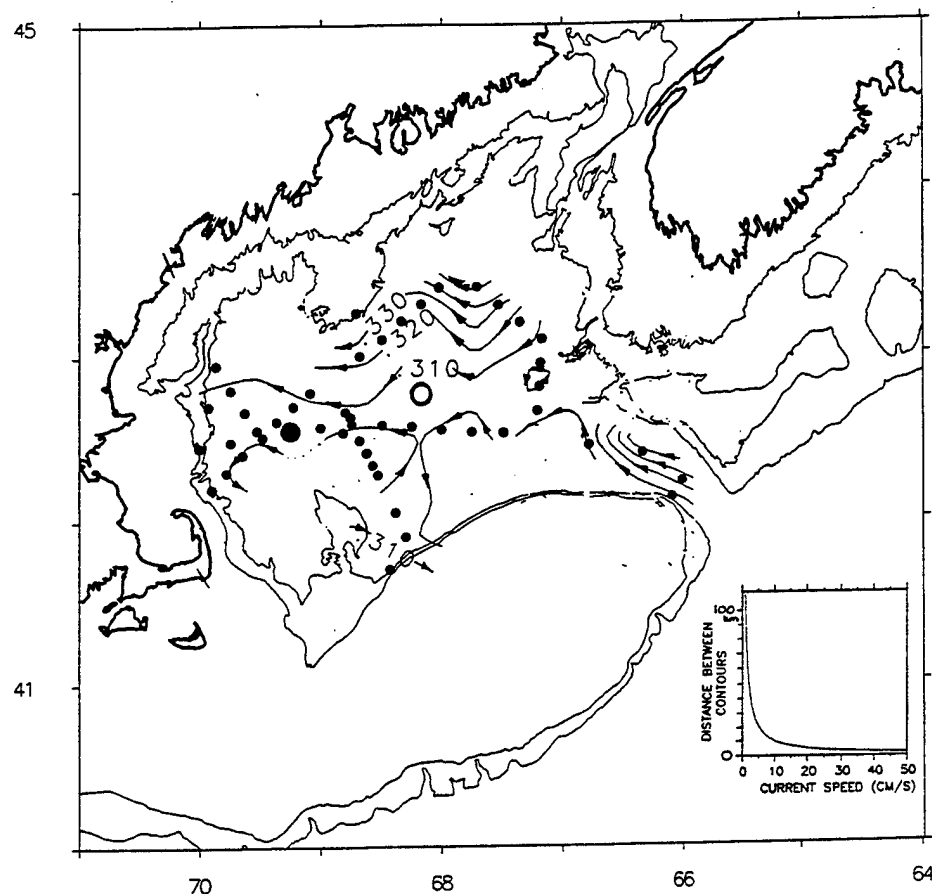
Figure 1. Surface dynamic topography (dynamic meters relative to 100 decibars) for the Gulf of Maine in early February 1987. The hydrographic survey stations (small dots) during the 5-15 February 1987 R/V Oceanus cruise, the Wilkinson Basin mooring (large dot) and the NDBC meteorological buoy (open circle) used in this study are located. The 100m and 200m isobaths are shown. Note the Wilkinson Basin cyclonic flow feature.

The Atmospheric Forcing: The meteorological forcing in Wilkinson Basin was estimated using meteorological records from the nearby Gulf of Maine (44005) National Data Buoy Center (NDBC) buoy (Figure 1). Bulk formulae were used to convert buoy measurements to estimated wind stresses and heat flux components. These time-series (Figure 2) reveal a major storm-induced cooling event that was bracketed by a short period of offshore wind-induced cooling beginning on 4 February and an extended period of strong cooling after 14 February. The storm-related surface cooling was due to high northeasterly winds and modest air-sea temperature differences. The pre- and post-storm cooling events were due to larger

22

air-sea temperature differences, but more moderate, dry offshore winds from the north.
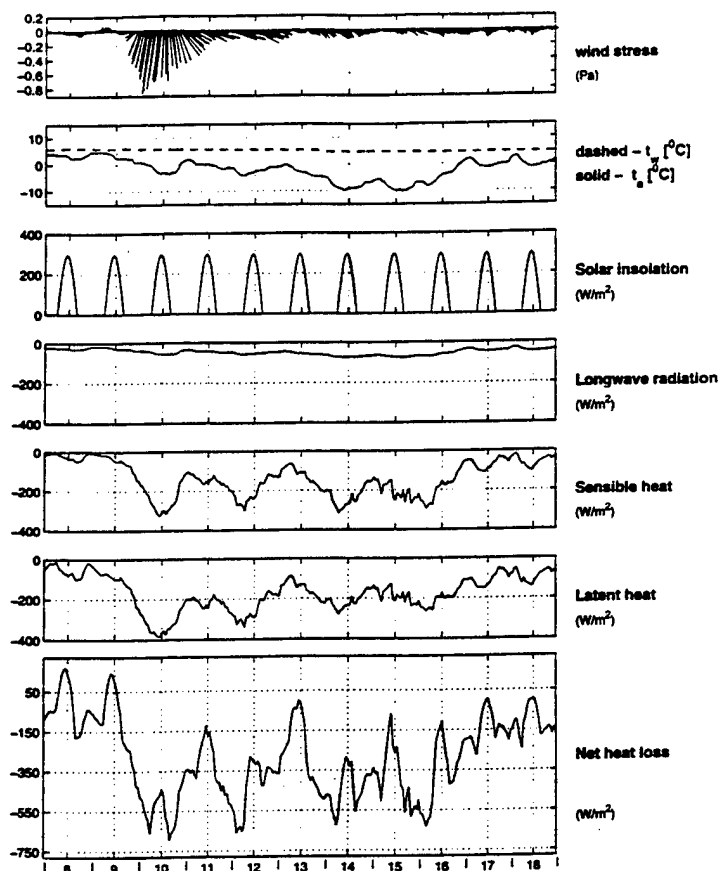

Figure 2. Time series of wind stress and thermodynamic surface forcing in Wilkinson Basin between 8 and 19 February 1987. The upper panel shows hourly wind stress vectors derived from winds on the NDBC buoy. The NDBC buoy air and mooring ocean temperatures in are in the next panel. Solar insolation, long-wave radiation, sensible heat flux, latent heat flux and net heat flux time series estimated from bulk formulae are in the lower panels.

The Ocean Response: The ocean response to this forcing was derived from measured temperature at 1m and Sea Bird temperature/conductivity at depths of 15m, 65m, 115m, 165m respectively in Wilkinson Basin. We found that intermittent, statically-unstable regions of the upper water column coincided with cold surface temperature anomalies during the 5-6 February period. After the brief period of warming, intense storm-induced surface cooling was established . Although there were episodes of cooling-induced static instability during this period, the water column below 15m actually became more stable due to increased salinity gradient. A comparison of the across-gulf hydrographic sections before and after the 9-10 February storm indicate lateral advection of fresher and colder (but less dense) upper water into Wilkinson Basin. Thus the 14 through 16 February cooling produced a much shallower mixed layer than the earlier two cooling events. A local heat budget for the upper ocean water column shows that decreases (increases) in heat content of the

23

upper 50m in Wilkinson Basin were consistent with local surface cooling (heating), but changes in the 50-150m depth range were not.
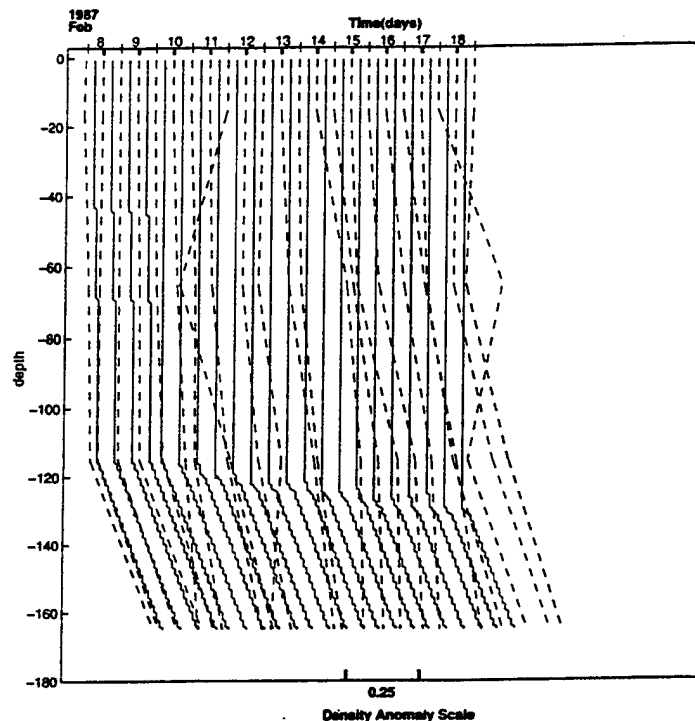

Figure 3. A ten-day sequence of 12-hourly PWP model density anomaly profiles (solid) resulting from the effects of surface forcing on the initial profile on the left. A corresponding sequence of observed profiles (dashed), derived by interpolating moored observations, is also presented.

Mixed Layer Modeling: The PWP one-dimensional mixed layer model was used to help understand the relative effects of convective overturning and direct wind mixing in the evolution of the winter mixed layer in the Wilkinson Basin in the two intervals of 4 and 6 February and 8 and 18 February, 1987. The PWP model, initialized with 4 February buoy-measured hydrography and forced with our estimated wind stresses and air-sea heat fluxes (Figure 2), maintained the relatively steady mixed layer depth of about 120m - very similar to what was observed.

On 7 February some unusual surface warming apparently produced a shallow (20m) layer of less dense water. These were the initial conditions at the beginning of the second PWP model run at midnight 8 February (Figure 3). During the first 2 days the *model* mixed layer deepened from 20m to 40m. Then near midnight on 10 February as the storm hit, with strong wind stress and surface cooling, the *model* mixed layer rapidly deepened from 40m to 90m and within a few hours to about 120 m, where it remained for the duration of the 10-day run. As diagnostic model experiments showed, convective overturning was required

24

for the model mixed layer to deepen to the observed 120 m depth, while direct wind mixing *alone* could deepen the model mixed layer to only about 75 m.

The *observed* mixed layer behaved rather differently from the model mixed layer. On 8 February, with weak winds and mid-day surface warming, the *observed* mixed layer at the buoy deepened precipitously and inexplicably to about 120m -unlike the *model* mixed layer. Furthermore, when the storm hit and the the model mixed layer was deepened rapidly, the *observed* mixed layer was shallowing, first to about 60m and then within a few days to about 20m.The model/observation discrepancies in the stability structure strongly suggest the importance of lateral advection in the Wilkinson Basin during and after the storm.

Observed salinity distributions combined with horizontal velocity estimates from a Dartmouth linear, finite element circulation model of the Gulf (FUNDY, Lynch et al.,1992) help to explain differences between PWP model and observational results. The model was forced with 36-hour average wind stress fields derived using the optimal spatial interpolation scheme, as described by Feng and Brown (1998), and NDBC wind measurements. Daily 3-D current fields were simulated by running the model in a steady state (i.e., very low frequency) diagnostic mode for each day of the study period. The currents at 8 model mesh nodes in the Wilkinson Basin (Figure 4) shows the daily average currents for 10 February, 1987, when the storm had the maximum intensity. While the Ekman transport in the upper 45m moved generally southwestward at about 8.5 km/day, the slower, deeper wind forced currents flowed in a clockwise circulation pattern around the Wilkinson Basin. These and the other simulated wind driven currents during this period were similar in suggesting that the flow structure is divided into two fairly distinct layers.

While the upper 40m advects salt from the east and northeast (very rapidly during the storm), the direction and speed of the deeper, more barotropic flow is generally different. The change of salinity due to lateral advection of the upper 40m of the water column in Wilkinson Basin, estimated from the product of the salinity gradients (derived from hydrography) and the model Ekman transports, was found produce a decrease of 0.14 psu. The very good agreement between this estimate and the corresponding measured salinity decrease of 0.15 psu strongly suggests an advection hypothesis. Thus it appears that the observed freshwater-induced restratification of the upper water column in Wilkinson Basin was due to the advection of water from the eastern and then northeastern Gulf.

Summary

(1)There were two types of cooling events in February 1987. The 5-6 and 14-16 February cooling events were characterized by modest offshore wind stress and very cold air temperatures. The very strong 9-11 February storm-induced cooling event was characterized by high wind stress and modest air-sea temperature difference.

(2) The observed and PWP model mixed layers were very similar during the 4-6 February, 1987 strong cooling event. The high heat extraction caused surface cooling-induced convection in the neutrally stable water column in the Wilkinson Basin, thus maintaining the

mixed layer depth at ~120 m. The cold (and dry)offshore winds produced minimal lateral advection.
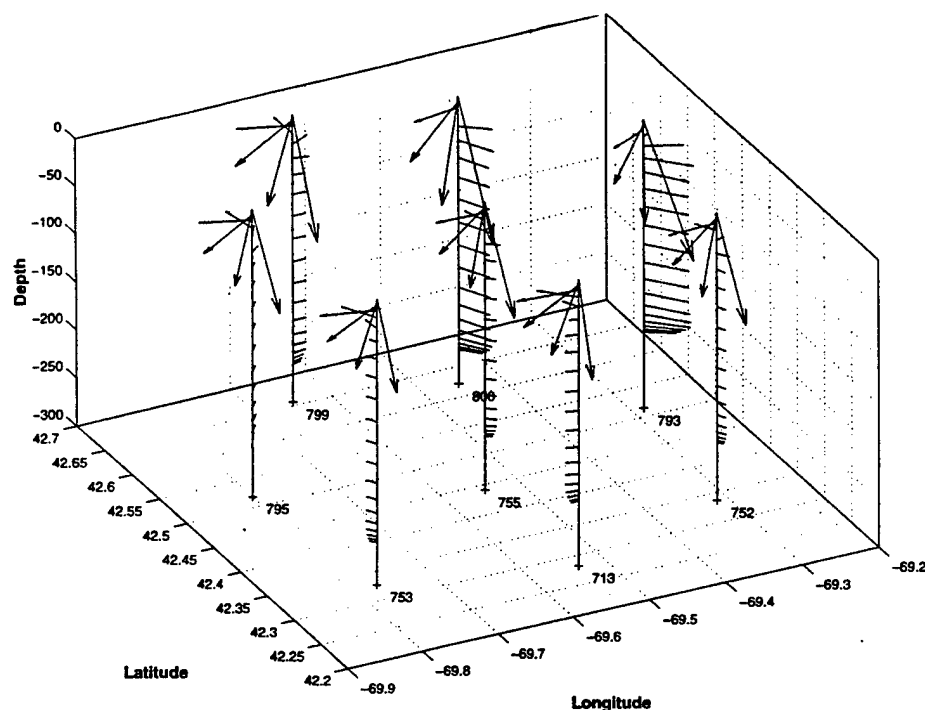
Figure 4. Diagnostic Fundy model current profiles resulting from the observed wind stress forcing for 9 February 1987 (during the storm). Note the distinct Ekman layer to a depth of about 50m and the very different direction of the rather depth-independent deeper flow. (In this perspective presentation, current vectors pointing directly away from the viewer can not be seen.)

(3) The PWP(1986) model results clearly suggest that free convection is the dominant process in deepening the Wilkinson Basin mixed layer to the observed pre-storm depth of about 120m during February 1987. The model results also suggest that, without convection, the observed wind stress would have caused vertical mixing to pre-storm depths of only about 65m.

(4) The results of the 8-18 February one-dimensional PWP model mixed layer depth history did not compare well with observed results because of unaccounted-for lateral advection

effects. The storm wind-forced lateral advection of fresher water from the northeastern gulf increased the local static stability of the water column. Thus, despite strong buoyancy-forcing, the mixed layer depth decreased from the pre-storm 120m to the post-storm 20mm. The intensive convective mixing period following the 9-10 February storm only cooled the upper water column.

(5) The FUNDY model results indicate a two-layered structure to the advection at the Wilkinson Basin mooring site. This suggests convective plumes, which are crucial to the mixed layer deepening, must be sheared by the lateral flow and thus are very 3-dimensional.

(6) The storm caused an enhanced clockwise circulation around the Wilkinson Basin in water deeper than 50m in the deep-water layer, which appears to have been fed by colder denser shallower water formed in adjacent coastal regions in the western gulf.

References

Brown, W.S., and Irish, J.D., 1993, The annual variation of water mass structure in the Gulf of Maine : 1986-1987. *J. Mar. Res.*, 51, 53-107.

Clarke, R.A. and J.C. Gascard, 1983. The formation of Labrador Sea water. Part I: large-scale processes, *J. Phys. Oceanogr.*, 13, 1764-1778.

Feng, H., and W.S. Brown, 1998, The wind-forced response of the western Gulf of Maine coastal ocean during spring and summer 1994, submitted *J. Geophys. Res.*

Gascard, J.C., 1991, Open ocean convection and deep water formation revisited in the Mediterranean, Labrador, Greenland and Weddell Seas. In: Deep Convection and Deep water Formation in the Oceans. P. Chu and J.Gascard, eds., Elsevier, Oceanogr.Ser., 157-181.

Hopkins, T.S. and N. Garfield III, 1979, Gulf of Maine Intermediate Water, *J.Marine Res.*, 37, 103-139.

Lynch, D.R., F.E. Werner, D.A. Greenberg, and J.W. Loder, 1992. Diagnostic Model for Baroclinic and Wind-Driven Circulation is Shallow Seas, *Continental Shelf Research*, 12, 37-64.

Price, J.F., Weller, R.A., Pinkel, R., 1986, Diurnal Cycling: Observations and Models of the Upper Ocean Response to Diurnal Heating, Cooling and Wind Mixing. *J. Geophys. Res.*, 91, 8411-8427.

Schott, F. and K.D. Leaman, 1991. Observations with moored acoustic doppler current profilers in the convection regime in the Golfe du Lion, *J. Phys. Oceanogr.*, 21, 558-574.

Schott, F., M. Visbeck, and J. Fischer, 1993. Observations of vertical currents and convection in the central Greenland Sea during the winter of 1988-1989, *J. Geophys. Res.*, 98, 14,402-14,421.

Stommel, H., 1972, Deep winter-time convection in the western Mediterranean Sea, In: Studies in Physical Oceanography, a Tribute to George Wust on his 80th Birthday, A.L. Gordon (ed.), Gordon and Breach 2, 207-218.

Application of Simple Profile Evolution Concepts: Analysis of a Dynamic Shoreline

Michael S. Bruno and Kelly L. Rankin
Stevens Institute of Technology
Hoboken, New Jersey 07030

I.   Introduction

There have been significant advancements over the last 10 years in our understanding of the physics responsible for sediment transport in the nearshore region. Much of this progress is the result of vastly improved field measurement capabilities. As these capabilities continue to evolve, they offer the promise of high-resolution data sets that will shed light on issues of paramount importance to the coastal engineering community, including the influence of coastal structures on nearshore hydrodynamics and sediment transport patterns, the generation and eventual fate of rip currents, and the accelerated erosion along localized stretches of shoreline, often termed "hot spots".

At present, the requirements of shoreline evolution models - e.g., the multi-year forecast of the shoreline configuration following a beach replenishment project - exceed the capabilities of even the most sophisticated algorithms. Indeed, even those models that can provide accurate representation of complex wave and current flow fields and the associated sediment transport rates, must employ wave forcing information that is (when available) only provided as averaged quantities or spectra representing the characteristics of individual wave realizations spanning time periods of several minutes to several hours. As a result, the majority of long-term shoreline evolution models currently in use treat the problem from the perspective of large spatial (order of several wavelengths) and temporal (order of hour) scales. These models are then employed in the simulation of shoreline behavior over length scales of tens of kilometers and time periods of several years. In these applications, the sediment transport problem is often separated into two components - the cross-shore transport which is assumed to dominate during severe storm (erosion) events and the alongshore transport which is assumed to drive the long-term evolution of the shoreline position and its response to coastal structures. This approach suffers from many weaknesses, particularly the absence of "communication" between the cross-shore and alongshore transport modes. However, it does provide a useful tool in the comparative evaluation of beach restoration projects and in the assessment of shoreline response to natural (e.g., storm) and human (e.g., coastal structures) influences.

The continued refinement of shoreline evolution models will require the conduct of high-resolution, long-term shoreline surveys coupled with continuous monitoring of oceanographic and meteorological conditions. In fact, such monitoring studies can themselves provide crucial information by identifying patterns of erosion and/or accretion in response to specific wave events. Such cause-and-effect information can be an important component of the data needed for effective coastal management and hazard mitigation planning. The following

describes the application of a multi-year monitoring study to the assessment of erosion potential along the developed shoreline of Manasquan, New Jersey.

II. Site description

Manasquan, New Jersey is located on the northern, headland portion of the Atlantic Ocean shoreline of the state, approximately 8 miles south of Asbury Park. The town is bounded on the south by Manasquan Inlet, as shown in Fig 1. Although the dominant deepwater wave direction in the region is from the north-of-east quadrant, the project area is influenced by the shadowing effect of Long Island to the northeast so that the long-term net alongshore sediment transport is directed toward the north. A sieve analysis of sand samples obtained in the intertidal zone along the Manasquan shoreline in May, 1997 indicated that the median grain size ranges from 0.45 mm to 0.52 mm. Manasquan Inlet was stabilized with the construction of parallel stone jetties in 1931-1933. The jetties were rehabilitated in 1979-1982 and have since functioned as an effective barrier to the net northerly alongshore sediment transport. In addition to the north inlet jetty, the Manasquan shoreline has several timber groins, constructed in 1939-1941 and stone groins, constructed at various times between 1931 and 1967. Recent accelerated erosion of a nourished beach along the southern portion of the shorefront prompted the following analysis.

III. Field Measurement Program

High-resolution beach profile surveys were obtained in the area at quarterly intervals beginning June, 1994 and ending September, 1996 at the profile lines indicated in Fig 2. Wave measurements were obtained from a U.S. Army Corps of Engineers nearshore wave gauge, located in 10 meter water depth at latitude 40.4^0 N, longitude 73.97^0 W, or just north of the study area. The gauge was installed in 1992 and continues to provide significant wave height, peak spectral period and direction at intervals ranging from 1 to 4 hours. Table 1 lists the measured beach width at each profile line for six survey periods, with the value indicating the width at the end of each period. These time periods were selected based on the availability of concurrent nearshore wave measurements. "ND" indicates no survey data. Fig 3 illustrates the profile change at line D - historically a highly erosional area - over the course of the study. Note the dramatic sand loss between the September 1995 profile and the February 1996 profile, and the large amount of accretion between the April 1996 and September 1996 surveys.

Time Period	Beach Width (meters)							# Hrs Erosion
	A	B	C	D	E	F	G	
6/94-9/94	58.5	52.1	51.8	44.2	74.7	58.8	63.4	4
9/94-11/94	58.2	57.9	44.2	42.7	67.1	ND	ND	52
6/95-9/95	57.9	58.5	53.3	57.0	77.4	58.2	ND	20
9/95-2/96	ND	47.2	36.6	33.5	65.2	54.9	ND	124
2/96-4/96	59.4	54.9	53.0	46.3	67.1	53.3	47.2	28
4/96-9/96	58.5	65.8	61.6	57.0	80.2	56.4	50.3	24

Table 1: Beach Width and Number of Hours of Strong Erosion

III. Analysis and Discussion

Our primary goal in the data analysis was the identification of a causal relationship between specific wave characteristics - e.g., height, steepness, direction - and shoreline response. This information could then be used in the assessment of proposed erosion mitigation strategies, using long-term wave observations to infer future conditions. With this in mind, our analysis of the Manasquan shoreline began with an attempt to develop a simple methodology to predict the profile response to known incident wave characteristics. We first examined the wave record with the aim of identifying the most effective erosion/accretion indicator. Initial attempts based on the total energy contained in the wave field during each monitoring period were unsuccessful. For example, as shown in Fig 4, the accretionary period from April 15 to September 15, 1996 was among the most energetic of all, even in comparison to the erosive period, September 1 to November 22, 1994. This result was in fact consistent with our expectation - based on our monitoring experience - that the shoreline behavior is controlled primarily by relatively short-lived extreme storm events rather than the total integrated wave energy over a given time period. In order to further explore this possibility, we defined an event-based erosion indicator based on the Profile Parameter, P, introduced by Dalrymple (1992):

$$P = \frac{gH^2}{w^3 T} \qquad\qquad (1)$$

where H is the wave height, here adopted as the significant wave height, w is the fall velocity of the bottom sediment, T is the peak spectral wave period, and g is the acceleration due to gravity. Dalrymple employed full-scale wave and beach profile measurements to find that a value of P greater than 9,000 indicates erosive conditions. Employing the methodology of Dietrich (1982), we determined a value of $w = 5.8$ cm/s for the average median grain size (0.47 mm) found along the Manasquan shoreline. Equation (1) was then employed to identify the time periods during each monitoring interval which would be expected to produce erosion. Table 1 lists the number of hours during each monitoring interval during which strongly erosive conditions occurred. These conditions correspond to periods when P = 23,000. The fact that this criterion differs from Dalrymple's value of 9,000 is the result of our use of significant wave height, H_s in (1) rather than the rms mean wave height($\cong 0.626$ H_s) used by Dalrymple.
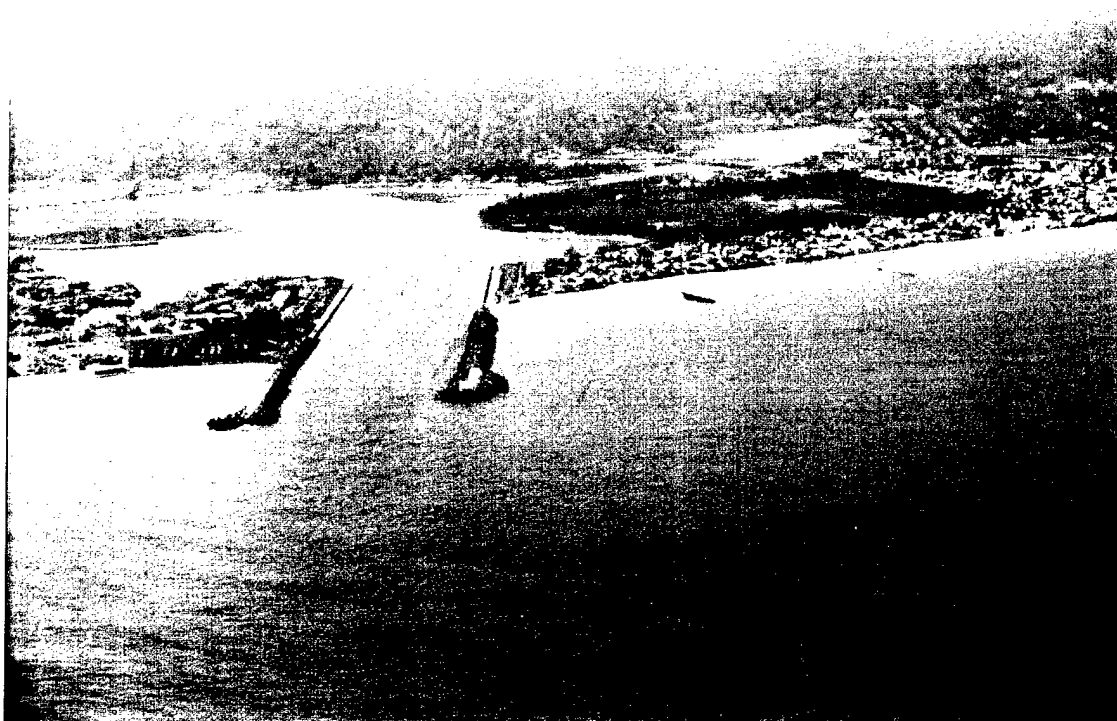
Figures 5 and 6 illustrate P as a function of wave direction for the (erosive) September 1995 - February 1996 period and the (accretionary) April - September 1996 period, respectively. Each data point represents a 4-hour wave observation. Note that as expected, the erosive period is characterized by significantly more occurrences of the Profile Parameter exceeding the erosion criterion. Interestingly, nearly all of the erosive wave "events" approach from the south-of-east quadrant (90 to 180 degrees). Should continued monitoring confirm this finding, future modifications to the Manasquan shorefront and structures should anticipate the potential for discontinuous erosion adjacent to shore-perpendicular structures, and (perhaps) a strong bias toward a northerly longshore sediment transport.

The use of the Profile Parameter in identifying periods of shoreline accretion is more problematic. Clearly, those time periods during which the parameter does not exceed the erosion criterion do not necessarily correspond to periods of accretion. We expect that a minimal

amount of wave energy is necessary to initiate and sustain onshore sediment transport. A dependence on wave steepness and sediment fall velocity, such as is contained in the Profile Parameter, is also expected. We are continuing to examine these and other possible contributing factors, such as the slope of the foreshore, in order to identify an appropriate parameter for shoreline accretion.

References

1. Dalrymple, R.A. 1992. Prediction of Storm/Normal Beach Profiles. J. Waterway, Port, Coastal, and Ocean Engrg. ASCE 118, No. 2, 193-20.
2. Dietrich, W.E. 1982. Settling Velocity of Natural Particles, Water Resources Res. `18, 1615-1626.
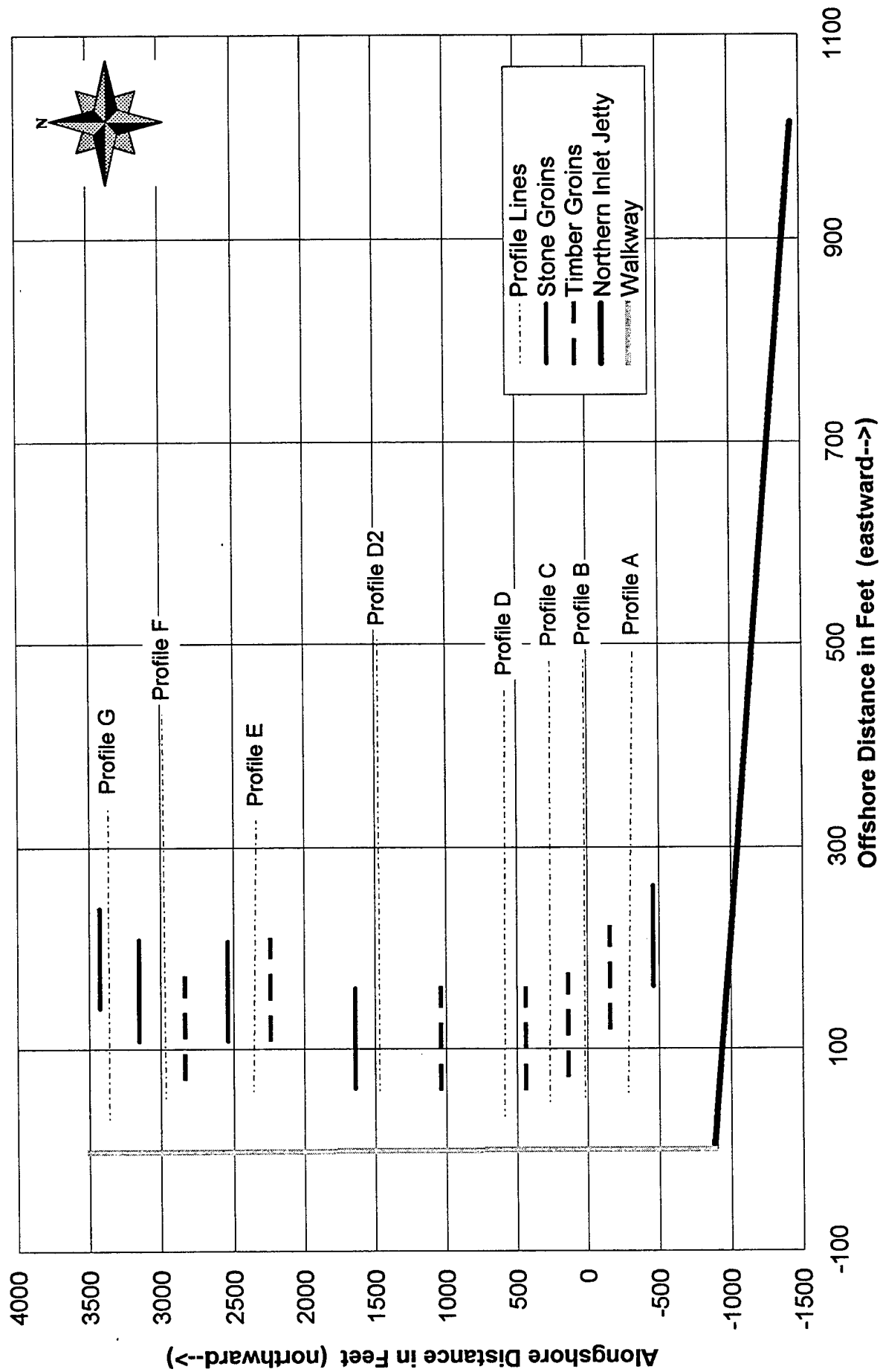
Manasquan, NJ - Plan View
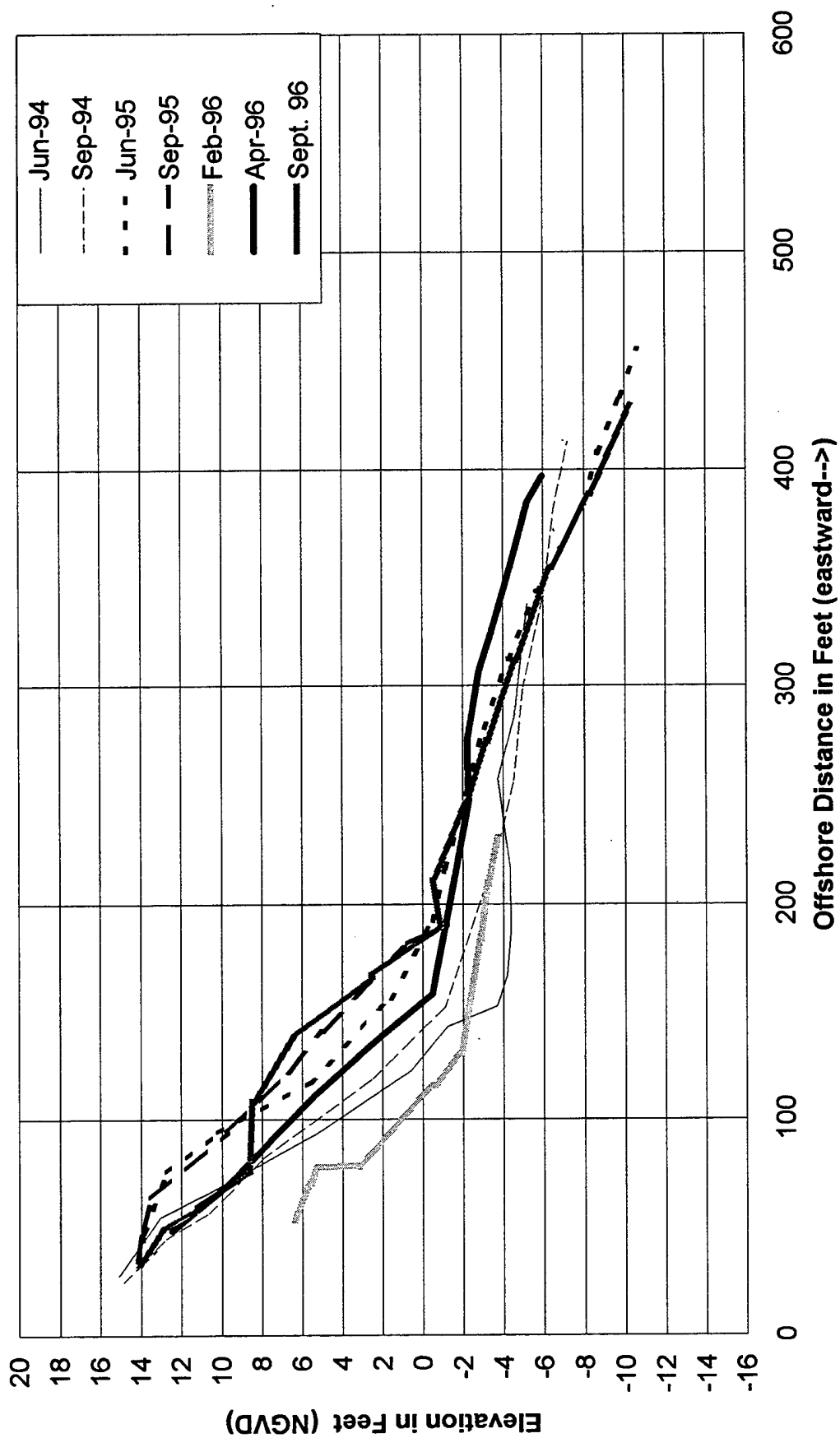

Figure 2

Manasquan, NJ - Profile D

Figure 3

Long Branch, New Jersey
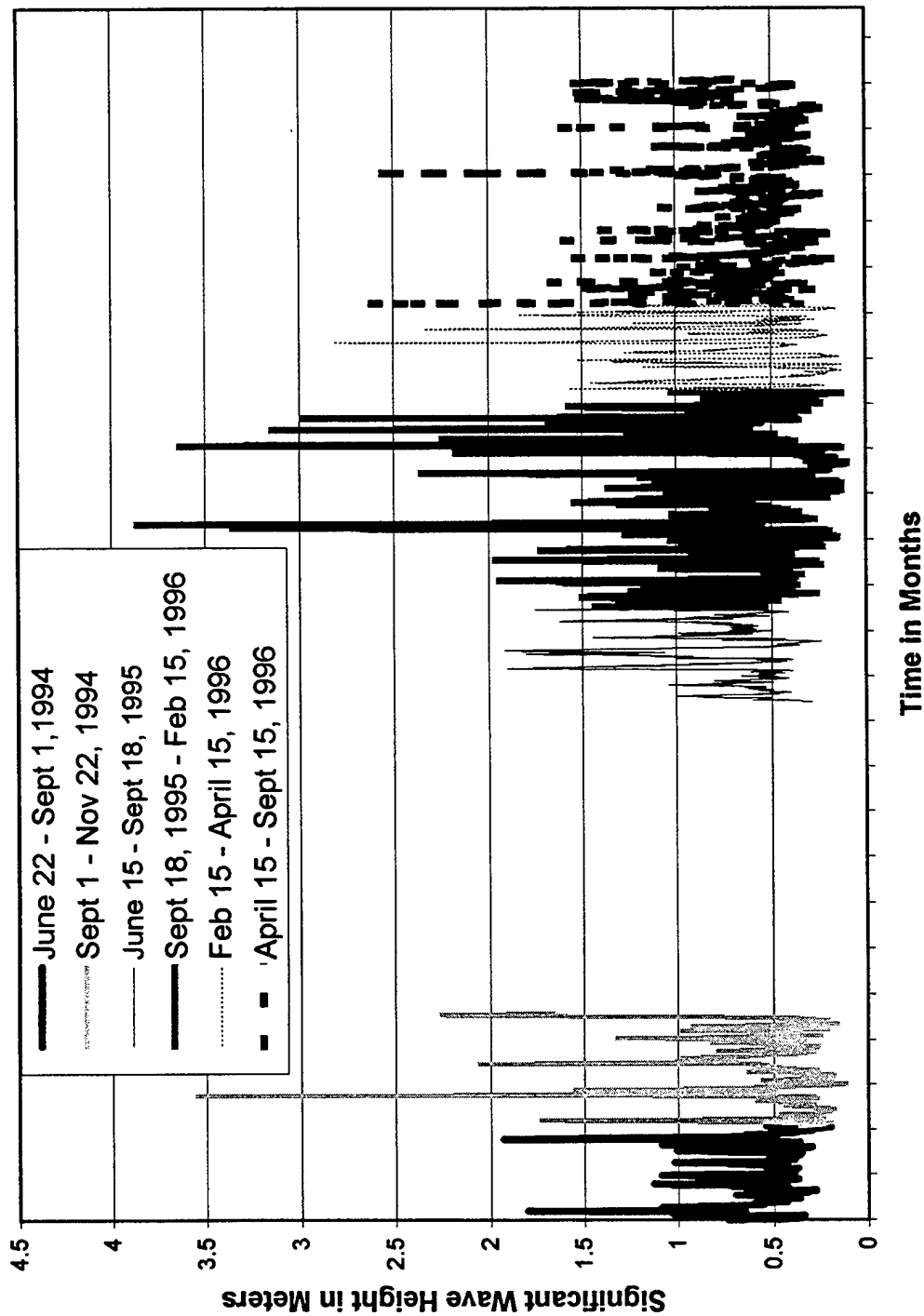

Significant Wave Height in Meters

Legend:
- June 22 - Sept 1, 1994
- Sept 1 - Nov 22, 1994
- June 15 - Sept 18, 1995
- Sept 18, 1995 - Feb 15, 1996
- Feb 15 - April 15, 1996
- April 15 - Sept 15, 1996

Time in Months

Figure 4

35

Long Branch, New Jersey
September 18, 1995 - February 15, 1996

Figure 5

Peak Spectral Direction in Degrees from North

Profile Parameter

36
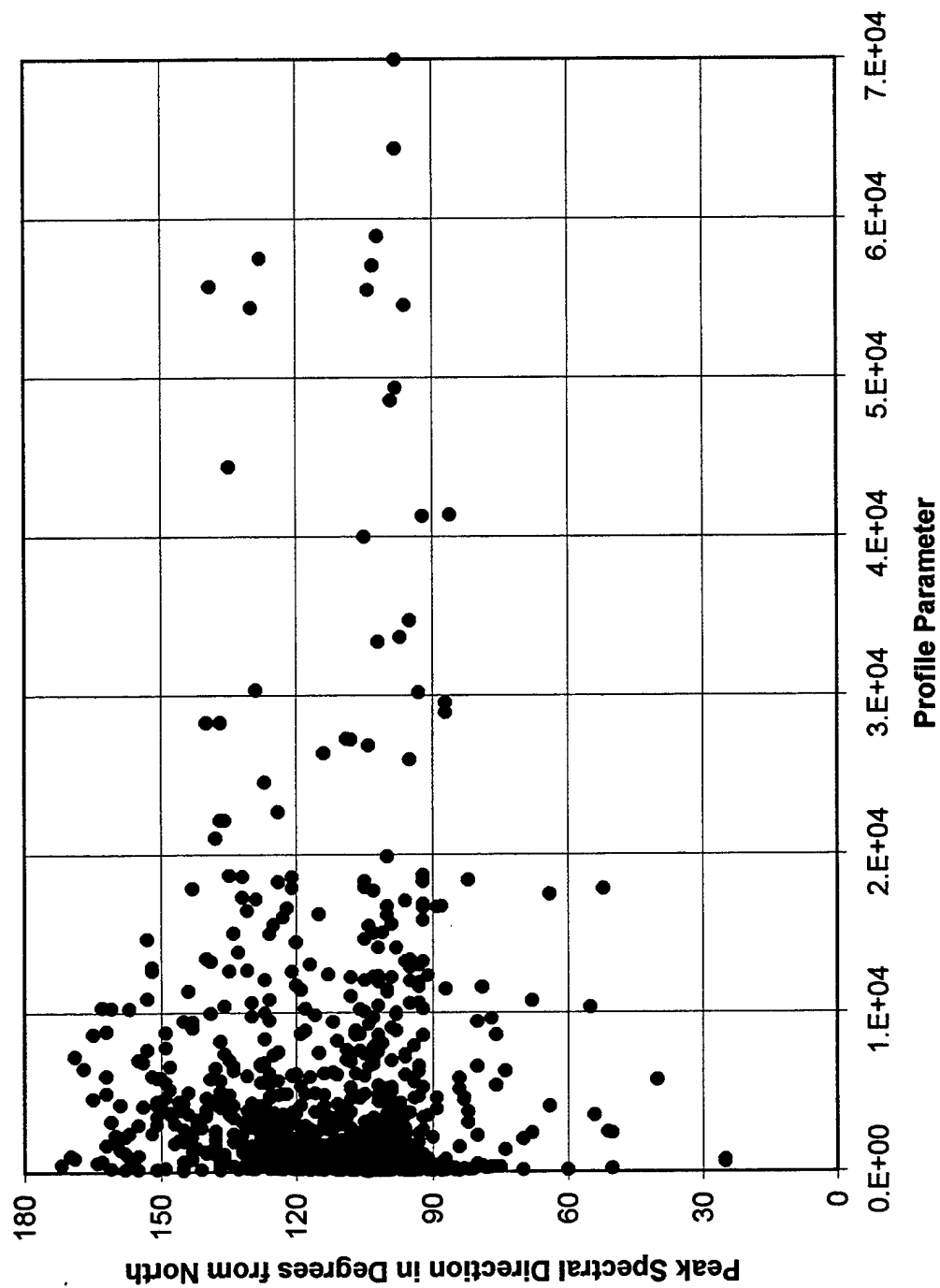
Long Branch, New Jersey
April 15 - September 15, 1996

Peak Spectral Direction in Degrees from North
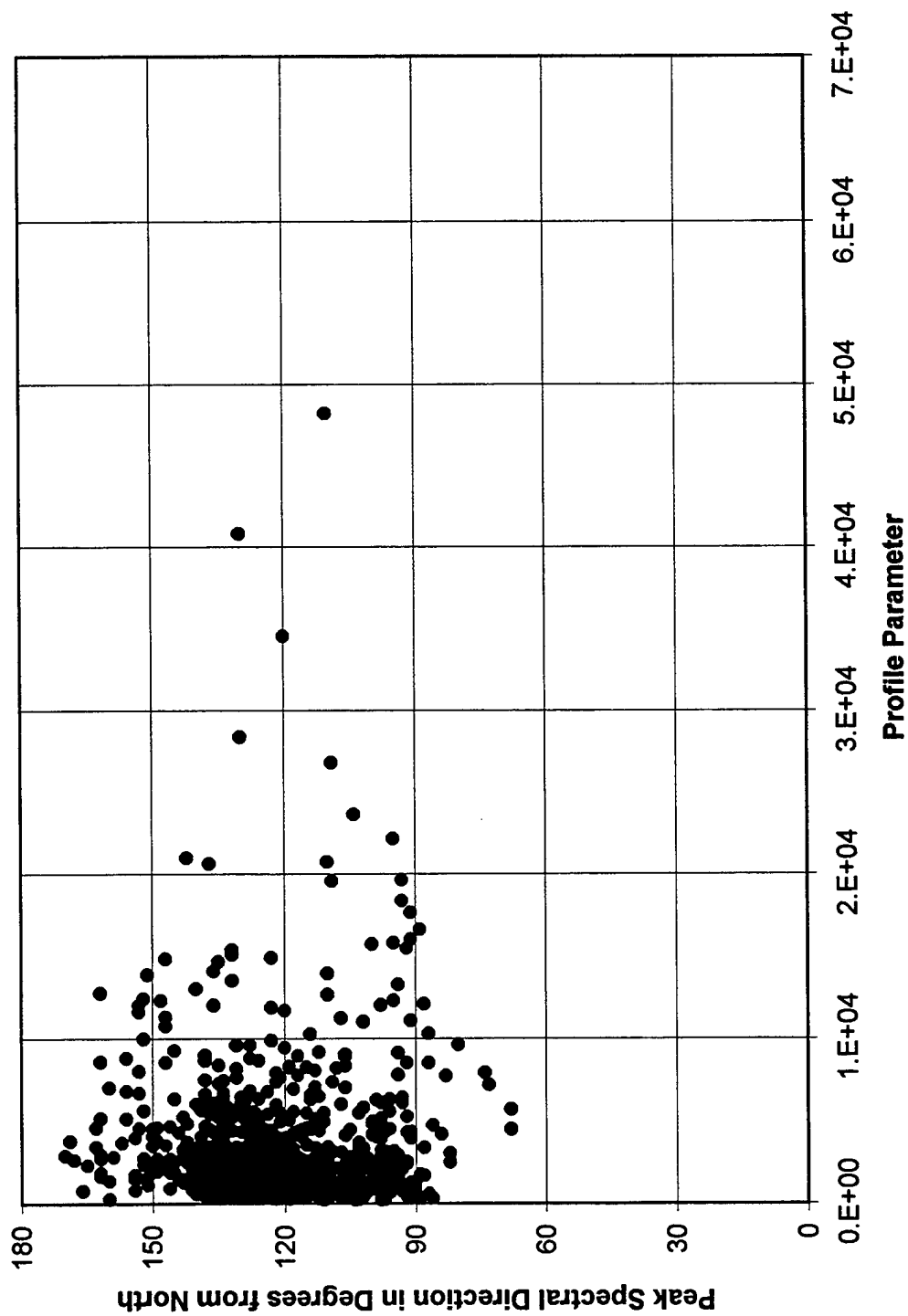
Profile Parameter

Figure 6

37

NEW PERSPECTIVES OF THE SEA FLOOR

Bradford Butman and Richard P. Signell

U.S. Geological Survey
Woods Hole, Massachusetts

Introduction

Sediment and sea floor characteristics have traditionally been determined by measurements made at fixed points or over scales of several meters. The separation between these measurements is typically several kilometers or more, leaving a large gap in our understanding of spatial variability in sediment transport processes. Multibeam echosounders and sidescan sonar are now being used to fill this gap, however, mapping bathymetry and sediment characteristics with 100% coverage over large areas of the coastal ocean (Gardner et al., 1998, Schwab et al., 1997; Goff et al., 1999). These maps are similar in detail to an aerial photograph, and show variability of seabed features over a wide range of spatial scales, from 10's of kilometers to several meters. These highly detailed views of the sea floor are providing a new framework for sediment transport studies in the coastal ocean.
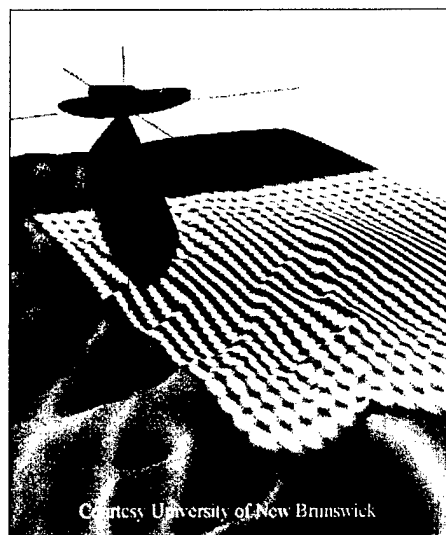

Figure 1: High-resolution multibeam echo sounders use sound from an array of 60-120 electronically separated transducers to measure water depth as well as sediment characteristics of the sea floor. Data is collected over swaths approximately 5 times the water depth in width. The beam footprint on the seafloor - the area over witch the backscatter is measured - varies with beam projection angle and water depth. In 50 m of water, a 2^0 beam produces a footprint on the seafloor of a few meters in water depths of 50 m.

New Images

Recent surveys of Massachusetts Bay (Valentine and Butman, 1998) and the New York Bight (Butman et al., 1998; Schwab et al., 1997) illustrate the rich information these techniques provide on morphology and texture of the ocean bottom. The Massachusetts Bay survey (Figure 2) includes the Stellwagen Bank National Marine Sanctuary, which supports large commercial and recreational fisheries and is essential habitat for marine mammals, including endangered species of whales. The region also
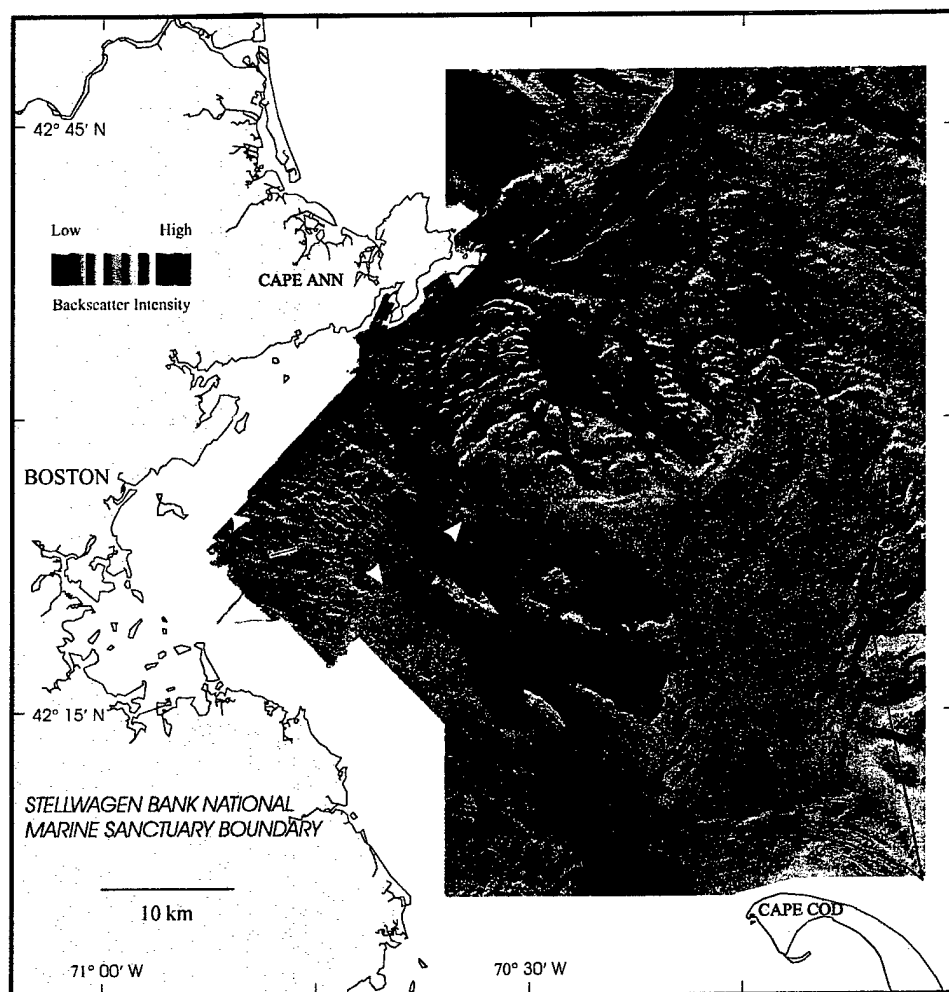
Figure 2. Sun-illuminated map of the region to the east of Boston Massachusetts. The backscatter intensity is draped over the topography. Red indicates high backscatter material (sand, gravel and rock); blue indicates low backscatter material (mud). Within each backscatter color, the intensity varies from dark to light depending on the sun illumination. The image illustrates shows a complex and wide variety of sedimentary environments and transitions between sediment types is often very sharp. Topographic features observed here were formed for the most part by glacial processes. Ice containing rock debris moved across the region, sculpting its surface and depositing sediment to form basins, knoll, banks and other features. Today, the sea floor is mainly modified by storm currents and waves from the northeast. These currents erode sand and mud from the shallow banks and transport them into the basins. Stellwagen Bank and Jefferys Ledge are shallow banks (20-40 m water depth) covered with sand and gravel. Stellwagen Basin (80-100 m) is floored with mud. In deeper water in the northeastern part of the image (85-140 m), a fine hummocky pattern was created by gouges (5-10 m deep and up to 120 m wide) caused by icebergs that grounded here. Present and past disposal sites (white arrows) are characterized by high backscatter material and are especially distinct when the background material is fine grained, such as in Stellwagen Basin. The easternmost arrow points to the presently active Masssachusetts Bay Disposal Site. The yellow rectangle in the western part of the map is the location of the new ocean outfall that will discharge treated sewage effluent from the Boston metropolitan area into Massachusetts Bay.
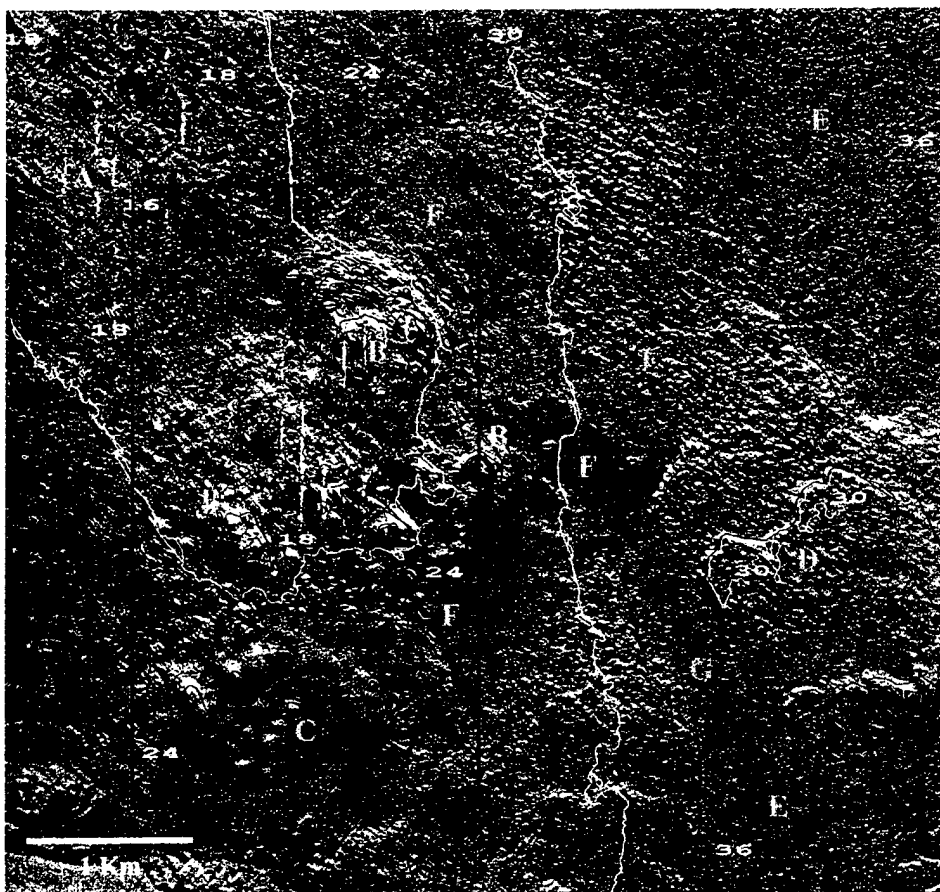
40

Figure 3: Sun illuminated bathymetry (with 2 m contours superimposed) for the region surrounding the Mud Dump Site (blue box) offshore of New York. The map shows the sea floor impacted by extensive disposal of dredged material, modern processes, and the underlying geologic framework. To create the image, the bathymetry was exaggerated 5 times and illuminated from an azimuth of $350°$ at an angle of $45°$. The shadows in the image accentuate the small scale variability of the bathymetry (relief of a few meters) that would be difficult to show in a traditional contour map. The white areas between swaths (that appear as 'tears' in the image) are data gaps where the swath width of the multibeam system narrowed over the shallow topography.

The most striking feature of the sea floor shown by this image is the variability in bottom morphology (and sediment texture) over scales of a kilometer or less, and the extensive features associated with disposal of dredged material on the sea floor. Features include: (A) a relatively smooth mound composed of material dumped since the 1800's and reworked into linear bed forms; (B) several mounds (as high as 10 m) of dredged material from more recent disposal; (C) a smooth, roughly circular region resulting from disposal of contaminated sediments and capping with sand; (D) outcrops of southeastward-dipping cretaceous-age coastal plain strata; (E) ubiquitous individual dumps of material, some apparently sitting atop the hard outcropping strata, some appearing as craters of order 50 m in diameter in the softer sediments; (F) an area of uniformly smooth topography to the northeast, east, and southeast of the Mud Dump Site composed of fine material, possibly winnowed from the disposed dredged material and transported downslope; (G) a channel, about 400 m wide and 4 m deep to the west of the outcropping cretaceous strata.

41

includes the site for the new ocean outfall that will begin discharging treated effluent from the Boston metropolitan region, beginning in 1999. The mapping was carried out to produce a series of maps that depict topography, backscatter, and the distribution of sedimentary environments and biological habitats (for example, Valentine et al., 1997, Valentine et al., in press). The New York Bight is offshore of the New York-New Jersey metropolitan region, one of the most populated coastal areas in the United States. The harbor estuary and offshore area are used for waste disposal, transportation, recreation, and commercial and recreational fishing. The Hudson Shelf Valley, the principal bathymetric feature of this region, is a potential sink for sediments and contaminants and/or a conduit for cross-shelf transport. The region has been used for disposal of sewage sludge as well as dredged and other material since the 1800's. The apex of the New York Bight was mapped as part of a USGS program to survey areas offshore of major metropolitan centers, and to provide a regional framework for studies of the transport and long-term fate of sediments and associated contaminants (Figure 3).

Implications for understanding sediment transport

These images of the sea floor provide a new perspective and framework for sediment transport studies in the coastal ocean. Benefits of these new surveys include:

New perspectives on processes: One of the most striking characteristics of the sedimentary environments shown in these new maps are the sharp boundaries between bottom characteristics, both in backscatter intensity and bathymetry. These suggest that sediment transport processes form and maintain sharp convergences and divergences of particle transport.

Regional perspective: The detailed mapping of large areas provides a regional perspective of the modern natural and anthropogenic processes causing transport and their effects on the sea floor. They provide information on the underlying geologic structures and the geologic history in controlling the present distribution of sediments. They also allow generalization of point measurements to larger areas of similar characteristics, for example in calculating sediment inventories, or determining sea floor roughness.

Design of field experiments: They allow instruments to be carefully placed and cores obtained in areas of interest, for example, either large areas representative of a larger region, or key locations where specific processes or events may occur.

New research directions: The spatial coverage and resolution of the new geologic maps allows investigation of benthic habitats on biologically relevant spatial scales of order 0.1 to 10 km that could not be resolved by previous studies. Understanding the role of sea floor geology and benthic processes in the life history and productivity of benthic populations is essential to develop and implement management strategies that will preserve biodiversity and promote a sustainable fishery.

Data interpretation: Interpretation of near bottom observations of sediment stress and concentration is simplest if the seafloor is spatially homogeneous over the advection length scale for a particular event. (h/u_{star}) x (advection velocity), where H is boundary

layer height and u_{star} is bottom stress. The rapid changes between sedimentary environments suggest that advection will often influence the suspended sediment concentration and transport observed at a single location.

Tests of sediment transport models: The bathymetric observations are of sufficient accuracy that repeated surveys may begin to provide an integrated test of sediment transport models.

Conclusion

Just as the wave-current interaction models of Grant and Madsen (1979) and Smith (1977) changed the way we think about sediment transport processes in the coastal ocean, high-resolution maps are changing the way we think of the effect of these processes on the sea floor. They will help bridge the gap between measurements made at scales of several meters and traditional point sampling measurements made at scales of kilometers. They will influence and guide sediment transport studies in the years to come. Bill Grant would have been excited by these new perspectives.

REFERENCES CITED

Butman, B., Danforth, W.W., Schwab, W.C., and ten Brink, M., Multibeam echosounder and backscatter maps of the upper Hudson Shelf Valley and adjacent shelf offshore of New York. U.S. Geological Survey Open File Report, in review.

Gardner, J.V., Butman, B., Mayer, L.A, Clarke, J.H., 1998, Mapping U.S. continental Shelves: Sea Technology, 39(6), p. 10-16.

Grant, W.D., and Madsen, O.S., 1979, Combined wave and current interaction with a rough bottom: J. Geophysical Res., 84, p. 1797-1808.

Goff, J.A, Swift, D.J.P., Schuur, C.L., Mayer, L.A. and Hughes-Clark, J.E., 1999, High-resolution swath sonar investigation of sand ridge and sand ribbon morphology in the offshore environment of the New Jersey margin, Marine Geology, accepted.

Schwab, W.C., Allison, M.A., Corso, W, Lotto, L.L., Butman, B., Bucholtz ten Brink, M., Denny, J., Danforth, W.W., and Foster, D.S., 1997, Initial results of high-resolution sea-floor mapping offshore of the New York - New Jersey metropolitan area using sidescan sonar: Northeastern Geology and Environmental Sciences, v. 19 (4), p. 243-262.

Smith, J.D., 1977, Modeling of sediment transport on continental shelves, in The Sea, V. 6, E.D. Goldberg, I.N. McCave, J.J. O'Brien and J.H. Steele, (eds.), Wiley Interscience, p.539-577.

Valentine, P.C., Baker, J.L., Unger, T.S., and Roworth, E.T., 1997, Sea floor topography of Quadrangle 1 in the Stellwagen Bank National Marine Sanctuary off Boston, Massachusetts: U.S. Geological Survey Open File Report 97-502, scale 1:25,000, 1 sheet.

Valentine, P.C., Baker, J.L., and Unger, T.S., in press, Sun-illuminated sea floor topography of Quadrangle 1 in the Stellwagen Bank National Marine Sanctuary off Boston, Massachusetts: U.S. Geological Survey Open File Report, scale 1:25,000, 1 sheet.

Valentine, P.C., Baker, J.L., and Unger, T.S., in press, Sea floor topography topography of the Stellwagen Bank National Marine Sanctuary off Boston, Massachusetts: U.S. Geological Survey Miscellaneous Investigations Series Map, scale 1:60,000, 1 sheet.

Valentine, P.C. and Butman, B., 1998, Mapping the Sea Floor and Biological Habitat of the Stellwagen Bank National Marine Sanctuary. USGS Fact sheet 078-98.

Organism-Flow-Sediment Interactions: An Eclectic Overview

Cheryl Ann Butman
Applied Ocean Physics and Engineering Department
Woods Hole Oceanographic Institution
Woods Hole, MA 02543

Introduction

Systematic, experimental studies of organism-flow-sediment interactions began in the early 1970's, but it took 15 years or more for this field to obtain broad-scale recognition. Now, biological oceanographers routinely measure flow and sediment parameters within the context of a wide range of benthic ecological studies, acknowledging that the hydrodynamic environment is one of the critical factors shaping organism distributions. There have been far fewer studies of organism effects on nearbed flows and sediment transport. Research in this area has a more checkered history. In fact, despite numerous demonstrations of significant effects of organisms on sediment transport, most sediment-transport models are still entirely abiotic.

This talk provides an eclectic overview of progress in the field of organism-flow-sediment interactions by providing two examples, one where advancements have been particularly encouraging, and one where progress has been somewhat discouraging. In addition, I briefly discuss some factors responsible for the magnitude of success. Examples discussed are those that sparked a passion in Bill Grant and in which he participated directly. I conclude with some research challenges for the future.

Effects of flows and sediment transport on organisms

The nearbed-flow and sediment-transport regime has been shown to affect virtually every major stage in the life history of benthic organisms. One important research tool has been the development of physical null models to test the importance of biology relative to the physics. This technique has been particularly fruitful in evaluating the role of physical versus biological processes in determining larval settlement and recruitment of benthic invertebrates.

Field and laboratory flume experiments have revealed that larvae initially reach the seafloor like passive particles, but for some species, whether the larvae stay or leave the depositional site depends on behavioral responses of the animals to aspects of the sediments or sedimentary environment. Recent work has also shown that, in the water column, larval behavior can be modified in response to a dissolved chemical cue. The cue presumably indicates a general region of acceptable adult habitat, and in response to the cue larvae cease swimming and sink. But, again, it is the nearbed flow regime that determines patterns of initial larval deposition on the bed. Because it is now known which stages of the larval-settlement process are biologically versus physically controlled, at least for some species, settlement can be predicted using a sediment-transport model. Such modelling assumes that larvae are transported passively toward the bed as particles with a specified gravitational sinking rate, but the model can also accomodate larval behaviors

in response to physical and chemical cues in the water column. Larval response to bed characteristics is embodied in a selectivity probability -- the probability of staying on the seafloor once deposited.

The broadest brush paints this field of research in highly successful hues. And, to first order, the use of physical null models has provided an experimental research framework that has yielded meaningful results. This success derives, at least in part, from using an appropriate physical model -- sediment particles to mimic settling larvae. However, larval behaviors, both in the water column and on the seafloor, can be highly species-specific. In fact, perhaps the greatest limitation to this research is that little more than a handful of species have been used in the larval-settlement experiments conducted in the lab. Of necessity, most species used in laboratory experiments are marine "lab rats" in that they were chosen largely because they do well under laboratory conditions. In the field, experiments are subject to the vagaries of larval availability and thus rarely have there been data for the same species under both laboratory and field conditions. In short, generalizations have been derived from highly specific information.

Effects of organisms on flows and sediment transport

Research on effects of organisms on flows and sediment transport has been discouraging in that a single parameter or group of parameters to account for biological effects has failed to emerge. Studies of biological effects on the critical stress to initiate sediment motion, for example, have yielded a wide range of results. Experiments have shown that, relative to the abiotic case, organisms can (1) *increase* the critical stress by binding sediments with mucus and by grading the bed (i.e., subducting fine sediments), and (2) *decrease* the critical stress by enhancing bed roughness and by increasing bed porosity ("loosening" the bed). Moreover, the magnitude of these effects is likely to depend on organism density, food availability and flow regime. Quantitative relationships between, for example, the critical stress and total polysaccharide content of the sediments may apply to some sandy nearshore sediments where bacterial binding predominates, but such relationships lack general predictive value because organism effects on sediment transport involve both secretions within or on the sediment bed, and physical alterations of the sediment surface (i.e., roughness) and bed (i.e., grading).

In analyzing potential factors responsible for the lack of recent progress in this field, it is tempting to point the finger at national funding agencies that have provided only scant support for studies of biological effects on sediment transport, especially relative to support provided for the abiotic case. However, it is unlikely that scads more research effort yeilding yet another and another spurious point on Shields' curve would go far toward elucidating meaningful predictive relationships between the biology and the physics. Rather, it is likely that the nature of biological systems is the culprit. That is, because organisms can affect nearbed flows and sediment transport in such a wide diversity of ways, with multiple effects that are complementary, compensatory or competitive, parameterizing biological effects for inclusion in sediment-transport models is either impossible or meaningless.

Rather than continuing to focus on single-species or chunks-of-community effects on sediment transport, perhaps a more fruitful research direction would be the elucidation of benthic habitats or seasons of the year where/when

biology is expected to have the largest effect. Biological effects in sandy nearshore habitats, for example, have long been considered neglible because of the high sediment-transport and physical-reworking rates in these areas. This presumption may well be valid, but it certainly requires testing.

Some future research challenges

Historically, more progress has been made in understanding flow and sediment-transport effects on ogranisms than the converse. Perhaps this is because the driving physical factors are inherently more predictable than the driving biological factors. Or perhaps this reflects a discipline bias -- there is little doubt that the strong interest of biologists in physical processes is underwhelmed by the relatively weak interest of physical oceangraphers in biological processes. Still, as mentioned above, because single-species or chunks-of-community effects on nearbed flows and sediment transport cannot yet be generalized -- with each case plotting as a unique point on curves like Shields' -- it is difficult to justify intensifying research effort *along the same lines*. The challenge is to develop a research approach that gets at the more general case of when, where and how much biology affects sediment transport. This problem may be best approached in the field utilizing new technology to measure sediment transport remotely.

There is an interesting, technique-driven dichotomy in the scale at which flow effects on biology have been studied. At the individual- to small-groups-of-individuals scale, laboratory flume studies have provided a wealth of information on how flow affects feeding, locomotion, reproduction, etc. of a wide variety of organisms. For larvae, flume studies on settlement have been done in patches of substrate of order centimeters to tens of centimeters in size. All of these laboratory studies are done on a few selected species (i.e., the taxonomic identity is known). At the other extreme, field studies of organism distributions (on the bottom or in the water column) relative to physical and biological factors are done at scales of 100's of meters to 10's of kilometers and greater. Instrumentation to collect organisms and to measure relevant aspects of the flow regime has improved dramatically over the last decade. For larvae, however, morphological identification to species has become a serious limitation to field studies, necessitating the development of molecular probes. A challenge of the next decade (or more) will be to bridge the experimental, sampling and conceptual gap between the large field and small laboratory scales of study. Inference in either direction may be spurious.

47

Internal Tides and Sedimentation on Continental Slopes

David A. Cacchione
Woods Hole Group, 715 Colorado Avenue, Palo Alto, CA 94303

Introduction

Current and temperature measurements obtained on a long-term mooring in 450 m water depth on the upper continental slope off northern California during STRATAFORM in 1997 reveal energetic tidal and higher frequency internal waves whose intensity and structure have considerable temporal variability. We describe these data and discuss implications of internal tidal wave dynamics for continental slope sedimentation and the generation of bottom and intermediate nepheloid layers in this region. A global model for the interaction of internal semi-diurnal tides and sediment deposition on continental slopes is presented in the context of these new results.

Evidence for intensified internal tidal flows over sloping oceanic boundaries has been mounting over the past 30 years. Time-series measurements of currents, temperature and salinity have documented significant energy levels of these flows over sloping topography, and field experiments have shown the intensification of these motions near the seafloor (Ericksen, 1982; Holloway and Barnes, 1998). The amplification of across-slope velocities associated with shoaling internal waves was originally proposed theoretically by Wunsch (1969), and more recently elucidated through numerical models that include non-linear and viscous effects (Slinn and Riley, 1996; Holloway and Barnes, 1998). Early laboratory studies of progressive internal waves over a linear bottom slope showed upslope amplification of the wave forms and near-bottom velocities for cases when the energy rays or characteristics were reflected upslope or were aligned parallel to the bottom slope (Cacchione and Wunsch, 1974). Later laboratory studies confirmed these results, and further elaborated on the nature of the turbulent boundary layer flows produced by the reflecting waves over the slope (Ivey and Nokes, 1989; Taylor, 1993).

Cacchione and Southard (1974) discussed the potential significance of shoaling internal waves for causing sediment movement on continental shelves and slopes. They proposed a simple model that predicted entrainment of natural sediment on shelves and slopes by internal waves. Laboratory experiments confirmed that shoaling interfacial waves could generate ripples and larger bedforms in artificial sediment (Southard and Cacchione, 1972). More recent studies also have found that internal waves of various types are potentially capable of resuspending and transporting sediment (Bogucki, et al., 1998).

Cacchione and Drake (1986) proposed a conceptual model for the generation and maintenance of bottom and intermediate nepheloid layers above continental shelves and slopes by turbulent shear caused by shoaling internal waves. This idea was also suggested

by Dickson and McCave (1986) based on an analysis of transmissometer profiles on the continental margin west of Ireland. The latter study proposed that well-defined intermediate and bottom nepheloid layers which emanated from bottom slopes in 400 to 600 m depths were caused by bottom erosion under internal tides and higher frequency internal waves. They calculated that the bottom gradient was aligned with the slope of the energy ray for the semi-diurnal internal tide, leading to increased velocities and erosion of the bottom sediment. No corroborating data from direct observations or current measurements were available to support this conclusion.

Results

An instrumented mooring was deployed on the upper continental slope in 450 m water depth in the STRATAFORM field area off northern California (Figure 1). Instrument clusters including temperature, salinity, current, and light transmission sensors were located on the mooring at 60, 180 and 435 m water depths. This mooring has been maintained at this site since September 1995. Locally the bottom slope has a gentle gradient of about 0.05 (2.8°), and the bottom is mantled with fine silt. The shelf break in this area is at 150-m depth. Here the analysis uses data collected from January 18 (Day 18) until April 15 (Day 107), 1997.

Internal semi-diurnal currents measured at about 15 m above the seafloor during this period occasionally exceed 35 cm/s; these strong currents are correlated with considerable mixing above the seafloor as indicated by concurrent temperature records. During these periods of enhanced internal tidal flows, downslope-directed currents persist for longer durations than upslope currents, leading to net downslope transport over many tidal cycles. The most striking example of this process occurred during Days 99-102 (Fig. 2). Current (upper) and temperature records for 3-day period when tidal fluctuations were largest over the entire deployment. Upslope flows are peaked and of shorter duration than downslope flows, leading to net downslope motion over this period. Hourly upslope speeds reach 33 cm/s; downslope speed is about 40 cm/s on day 100. Hourly temperature data from the three bottom sensors indicate periods of mixing during days 100.8 – 102 (periods of temperatures coalescing). Times when temperatures are falling are correlated with upslope flows, suggesting movement of deeper cold water associated with internal tidal motion. The general structure of the velocity and temperature records suggests bore-like propagation of the internal tide upslope. Holloway and Barnes (1998) have described these types of internal tidal motions above a sloping bottom recently from numerical simulations and other field data.

Discussion

We propose that the strong internal tidal currents and associated turbulent mixing retard the settling of fine-grained materials onto the seabed, thereby inhibiting deposition along this section of the slope as observed in surficial sediment samples. Net downslope flow

provides a mechanism for transport of suspended materials into deeper water or into intermediate nepheloid layers. It is not known whether the episodic, strong internal tidal currents resuspend the local bottom sediment along this portion of the slope.

Based on CTD profiles taken in this region during the mooring deployments, the slope of the characteristics for the internal M2 tide are approximately critical for bottom slopes at the shelf break and in deeper water (about 500 m). Power spectra of the cross slope component for the middle and lowest current meters indicate that the energy at M2 is largest near the bottom, and that substantially elevated energy levels are found throughout the frequency band from M2 to M4. The latter overtide is approximately critical at the 450 m site, and also is substantially more energetic in the across-slope flows near the bottom.

Conceptual Model

Semi-diurnal internal tidal currents are likely major factors in shaping continental slopes. Continental slopes are generally narrow physiographic seafloor features that mark the transition from shallow continental to deeper oceanic domains. Continental slopes span a depth range of about 2500 m, with the shallow edge averaging about 120-150 m. The regional gradients of continental slopes generally fall in the range of $0.5° - 5°$, but locally these gradients can be much steeper.

As the sediment deposition through time progrades the surface of the continental slope, a gradual reduction in the steepness of the slope surfaces might result. The bottom shear and energy dissipation along the slope associated with the semi-diurnal internal tide will likely increase as the slope surface approaches "critical." The turbulent mixing and shear associated with this process will inhibit deposition of the fine-grained suspended materials, creating intermediate and bottom nepheloid layers, and will cause the regional slope to reach an equilibrium gradient.

References

Bogucki, D., T. Dickey, and , L. Redekopp, 1997. Sediment resuspension and mixing by resonantly generated internal solitary waves, J. Phys. Oceanography, 27, 1181-1196.

Cacchione, D.A. and D.E. Drake, 1986. Nepheloid layers and internal waves over continental shelves and slopes, Geo-Marine Letters, 6, 147-152.

Cacchione D.A. and J.B. Southard, 1974. Incipient sediment movement by shoaling internal gravity waves, J. Geophys. Res., 79, 2237-2242.

Cacchione, D.A. and C.I. Wunsch, 1974. Experimental study of internal waves over a slope, J. Fluid Mechanics, 66, 223-239.

Dickson, R.R. and I.N. McCave, 1986. Nepheloid layers on the continental slope west of Porcupine Bank, Deep-Sea Res., 33, 791-818.

Eriksen, C.C., 1982. Observations of internal wave reflection off sloping bottoms, J. Geophys. Res., 87, 525-538.

Holloway, P.E. and B. Barnes, 1998. A numerical investigation into the bottom boundary layer flow and vertical structure on internal waves on a continental slope, Cont. Shelf Res., 18, 31-66.

Ivey, G.N. and R.I. Nokes, 1989, Vertical mixing due to the breaking of critical internal waves on sloping boundaries, J. Fluid Mechanics, 204, 479-500.

Southard, J.B. and D.A. Cacchione, 1972. Experiments on bottom sediment movement by breaking internal waves, in Shelf Sediment Transport, Process and Pattern, ed. by Swift, D.J.P., Duane, D.B. and Pilkey, O.H., Dowden, Hutchinson and Ross, Stroudsburg, PA, 83-98.

Taylor, J.R., 1993, Turbulence and mixing in the boundary layer generated by shoaling internal waves, Dynamics of Atmospheres and Oceans, 19, 233-258

Slinn, D.N. and J.J. Riley, 1996. Turbulent mixing in the oceanic boundary layer caused by internal wave reflection from sloping terrain, Dynamics of Atmospheres and Oceans, 51-62.

Wunsch, C.I., 1969. Progressive internal waves on slopes, J. Fluid Mechanics, 35, 131-144.
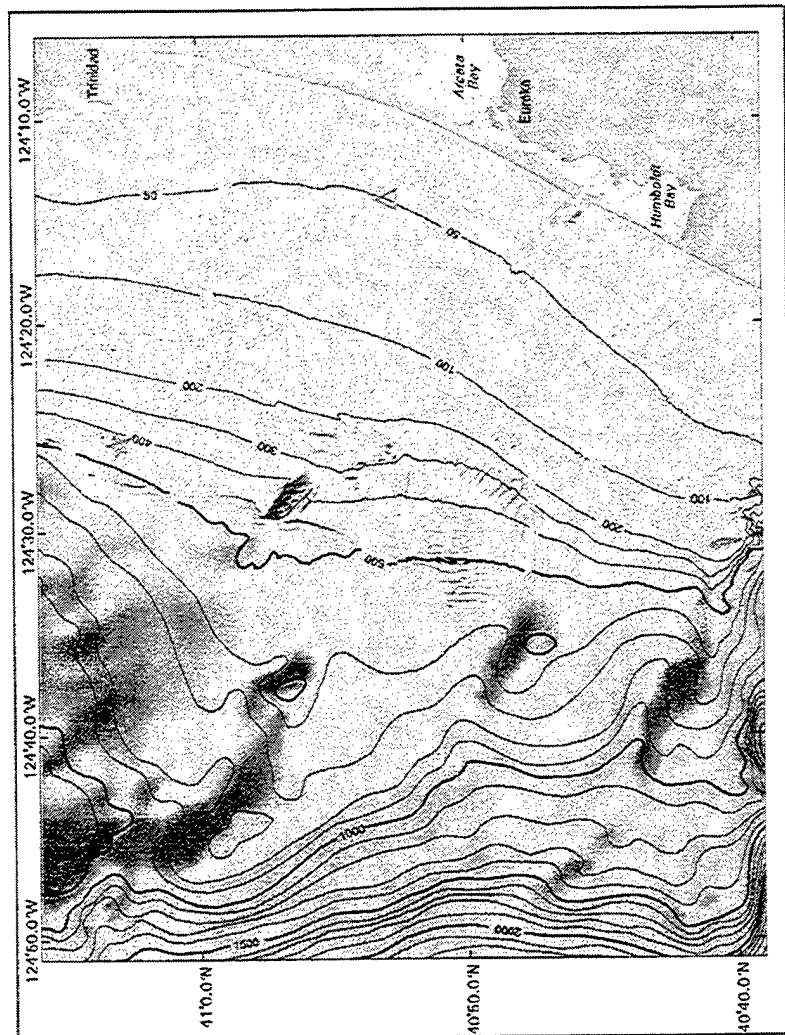
Figure 1. Color-shaded bathymetry and relief of the northern California continental shelf and slope. Generalized bathymetry obtained from the USGS digital bathymetric data base. Detailed multi-beam bathymetric data in the STRATAFORM study area (outlined in white) provided by L. Mayer (personal communication). A 60-m horizontal grid spacing is used for all data. The long-term mooring site is marked by a star; the inner shelf instrumented GEOPROBE tripod is shown as a triangle. The shelf break shoreward of the mooring site is at about 160 m depth.
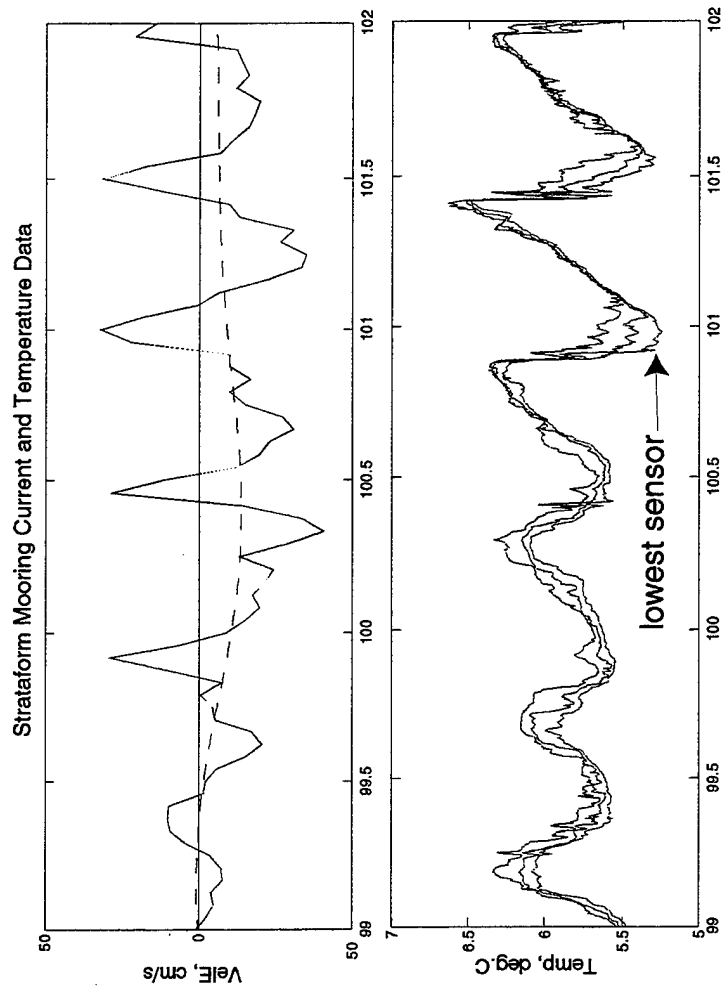
Figure 2. Current (upper) and temperature records for 3-day period when tidal fluctuations were largest over the entire deployment. Solid blue line in upper panel is hourly current averages of across slope flow (+ upslope); dashed line is low pass filtered current. Note that the upslope flows are peaked and of shorter duration than downslope flows, leading to net downslope motion over this period. Hourly upslope speeds reach 33 cm/s; downslope speed is about 40 cm/s on day 100. Hourly temperature data from the three bottom sensors (lowest is at 435 m; middle at 400 m; and upper at 360 m). Note the periods of mixing during days 100.8 - 102 indicated by the temperatures coalescing. Times when temperatures are falling are correlated with upslope flows, suggesting movement of deeper cold water associated with internal tidal motion. The general structure of the velocity and temperature records suggests bore-like propagation of the internal tide upslope.

Ocean Currents Near the Congo River Outfall

Cortis Cooper
Senior Research Associate
Chevron Petroleum Technology *Company*
San Ramon, CA ckco@chevron.com

With an average discharge of 40 k m3/s the Congo River is second only to the Amazon. Several features make the mouth of the Congo River unique. Unlike most rivers, the Congo has no major delta; instead it ends in a long deep trench (Figure 1). What processes maintain the trench? This remains a mystery though one obvious suspect is strong, sediment-scouring currents.

Published oceanographic work on the seaward side of the mouth have been limited to four studies Berrit (1966), Meulenbergh (1974), Wauthy (1977), and Eisma and Van Bennekom (1978). These studies have involved synoptic CTD sections and some limited synoptic current profiles within a few km of the mouth. No current measurements longer then a few days have apparently been published.

Since 1990, Chevron has collected substantial current data around the mouth of the river. While these measurements have not been comprehensive, they are starting to shed some further light on the oceanography in this region. The primary focus of the measurements has been to identify extreme currents that might pose a hazard to offshore construction and operations. Figure 1 shows the sites of data collection while Table 1 provides a timeline and details of the measurements. Substantial new measurements will be made in the coming year from 40 near-surface drifting buoys, a platform-based station with meteorology, a deepwater current mooring (Sites A and B in Figure 1), and further ADCP measurements from a mobile drilling rig.

A complete analysis of the data is planned at the end of next year when most of the collection will be complete. Our interim analysis shows the following

1. Astronomical barotropic tides in the region are small. Mean range is about 1.1 m and observed currents are less then 5 cm/s.

2. Winds are dominated by the SE trades. The mean wind speed is 3.5 m/s directed from the south.

3. Near-surface currents away from the river mouth seem to be dominated by the Trade winds. Currents are persistently directed to the west-northwest and average roughly 0.4 m/s.

4. The river plume reaches speeds of at least 1.5 m/s, with the river currents clearly evident up to 100 km from the mouth of the river. The plume does not seem to exceed 4 m in depth.

5. Episodic barotropic current events lasting several days and recurring every 7-10 days are evident on the outer shelf. Their origin has not yet been determined though it is known that the events are not generated by local wind events.

6. Bursts of currents have been observed near the Canyon. These bursts occupy the water column from the bottom up to 100 m. They last only a few hours and their origins are yet to be determined.

Table 1:   Time line of measurements taken offshore Angola in recent years.

			90			91	95			96	97				8				99		
Region	No.	Depth (m)	Q2	Q3	Q4	Q1	Q2	Q3	Q4	Q1	Q1	Q2	Q3	Q4	Q1	Q2	Q3	Q4	Q1	Q2	Q3
[1]Area C	3	85	—	—	—	—															
[2]Kuito	1	350											—	—	—	—	—					
[2]Nym	1	250								—												
[2]Nkassa1	1	125											—									
[2]129	1	65													—							
[1]Exx1	5	1000					—	—	—	—												
[1]Exx2		280						—	—													
[3]WADS 1	8	NA														—	—	—				
[3]WADS 2	40	NA														—	—	—				
[4]Sanha	3	125														—	—	—	—	—		
[1]A	5	1500												—	—							
[1]B	5	1000																			—	—

[1]Mooring of conventional "point" current meters - Aandera RMC4's or equivalent.
[2]150 kHz ADCP deployed from a drilling vessel 10-20 m below the surface looking down.
[3]Satellite-tracked drifting buoys, roughly 70% drogued at 0.5 m; the rest from 2-4 m.
[4]Platform based system with wind, tide, wave, & "point" current meters (3 levels).
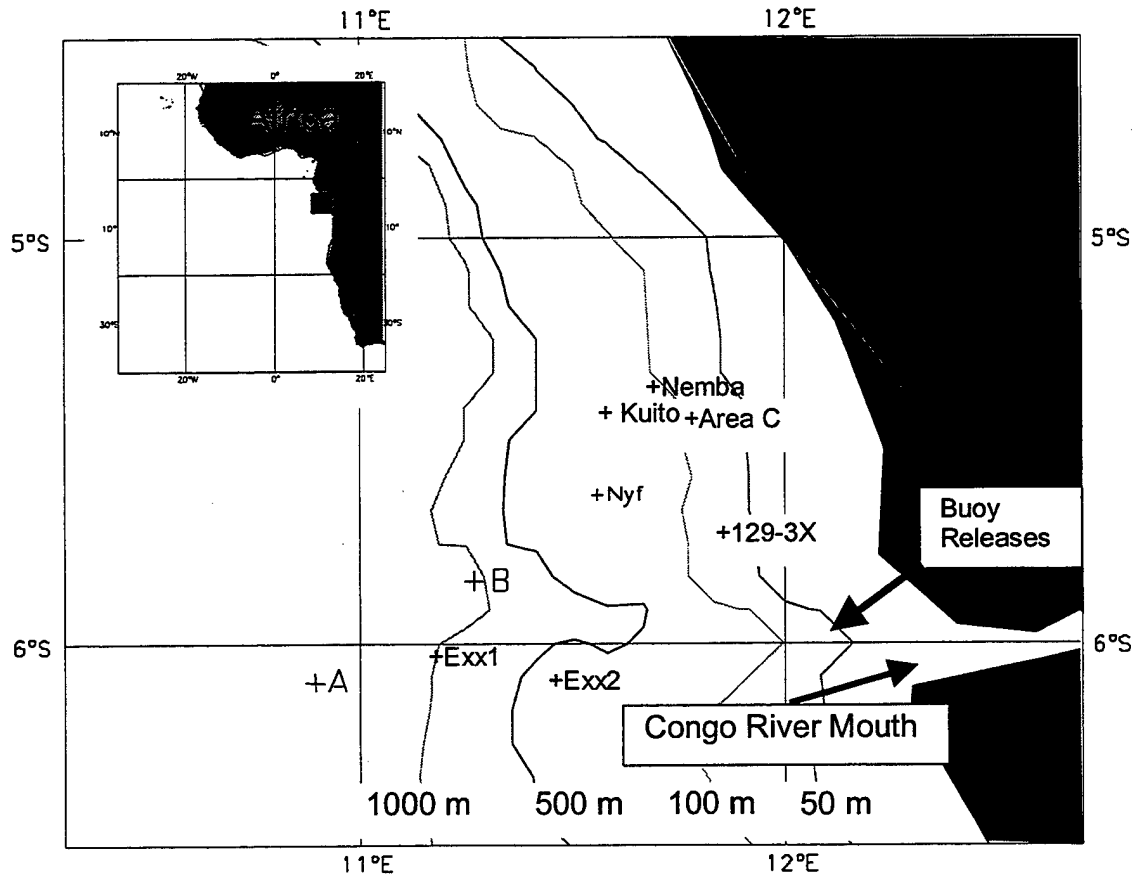
Mixing in a Bottom Layer Associated with the New England Shelf/Slope Water Front

Timothy F. Duda. Chris R. Rehmann and James R. Ledwell
Applied Ocean Physics and Engineering Department
Woods Hole Oceanographic Institution
Woods Hole, MA 02543

Abstract: Towed transects of scalar (conductivity) microstructure were made in a near-bottom layer of warm salty water intruding onto the continental shelf south of New England in August 1997. The layer was known to be moving onto the shelf because of a concurrent dye injection and tracking experiment in the layer. The Osborn-Cox model was used to estimate the diapycnal eddy diffusivity as a function of depth using the mean variances of the measured scalar gradients. The diffusivity decreases rapidly with distance above the bottom, with a minimum at the interface separating the layer from the "cold pool" water above. At the interface, about five meters above the bottom, diffusivities estimated from the Osborn-Cox model, from the dispersal of the dye cloud centered at the inferface, and from the rate of dye cooling all agree at $6 \times 10^{-6} \mathrm{m}^2/\mathrm{s}$. The diffusivity scales as N^{-3} in the layer and just above it (N is the Brunt-Vaisala frequency), consistent with observations of shear-driven entrainment across interfaces in laboratories under the assumption of steady shear. The scaling is closer to N^{-1} in the water column above. The strong decay of diapycnal diffusivity to very low values only a few meters off the bottom at the interface allows the warm-salty layer (the toe of the shelf-break front) to extend many kilometers onto the shelf despite its thinness.

Procedures

Towed measurement of microstructure can be an effective way to observe small-scale gradients of fluid properties which are often indicative of turbulent activity. Both dynamical properties such as velocity and (nearly) passive properties such as temperature are strained by turbulent flow, with resultant increases in mean-square value and in variance at high wavenumber. Observing these gradients along horizontal paths provides a large quantity of data at a specific depth in the water column. The towed observations used here to derive mixing rates near the seafloor were collected as an enhancement to a program of tracer dispersal experiments on the continental shelf.

During the late-summer periods of 1995 through 1997 a series of five dye-injection and tracking experiments were conducted by our group using techniques adapted from previous deep-water experiments [*Ledwell and Bratkovich*, 1995; *Ledwell and Watson*, 1991; *Ledwell, Watson and Law*, 1993]. Injections took place near 40.5 N, 70.5 W, approximately 100 km south of Martha's Vineyard, Massachusetts, in 70 m-deep water. Fluorescent dye was injected in km-long streaks on isopycnal surfaces and subsequently mapped three times over the next five days. The observed vertical growth of the patches provided estimates of diapycnal (essentially vertical) diffusivity K, and the observed lateral expansion provided estimates of horizontal diffusivity. The values of K recorded for five values of N, but possibly influenced by other variable factors, ranged from about 0.7 to $3 \times 10^{-5} \mathrm{m}^2/\mathrm{s}$, following roughly N^{-1}.

A system to measure microscale gradients of conductivity was fitted to the dye sampling system during the third and final cruise. The system was towed near the dye patches at approximately 2 m/s, undulating vertically under automatic winch control. A 400-Hz sampling rate allowed full utilization of the 1-cm (wavelength) resolution capability of the sensor.

The majority of the data were taken during ten non-undulating tows near the bottom (71 m depth) in the vicinity of a dye patch injected roughly 5 meters above the bottom. Injection was in water of density anomaly 26.14 kg/m^3 in a sharp interface layer above a bottom layer of warm, salty water of lesser vertical density gradient. Each tow was approximately 2.5 km in length. A spectral method was used to compute the temperature gradient variance at one-second intervals, using the conductivity to temperature correction schemes of *Washburn, Duda and Jacobs* [1996]. The dissipation rate of thermal variance χ_T is proportional to this variance. Figure 1 shows one tow path trajectory and χ_T along the path.
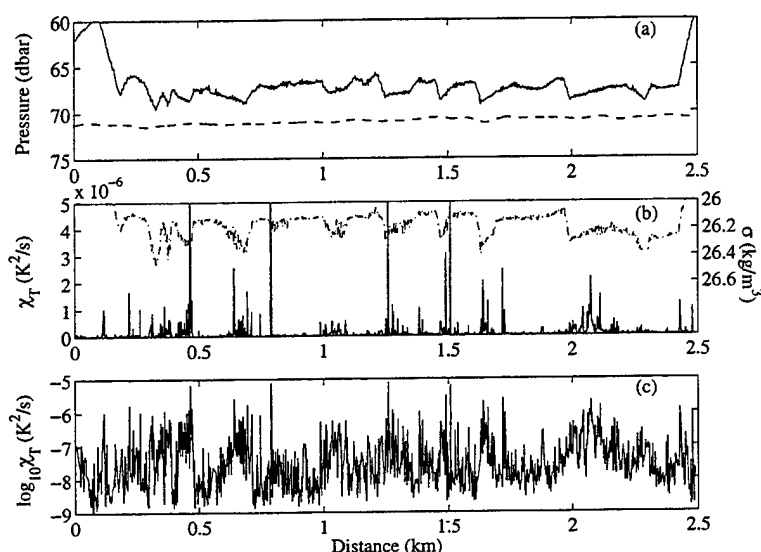

Figure 1. (a) The sled depth and bottom are shown. (b) Density along the track (dash) and dissipation rate χ_T are shown. (c) Log of χ_T along the track is shown.

Results

The Osborn-Cox relation [*Osborn and Cox*, 1972] for steady state homogeneous stratified turbulence provides an estimate of turbulent diffusivity K as a function of χ_T and the mean temperature gradient. In the model, $K = \chi_T/2(dT/dz)^2$. Figure 2 shows mean gradient, χ_T, K and heat flux results from the transects. The zone of peak gradient, 64 to 66 dbar, has the lowest diffusivity. The K estimate in this zone is a factor of two lower than the estimate from the dye. These may be consistent with equal estimates when uncertainties are taken into account.

The reduced gradient within a few meters of the seafloor coupled with χ_T values comparable to those in the interface above give elevated K values. The diffusivity times the gradient, the flux, also rises near the bottom. The picture seems to imply heat flux out of the bottom, but the profile in the bottom few meters is probably not to be trusted. Only the existence of elevated K should be relied upon.
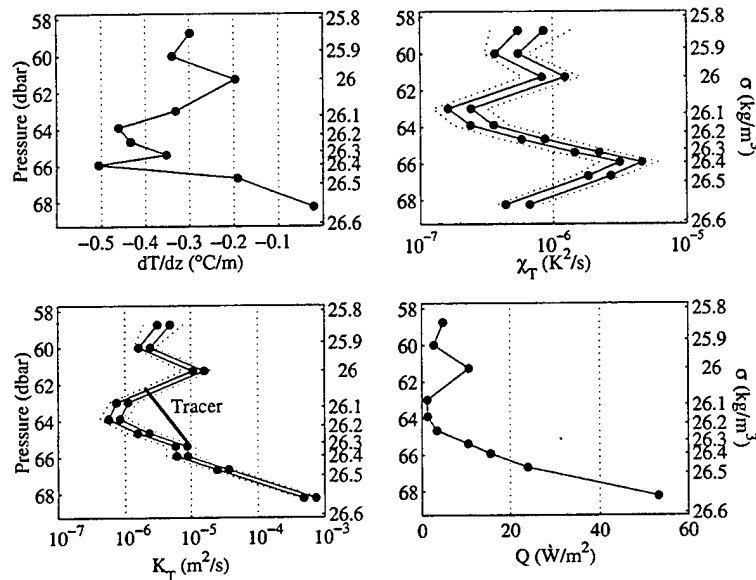
Figure 2. (a) The sled depth and bottom are shown. (b) Density along the track (dash) and dissipation rate χ_T are shown. (c) Log of χ_T along the track is shown.

If K is plotted against N (Figure 3) a power-law relation is seen. The relation compares well with laboratory experiments of shear-driven entrainment across an interface between two layers reviewed by *Christodoulou* [1986] and *Fernando* [1991], which suggest $K \propto N^{-3}$ for Richardson number greater than one and constant layer thickness, interface thickness, and velocity difference across the interface.

These preliminary results suggest much lower diffusivity rates than assumed in many models of the shelf break front and the other features of the coastal environment (see, for example, *Lentz* [1995] and *Chapman and Lentz* [1994] and work cited therein). This reduced diffusivity allows the front to be close to horizontal, as it was observed to be during our study, with isotherms spanning 40 km horizontally as they descend from surface to bottom near the shelf break. This is a factor of eight flatter frontal slope than computed by *Chapman and Lentz* [1994]. Comparison of the low K values observed in this coastal study with open ocean results at lower N conditions imply that stratification may either inhibit turbulent mixing and diffusion, or that the geometry of the shelf inhibits motions (internal or inertial waves) which are necessary to drive mixing.

References

Chapman, D. C. and S. J. Lentz, Trapping of a coastal density front by the bottom boundary layer, *J. Phys. Oceanogr.*, *24*, 1464–1479, 1994.

Christodoulou, G. C., Interfacial mixing in stratified flows, *J. Hyd. Res.*, *24*, 77–92, 1986.

Fernando, H. J. S., Turbulent mixing in stratified fluids, *Ann. Rev. Fluid Mech.*, *23*, 455–493, 1991.

Ledwell, J. R. and A. Bratkovich, A tracer study of mixing in the Santa Cruz Basin, *J. Geophys. Res.*, *100*, 20681–20704, 1995.

Ledwell, J. R. and A. J. Watson, The Santa Monica Basin tracer experiment: A study of diapycnal and isopycnal mixing, *J. Geophys Res.*, *96*, 8695–8718, 1991.

Ledwell, J. R., A. J. Watson and C. S. Law, Evidence for slow mixing across the pycnocline from an open-ocean tracer-release experiment, *Nature*, *364*, 701–703, 1993.

Lentz, S. J., Sensitivity of the inner-shelf circulation to the form of the eddy viscosity profile, *J. Phys. Oceanogr.*, *25*, 19–28, 1995.

Osborn, T. R. and C. S. Cox, Oceanic fine structure, *Geophys. Fluid Dyn.*, *3*, 321–345, 1972.

Washburn, L., T. F. Duda and D. C. Jacobs, Interpreting conductivity microstructure: Estimating the temperature variance dissipation rate, *J. Atmos. Ocean. Technol.*, *13*, 1166–1188, 1996.
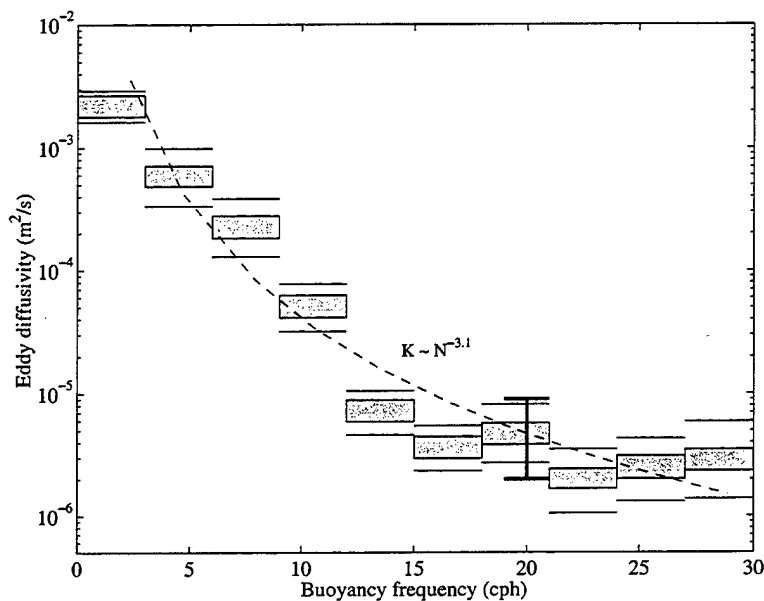
Figure 3. Diffusivity shown in the previous figure is plotted versus stratification strength, N.

Diffusion Versus Advection Dominated Suspension on the Inner Shelf Under Storm and Swell Conditions, Duck, N.C.

G. Lee[1], C.T. Friedrichs[1], L.D. Wright[1], and C.E. Vincent[2]
[1]Virginia Institute of Marine Science, School of Marine Science,
College of William and Mary, Gloucester Point, VA 23062, USA
[2]School of Environmental Sciences, University of East Anglia,
Norwich NR4 6TJ, UK

Introduction

A first approximation for sediment transport under waves and currents on the continental shelf is given by vertically integrating the product of wave-averaged horizontal velocity and wave-averaged sediment concentration. Models following this approach generally solve the steady state diffusion equation (e.g., Glenn & Grant 1987).

$$w_s C + \varepsilon_s \, dC/dz = 0 \tag{1}$$

where $C(z)$ is wave-averaged sediment concentration at height z above the bed, w_s is sediment fall velocity, and ε_s is eddy diffusivity. This equation simply states that the mechanism for sediment suspension is a diffusive process such that upward sediment flux by turbulent diffusion is balanced by downward flux due to gravitational settling.

To obtain an expression for ε_s, the assumption is made here that

$$\varepsilon_m = \varepsilon_s = \kappa u_{*cw} z \text{ for } z < \delta_w, \quad \varepsilon_m = \varepsilon_s = \kappa u_{*c} z \text{ for } z > \delta_w \tag{2}$$

where κ is Von Karman's constant (~0.4), u_{*cw} is maximum shear velocity within the wave boundary layer of thickness δ_w, $= 2\kappa u_{*cw}/\omega$, ω is wave radian frequency and u_{*c} is wave-averaged shear velocity (Grant & Madsen 1986; Glenn & Grant 1987). Integration (1) using (2) yields the Rouse equation. The vertical distribution of suspended sediment predicted by the Rouse equation is reported to agree well with measurements in unidirectional stream flow (e.g., Vanoni 1975) and over a plane bed under waves in flumes (Ribberink & Al-Salem 1994).

When sharp-crested ripples are present under regular waves, laboratory results indicate that the dominant process of sediment suspension is no longer diffusion, but rather vertical advection associated with the cyclic development and convection of large vortices (Ribberink & Al-Salem 1994). The vertical distribution of suspended sediment concentration can then be described by an advection-diffusion model that incorporates vertical advection of sediment associated with large-scale eddy motion in the presence of bed forms (Nielsen 1992). Under conditions dominated by vertical advection, the assumption of (1) is expected to fail.

In this paper, we examine the relationship between eddy viscosity and eddy diffusivity during storm and swell conditions observed on the inner shelf off Duck, N.C. Our interest lies, in particular, into what conditions the assumption of (1) is valid. Further, we test the ability of a Rouse-type diffusion model (Grant & Madsen 1986; Glenn & Grant 1987) versus a combined advection and diffusion model (Nielsen 1992) to reproduce observed sediment profiles.

Field Experiment

The Virginia Institute of Marine Science deployed an instrumented benthic boundary layer tripod at depth of 12 m on the inner shelf off Duck, N.C., between 26 September and 22 October 1996. Instrumentation set to burst sample every two hours included five

electromagnetic current meters (EMCMs) at heights of 8, 38, 68, 98 and 125 cm above the bottom (cmab), a pressure sensor at 195 cmab, three acoustic backscatter sensors (ABSs) at 88 cmab, and an acoustic Doppler velocimeter (ADV) at 19 cmab. The EMCMs and pressure sensor sampled at 1 Hz for burst durations of 34 min, while the ABS and ADV sampled at 5 Hz for about 12 min.

On 3 October 1996, a northeaster developed in the area and lasted about four days. During the storm, the current was predominantly along coast and toward the south, reaching about 50 cm/s near the beginning of the storm before gradually decreasing. Near bottom orbital velocity was about 40 cm throughout the storm, and the wave period was about 9 s. Toward the end of the deployment, the tripod recorded an extended period of well organized swell. The wave period during the swell was about 12 sec and near bottom orbital velocity reached about 30 cm/s. During the swell dominated period, the current speed was relatively weak (< 20 cm/s).

Estimating Eddy Diffusivity and Eddy Viscosity

Apparent eddy diffusivity, ε_s, is estimated from (1), while eddy viscosity, ε_m, is estimated from (2). C and dC/dz are given by burst-averaged sediment concentration profiles obtained from the ABSs, and w_s is based on the median sediment size in the bed obtained by divers at the time of deployment. Two methods are used to determine u_{*c}: (i) the observed best-fit log profile ($u = u_{*c}/\kappa \log(z/z_0)$) and (ii) the Grant and Madsen (1986) model for wave-current interaction. The later model is also used for estimating u_{*cw}. We apply the Grant and Madsen model because of its simplicity and its wide application in the literature. Ripple geometry is predicted using mean bed grain size (0.17 mm) input into Wiberg and Harris (1994). Equivalent bottom roughness is then predicted using the Nielsen (1992) formulation. The effects of sediment-induced stratification are assumed to be negligible over the sandy beds found at 12 m depth off Duck.

Figure 1 displays profiles of ε_s and ε_m estimated as described above for storm and swell conditions. Apparent eddy diffusivity profiles are estimated independently using each of the three ABS transducers (Channels 1, 2 and 3 = 1, 3 and 5 MHz). Under storm conditions, the vertical structure of eddy viscosity is relatively consistent with diffusivity, both inside the wave boundary layer and about 20 cm into the current boundary layer. Even above that, ε_m associated with u_{*c} still provides an upper bound on observed ε_s. Under swell, the vertical structure of ε_s is likewise relatively consistent with ε_m within the wave boundary layer. But above the wave boundary layer ε_s continues to increase as if still determined by u_{*cw}.

Figure 2 displays time-series of shear velocities during storm and swell. $u_{*c,\varepsilon s}$ was inferred from the eddy diffusivity profiles (Channel 2) using (2). As described above, $u_{*c,\varepsilon s}$ agrees well with u_{*cw} during swell and with u_{*c} most of the time during the storm. It is noted, however, that $u_{*c,\varepsilon s}$ follows a projection of u_{*cw} above the wave boundary layer during several bursts on October 6. This is discussed further below.

Diffusion-dominated vertical distribution of suspended sediment

In this section, we apply a two layered Rouse model of Glenn and Grant (1987) for suspended sediment distribution to the above storm and swell dominated observations. For the model, we use seven grain sizes to reproduce the distribution observed in the bed, set the reference concentration to match the observed concentration at 1 cm above the bed, and neglect the effects of sediment-induced stratification. In addition, a mixing depth is incorporated into the model, following Wiberg et al. (1994) such that

$$\delta_m = q_{bl}T/c_b\lambda + \delta_b \tag{3}$$

where δ_m is mixing depth, q_{bl} is bedload transport rate, T is wave period, c_b is volume concentration of the bed (~0.65), and λ is ripple length. δ_b represents a background mixing depth, set to 1 mm. This is useful when flow conditions are so weak that there is no bed load transport. The bedload transport rate is estimated from the Meyer-Peter and Müller (1948) equation, $q_{bl} = 8(\tau_{sf}-\tau_{cr})^{1.5}/(\rho_s-\rho)g$, where τ_{sf} is skin friction shear stress, τ_{cr} is critical shear stress, ρ_s is sediment density, ρ is sea water density and g is acceleration of gravity.

Figure 3 shows the vertical distribution of suspended sediment from the bed level to 50 cm above the bottom during storm and swell conditions. The Rouse model reproduces the storm data quite well, while it considerably underestimates concentration above the wave boundary layer during swell conditions. This is consistent with the observations of apparent eddy diffusivity: vertical diffusion appears to be dominant during the storm, whereas vertical advection appears to dominate during swell.

Criteria delineating diffusion and advection processes

Figure 4a displays time-series of observed and modeled sediment concentrations at 5 and 30 cm above the bed during storm and swell conditions. The bursts for which the Rouse model fails to reproduce the observations above the wave boundary layer are hatched, signifying that the assumption of (1) is invalid. These periods include most of swell cases and several bursts during the storm on October 6 which correspond to the cases when $u*_{c,\epsilon s}$ follows $u*_{cw}$. These events correspond to times of weak current (~< 10 cm/sec, Figure 4b).

In order to further examine under what conditions the assumption of (1) is invalid, we introduce a scaling parameter, R, which is a ratio of vertical advection velocity to the mean current, $u_{c,\delta}$, at the top of the wave boundary layer. Here, the vertical advection or "jet" velocity, u_j, is scaled to $(\eta/\lambda)u_b$ where η is the ripple height and u_b is the near-bottom orbital velocity. Andreopoulos and Rodi (1984) reported through laboratory experiments that at small ratios of jet-to-crossflow velocity (R < ~0.5) , the jet is immediately bent over by the crossflow, while at higher R-values (R > ~0.5) the jet penetrates further into the crossflow. That is, at small R-values, diffusion by current shear outside the wave boundary layer will be the dominant process. For cases of higher R-value, current shear may be insignificant and sediment suspension is dominated by jet-like advection associated with ripple vortex shedding.

Figure 4c contains a time-series of the scaling parameter, R, where we have used the Wiberg and Harris (1994) model to estimate η and λ. In general, the assumption of (1) fails when R > ~0.3-0.5. This is roughly consistent with the observations of jet penetration by Andreopoulos and Rodi (1984).

Combined diffusion and advection model of vertical distribution of suspended sediment

In this section, we apply the combined diffusion and advection model of Nielsen (1992). The steady state combined advection and diffusion equation of Nielsen (1992) is

$$w_s C + \epsilon_s \, dC/dz - PF(z) = 0 \qquad (4)$$

where $P = w_s C_o$ is the wave-averaged pickup rate and F(z) is a probability function that a given particle can reach a certain level, z. Empirical results suggest a probability function of the form:

$$F(z) = (1 + 11z(k_b A_b)^{-1/2})^{-2} \qquad (5)$$

where k_b is the Nikuradse roughness and A_b is the near-bottom orbital excursion. Nielsen assumes $\epsilon_s = 0.016 \omega k_b A_b$ is constant with height. Then integration of (4) and (5) yields

$$C(z) = \frac{P}{w_s} e^{-w_s z/\varepsilon_s} \left(\frac{w_s}{\varepsilon_s} \int_0^z \frac{e^{w_s z'/\varepsilon_s}}{(1 + 11z'(k_b A_b)^{-1/2})^2} dz' + 1 \right) \tag{6}$$

Concentrations predicted by the combined diffusion and advection model are shown in Figure 5. The combined model reproduces the storm data reasonably well. However, the Rouse model works better than the combined model under storrm conditions. During swell conditions, the combined diffusion and advection model does better reproducing observed concentrations above the wave boundary layer. Nonetheless, it is not entirely satisfying in that the combined model is more empirically based and also fails to reproduce observed concentration profiles with very steep gradients.

References

Andreopoulos, J. & W. Rodi (1984) Experimental investigation of jets in a crossflow. J. Fluid Mech., 138: 93-127.

Glenn, S.M. & W.D. Grant (1987) A suspended sediment stratification correction for combined wave and current flow, J. Geophys. Res., 92: 8244-8264.

Grant, W.D. & O.S. Madsen (1986) The continental shelf bottom boundary layer, Ann. Rev. Fluid Mech., 18: 265-305.

Meyer-Peter, E. & R. Müller (1948) Formulas for bedload transport. In: Proceedings of the Second Meeting, International Association of Hydraulic Research. Stockholm, Sweden, pp. 39-64.

Nielsen, P. (1992) Coastal Bottom Boundary Layers and Sediment Transport, World Scientific, Singapore, 324 p.

Ribberink, J.S. & A.A. Al-Salem (1994) Sediment transport in oscillatory boundary layers in cases of rippled beds and sheet flow, J. Geophys. Res., 99: 12,707-12,727.

Vanoni, V.A. (1975) Sedimentation Engineering, ASCE, New York, 745 p.

Wiberg, P.L., D.E. Drake & D.A. Cacchione (1994) Sediment resuspension and bed armoring during high bottom stress events on the northern California inner continental shelf: measurements and predictions. Cont. Shelf Res., 14: 1191-1219

Wiberg, P.L. & C.K. Harris (1994) Ripple geometry in wave-dominated environments, J. Geophys. Res., 99: 775-789.
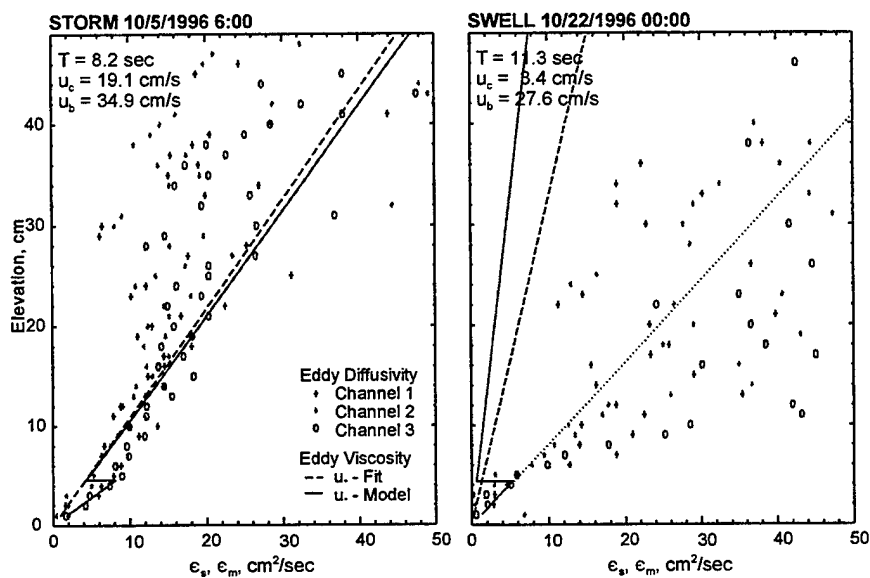
Figure 1. Eddy viscosity and diffusivity profiles during storm and swell conditions. Eddy viscosity using u_{*cw} above the wave boundary layer is shown by dotted line for the swell case. Wave period (T), current speed at 1 mab (u_c) and near-bottom orbital velocity (u_b) are also shown in the figure.
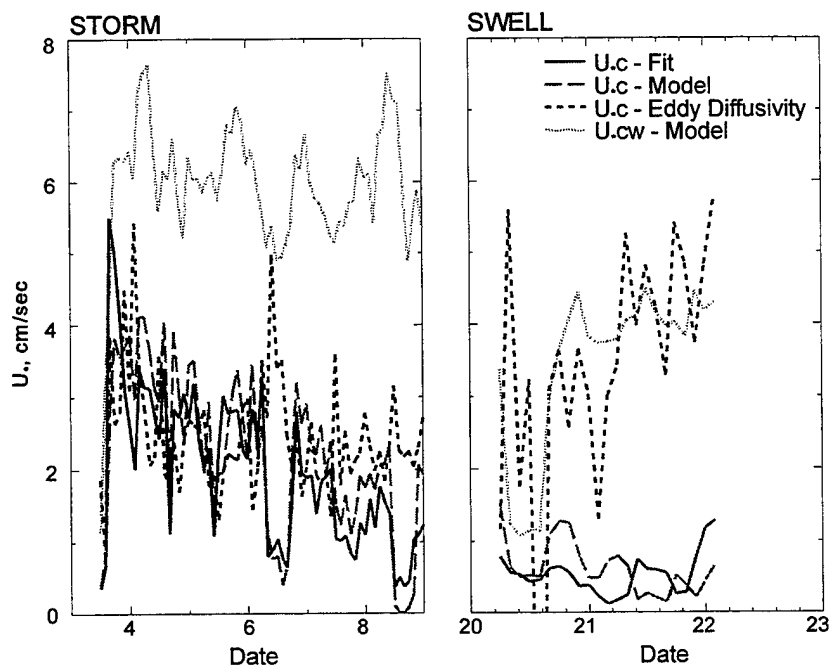

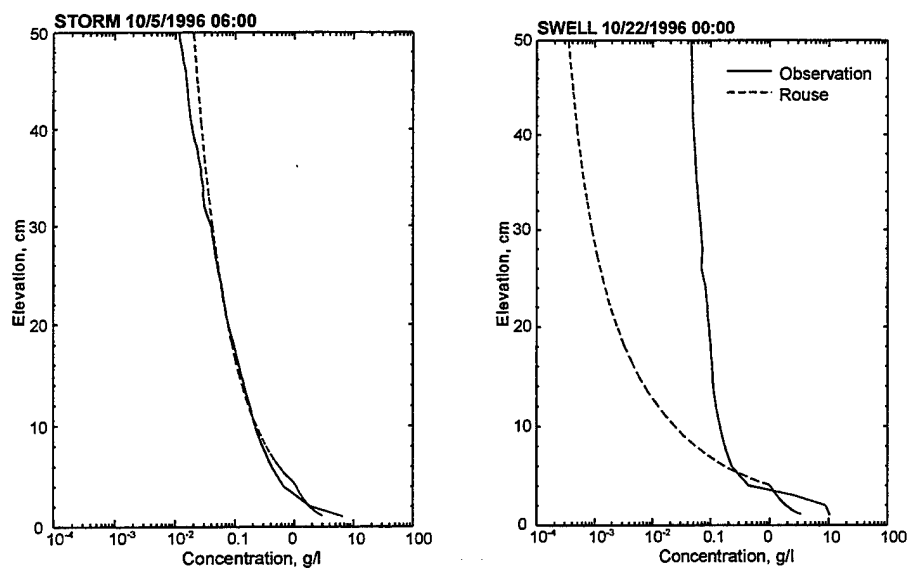Figure 2. Time-series of shear velocities during storm and swell

Figure 3. Comparison of vertical sediment concentration profiles during storm and swell conditions
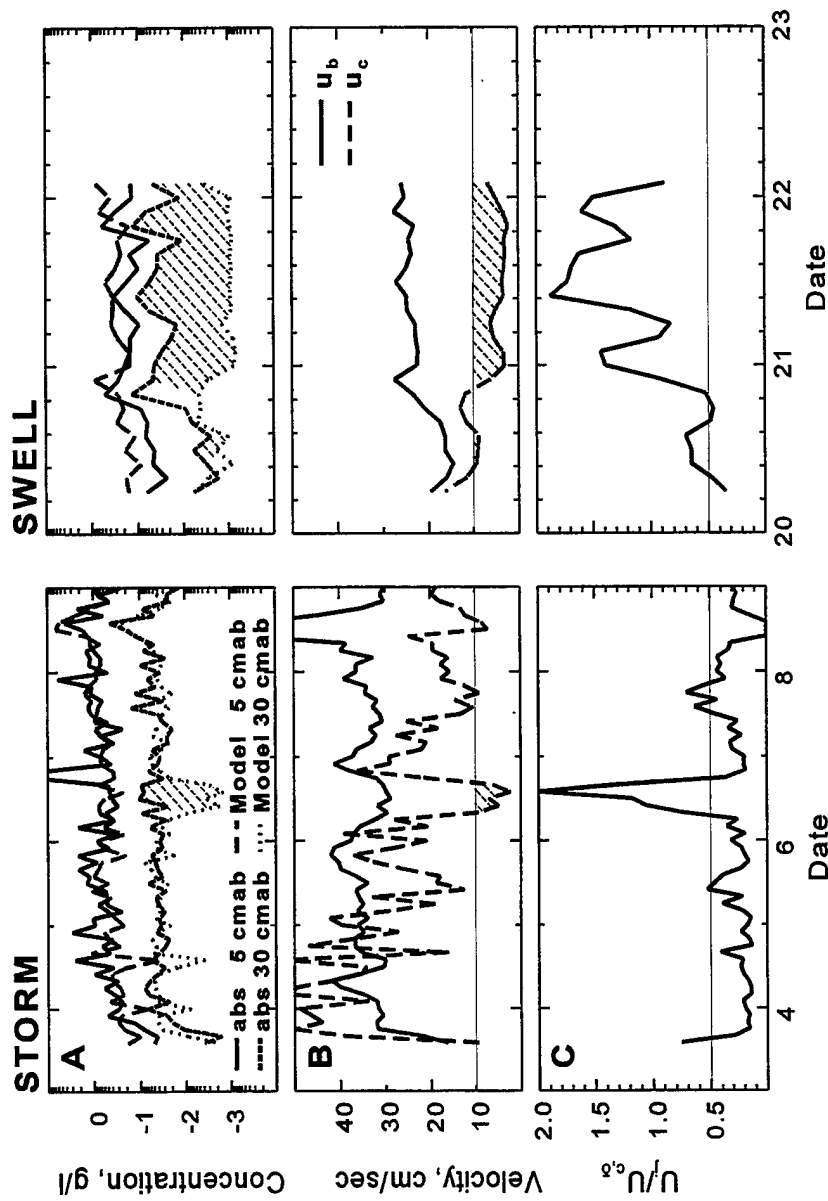
Figure 4. a. Time-series of modeled and observed concentrations at 5 and 30 cmab during storm and swell conditions; b. Near-bottom orbital velocity and current velocity at 1 mab; c. scaling parameter of vertical advection velocity to mean current. Hatch represents the time when the assumption of (1) is invalid.
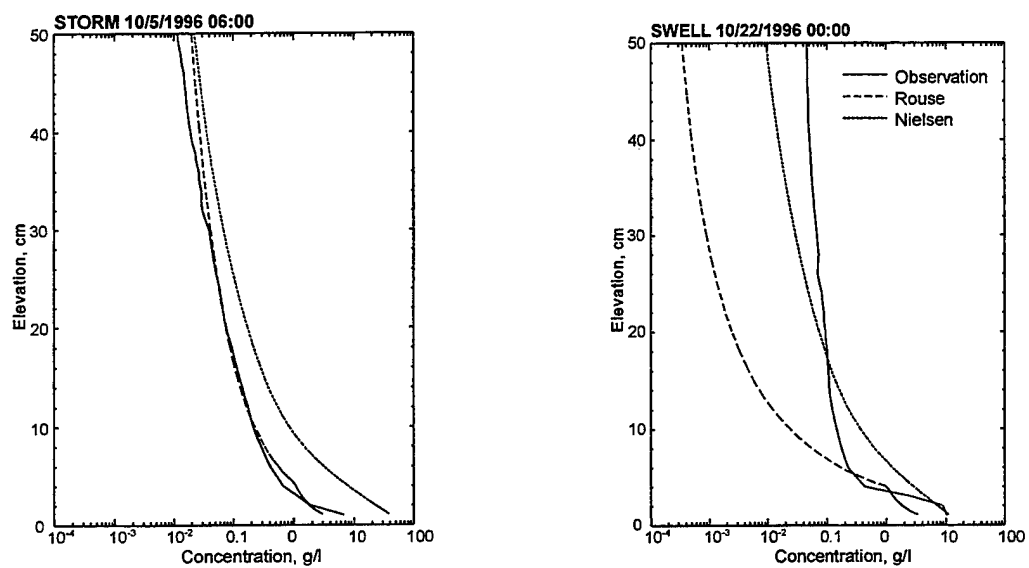
Figure 5. Vertical sediment concentration profiles during storm and swell conditions

Shelfbreak Frontal Structure during Spring, 1996: SeaSoar Observations from the ONR Shelfbreak PRIMER Experiment

Glen Gawarkiewicz, Robert Pickart,
Frank Bahr, and Robert Beardsley
Physical Oceanography Department
Woods Hole Oceanographic Institution.

Over the last six years, the dynamics of the bottom boundary layer over a stratified continental shelf have been studied using theoretical and numerical methods by many investigators. A particularly important area of importance for the dynamics of stratified bottom boundary layers is the shelfbreak, where a strongly stratified front intersects the bottom in many regions such as the Middle Atlantic Bight. Prior modelling work (Gawarkiewicz and Chapman, 1992; Chapman and Lentz, 1994) suggests that the bottom boundary layer detaches into the frontal zone, leading to an upwelling circulation within the front. In order to gain further insight into shelfbreak frontal processes, SeaSoar surveys were conducted from May 7-9, 1996, to examine the shelfbreak frontal and velocity structure.

The frontal configuration during this time period was relatively straight, with strong cross-shelf temperature, salinity, and density gradients near the surface. This resulted in strong geostrophic velocity shears in the upper 20 m of the water column, and maximum alongshelf velocities as large as 60 cm/s. Near the foot of the front, stratification was strong, as was the cross-shelf density gradients. A particularly interesting feature in the ADCP velocity field is a mid-level jet resulting from the thermal wind shear of the cross-shelf density gradients near the foot of the front. The cross-shelf velocity field is indicative of a double-sided convergence near the bottom in the vicinity of the foot of the front, which is similar to the model of Chapman and Lentz (1994).

Careful analysis of the stratification within the frontal zone reveals a layer of very weak or non-existent stratification which is suggestive of the detached bottom boundary layer. This is consistent with the result of recent dye releases within the front undertaken by R. Houghton of Lamont Doherty Earth Observatory. This layer extends to within 30 m of the surface, indicating that the detachment process affects the frontal structure throughout much of the frontal zone. Further work will be necessary to understand how this layer is affected by the numerous forcing and instability processes affecting the front.

Coastal Predictive Skill Experiments at the Long-term Ecosystem Observatory

Scott Glenn

Rutgers University

Overview

The Long-term Ecosystem Observatory (LEO-15) was installed on the ocean floor in 15 m of water approximately 10 km offshore Tuckerton, NJ in September, 1996. The subsea observatory was constructed through a NSF-funded partnership between the Institute of Marine and Coastal Sciences (IMCS) at Rutgers University and the Ocean Systems Laboratory (OSL) at the Woods Hole Oceanographic Institution. It is now operated by Rutgers with continuing support from NOAA's Mid-Atlantic Bight National Undersea Research Center.

LEO-15 is the site of numerous multi-institutional inter-disciplinary research efforts that have involved over 50 researchers from over 20 institutions. The most recent was the first in a series of Coastal Predictive Skill Experiments sponsored by the Office of Naval Research, the National Ocean Partnership Program, and the Middle Atlantic Bight National Undersea Research Center. A coastal adaptive sampling network centered on the LEO-15 site was operated during July of 1998 to study coastal upwelling and its affect on phytoplankton distributions and in-water optical properties. The observation network included three satellites and one aircraft, a shore-based high-frequency radar, five surface vessels, and four different Autonomous Underwater Vehicles (AUVs). Real-time surface data from satellites and shore-based remote sensing systems combined with real-time subsurface data from LEO-15 proved to be a critical mission planning device for scientists directing the coordinated shipboard and AUV sampling patterns. Selected remote sensing and shipboard datasets were post-processed within hours of collection for assimilation by a numerical forecast model. Data assimilative forecasts run twice per week provided additional long-term (2-5 day) guidance to mission planners.

Remote Sensing Systems

Remote sensing data was acquired from 3 satellites, including sea surface temperature from the Advanced Very High Resolution Radiometer (AVHRR) on the NOAA Polar Orbiting Environmental Satellites (POES), ocean color from the Sea-Viewing Wide-Field-of-View Sensor (SeaWiFS) on the SeaStar satellite, and surface roughness from the Synthetic Aperture Radar (SAR) on the Canadian RADARSAT. AVHRR and SeaWiFS data was collected in real-time at the IMCS Marine Remote Sensing Laboratory in New Brunswick, while the RADARSAT data was acquired by scientific partners at NOAA. On one Sunday in July, hyperspectral ocean color data was collected with the AVIRIS in an overflight by a Navy research plane.

Ocean surface current fields where observed from a shore-based COastal raDAR (CODAR) HF-radar. Two transmit/receive sites where set up on the barrier island beaches approximately 15 km north and south of LEO-15. Real-time radial vectors from each beach site where transmitted to a central processing system at the Rutgers Marine Field Station in Tuckerton. There it was converted to vector fields, detided, filtered and made available on the World Wide Web. Some of the most useful products for mission planning were the overlays of the CODAR-derived surface currents on the AVHRR-derived surface temperatures, and maps of surface convergence/divergence derived from the current vectors.

LEO System

The LEO-15 system consists of two instrument platforms (or nodes) housed within trawl-resistant steel shells that are anchored to the sea bottom. The instrument nodes are linked to shore via an electro-fiber optic cable that provides power and remote access over the Internet. The nodes are equipped with video cameras, acoustic hydrophones, stationary tide, wave and current sensors, instrumented vertical profilers, and 8 guest ports to plug in additional sensors. The vertical profiler can be controlled from any remote site via the Internet. Similarly, scientists with instruments plugged into the guest ports can communicate and control their sensors from their home institutions.

During the July experiment, nearshore temperature and salinity profiles were collected using the profiling sensors on the node. Initially the profilers were manually cycled vertically through the water column, but as confidence grew, they were programmed to autonomously cycle once every hour, continuously, day and night. Current profiles were collected using an Acoustic Doppler Current Profiler (ADCP) plugged into one of the node guest ports and controlled from shore. Datasets from both instruments were processed and displays updated on the World Wide Web every 15 minutes.

Survey Vessels

Five vessels were used during the July experiment, one to support divers and node operations, two to support AUV operations, one for physical surveys, and one for biological/optical surveys. The physical survey vessel (R/V Caleta) was equipped with two new instrument systems, an ADCP towed at the surface alongside the survey vessel and an undulating CTD/Fluorometer towed behind the vessel.

The ADCP was mounted on an aluminum Small Water Area Twin Hull (SWATH) towbody designed by Gold Coast Yachts and constructed by Rutgers. The design incorporated many improvements identified in tests with an earlier version developed jointly with Stevens Institute of Technology. The subsurface pontoons on the new vessel were designed to provide nearly all the buoyancy, and the vertical struts responsible for the remainder were extended from a few inches to 2 ft. Other than the vertical struts, the new SWATH had virtually no above surface superstructure. The design improvements enabled the SWATH to be towed through surface waves rather than over, greatly reducing vehicle motion and allowing us to tow, for the first time, directly into a short windsea.

The undulating CTD also was redesigned based on our previous summer's experience. The towing bridle on a Guildline Minibat was replaced with a stronger version, and skids were added for the inevitable collisions with the sandy bottom. A Falmouth Scientific Inc. (FSI) Mini-CTD and a WetStar Fluorometer were small enough to be mounted internally, resulting in more streamlined sensor payload. Maneuverability of the redesigned vehicle was improved, especially for close approaches to the bottom, but was still highly dependent on towing cable length. Optimal towing speed remained near 5.5 knots. By far the greatest improvement was the real-time CTD data display, redesigned by FSI specifically for towed vehicles. The display allows users to view a trace of the pressure record versus time, with the color of the line based on the temperature, salinity, or fluorometer readings. A real-time CTD cross-section results, which combined with the real-time ADCP cross-sections, enabled survey crews to observe features and radio locations to other vessels operating in the vicinity.

Autonomous Underwater Vehicles

Multiple AUV operations at LEO were nearly a daily activity during the month-long experiment. The autonomous vehicles included two Remote Environmental Measuring UnitS (REMUS) AUVs constructed and operated by the WHOI Ocean Systems Laboratory (OSL). One of the WHOI REMUS AUVs was designed for docking tests, the other for ADCP/CTD surveys. A third turbulence REMUS was constructed by OSL and operated by the Naval Underwater Warfare Center (NUWC) during the experiment. In preparation for next year, a pair of Multi-Trip Lagrangian autonomous CTD profilers constructed and operated by Webb Research Corporation (WRC) were tested.

For the docking tests, a REMUS docking station was installed at LEO-15 and plugged into one of the node guest ports. On numerous occasions, the docking REMUS vehicle would be programmed to swim into the docking cone, establish an electrical connection, recharge its batteries, and be reprogrammed for another mission. It would then be instructed to exit the station and, after performing the new mission, return.

The WHOI survey REMUS was programmed to run along a 20 km cross-shelf line marked by a series of transponders placed a 4 km intervals. The REMUS AUVs were capable of completing the full 20 km interval on rechargeable lead-acid batteries in about 3 hours. The REMUS surveys were coordinated with shipboard ADCP/CTD surveys to provide either multiple coverage of the same line or simultaneous coverage of two parallel lines. Disposable lithium batteries tested near the end of the experiment increased the range capability to 60 km, enabling the cross-shelf line to be surveyed three times in one day, with matching coverage on a parallel line by the R/V Caleta.

Instrumentation on the NUWC turbulence REMUS included the same internal ADCP/CTD configuration as the WHOI survey vehicle, with an additional external sensor suite consisting of an Acoustic Doppler Velocimeter (ADV), two additional fast-response CTDs, and a shear probe all mounted on stings. Surveys by the turbulence REMUS designed to acquire horizontal transects of turbulent properties across the different fronts associated with the upwelling centers. The turbulence REMUS was deployed once each week in a critical location determined by the real-time data.

The Multi-Trip CTDs were tested at both a deep offshore site and a shallow inshore site. The deep offshore site (22 m) was visited to gain experience sampling the strong summer pycnocline occurring near mid-depth, a monitoring task to be fulfilled next year by the WRC ALACE Glider AUVs. The inshore site was chosen to monitor the surfacing of the pycnocline during an upwelling event. This was a challenging task with water depths less than 10 m and the pycnocline to be sampled lying only 2 m above the bottom. Communicating with the Multi-Trip from the support vessel via a FreeWave transceiver, WRC scientists were able to test numerous profiling configurations, including varying the descent rate and altimeter range, to optimize settings for this situation.

Forecasting System

An ocean forecasting system was assembled for the purpose of assimilating the above datasets and providing forecast guidance for adaptive sampling. The numerical ocean model used to generate the ocean forecasts was the Rutgers Regional Ocean Modeling System (ROMS v1.0), the most recent version of the original S-Coordinate Rutgers University Model (SCRUM). Surface forcing was provided by atmospheric forecasts from the Navy Operational Regional Atmospheric Modeling System (NORAPS) and the Navy Operational Global Atmospheric Modeling System (NOGAPS) acquired over

the World Wide Web. Ocean data assimilation was via a multi-variate Optimal Interpolation (OI) scheme.

The forecasting scheme evolved from our need to fix the shipboard and AUV sampling strategies for a two day period twice a week (Monday/Tuesday and Thursday/Friday). Two day survey patterns were desired to try to resolve both tidal and inertial oscillations in the towed ADCP data. Forecast model runs therefore where targeted for submission on Sundays and Wednesdays, and required to run for at least 3 days into the future. Since the NORAPS higher resolution atmospheric forecasts were only available for 3 days, forcing from the larger scale NOGAPS model was used for forecast days 4-5.

Preliminary Observations

The experiment began during the relaxation of the first major upwelling event of the summer. As usual, the relaxation process was accompanied by a period of eddy formation and propagation as the warm surface water returned from offshore. This was followed by a quiescent time with very low winds and relatively flat isotherms throughout the study area. Stronger upwelling winds eventually returned, and the formation of a typical upwelling center was observed, including the meandering of the northward-flowing warm surface jet around the cyclonic eddy formed within the northeast quadrant of the upwelling center. One important discovery this year was the observation of a nearshore subsurface jet of southward flowing cold water that fed into the upwelling center on the shoreward side. The experiment ended with a mixing storm on the last day of July in which strong northeasterly winds and large waves destroyed the upwelling center and the near-shore stratification.

HIGH-FREQUENCY RADAR REMOTE SENSING: A NEW TOOL FOR COASTAL OCEANOGRAPHY

Hans C. Graber
Radar Ocean Sensing Laboratory
Division of Applied Marine Physics
Rosenstiel School of Marine and Atmospheric Science
University of Miami
Miami, Florida 33149, USA

Abstract:

The littoral ocean with its complicated coastline and complex bathymetry poses great challenges to oceanographers, coastal managers, and warfighters who, increasingly, need to understand and predict its behavior. However, the prediction of coastal environmental parameters is particularly difficult because winds, waves, and currents interact with the boundaries on much smaller space and time scales than in the open "deep blue" ocean. As a result, the dynamics of coastal waters and the resulting circulation are dependent on many physical mechanisms and interactions that are not well understood and have not been measured extensively with the necessary spatial and temporal resolution. Conventional measurement techniques are limited to single-point, temporal observations (e.g., current or wave measurements from a mooring) or to poorly resolving spatial snapshots (e.g., ship surveys or drifting buoy arrays). The broad spectrum of societal and environmental issues that arise from our increasing interest in (and dependence on) the coastal ocean (e.g., coastal pollution, fisheries recruitment, search and rescue, beach erosion, and sediment transport) demand that we improve our ability to monitor coastal processes, and to fine-tune models to more accurately predict impending changes.

With the advent of high frequency (HF) radars some forty years ago, it became feasible to observe, simultaneously, large regions of coastal ocean and construct maps of surface currents, waves, and wind direction. Depending on the system configuration, horizontal resolutions can be hundreds of meters to tens of kilometers while offshore ranges are tens to hundreds of kilometers. The shore-based, non-invasive nature of this remote sensing technology means that, in principle, these two-dimensional observations can be collected continuously for relatively low costs compared with at-sea measurements. The potential of HF radars to advance our understanding of coastal oceanography by providing much of the necessary space-time observations is tremendous.

Measurements from several experiments will illustrate the use of HF radar data in studying the retention of coral reef fish larvae, wave height variability during an extra-tropical storm and tidal dynamics along the US East Coast,

Chlorophyll as a tracer of small-scale hydrodynamics on the seabed: preliminary studies

Jon Grant and David Adler
Department of Oceanography
Dalhousie University
Halifax, Nova Scotia
Canada B3H 4J1
email: jon.grant@dal.ca

Introduction

Microtopography at the sediment-water interface has a major impact on small-scale hydrodynamics and the subsequent deposition of fine material to the seabed. Ripples and other bedforms provide an example of physically generated micro-structure that affect deposition, and biogenic features such as faunal feeding pits play a similar role (Yager et al. 1993). The sedimentation of particulate organic matter is also influenced by local topography, and as a consequence, the distribution of organisms that depend on this material for food (Sun et al. 1993, Boon et al. 1998). Photopigments provide a useful tool for the study of these processes because they are (1) low density and indicative of fine sediment deposition, (2) easily measured by chemical analyses (3) an important labile food source for benthic fauna, and (4) a direct measure of benthic-pelagic coupling in aphotic sediments. Despite these advantages, there are few studies of chlorophyll with respect to small-scale hydrodynamics at the sediment surface.

In the present study, we combine image analysis, chlorophyll sampling, and spatial statistics to examine the correspondence between visible topography on the sediment surface and levels of photopigments. Our null hypothesis is that chlorophyll deposition will be enhanced by negative relief on the seabed. The general approach and preliminary results are presented herein.

Approach

We include several environments in this study in order to examine a range of both sediment transport regimes as well as sources of microalgal input to the sediments. Their inclusion is rationalized as follows:

(1) Intertidal sand - Eastern Passage, Nova Scotia; intertidal sands contain chlorophyll derived from benthic microalgae as well as phytodetritus. Sediment transport and ripple relief are well known to affect the distribution of chlorophyll (e.g. Grant et al. 1986).

(2) Intertidal mud - Minas Basin, Bay of Fundy; also containing both autochthonous and allochthonous chlorophyll, but perhaps less influenced by sediment transport, and more by bioturbation (Daborn et al. 1991).

(3) Arctic shelf mud - northern Baffin Bay (500 m); contains chlorophyll derived only from phytoplankton and ice algae during brief seasonal pulses

This list of sites and possibilities is neither exhaustive nor mutually exclusive, and reflects sites of opportunity as well as the initial thinking summarized in this paper. Specifically, the results presented here are for an initial trial of the approach in intertidal sand (Eastern Passage)

conducted in June 1998. Small ripples as well as polychaete burrows and feeding structures were present. Defined quadrats were photographed with a digital camera, after which chlorophyll sampling locations were marked with vial lids and the quadrat photographed again. The heights of various pits and mounds in the photograph were measured by ruler to the nearest 5 mm. The XY coordinates of the measured features were digitized from a color print using a digitizing pad. The vertical relief (Z) of each point was added to the grid, and the data imported to Surfer (Golden Software) where surface contour plots were made. A similar plot was produced using the chlorophyll sample data (acetone extraction and fluorometry) as the Z variable, and the contour surfaces compared.

A description of the 3-dimensional sediment surface may be achieved by regressing elevation (Z) and chlorophyll as polynomial functions of X and Y. If the trend surfaces of each dependent variable versus X and Y match, then all of the variation in chlorophyll may be explained by relief at the sediment surface. Grant et al. (1997) applied trend surface analysis to physical sediment reworking at 10^1-10^2 m scales on an intertidal sandflat. Legendre et al. (1997) provide more information on this approach.

Preliminary results and discussion

A digital photograph of the sampled sediment surface is depicted in Fig. 1. Various features include polychaete burrows, feeding pits, and fecal mounds (*Arenicola marina* is common at this site as are numerous spionids), and faint ripples. Samples were taken after a period of calm weather; more defined ripples characteristic of this site would be of interest in future sampling. Based on the low relief and initially crude resolution of elevation, these features were characterized only as 0, ±5 or ±10 mm in the Z dimension.
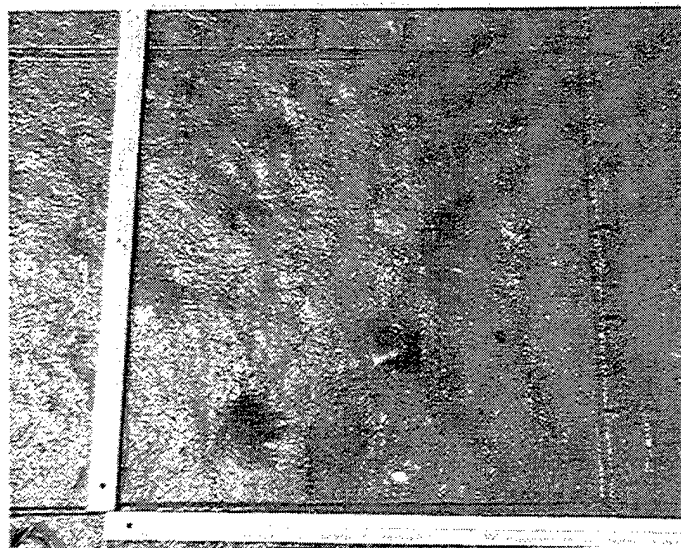
Fig. 1. Photograph of the sediment surface showing *Arenicola marina* feeding pit (lower left) and fecal pile (lower center), ripple trough (left center) and other small-scale features. Ruler on left is 50 cm in length.

A grid surface plot of this quadrat (Fig. 2A) indicates the relief derived from digitizing Fig. 1. Overlaying a similar plot using chlorophyll instead of elevation (Fig. 2B) provides a visual comparison of the two surfaces. Chlorophyll is generally high due to diatom growth in calm weather and there is some suggestion of elevated chlorophyll in the depressions along the western side of the quadrats.
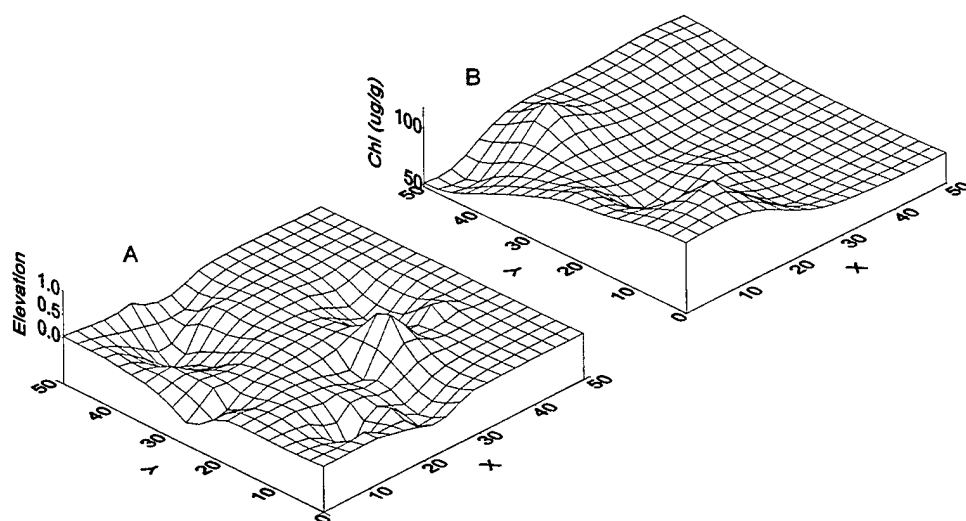
Fig. 2. Kriged surface plot of A. elevation (cm; n=58) and B. chlorophyll content (n=16) from quadrat shown in Fig. 1.

In order to quantitatively compare these two surfaces, a regression of chlorophyll versus elevation at the sampling locations is performed, and the residuals calculated. If the resulting unexplained variance in chlorophyll is a significant polynomial function of X and Y, then there is spatial structure in chlorophyll that is not due to surface relief. In the present example, elevation categories are not sufficiently detailed to regress against chlorophyll. However, since undertaking the initial intertidal studies, a more precise method of measuring vertical relief has been developed using calipers and a fixed upper reference point.

It is of interest to look for spatial structure in chlorophyll even without subtracting the variance due to elevation. A polynomial regression of chlorophyll using XY monomials (X, Y, X^2, Y^2, XY etc.) is not significant in the present example, suggesting a lack of spatial pattern at this scale. Because the sampling was conducted after an extended calm, chlorophyll results reflect growth of benthic diatoms, a process that may show less spatial pattern. In any case, greater sample sizes (as used subsequently) would provide additional power to the polynomial regression.

Although we have used only elevation as an independent variable and as a surrogate for deposition, other physical and biotic variables are desirable. These include direct measures of flow as we have done in previous flume work relating chlorophyll deposition to biogenic structure (Pilditch et al. 1998). Indicators of bioturbation such as oxygen penetration or carbohydrate content would also provide useful comparators. In more recent studies of Arctic sediments, we have co-sampled the chlorophyll grid for bacterial abundance. Where several independent variables are available, a multiple regression would be used to isolate residual variance for examination of remnant spatial structure.

It is apparent that depth need not be exclusively an indicator of deposition. For example, reduced chlorophyll might be associated with grazing in depressions caused by deposit-feeding worms, in which case elevation and sediment pigments might be positively associated. A sample set from rippled sands is of interest because sediment chlorophyll is known to be buried by ripple migration (Jenness and Duineveld 1985), providing an end member of boundary layer control of pigment distribution.

Several studies have used spatial autocorrelation to examine the distribution of sediment microalgae and co-dependence of grazing fauna (Sun et al. 1993), or define characteristic spatial scales of faunal dispersion (Eckman and Thistle 1988). Surface trend analysis differs in that the sampling scheme is less rigid and there is an emphasis on the presence of patterns rather than on scales of patchiness. Use of this technique with benthic microalgae is complex since they have growth patterns as well as responses to sediment transport. It is important to note that while benthic microalgae are affected by sediment transport, they also regulate resuspension/deposition by binding the sediment surface with extracellular material. The work of Bill Grant et al. (1982) was the first to quantify this effect in terms of boundary layer flow.

The deposition of phytodetritus to sediments in aphotic waters is somewhat different than the intertidal case in that pigments always originate from the water column and reach the sediment through passive deposition, where they may be reworked by fauna or redistributed by near-bottom flow. Trend surface analysis of sediment pigments and topography combined with other bed characterizations (e.g. roughness as in Wheatcroft (1994)) appears to be a useful approach for investigation of deposition and residence time of organic material in the sediments.

References
Boon, A. R., and G. C. A. Duineveld. 1998. *Mar. Ecol. Prog. Ser.* 162: 33-43.
Daborn, G. R., and others. 1993. *Limnol. Oceanogr.* 38: 225-31.
Eckman, J. E., and D. Thistle. 1988. *Deep-Sea Res.* 35: 1565-78.
Grant, J., U. V. Bathmann, and E. L. Mills. 1986. *Estuar. Coast. Shelf Sci.* 23: 225-38.
Grant, J., S. J. Turner, P. Legendre, T. M. Hume, and R. G. Bell. 1997. *J. Exp. Mar. Biol. Ecology* 216: 33-50.
Grant, W. D., L. F. Boyer, and L. P. Sandford. 1982. *J. Mar. Res.* 40: 659-77

Jenness, M. I., and G. C. A. Duineveld. 1985. *Mar. Ecol. Prog. Ser.* 21: 283-87.

Legendre, P., and others. 1997. *J. Exp. Mar. Biol. Ecol.* 216: 99-128.

Pilditch, C. A., C. W. Emerson, and J. Grant. 1998. *Cont. Shelf Res.* 17: 1869-85.

Sun, B., J. W. Fleeger, and R. S. Carney. 1993. *J. Exp. Mar. Biol. Ecol.*: 73-90.

Wheatcroft, R. A. 1994. *Cont. Shelf Res.* 14: 1167-90.

Yager, P. L., A. R. M. Nowell, and P. A. Jumars. 1993. *J. Mar. Res.* 51: 209-36.

Control of Sediment Transport Reference Concentration by Flux Rate Boundary Conditions

Thomas F. Gross,
NOAA/NOS/CS/CSDL/OP
1315 East-West Highway
Silver Spring, MD 20910
301/713-2809, ext. 139 fax 301/713-4501

When a sediment suspension is in steady state with the processes of erosion, deposition, resuspension and settling velocity, there must be either a limiting source of seabed sediment or a negative feedback process which limits further seabed erosion. The limiting process can be either suppression of near bed turbulent shear stress by stratification effects, suppression of shear stress by work required to maintain a bedload, or simply such a large suspended load that settlement can balance erosion. All processes can act together and their relative importance spans a parameter space governed by non-dimensional ratios of velocity scales,; turbulent shear velocity, particle fall velocity and erosion velocity. This parameter space is explored with the aid of a one dimensional energy closure suspended sediment model. Bottom boundary conditions are expressed as flux terms, rather than parameterized concentration. The rate of erosion velocity is a difficult parameter to quantify. This modeling exercise provides some guidance as to what range of conditions the rate of erosion will be an important factor in dictating suspended sediment load.

Alongshore Momentum Balances in Shallow Water

Steve Lentz (Woods Hole Oceanographic Institution),
Falk Feddersen & R.T. Guza (Scripps Institution of Oceanography),
Steve Elgar (Washington State University),
T. H. C. Herbers (Naval Postgraduate School)

Mean alongshore currents have been studied extensively in the surf zone and on the continental shelf. Mean alongshore currents in the surf zone are driven primarily by obliquely incident breaking waves (Whitford and Thornton, 1993 and references therein), whereas forcing by alongshore wind stress and pressure gradients are dominant on the shelf (Lentz, 1994 and references therein). Concurrent observations of currents, waves, and wind were collected for about 3 months on a 16 km-long transect extending from the shoreline to the 26 m isobath (Figure 1) as part of the Duck94-Coop experiment conducted during Fall 1994 at Duck, NC (Butman, 1994). Mooring or fixed towers supported vertical stacks of flowmeters at 5 sites in depths between 4 and 26 m and 14 additional flowmeters were deployed shorewards of the 4 m isobath. A lightning strike electrocuted some instruments. Others washed ashore.

Lentz et al. (submitted) show that the bottom drag and acceleration of vertically averaged alongshore currents at all mooring and tower sites are usually driven by alongshore wind stress and pressure gradients (Figure 2). An exception is when the 4-m site is within the surf zone so that breaking-wave driven currents are strong. The wind and wave forcing often reinforce each other, but occasionally the alongshore wind and wave forcing have opposite signs. When energetic swell opposes the wind the mean longshore current changes sign between the 4-m (within the surf zone) and deeper (seawards of the surf zone) sites (September 22, October 12-16, Figure 2a). The surf zone is narrower with less energetic swell, and similar current reversals sometimes occur farther shorewards near the crest of the sand bar.

Feddersen et al. (1998) focus on the region shallower than the 8 m isobath and consider cross-shore integrated alongshore momentum balances that do not require parameterization of poorly understood processes (eg. lateral mixing and wave rollers) that may be important to local momentum balances within the surf zone. Analysis of momentum balances over different cross-shore regions shows that in the surf zone wave forcing dominates forcing by wind and large scale pressure gradients. Wind stress contributes roughly 1/3 of the forcing shorewards of the 8 m isobath and the momentum balance over this region closes well (Figure 3). Although the surf zone and shelf studies use different drag laws (quadratic and linearized, respectively), in each case the drag coefficient is at least a factor of 3 larger within the surf zone than seawards of the surf zone. The causes of the increase are not understood.
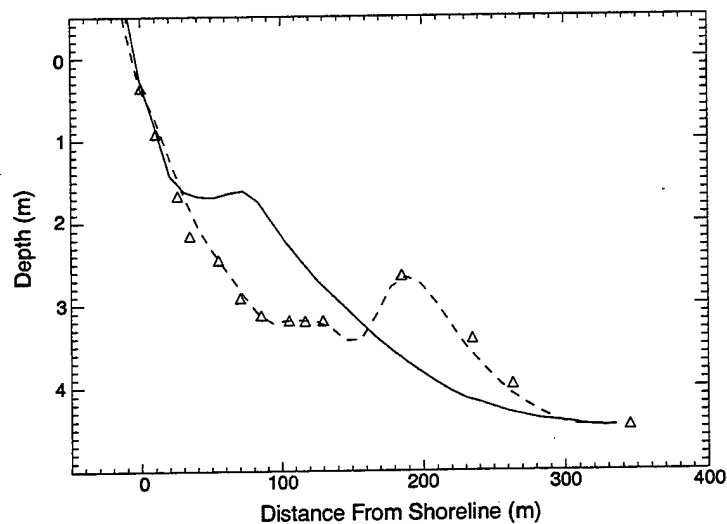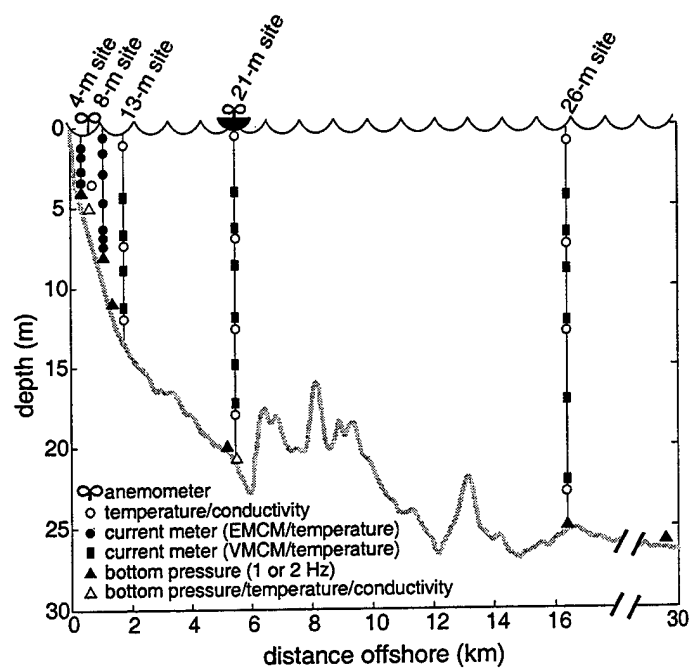
Figure 1: Upper: Cross-shelf instrument transect at Duck, NC. Thick curve is the seafloor. From Lentz et al. (submitted). Lower: The landward 0.4 km of the transect. A triangle represents a colocated bottom-mounted pressure sensor, current meter, and sonar altimeter. Bathymetry observed on August 25 (solid curve) and October 26 (dashed curve) is shown. From Feddersen et al. (1998).
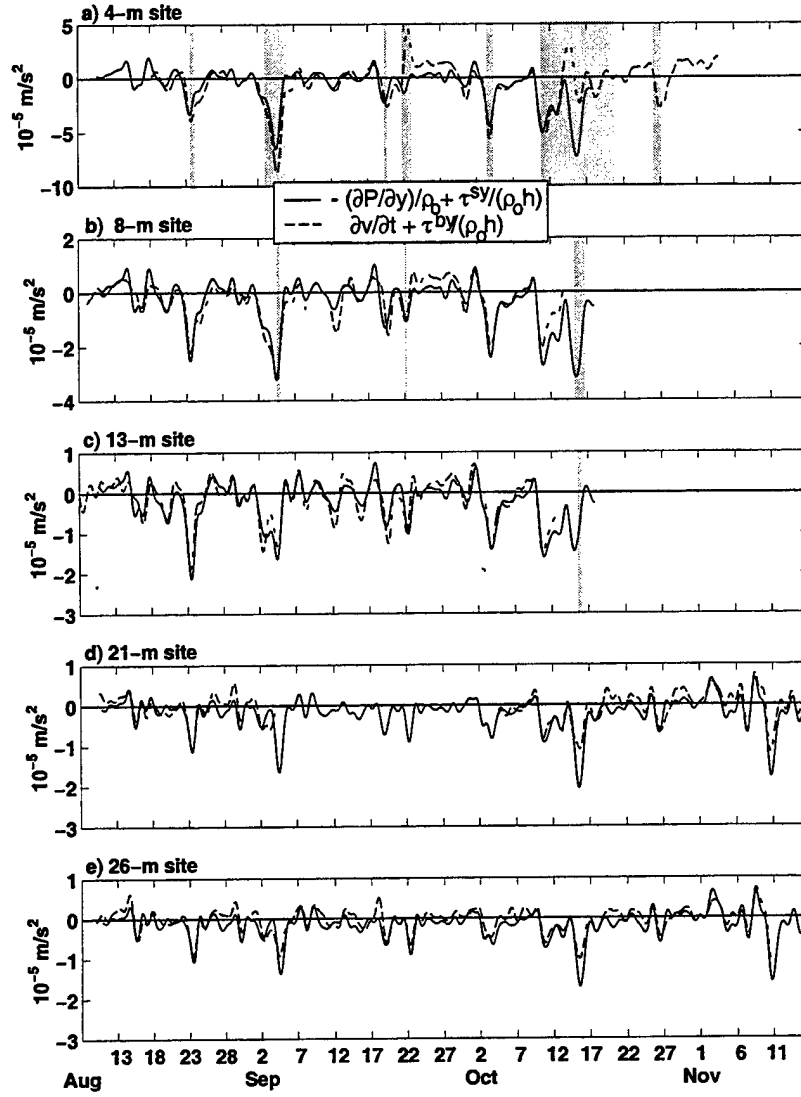
Figure 2: Time series of the combined alongshelf wind stress τ^{sy} and pressure gradient $\partial P/\partial y$ forcing $(\tau^{sy}/(\rho_o h) - (\partial P/\partial y)/\rho_o)$ and the response $(\partial \tilde{v}/\partial t + \tau^{by}/(\rho_o h))$ at each mooring site (ρ_o is a reference density, h is the water depth, y and t are the alongshore and time coordinates, and $\tilde{v}$ is the vertically averaged mean alongshore current). The bottom stress τ^{by} is estimated using a linear drag law ($\tau^{by} = r\tilde{v}$ where r is a constant drag coefficient.) The wave-induced radiation stress $\partial S_{xy}/\partial y$ is not included in the forcing. Thus, when a site is within the surf zone (shaded regions), discrepancies may be large. Squared correlations (excluding surf zone observations) between the forcing and response are greater than 0.65 at all sites. From Lentz et al. (submitted).
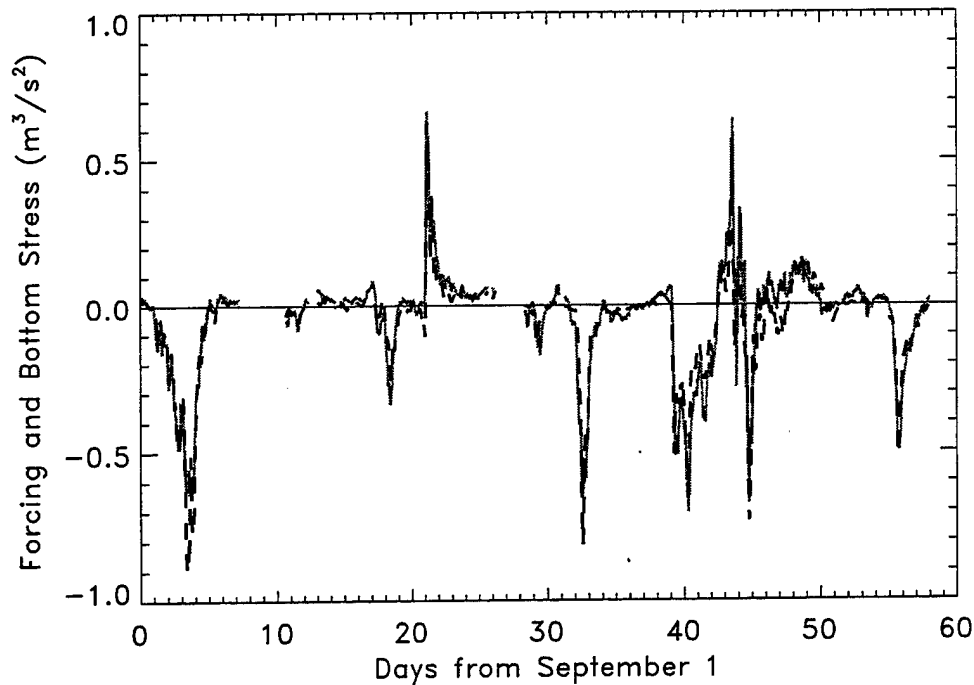
Figure 3: Hourly total forcing (wave + wind, $-\frac{S_{yx}}{\rho_o}|_{x_{8m}} + \int_0^{x_{8m}} \frac{\tau^{sy}}{\rho_o} dx$, solid) and quadratic bottom stress ($c_f \int_0^{x_{8m}} < |\vec{u}|v > dx$, dashed) integrated from the shoreline to 8-m depth versus time. (x is the cross-shore coordinate, x_{8m} is the coordinate of the 8 m isobath, c_f is a constant drag coefficient, v is the instantaneous alongshore velocity, and $\vec{u}$ is the instantaneous velocity vector). The correlation coefficient squared is 0.87. From Feddersen et al. (1998).

Acknowledgements

References

Butman, C. A., CoOP: Coastal Ocean Processes Study - Interdisciplinary approach, new technology to determine coupled biological, physical, geological processes affecting larval transport on inner shelf, Sea Technology, 35, 44–49, 1994.

Feddersen, F., R. T. Guza, Steve Elgar, T. H. C. Herbers, Alongshore momentum balances in the nearshore, J. Geophys. Res., 103, 15,667-15,676, 1998.

Lentz, S., R. T. Guza, S. Elgar, F. Feddersen, T.H.C. Herbers, Momentum balances on the North Carolina Inner Shelf, J. Geophys. Res., submitted.

Lentz, S. J., Current dynamics over the northern California inner shelf, J. Phys. Oceanogr., 24, 2461–2478, 1994.

Suspended Sediment Flux and Sediment Redistribution on the Continental Shelf

Courtney Harris
Patricia Wiberg
Department of Environmental Sciences
University of Virginia, Charlottesville, VA.

Introduction: Sediment transport on many continental shelves, including those off the U.S., is dominated by resuspension during energetic wave events. Resuspension events modify sea-floor stratigraphy by preferentially entraining and transporting fine sediment. To quantify this process, a two-dimensional, time-dependent solution to the transport equation has been formulated to account for advection and diffusion of suspended sediment in the bottom boundary layer of continental shelves (Harris, 1999; Harris and Wiberg, in prep.). Changes to sea bed stratigraphy resulting from resuspension and redistribution of sediments are calculated by conserving sediment mass between the water column and sea floor. Previous efforts at predicting suspended sediment concentrations in this environment usually neglected both time-dependence and spatial non-uniformities but compare well to field measurements (e.g. Wiberg, et al., 1994). The two-dimensional, time-dependent approach taken here is advantageous in shelf areas that display high spatial gradients in sediment availability or flow energy or contain abundant fine silts that require a long time to equilibrate with the flow field. This model has been used to determine the relative significance of time-dependence and spatial nonuniformity on shelf sedimentation patterns.

This study follows the path forged by Bill Grant in several ways, most obviously by using a theoretical, quantitative approach combined with field measurements to study shelf flows and sediment transport. The success of the wave-current interaction model developed by Grant and Madsen (1979) and Smith (1977), subsequent suspended sediment models (see, e.g. Smith, 1977; Glenn and Grant, 1987; Wiberg et al., 1994) and advances numerical computing facilitate extending these models to two spatial dimensions. This work has been conducted as part of the STRATA FORmation on Margins project (STRATAFORM), developed in the wake of the CODE and STRESS experiments in which Bill Grant and his legacy was a driving force (see Nittrouer and Kravitz, 1995; Beardsley and Lentz, 1987; and Trowbridge and Nowell, 1994). The STRATAFORM initiative is to investigate through field and theoretical methods, the mechanisms through which shelf stratigraphy is formed and modified over time-scales ranging from single storm or depositional events to eons.

The time-dependent, two-dimensional modeling framework allows us to evaluate the significance of flux divergence and time-dependence in sediment transport and bed reworking on the continental shelf. The calculations require as input driving wave properties and current velocities, sediment size distributions along the modeled transect, and hydrodynamic sediment properties. The model calculates suspended sediment concentration and sediment flux as a function of height above the bed along the transect for each grain size modeled. Net erosion and deposition are also calculated for each grain size, and used to evaluate changes to fine-scale sediment grading with depth in the bed.

Objectives: The contributions of various sources of time-dependence and flux divergence are explored by contrasting sedimentation patterns of a set of increasingly realistic shelf systems to a series of increasingly realistic flow fields. First, a uniform system to steady waves and currents is considered. Next, the same steady forcing functions are used to drive calculations on a cross-shelf system representing the Eel River shelf off northern California, the site of much STRATAFORM research, to illustrates the sources of flux divergence along a realistic cross-shelf transect. The final cases considered the response of the cross-shelf transect to time varying wave and current time series to evaluate the response of a cross-shelf transect to more realistic forcing functions. In this manner, we address several objectives:

- Demonstrate the ability of a two-dimensional, time-dependent transport model to predict the redistribution of sediment in the bottom boundary layer of continental shelves.

- Evaluate the significance of time-dependent and spatial terms in the advection and diffusion of sediment in the bottom boundary layer.

- Compare the sources of time-dependence (such as sediment advection and unsteady forcing functions) and non-uniformity (from gradients in flow energy and sediment availability) in this system.

- Apply the calculations using field data obtained on the Eel River shelf.

Uniform calculations: Though the uniform, time-dependent case is the most abstract case considered, it provides a framework with which to introduce the calculations and is most similar to previous efforts at modeling resuspension processes. Comparison of the uniform and two-dimensional calculations highlight the contribution of flux divergence to bed reworking, and demonstrate the utility of solving the two-dimensional problem. The forcing conditions used for this case were steady waves with significant heights of 5m, and geostrophic currents with speeds of 10cm/s directed off-shelf and poleward. Model calculations of bottom boundary layer velocity are driven by a prescribed reference velocity at the top of the model grid (the height of the Ekman layer) and decrease to zero at a roughness height dependent on shear stress and sediment size (figure 1a). Because this model is most concerned with sediment transport calculations, the velocity calculations have been simplified by neglecting density stratification, advection of momentum, and time dependence in the velocity field. The suspended sediment concentration for each grain size is numerically calculated using a flux boundary condition close to the sea floor, turbulence profiles provided by the velocity calculations, and the two-dimensional, time-dependent transport equation. The product of the velocity and suspended sediment calculations provide estimates of suspended sediment flux (figure 1). During an energetic flow event, entrainment of the finer sediment fractions lowers the surface of the sediment bed (figure 2). In a uniform system, all of the sediment removed from the bed can be accounted for by the volume of overlying suspended sediment. As flow conditions wane, suspended sediment settles back to the bed, and the bed surface returns to it's original location (figure 2a). Because the uniform model does not account for changes in sediment or flow properties along the flow
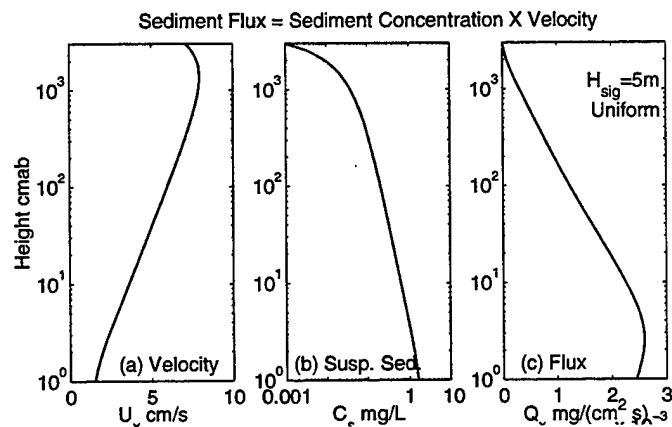
Figure 1: Calculations of (a) velocity, (b) suspended sediment concentration, and (c) suspended sediment flux for a uniform transect that has reached steady state.
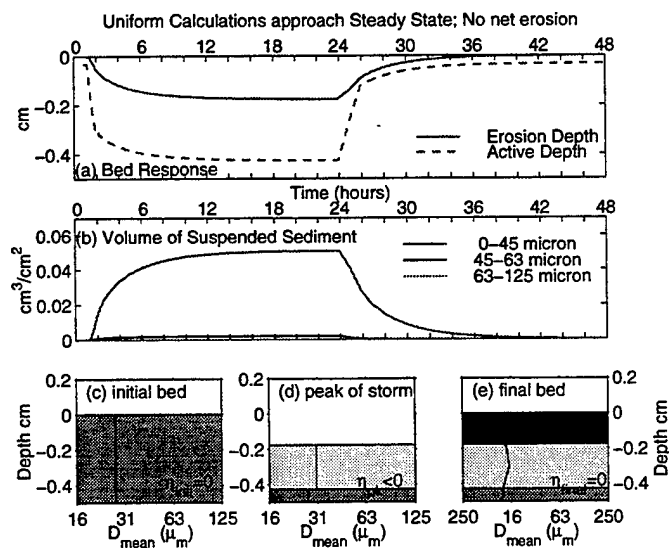

Figure 2: Calculations of (a) erosion depth and (b) volume of sediment in suspension for the uniform transect as it approaches steady state. Small size grading of (c) the initial bed, (d) at the peak of the resuspenson event, and (e) once all sediment has been redeposited.

path, it can not directly account for flux divergence, and no net erosion or deposition is calculated. However, the uniform model captures the time-dependent response of the system, predicts peak suspended sediment volumes and sediment concentrations, and also can be used to estimate the characteristics of the fining-upward bed created by resuspension and deposition (figure 2c–e).

Cross-shelf transect; steady forcing: Continental shelves exhibit variations in flow conditions and sediment properties that create spatial gradients in sediment flux that can account for significant net erosion and deposition. This is illustrated by considering a cross-shelf transect based on the Eel River shelf, off of northern California (figure 3). This
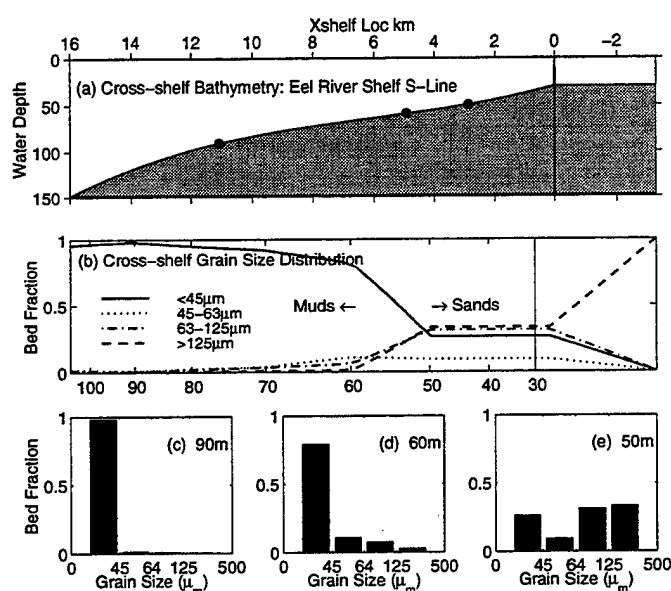

Figure 3: Transect used to represent the Eel River shelf. (a) Model bathymetry and (c) cross-shelf grain size distributions used, based on (d)–(e) surficial grain size distributions from several locations on the Eel River shelf provided by D. Drake, pers. comm.

shelf is approximately 20km wide, with the shelf break occurring at a water depth of about 150m, and exhibits a sharp transition between sandy and muddy beds at a water depth of approximately 60m. It contains primarily fine sands up to a water depth of 50m, and muddy sediment derived from winter flooding of the Eel River in the mid-shelf region between water depths of 70m and 90m. To examine flux divergence in this setting, a transect modeled after the Eel River shelf (figure 3) was subject to the steady energetic flow case considered above. Here, when flow energy increases, the system at first shows a similar response to that calculated for a uniform system, with entrainment of fine sediment and erosion across the model grid (figure 4). However, fine sediment makes up a small portion of the bed at the upstream, shallow portion of the transect, where wave shear stresses are most effective at entraining sediment (figure 3c). The available fine sediment is quickly
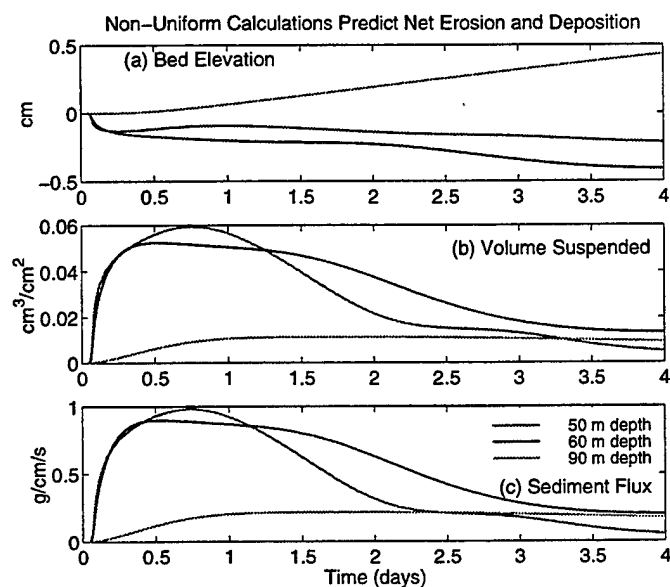
Figure 4: Calculations of (a) bed elevation, (b) volume of suspended sediment, and (c) sediment flux for three water depths (see legend) subjected to steady energetic waves.

eroded from the upstream locations, and advected off-shelf. As the fine sediment source is depleted, flux and suspended sediment calculations decrease, so that the system displays a time-dependent response to steady forcing functions (figure 4). The source of this time-dependence is the evolution of the sea bed. For the waves and current velocity considered here, this system shows flux divergence and therefore erosion shoreward of approximately 60m, from the combination of high wave shear stress and lack of fine-grained sediment. Further downstream, the wave shear stress decreases to below that needed to suspend significant amounts of sediment, and flux convergence in this area results in deposition. For moderate wave energies where the wave-current base does not exceed the critical shear stress of the sediment over the mid-shelf mud bed, the flux divergence that comes from the gradient in wave shear stress dominates the depositional pattern. More energetic waves are required before the presence of readily available fine sediment in the mid-shelf can be entrained in great quantities.

Cross-shelf transect; storm forcing: Actual resuspension events are driven by increases in wave-current shear stress due to the presence of energetic waves that may persist for a few hours or days. To examine flux divergence patterns over the time-scale of a single resuspension event, the cross-shelf model transect for the Eel River shelf was subjected to a six-day long, smoothly-varying time-series of waves (figure 5). The event had peak wave heights of 5m and wave periods of 10s. A steady current velocity of 10cm/s was used, which is representative of mean currents on this shelf, and was directed off-shelf and poleward. Estimated shear stresses for this event were capable of resuspending sediments
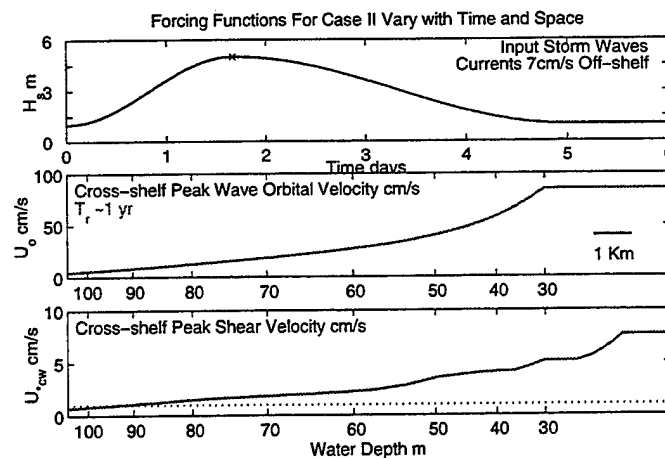
Figure 5: Driving forces used to represent a six-day long moderate storm. (a) Significant wave height. (b) Wave oribital velocity and (c) shear velocity with depth in the bed.

to a water depth of approximately 80m. The high shear stresses, combined with off-shelf directed flow remove fine sediment from the shallow portion of the model grid and transport it to the mid- and outer-shelf where it is deposited as a fining upward layer (figure 6). The net erosion and deposition over the course of the resuspension event depends on the flux divergence at each grid point. In the beginning of the resuspension event, entrainment of sediment increases the volume of suspended sediment at a location and lowers the sediment bed. But by the end of the resuspension event, all of the suspended sediment has settled back to the bed, and the final location of the bed surface at each point equals the time-integrated sediment flux divergence, corrected for bed porosity.

Cross-shelf transect; realistic forcing: During a resuspension event the bottom boundary layer current velocities are variable and time series of significant wave height are often spiky. The time-scales over which the forcing conditions change influence the manner in which the suspended sediment and flux fields respond during a resuspension event. To examine this, we used the cross-shelf model transect based on the Eel River shelf, and a time-series of waves and currents measured at this location in January, 1996 (Ogston and Sternberg, in press, figure 7). As is typical, the current velocity fluctuates widely during this 8-day time series, ranging from approximately 40 cm/s on-shore to 50 cm/s offshore, but the mean cross-shelf currents of about 7 cm/s off-shelf are similar to the one used for the simplified model runs. Peak wave heights during this time reached 6.5m, but were often similar to the value used previously (5m).

Though shear velocities are not much higher for this case, predicted volumes of suspended sediment are significantly increased compared to previous cases. This is particularly apparent over the muddy bed (90m, figure 8). The volume of suspended sediment responds to the fluctuations in the forcing functions, particularly the current velocity. Sediment is dispersed from the muddy bed (70-90m), and deposited both off the shelf and
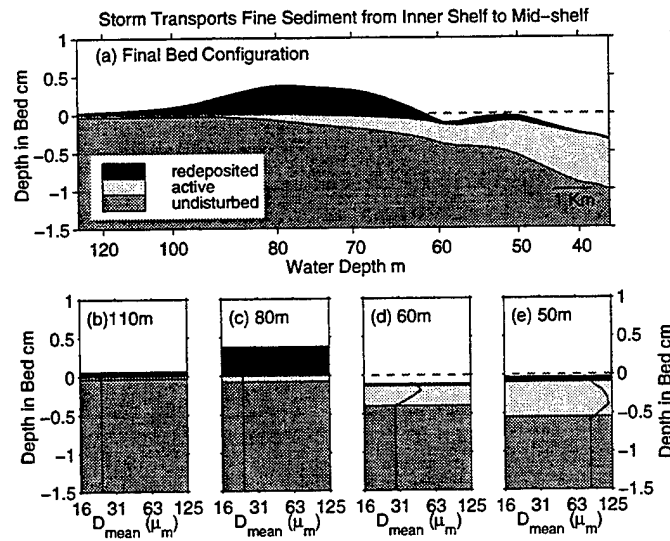
Figure 6: (a) Final configuration of sediment bed as reworked by the time series shown in figure 5. (b–e) Small scale bed grading shown for several water depths.
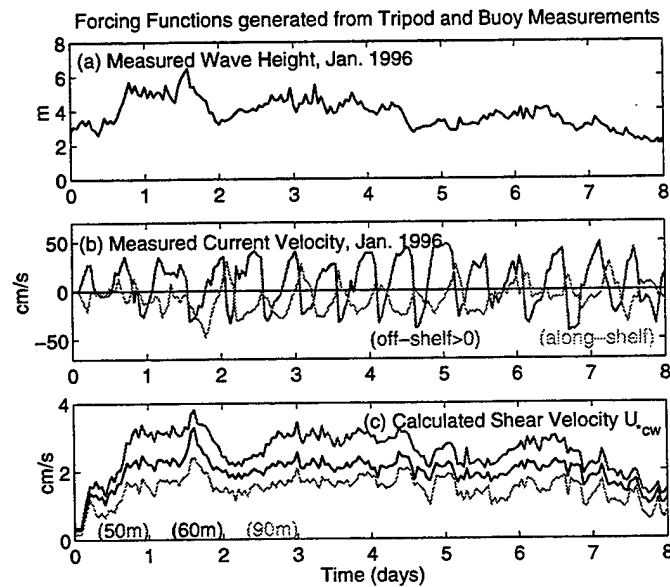

Figure 7: Measured (a) waves and (b) current velocities used to drive model calculations. Wave heights from NDBC buoy 46022, current velocity measured 123 cmab (Ogston and Sternberg, in Press).
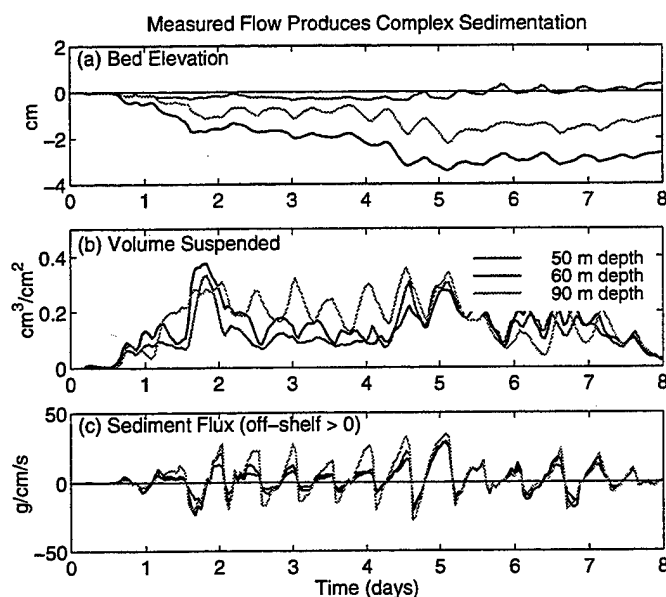
Figure 8: Flux divergence, volume of suspended sediment, and bed elevation calculated for time series in figure 7 for several water depths (see legend).

on the inner shelf (figure 9). However, fine-grained sediment deposited on the inner shelf would form a transient deposit, because the wave energy in this region is usually more than adequate to suspend this sediment. The fact that fine grained sediment does remain on the mid-shelf mud bed implies that another process must be limiting the suspension of sediment in this region.

Summary of Results:

- The two-dimensional, time-dependent transport model can be used to quantify suspended sediment transport and bed reworking by resuspension in the continental shelf bottom boundary layer.

- Calculations of net erosion and sediment redistribution can be accomplished directly by using a two-dimensional approach.

- Both sediment availability and wave energy affect flux divergence patterns in a shelf such as the one off-shore of the Eel River. For a moderately energetic storm, the gradient in wave energy is more significant than the gradient in sediment availability.

- Advection of sediment by realistic current velocities can increase suspended load across the shelf.

- The major source of time-dependence in the system appears to be the unsteadiness of waves and current velocities in the bottom boundary layer. The suspended sediment
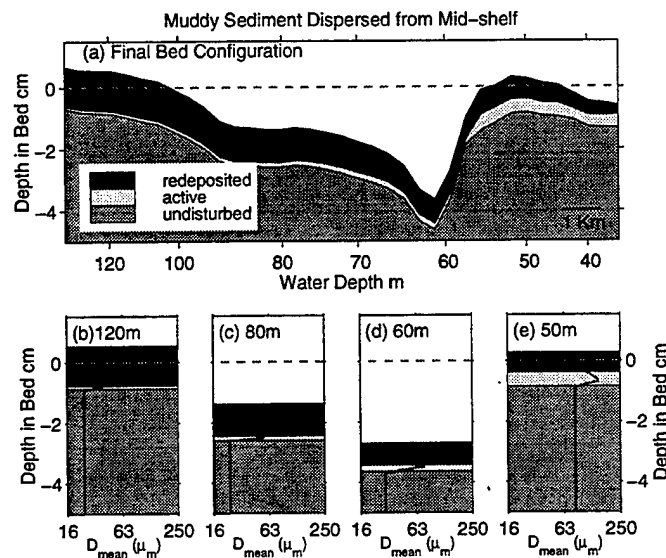
Figure 9: (a) Final configuration of sediment bed as reworked by the time series shown in figure 7. (b–e) Small scale bed grading shown for several water depths.

field would seldom be equilibrated in such a rapidly fluctuating system.

- The mean off-shelf flows measured on the Eel River shelf during energetic times implies a net off- shore transport. Calculations predict some transport towards shallower waters during times of tidally-influenced on-shore flow. However, such deposits would be unlikely to persist, because of the high wave energies combined with net-offshore flow would eventually remove the fines.

Conclusions: A two-dimensional, time-dependent solution to the advection/diffusion equation has been used to predict the transport of suspended sediment in the bottom boundary layer of continental shelves (Harris, 1999; Harris and Wiberg, in prep.). By accounting for entrainment and deposition of suspended sediment, these calculations are also used to predict changes to sea bed stratigraphy from resuspension processes (Harris, 1999; Harris and Wiberg, in prep.). The model described here could be improved by including a more sophisticated representation of shelf circulation, by accounting for density-induced stratification, advection of momentum, and time-dependence in the velocity calculations. Incorporation of sediment transport into circulations models is an exciting direction in which to take this work. However, even with these limitations this model provides a promising step forward in our ability to model sedimentation in the coastal zone. Unlike the one-dimensional, steady sediment resuspension models from which this model grew, the two-dimensional, time-dependent approach enables us to calculate net erosion and deposition. By numerically representing the resuspension and redistribution of shelf sediments due to energetic

bottom boundary layer flows, we are able to evaluate the relative importance of flux divergence and advection in shelf sedimentation and predict shelf-wide sediment transport and bed reworking. This takes a natural step in the direction pioneered by Bill Grant and his colleagues (Grant and Madsen, 1979; Smith, 1977; Glenn and Grant, 1987).

References

- Beardsley, R. and S. Lentz (1987). The coastal ocean dynamics experiment collection: an introduction. Journal of Geophysical Research, Vol. 92(C2), 1455-1463.

- Glenn, S. and W. Grant (1987). A suspended sediment stratification correction for combined wave and current flows. Journal of Geophysical Research, Vol. 92(C8), 8244-8264.

- Grant, W. and O. Madsen (1979). Combined wave and current interaction with a rough bottom. Journal of Geophysical Research. Vol. 84(C4), 1797-1808.

- Harris, C.K. 1999. The importance of advection and flux divergence in the transport and redistribution of continental shelf sediment. Ph.D. Thesis. University of Virginia, Charlottesville VA.

- Harris, C. and P. Wiberg (in prep.). A two-dimensional, time-dependent model of suspended sediment transport and bed reworking for continental shelves. Computers and Geosciences.

- Ogston, A. and R. Sternberg (1999). Sediment transport events on the Northern California continental shelf. submitted to Marine Geology. In Press.

- Nittrouer, C. and J. Kravitz (1995). Integrated continental margin research to benefit ocean and earth sciences. EOS, Transactions, American Geophysical Union. Vol. 76(12), 121, 124, 126.

- Smith, J.D. (1977). Modeling of sediment transport on continental shelves. In E. Goldberg, I. McCave, J. O'Brien, and J. Steele (Eds.), the Sea, Volume 6; Marine Modeling, Chapter13, pp. 539-577. New York: John Wiley.

- Trowbridge, J. and A. Nowell (1994). An introduction to the sediment transport events on shelves and slopes (stress) program. Continental Shelf Research. Vol. 14(10/11), 1057-1061.

- Wiberg, P., D. Drake, and D. Cacchione (1994). Sediment resuspension and bed armoring during high bottom stress events on the northern California continental shelf: measurements and predictions. Continental Shelf Research. Vol. 14(10/11), 1191-1219.

On Remotely Probing the Structure of the Bottom Boundary Layer Over an Evolving Seabed

Alex E. Hay[1], Carolyn Smyth[1], Len Zedel[2] and Todd Mudge[1]

[1]Department of Oceanography, Dalhousie University,
Halifax, Canada

[2]Department of Physics and Physical Oceanography, Memorial University of
Newfoundland, St. John's, Canada

Introduction

In their pivotal review of the continental shelf bottom boundary layer, Grant and Madsen (1986) identified some of the measurement problems which at that time impeded progress toward improved knowledge of the dynamical processes operating at and above a mobile seabed. A consequence of their discussion of both the need for improved observations and the difficulties in obtaining them has been the development over the ensuing decade of a range of new sensors which are providing unprecedented views of this complex environment.

In this paper, results are presented from a nearshore field experiment in which several recently developed sensors were deployed to remotely probe the vertical structure of the flow and suspended sediment fields in the bottom boundary layer, simultaneous with detailed remote measurements of bed topography. The motivation for making remote measurements is the need to minimize flow disturbance in the vicinity of the bed. The sensors deployed included rotary imaging sonars (Hay and Wilson, 1994); a coherent Doppler profiler, or CDP (Zedel and Hay, 1998a and b); and a laser-video imaging system (Crawford and Hay, 1998). Results from the CDP and the rotary sonars are presented here.

The Experiment

The experiment was carried out in 3.5 m mean water depth at Queensland Beach, Nova Scotia, in September 1995. Particular features of this site are that it is a planar pocket beach facing a narrow opening onto the continental shelf, so that waves tend to be normally incident to the shoreline, and longshore currents small. The instruments were mounted approximately 70 cm above the bottom, on a horizontal mast cantilevered in the seaward direction away from a quadrupod support frame (see Crawford and Hay, 1998). The median sand grain diameter was 170 μm. The deployment lasted 11 days. One major storm event was captured. Otherwise the forcing was moderate to weak.

Results

Bed State

The 2-dimensional images of the seafloor obtained with the rotary fan beam sonar were used to characterize the state of the seabed as a function of time. Figure 1 shows 4 m × 2 m rectangular subimages, taken from the full 5-m radius fanbeam images, of the seabed on the seaward-facing side of the frame. The subimages illustrate the different bed states which were observed, and are presented in order of increasing hydrodynamic forcing from irregular ripples at the top (low energy), through cross and linear transition ripples, to flat bed at the bottom (high energy).
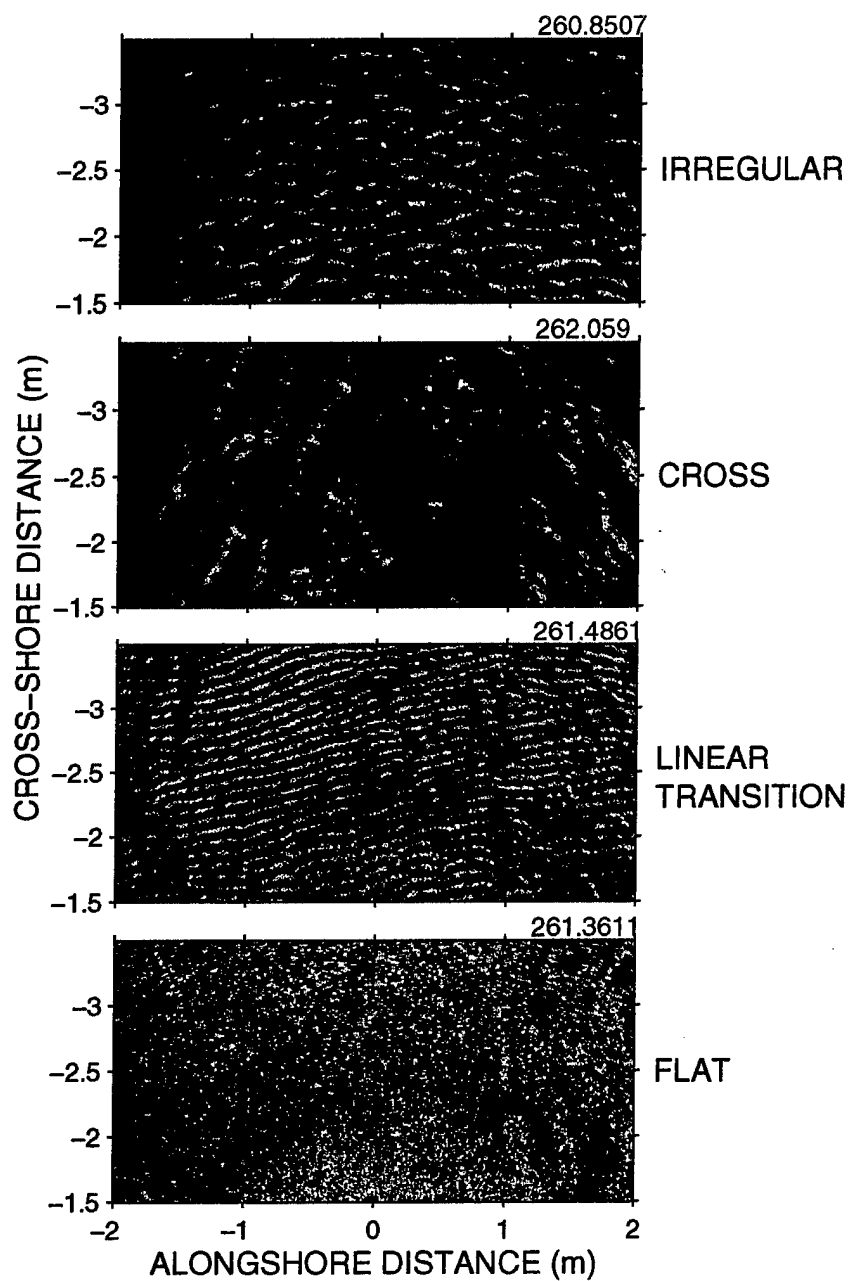
Figure 1: Characteristic bed states during the Queensland experiment. Each panel is a 4 m × 2 m subimage from a 10 m diameter rotary fan beam image. The offshore direction is toward the top of each panel. The $x - y$ origin is the location of the fan beam sensor.

Figure 2 shows the evolution of bed state during the experiment. The solid light blue circles in Figure 2d indicate different ripple classes, representing distinctly different bed states, determined visually from the fan beam imagery. As in Figure 1, bed state categories are: flat bed (Fl), linear transition ripples (Tr), cross ripples (Cr) and irregular (or short-crested) ripples (Ir). A strong correspondence between ripple class and grain roughness Shields parameter is indicated, illustrating the previously mentioned close association in these data between bed state and forcing energy.

The upper 3 panels in Figure 2 show results from radial spectral analysis of the fan beam data in a 60° azimuthal sector, centred on the offshore direction. The spectra have been averaged into 3 spatial frequency bands: high (10-15 cycles/m), intermediate (3-10 cycles/m) and low (0.5-3 cycles/m). Typically, most of the energy is in the intermediate band, so the spectra are yellow, as opposed to red. The spectral yellowing is due to the 0.5 cpm high-pass filter used to remove beam pattern effects prior to computing the spectrum, and to the fact that the fan beam detects variations in bottom slope, as opposed to bed elevation. Flat bed is evident during the peak of the storm, when $\Theta_{2.5}$ exceeded 0.7, as low energy in all three bands. Transition ripples are the relatively narrow (in azimuth) and short-lived peak in the high frequency band, centred on roughly 10° azimuth, and occurred during the storm for $\Theta_{2.5}$ about 0.5. Cross ripples occurred both as the storm waxed and waned, and later during moderate forcing conditions on days 264-265 ($0.2 \leq \Theta_{2.5} \leq 0.4$). Cross ripple occurrence was associated with increased radial spectral energy at low frequencies, with distinct peaks at $\pm 20°$ azimuth, and with reduced radial spectral energy at mid frequencies, centred on 0° azimuth. Irregular ripples are evident as higher, more (azimuthally) isotropic energy in the intermediate band, and occurred during periods of weak forcing ($\Theta_{2.5} \leq 0.1$).

CDP Data

Figure 3 shows time series of vertical profiles of the mean on-offshore horizontal velocity U, the rms vertical velocity in the incident wave band $\tilde{w}_{rms}$, and mean suspended sediment concentration C. These data were obtained with the CDP. The $\tilde{w}_{rms}$ data decay toward the bed during the peak of the storm, consistent with wave orbital motions in intermediate water depth. For much of the remainder of the record, the vertical motions in this frequency band are bottom intensified, especially during periods of well-developed irregular ripples (Figure 2). Mean suspended sediment concentrations do not show any particular correspondence to these bottom intensified wave motions.

Horizontal velocities determined with the CDP extend only to within about 5 cm of the bed. U was negative (offshore) during the peak of the storm, consistent with mass flux conservation arguments associated with the wave-induced Stokes drift at the surface, and of variable sign during the remainder of the record. There are periods of bottom-intensified mean flow, directed either onshore (e.g. Yearday 269), or offshore (e.g. Yearday 263). The mean cross-shore velocities were small (less than 5 cm/s), indicating that wave motions were the dominant forcing term in the bottom boundary layer during this experiment.

Wave Bottom Boundary Layer Model Comparison

Figure 4 shows vertical profiles of the incident wave band $\tilde{w}_{rms}$, ensemble-averaged for many data runs for the different bed states: 12 runs for flat bed; 13 for linear transition ripples; 36 for cross ripples; and 92 for irregular ripples. (The time duration of each CDP run was about 8 min.) At heights greater than O(10 cm) above the bottom, the profiles

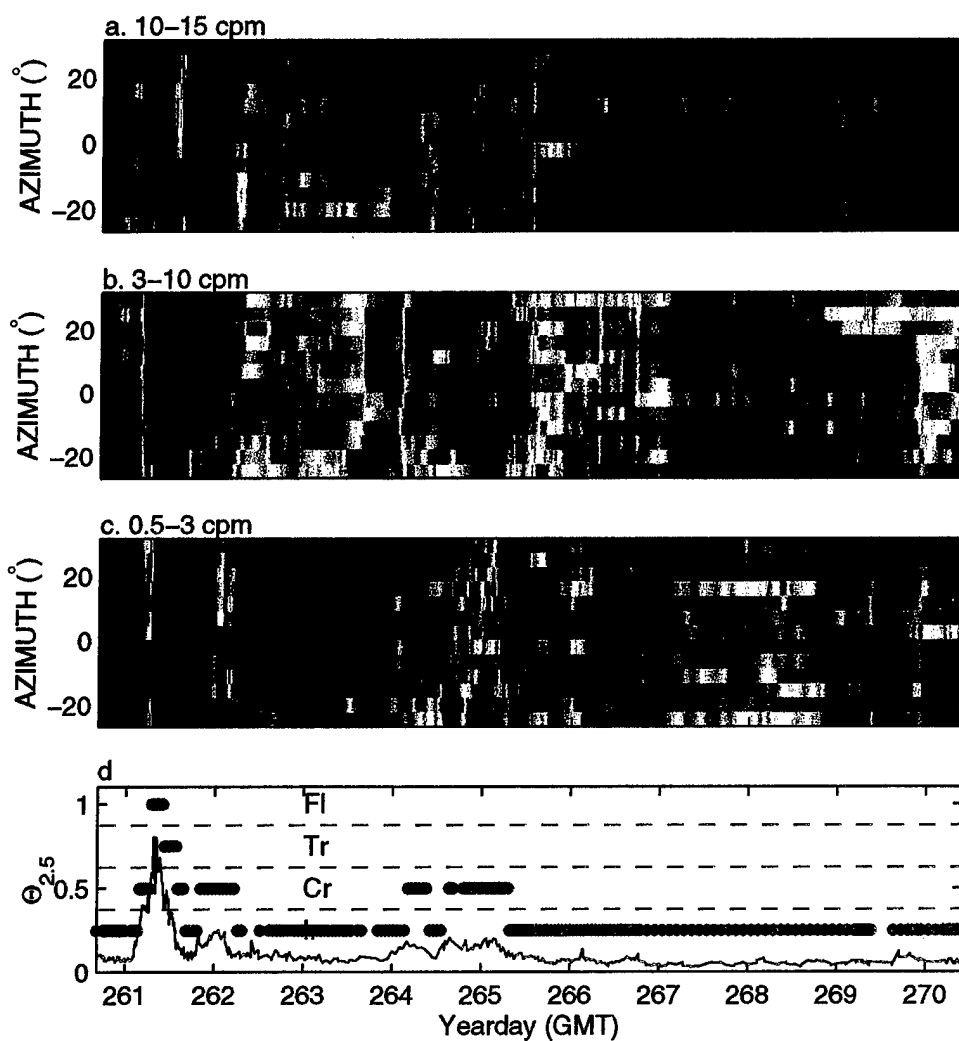Figure 2: Bedform characteristics during the Queensland experiment: a. high spatial frequency band versus time and azimuth; b. intermediate; and c. low. Blue means low spectral energy; red high. The different bed states (see text) are indicated in d. flat bed (Fl), high energy transition ripples (Tr), cross ripples (Cr) and Irregular ripples (Ir), together with $\Theta_{2.5}$, the grain roughness Shields parameter.
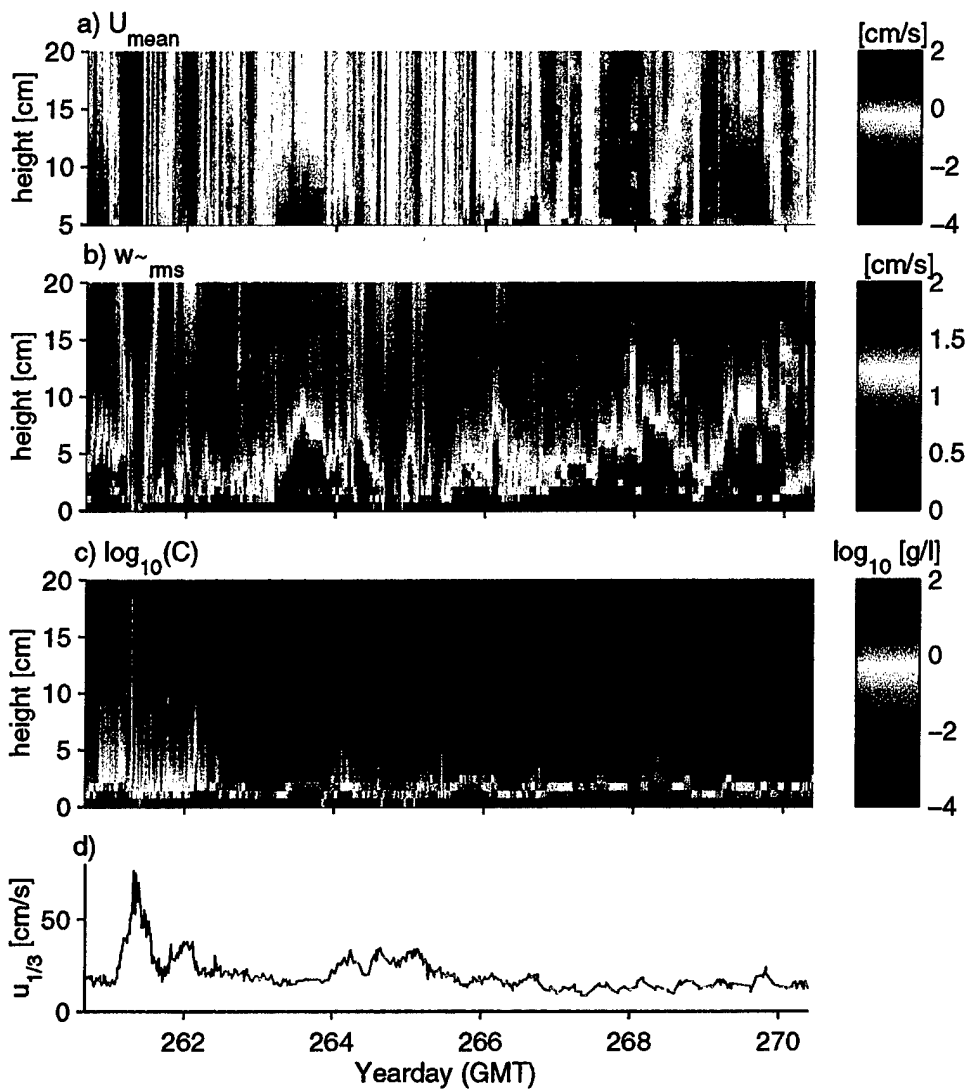
Figure 3: CDP results. Vertical profiles of: a. the mean on-offshore horizontal velocity U; b. vertical velocity in the incident wave band $\tilde{w}$; c. mean suspended sediment concentration C; and d. significant wave orbital velocity, $u_{1/3}$.

show the linear decay toward the bed expected on the basis of linear wave theory. Closer to the bed, many of the profiles exhibit a pronounced peak at about 3 cm height. This peak is more pronounced for the lower energy, steeper (Figure 2) ripple types, and is absent for the flat bed runs. For heights less than about 3 cm, the profiles decay sharply to near zero values at the bed.

Vertical profiles of the rms wave orbital velocity were computed assuming linear wave theory. The effects of flow over the ripple topography were computed using the potential flow theory developed by Davies (1983). These calculations used ripple wavelengths and amplitudes for the three spatial frequency bands shown in Figure 2, determined from the rotary pencil beam profiles (not shown). The effects of bottom friction were included using an eddy viscosity model of the Wave Bottom Boundary Layer (WBBL) similar to the Grant and Madsen model, with the time-independent eddy viscosity varying with height z as $\kappa u_* z$, κ being von Karman's constant and u_* the friction velocity.

The model results are shown in the lower panel of Figure 4. They compare favorably with the measurements, at least as far as the qualitative shapes of the profiles for the different bed states are concerned. The profiles for rippled beds exhibit a near bottom peak, whereas the flat bed profile does not, much like the measurements. The magnitudes of the peaks are not well reproduced however. It is possible that this quantitative difference between theory and experiment is due in part to including the low spatial frequency band amplitude and wavelength in the model. This scale makes a significant contribution to the vertical structure, but its inclusion in the theory may not be justified for comparisons with the present data. At large distances from the boundary, the model predictions are lower than the measurements for all bed states. The reasons for this difference are not yet understood, and are being pursued.

The good qualitative agreement between the shapes of the measured and predicted profiles is encouraging. In particular, the model results demonstrate that the near bottom peak in $\tilde{w}_{rms}$ for rippled beds is associated with potential flow over the ripple topography, combined with a thin frictional layer near the bed. For the flat bed case, the measured and predicted profiles both become nearly height-independent in the region immediately above the bottom frictional layer: this is also an inviscid effect, and is associated with oscillatory flow over a finite mean bottom slope (about 1° at the instrument location).

Summary

The above comparisons between measurements and second order potential flow theory demonstrate that bedform geometry and O(1°) bottom slopes have first order effects on vertical wave orbital velocities in the WBBL.

These results also demonstrate a new and comprehensive measurement capability for investigating sediment suspension processes and the evolution of the seabed. Several important science questions arise. Central among these is the observed high degree of 3-dimensionality in bedform geometry at low to intermediate bottom shear stresses. This 3-dimensionality is often not part of the textbook view of bedforms, particularly bedform modelling, and both its causes and effects on sediment suspension and bottom boundary layer structure need further study.
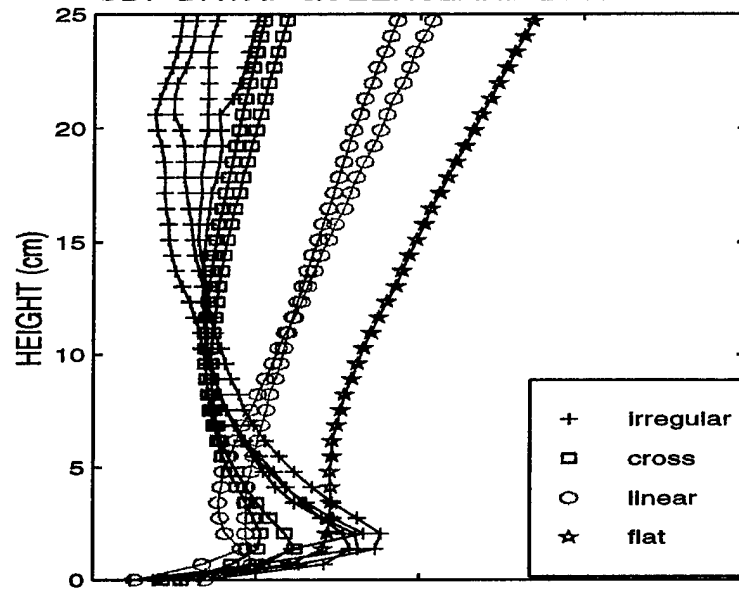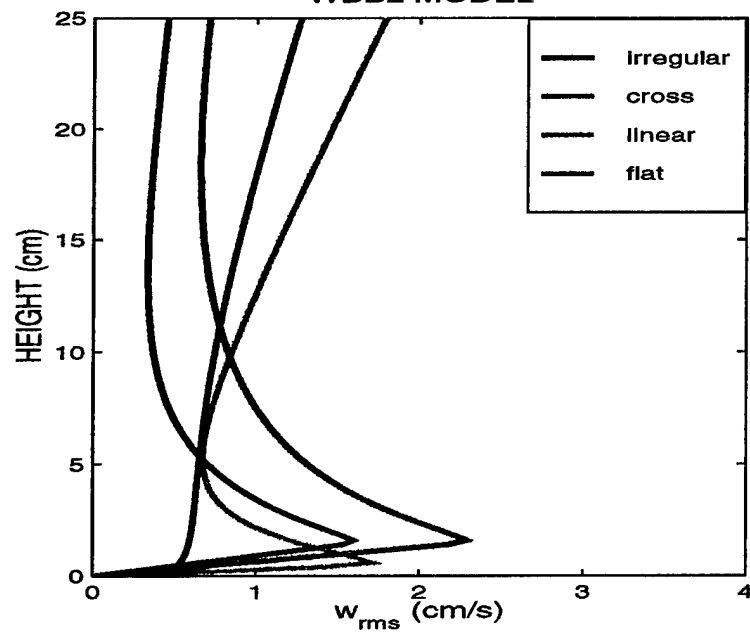
Figure 4: Vertical profiles of w_{rms} in the incident wave band for different bed states: upper panel, measured (ensemble-averaged CDP profiles); lower panel, model predictions.

References

Crawford, A. M., and A. E. Hay. 1998. A Simple System for Laser-Illuminated Video Imaging of Sediment Suspension and Bed Topography. IEEE J. Oceanic. Eng. 23(1), 12-19.

Davies, A. G. 1983. Wave Interactions with Rippled Sand Beds. In *Physical Oceanography of Coastal and Shelf Seas*, B. Johns (editor), Elsevier, 1-65.

Grant, W. D., and O. S. Madsen, 1986. The continental shelf bottom boundary layer, *Ann. Rev. Fluid Mech.*, *18*, 265–305.

Hay, A. E., and D. J. Wilson, 1994. Rotary sidescan images of nearshore bedform evolution during a storm, *Mar. Geol.*, *119*, 57–65.

Zedel, L., and A. E. Hay, 1998a. A Coherent Doppler Profiler for High Resolution Particle Velocimetry in the Ocean: Laboratory Measurements of Turbulence and Particle Flux. *J. Atmos and Ocean. Tech.* (in press).

Zedel, L., and A. E. Hay, 1998b. Direct Observations of Wave Induced Sediment Flux and Turbulent Velocities in a Wave Flume. *Proc. 26th Int. Conf. Coastal Engineering*, 22-26 June 1998, Copenhagen (in press).

Suspicions about Settling Columns

Paul S. Hill *and Timothy G. Milligan [†]

1 Introduction

Field-deployed settling columns show that the clearance rate of fine sediment depends on initial concentration (Dyer et al., 1996). A compelling and widely accepted explanation for such data is that fine sediment sinks in particle agglomerates called flocs, whose size and settling velocity increase with increasing concentration. Direct observations of flocs in the field and in the laboratory, however, do not support the hypothesis that size and settling velocity vary with concentration (ten Brinke, 1994; Milligan and Hill, 1998).

Floc breakup and reformation within settling columns has been proposed an alternative explanation for the observed dependence of clearance rate on concentration (Milligan and Hill, 1998). According to this hypothesis, component particles and small flocs are liberated from larger flocs during sampling. These particles then recombine into large flocs and sink out at a floc settling velocity that does not depend on concentration. The time required to complete this two-step removal pathway decreases as concentration grows because the time required for formation of flocs scales inversely with concentration, not because of any concentration dependence of floc settling velocity. With the goal of evaluating this alternative hypothesis, this work develops a simple model of aggregation and sedimentation in a settling column and compares predicted and observed responses of clearance rate to increasing concentration.

2 Methods

To compare modelled and observed behavior of settling columns use is made of an outstanding data set from a study designed to assess the performance of various instruments designed to estimate settling velocity (Dyer et al., 1996). Model results are compared with data from the University of Copenhagen and the University of Hamburg "Owen Tubes", and data from the "VIS", which observes flocs directly, are used to constrain floc properties in the model.

An Owen Tube is a 1-m long 51-mm internal diameter tube. It is lowered horizontally into the water with both ends open. At the appropriate depth the tube is sealed, returned to deck, and placed in a vertical position. Subsamples are withdrawn from the bottom of the tube at preset times. Each withdrawal time is converted to an effective settling velocity by dividing the column height by the time. Cumulative mass fraction in the column is plotted as a function of effective settling

*Dalhousie University, Halifax, Nova Scotia, Canada, B3H 4J1
[†]Bedford Institute of Oceanography, Dartmouth, Nova Scotia, Canada B2Y 4A2

Table 1: Model inputs

Variable	Value
maximal floc diameter	545 μm
maximal floc settling velocity	4 mm s^{-1}
floc fractal dimension	2.31
minimal particle diameter	1 μm
grain density	2966 kg m^{-3}
maximal initial floc size	200 μm
temperature	15°C
salinity	5 PSU

velocity. The effective settling velocity for which half of the total mass remains in suspension is determined graphically and given the symbol w_{50}.

A geometric sectional model is used to simulate aggregation and sedimentation (Jackson and Lochmann, 1992) in an Owen Tube. The model adopts three, major, simplifying assumptions. First, the suspension is well-mixed. Second, particle encounter occurs only by differential settling of particles. Third, disaggregation does not occur within the sealed tube.

Aggregation models require numerous inputs (Hill, 1992) (Table 2). When possible, data from the Dyer et al. (1996) study are used to define them. Maximal floc size and settling velocity and floc fractal dimension are estimated based on data from the VIS (Dyer et al., 1996) . Minimal particle size is assumed to be 1 μm, and density of the smallest particle is calculated to match floc settling velocities to the size-settling velocity relationship observed by the VIS. Initially, particle mass is assumed to be inversely proportional to particle diameter from a minimum size up to some maximum. Initial maximal particle size is set so minimal w_{50} generated by the model equals the observed minimum in the Owen Tubes in the Dyer et al. (1996) study. Temperature and salinity, which are used to calculate fluid density and viscosity, are representative values from Dyer et al. (1996).

Contact and sticking efficiencies cannot be constrained with data from Dyer et al. (1996), and their values are not well-constrained in the literature (Hill, 1992; Li and Logan, 1997). Contact efficiency is the fraction of particles that make contact upon encounter. Two basic models describe this process. The first, called the "rectilinear model" assumes no hydrodynamic deflection of particles around one another, so contact efficiency equals unity for all particle interactions. The second, called the "curvilinear model" assumes particles are impermeable and accounts for hydrodynamic deflection. It imposes severe constraints on contact between all but similarly sized particles, and slows aggregation rates substantially (Hill, 1992). Sticking efficiency is the fraction of particles making contact that actually adhere. Its value is thought to range between approximately 0.1 to 1 for marine particles (Hill, 1992). Because of the lack of constraint on these efficiencies, end-member simulations are run. In the first, a rectilinear model of contact is used, and sticking efficiency is assumed equal to unity. In this simulation aggregation is operating
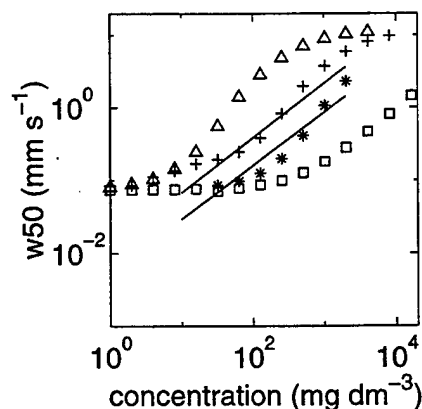
Figure 1: Model and observed dependence of w_{50} on sediment concentration in an Owen Tube. The two solid lines are best fits to data from the University of Copenhagen and University of Hamburg Owen Tubes. Triangles, pluses, and asterisks are the rectilinear model with sticking efficiencies of 1.0, 0.1, and 0.05, respectively. Squares are from the curvilinear model with a sticking efficiency of 1.0. Note the similar approximately linear increase in w_{50} with increasing concentration in all models and observations.

as fast as possible. In the second, a curvilinear model of contact is used, and sticking efficiency is left as unity. This model underestimates aggregation rate substantially (Hill, 1992; Li and Logan, 1997). The simulations are run at a range of concentrations. The variable w_{50} is calculated by dividing column height by the time required to remove half of the original mass by sinking.

3 Results

Modelled w_{50} responds to concentration in a way consistent with observations, both for rectilinear and curvilinear models (Figure 1). When concentration is low, w_{50} takes a constant value. As concentration increases, w_{50} increases in nearly linear fashion as observed in Owen Tubes. At high concentration, w_{50} asymptotes to a constant value. The only significant difference between the two simulated responses is that the nearly linear increase in w_{50} with concentration occurs at higher concentrations with the curvilinear model.

Model behavior is simple to understand. At low concentrations, aggregation occurs so slowly that sediment sinks out before significant modification of the size distribution has occurred. At high concentrations, the step of reforming flocs occurs so rapidly as to be practically instantaneous. The value of w_{50} is set by column height and maximal floc settling velocity, neither of which are concentration dependent. At intermediate concentrations, aggregation and sinking occur over similar time scales. As concentration grows, aggregation time falls, so the overall removal process takes less time.

The observation that each simulation produces similar behavior even though their underlying physics differ significantly indicates that a nearly linear increase in

clearance rate over a certain range of increasing concentration is a robust feature of suspensions in which aggregation and sedimentation are occurring. The observation that the fast, rectilinear and slow, curvilinear simulations bracket the Owen Tube data indicates that aggregation can act fast enough to produce observed behavior. With sticking efficiencies in the range 0.05–0.1, which are realistic (Hill, 1992), the rectilinear simulation produces values of w_{50} closely matching those from the Owen Tubes (Figure 1).

4 Conclusion

Floc reformation and sinking can account for observed clearance rates in Owen tubes as well as accommodate observations that floc size and settling velocity do not depend on sediment concentration. This hypothesis is more consistent with current understanding of flocs than is the widely held view that floc settling velocity in concentration dependent. Adopting it renders Owen Tubes obsolete because the behavior of suspensions within them is linked inextricably to the unknown degree of breakup caused during sampling. In situ, direct observation of flocs is the only viable method of characterization.

References

Dyer, K. R., Cornelisse, J., Dearnaley, M. P., Fennessy, M. J., Jones, S. E., Kappenberg, J., McCave, I. N., Pejrup, M., Puls, W., Van Leussen, W. and Wolfstein, K. (1996). A comparison of in situ techniques for estuarine floc settling velocity measurements, *Journal of Sea Research* **36(1-2)**: 15–29.

Hill, P. S. (1992). Reconciling aggregation theory with observed vertical fluxes following phytoplankton blooms, *Journal of Geophysical Research* **97(C2)**: 2295–2308.

Jackson, G. A. and Lochmann, S. E. (1992). Effect of coagulation on nutrient and light limitation of an algal bloom, *Limnology and Oceanography* **37(1)**: 77–89.

Li, X. and Logan, B. E. (1997). Collision frequencies of fractal aggregates with small particles by differential settling, *Environmental Science and Technology* **31(4)**: 1229–1236.

Milligan, T. G. and Hill, P. S. (1998). A laboratory assessment of the relative importance of turbulence, particle composition, and concentration in limiting maximal floc size, *Journal of Sea Research* **39(3/4)**: 227–241.

ten Brinke, W. B. M. (1994). Settling velocities of mud aggregates in the Oosterschelde tidal basin (the Netherlands), determined by a submersible video system, *Estuarine Coastal and Shelf Science* **39**: 549–564.

LABORATORY EXPERIMENTS FOR EVALUATING THE EFFECTS OF WIND FORCING ON SHALLOW WATERS WITH EMERGENT VEGETATION

Harry L. Jenter[*]
U.S. Geological Survey

INTRODUCTION

Little is known about the effects of wind forcing on circulation in shallow waters with emergent vegetation. An investigation of those effects through laboratory experiments, supplemented by the analysis of historical wind data, is being conducted as part of the South Florida Ecosystem Program of the U.S. Geological Survey (USGS). A primary goal of this investigation is to formulate an improved wind-stress term for quantifying wind-to-water momentum transfer in numerical flow models of the Everglades. One such model is being developed at the USGS to aid in the design and evaluation of restoration plans and actions for the South Florida ecosystem. A unique set of laboratory experiments conducted to support this modeling effort is described below.

FLUME AND WIND COWLING

The laboratory experiments were conducted in a 200-foot-long, 6-foot-wide, 4-foot-deep flume in which a bed of sawgrass, *Cladium jamaicense*, was growing for more than 2 years. Sawgrass is one of the predominant vegetation types in the Everglades. A removable-lid wind cowling, 100 ft long and 4 ft high, covered the upstream half of the flume. Because the density of sawgrass in the flume was approximately that of sawgrass in the Everglades, it was possible to adjust the discharge in the flume to give simultaneously small water-surface slopes and flow velocities typical of those found in the Everglades.

The wind cowling was a rectangular channel made of plywood with various structural modifications to ensure a nearly uniform, steady wind field. Window screening covered the inlet to eliminate any large scale turbulent eddies entering the cowling. In addition, rounded edges made of 3-inch-diameter plastic pipe, cut in half, were added to the inlet to reduce any secondary circulation created by the blunt edges of the plywood walls and ceiling. Wooden bevels, approximately 4 inches wide, were added to all interior right angle joints to diminish any secondary flows generated in the corners.

Short pieces of ribbon stapled to the interior walls and ceiling of the wind cowling provided visual confirmation that the air flowing in the test section was free of any large turbulent eddies. Tests with a bank of three cup-style anemometers positioned across the cowling at the same vertical level confirmed that the wind field was symmetric and nearly-uniform across the middle half of the flume at all heights above the vegetation.

Wind in the experiments was generated by a bank of four 4-foot-diameter ventilation fans arranged in a 2 by 2 array and positioned so as to draw air through the enclosed flume. The cross-sectional area of the fan bank was substantially larger than the cross-sectional area of the cowling covering the flume, which required an expansion section of cowling

to be built. This expansion section was significantly shorter than that found in a typical wind tunnel and, thus, required modification to improve the efficiency of the fan bank. Large 12-inch-wide vanes were added in the expansion section to direct the air toward the upper fans. In addition, a sharp, 1-inch-wide, metal ridge was added along the roof of the cowling just upwind of the expansion section, to induce turbulence in the expansion section and thus, to deliver more air to the upper fans. These mechanisms appear to have worked very well because the rated volume capacity of the fans matched the measured volume of air movement in the enclosed flume to within 10 percent.

The entire expansion section was built to be portable so that it could be removed as a single piece from one end of the test section of the cowling and moved to the other end. This allowed experiments to be conducted in which the wind either coincided with or opposed the unidirectional water movement in the flume. The test section of the cowling was fitted with a lid constructed of 4-foot by 6-foot plywood panels that were removed nightly so that a bank of high-intensity mercury-halide grow lamps could illuminate the sawgrass. Some of the removable panels were modified to allow vertical positioning of the anemometers and current meters and reading of hook gages through the roof of the cowling. Additional access to the test section of the cowling was possible through 2-foot by 2-foot plexiglass doors mounted in the side of the cowling, flush with the interior walls of the test section. These doors also served as observation windows when closed.

INSTRUMENTATION AND MEASUREMENTS

The cowling was instrumented with a bank of three anemometers positioned at different heights across a lateral cross section to measure the vertical profile of wind speed. The flume was instrumented with a pair of acoustic Doppler current meters that were positioned at a number of heights in the water column to measure vertical profiles of velocity. A third acoustic Doppler current meter was employed to measure flow through a horizontal pipe manometer used for determining the water-surface slope. An independent evaluation of water-surface slope was obtained from a pair of hook gages positioned near the upstream and downstream ends of the test section.

Aanderaa** Model 2740 cup-type anemometers, with a rated accuracy of approximately .4 mph, were used to measure the wind speed. The anemometers were positioned nominally 1, 2 and 3 ft above the vegetation. Average wind speed was recorded every 30 seconds for the duration of each experiment.

Each current meter used in the experiment was a SonTek 10 MHz ADV (acoustic Doppler velocimeter) with a rated resolution of .0003 ft/s (.1 mm/s) in a range of ±.1 ft/s (±3 cm/s). Each ADV sampled the three components of velocity at 20 Hz. Samples were collected in 2-minute bursts at each height. One of the paired profiling current meters was fitted with an up-looking probe for measuring flow within .1 ft of the water surface. The other paired current meter was fitted with a down-looking probe for measuring flow very near the bottom of the water column. Velocity measurements were collected in the water column in vertical increments of .2 ft from the surface to the bottom at two locations nominally one-third of the flume width from each wall. After a set of profiles was collected, the paired current meters were swapped and the vertical-profile sampling was repeated so that both velocity-measurement locations would have measurements

from very near the bottom and very near the water surface. Measurements were occasionally contaminated by vegetation drifting into the sampling volume of a velocity probe. These were detected by a technician who graphically monitored all of the velocity data as they were collected. Contaminated measurements were discarded, and the measurements were repeated after the vegetation was removed from the sampling volume. In addition to visually monitoring the signal quality for each measurement, the signal-to-noise ratio and signal-correlation data were recorded at the same sampling rate as the velocity data. These were later analyzed to confirm data integrity.

To determine water-surface slopes, an 8-foot-long plastic pipe with a short elbow at one end was positioned horizontally below the water surface and parallel to the flow direction with the elbow at the upstream end and pointing down. The centerline velocity in the pipe was measured by inserting a side-looking probe mounted on the third ADV into the downstream end of the pipe. The water-surface slope was determined from the centerline velocity by applying a rating equation developed from data collected in the flume under carefully controlled conditions. This "pipe manometer" technique appears to be an accurate means of measuring the small water-surface slopes driving flows with magnitudes typical of those found in the Everglades (J. K. Lee, USGS, oral communication)

Hook gages, positioned near the upstream end of the test section and near the downstream end, were used to provide an independent estimate of the water-surface slope. This estimate was likely less accurate than that obtained with the "pipe manometer" method because of the small longitudinal separation of the gages. To locate the water surface with a hook gage, the hook is positioned below the water surface and raised until the sharp tip of the hook makes a small dimple at the water surface. This dimple sparkles when illuminated from above. At each hook-gage location, a datum was established by making measurements with a horizontal water surface (no-flow conditions). This reference elevation at each hook-gage location was then subtracted from the hook-gage readings made at that location during a wind experiment to give the water-surface elevation. Water-surface slope was calculated by subtracting the hook-gage elevations at either end of the test section. Two factors reduced the accuracy of this calculation. The first was that the slopes were so small that the separation of the gages required an accuracy of vertical positioning on the order of .003 ft (1 mm). The second was that the actively growing plants were transpiring during the experiment and, thus, changing the water level continuously. Because of this transpiration, time series of hook-gage measurements were collected at each gage location, the rate of fall of the water surface was estimated, and all measurements used to obtain reference elevations were adjusted to refer to a horizontal water surface at a fixed time.

Over the 10-month duration of the wind experiments, three surveys of vegetation density and other plant characteristics were conducted. During each survey, vegetation samples were collected from eight 1 ft by 1.5 ft areas located randomly in the flume. Vegetation was sampled in .65-foot (20-cm) bins vertically from the bottom of the water column to the top of the emergent plant canopy. It was then dried, sorted, measured, and weighed. Vegetation was transplanted to fill in the sampled areas. In addition, vegetation was periodically trimmed to maintain a fairly uniform plant height of approximately 4 ft. There was substantial variability around this height, however, because the plants were

growing rapidly. Consequently, vegetation height was also estimated for each experiment.

EXPERIMENTAL PARAMETERS

The suite of experiments conducted was designed to mimic a representative range of wind, water-depth, and flow-velocity conditions found in the Everglades wetlands. The range of winds studied was nominally 0 to 20 mph. This almost completely bracketed the range of 15-minute-averaged winds observed in the eastern Everglades during 1996 and 1997, 0 to 22.5 mph, as determined from analysis of historical data (E. German, USGS, written communication).

Water depth was maintained at either 1 or 2.5 ft. With a nominal vegetation height of 4 ft, this exposed either 3 or 1.5 ft of vegetation above the water surface, respectively.

Discharges through the flume were varied from 0 to .84 cfs at a water depth of 1 ft, and from 0 to 2.2 cfs at a water depth of 2.5 ft. This discharge range represents a flow speed range of 0 to .15 ft/s (0 to 4.5 cm/s), completely bracketing all but the most extreme flows observed in the Everglades wetlands. Experiments were conducted with discharges in the same direction as the wind and with discharges opposite the direction of the wind.

Most of the wind experiments were conducted with the water surface exposed directly to the wind. However, a small subset of experiments was conducted with the water surface covered by sponges. The purpose of these experiments was to simulate the effect of periphyton, commonly occurring algal mats, which form on the water surface in the Everglades. Periphyton may have a significant effect on the wind's ability to affect flow on small spatial scales.

DATA PRODUCTS

The profiles of water velocity and wind speed collected in these experiments, along with the measured water-surface slopes, will be used to calculate terms in the horizontal momentum balance for the flume. Surface wind stresses will be inferred from the resulting momentum deficits. The surface stresses will be related, in turn, to measured characteristics of the wind and vegetation profiles.

These experiments have produced a very large archive (nearly 500 megabytes) of data from which much can be learned about the effects of wind on water movement in shallow waters with emergent vegetation. The final year of this project will be devoted to analyzing these data and using the results to formulate improved relations for treating these effects in numerical models.

---

* Harry L. Jenter; Research Hydrologist; USGS; 12201 Sunrise Valley Drive; Mailstop 430; Reston, Virginia 20192; U.S.A.; (703) 648-5916; *hjenter@usgs.gov*.
** All brand names are for identification purposes only and do not constitute endorsement by the USGS.

High Concentration Suspensions in Coastal Sediment Transport: Observations from Field Investigations

Gail C. Kineke
Dept. of Geology and Geophysics, Boston College,
Chestnut Hill MA 02467

Introduction

High-concentration suspensions of fine sediments, or fluid muds, have been investigated for several decades, often in conjunction with dredging activities or rivers with extremely high suspended-sediment concentrations. Studies have been specific to particular sites such as the Severn or Gironde estuaries, the mud banks of the Surinam coast, and the Huanghe (Kirby and Parker 1983, Allen et al. 1980, Wells and Coleman 1981, Wright et al. 1990). An interdisciplinary study on the Amazon shelf from 1989 to 1991 (AMASSEDS) added to the field observations of fluid muds, and demonstrated the critical role these suspensions play in sediment dispersal and the influence they have on a variety of processes ranging from modifying tidal wave propagation to inhibiting geochemical exchange between the water column and seabed (Kineke et al. 1996).

Fluid muds on the Amazon shelf are responsible for the sediment dispersal via bottom gravity flows and the dispersal route is distinct from the path of the surface plume. While the Amazon system is extremely large in terms of river discharge, it is moderate in terms of source suspended-sediment concentrations, and it is not the high concentrations of the source waters that are the factor in fluid mud formation. Necessary ingredients for fluid muds are moderate sediment concentrations and an effective trapping mechanism. The fluid muds occurring on the Amazon shelf are "extreme", on average 1-2 m thick over an area of thousands of square km and persist for at least 4-6 weeks, but the conditions that produce fluid muds need not be extreme. Fluid muds might be quite common and an important consideration for sediment transport in many estuarine and shelf environments. Where present, transport via gravity-driven flows might become more important than by mean circulation or wave-current boundary layer flow.

Since the Amazon study, an ongoing research program investigating fine-sediment transport in a variety of shelf and estuarine settings has revealed some unexpected observations regarding the occurrence of fluid muds. While many of the dynamics of fluid muds are far from resolved, the observations are useful in identifying common processes and areas of necessary future research.

Background

A rigorous definition of "fluid mud" is still debatable, but a general working definition is a nearbed fine-grained suspension with concentrations of sediment around 10 g/l or greater. Grain size, density, and state of the suspension will alter this threshold, but generally between 2-10 g/l the characteristics and behavior of the suspension begin to change. A lutocline (density gradient due to suspended sediments) develops due to a maximum in settling flux and the onset of hindered settling. A floc framework begins to develop that can lead to viscoelastic behavior. The lutocline is usually such a sharp

interface that gradient Richardson numbers exceed the critical value, effectively inhibiting mixing and reducing the stress reaching the bed. The viscosity of the suspension can be much greater than water, and non-Newtonian behavior can develop.

Some of the first observations of fluid muds were made with echo sounders and the identification of a false bottom. Common optical methods for suspended sediment measurements (transmissometers and Optical Backscatterance Sensors, OBS) will go off-scale, although OBSs have been calibrated for concentrations in the range of ~50-350 g/l using in situ pumped samples. Another indicator for fluid mud is that they sometimes have an anomalous temperature and salinity signal, indicating an unstable density structure were it not for the added mass of the suspended sediment. Thus, although the concentrations within the fluid mud might be difficult to measure, their presence can be documented and attention to altered boundary conditions for sediment transport modeling could be addressed.

While some experiments have shown the generation of a thin fluid mud layer under surface gravity waves, the thickness of the layer is limited by the thickness of the wave boundary layer (Mehta et al. 1994). In many environments, fluid muds have been observed to be 10s of cm or more, exceeding the thickness of the wave boundary layer. More commonly, fluid muds appear to be the result of rapid settling exceeding consolidation. Examples from different environments provide insight on the dominant processes and focus attention on remaining questions and sampling needs.

Examples from Field Observations
Fluid muds on the Amazon Shelf are noteworthy because of the extent (5,000-10,000 km^2) and thickness (average 1-2 m and as much as 5m). The fluid muds form primarily through trapping mechanisms along the bottom salinity front on the inner shelf and supplied sediment to the subaqueous delta via bottom gravity flows. While freshwater input is extremely large, suspended sediment concentrations are moderate, that is 100s of mg/l as opposed to 10s of g/l (Kineke et al. 1996).

By comparison, the Atchafalaya River and Shelf system is characterized by a fraction of the river discharge and comparable suspended-sediment concentrations in the river (Table 1). In this environment, fluid muds approximately 1m thick are consistently observed within the dredged river channel where the along-channel salinity gradient is strongest. This is well downstream of the landward extent of salt intrusion where the traditional concept of a turbidity maximum occurs. On the inner shelf, fluid muds appear to be ephemeral and related to wind wave events. For example, in March 1998 a cold front passed where the average wind speed increased from 10 to >30 kts over a two-hour period, and continued to blow over 30 kts for 6-8 hours. In 5 m water depth the suspended sediment concentrations went from a Rouse-type profile with a maximum bottom concentration of ~ 500 mg/l to a well-mixed water column with concentrations of 1.3 g/l. Within 2 hours of the wind speed decreasing, a fluid mud layer approximately 1 m thick formed with bottom concentrations of 25 g/l. Significant wave height measured seaward in 13 m of water decreased from ~ 1m to 10 cm over the time period that fluid muds appeared. While resuspension provided the sediment to the water column, the fluid mud appears to have formed from rapid settling once the wind stress was relaxed.

Several southeastern estuaries (Table 1) are currently being investigated, and unexpectedly, fluid mud has been observed in each one. This is unexpected because two of the estuaries, the Satilla River, GA and the Ashepoo River, SC are coastal plain estuaries with negligible sediment concentrations. In the case of the Satilla, fluid muds appeared approximately 2 hours after maximum flood currents and overlie a sandy substrate. In the case of the Ashepoo, the fluid muds are observed in the region of a "mud reach" that appears to result from the mixing of organic rich waters of the Ashepoo with the waters from the Edisto River (a piedmont river) through a narrow man-made cut. Sediments rapidly aggregate and settle in a region of high accumulation rates with a fluid mud layer 10-50 cm thick, and serve as a source for further resuspension and settling. Another estuary, Winyah Bay, SC, has persistent fluid mud in the region of a salinity front that appears to be morphologically controlled.

In a drastically different system of a mountainous river on a convergent margin, the Sepik River, Papua New Guinea, the processes of flow convergence and rapid settling appear to form fluid mud at the head of a submarine canyon which then feeds a hyperpycnal flow. This results in different geochemical and grain size signals in sediments delivered via the surface plume, and the subsurface, hyperpycnal plume.

Table 1. Conditions of Environments with High Concentration Suspensions

	river discharge m³/s	tidal range m	tidal currents cm/s	source (background) concentration mg/l
Amazon shelf	100,000-220,000	>2	±100-200	<500 river 100s shallow shelf
Atchafalaya River and shelf	5,000	~0.5	~ 10	100-300 river 10-300 shallow shelf
ACE Basin, SC (Ashepoo R.)	? not gauged	~2.5	60-100	10 mg/l
Winyah Bay (Pee Dee R.)	500	1	50-100	40 mg/l
Satilla River, SC	70	2-3	±100	10 mg/l
Sepik River, PNG	~5,000	<1m	?	150 mg/l

Remarks and Implications

High concentration suspensions, or fluid muds, are not uncommon. They have been observed in systems as different in scales as the Amazon River, the largest river in the world, and the Satilla or Ashepoo Rivers in the southeastern US that have minimal sediment and river discharge. Occurrence of fluid muds is not dependent on initial concentration of source waters, but fluid muds can form in areas of effective trapping due to convergence of water masses or rapid settling. Rapid settling can be the result of high settling flux due to high concentrations from resuspension, high particle settling

velocities from the formation of aggregates, or rapid decrease in turbulent stresses (e.g. decrease in wind stresses).

Fluid muds influence mixing and water column/seabed exchange, effectively decrease the shear stresses reaching the bed, and dominate sediment transport. If overlooked, estimates of particle and chemical fluxes can be in error, both in magnitude and direction. We must be aware of the possible occurrence of these nearbed suspensions in environments where fine sediments are present, and develop new methods for measurement of water, sediment and flow properties in the presence of fluid muds for both site-specific studies, and to improve parameterization of sediment transport models.

References
Allen, G.P. , J.C. Salmon, P. Bassoulet, Y. Du Penhoat, and C. De Grandpre. (1980). Effects of tides on mixing and suspended sediment transport in macrotidal estuaries. Sedimentary Geology, 26:69-90.

Kineke, G.C., R.W. Sternberg, J.H. Trowbridge, and W.R. Geyer (1996). Fluid mud processes on the Amazon Continental Shelf. Continental Shelf Research 16:667-696.

Kirby, R. and W. R. Parker (1983). Distribution and behavior of fine sediment in the Severn Estuary and Inner Bristol Channel, U.K. Canadian Journal of Fishery and Aquatic Sciences. 40(Suppl. 1):83-95.

Mehta, A.J., S.-C. Lee and Y. Li (1994). Fluid mud and water waves: a brief review of interactive processes and simple modeling approaches. US Army Corps of Engineers, CR DRP-94-4, 79 pp.

Wells, J.T. and J.M. Coleman (1981). Physical processes and fine-grained sediment dynamics, coast of Surinam, South America. Journal of Sedimentary Petrology. 51:1,053-1,068.

Wright, L.D., W.J.Wiseman, Z.-S. Yang, B.D. Bornhold, G.H. Keller, D.B. Prior, and J.N. Suhayda (1990). Processes of marine dispersal and deposition of suspended silts off the modern mouth of the Huanghe (Yellow River). Continental Shelf Research 10:1-40.

Mean current profiles over the northern California shelf in fall and winter

Steve Lentz and John Trowbridge
Woods Hole Oceanographic Institution

The characteristics and dynamics of continental shelf flows on time scales of months or longer are not well understood. (For convenience flows time-averaged over months are referred to as *mean* flows.) Mean flows on shelves have been interpreted in the context of the Arrested Topographic Wave model proposed by *Csanady* (1978) which is relevant to unstratified flows. However, recent theoretical studies suggest that for a stratified flow over a sloping bottom, adjustment of the density field within the bottom boundary layer may reduce or even eliminate the bottom stress acting on low-frequency flows (*Garrett et al.*, 1993; *Chapman and Lentz*, 1997). A sequence of field programs on the Northern California shelf between 1981 and 1990 provide an opportunity to characterize the vertical structure of the mean flow during fall and winter, its year to year variation and the associated dynamical balances.

Moored current observations spanning the water column have been acquired at a mid-shelf site (designated C3) off Northern California during three different field programs in the fall and/or winter of four different years (*Lentz and Chapman*, 1989; *Largier et al.*, 1993; *Dever*, 1997; *Trowbridge and Lentz*, 1998). Mean wind stresses for fall and winter from these studies ranged from -0.2 to -0.6 dynes/cm^2 alongshelf (upwelling favorable) and 0.0 to 0.2 dynes/cm^2 cross-shelf. (Alongshelf is positive toward 317°T and cross-shelf is positive onshore.) Mean current profiles for the fall and winter from these studies all have similar vertical structure (Figure 1). The alongshelf flow is poleward across the water column, with a mid-depth maximum of 5 - 10 cm/s. Year to year variations are largest in the upper water column and decrease with depth. The exception to this structure is March-May 1989 (winter89b) when the mean alongshelf flow was equatorward in the upper half of the water column and approximately zero in the lower half of the water column, possibly due to a meso-scale feature impinging on the shelf (*Largier et al.*, 1993).

The mean cross-shelf flow is offshore at about 2 cm/s in the upper 20 m of the water column and offshore at about 1 cm/s within 20 m of the bottom. Between these surface and bottom layers there is a 30-40 m thick onshore flow of about 2 cm/s. The mean cross-shelf current profiles are consistent from year to year. Maximum differences at any depth are generally less than 2 cm/s; less than variations in the mean alongshelf flow. The interior onshore transport ($\sim$1.9 m^2/s for winter 1989a) is about equal to the sum of the near-surface ($\sim$1.2 m^2/s) and near-bottom ($\sim$0.6 m^2/s) offshore transports so the net cross-shelf transport (depth-averaged cross-shelf flow) is small.

Fall and winter mean current profiles from sites 30 km south of C3 (R3) (*Lentz and Chapman*, 1989) and 8 km offshore of C3 (C4) (*Trowbridge and Lentz*, 1998) have the same vertical structure, as do fall/winter mean profiles at four other midshelf sites off northern California (*Largier et al.*, 1993), suggesting this pattern may be typical along this coast, at least at sites between prominent capes. Mean current profiles from two mid-shelf sites off Peru (15°S) during fall (March - May) 1977 also show a similar vertical structure (*Smith*, 1981).
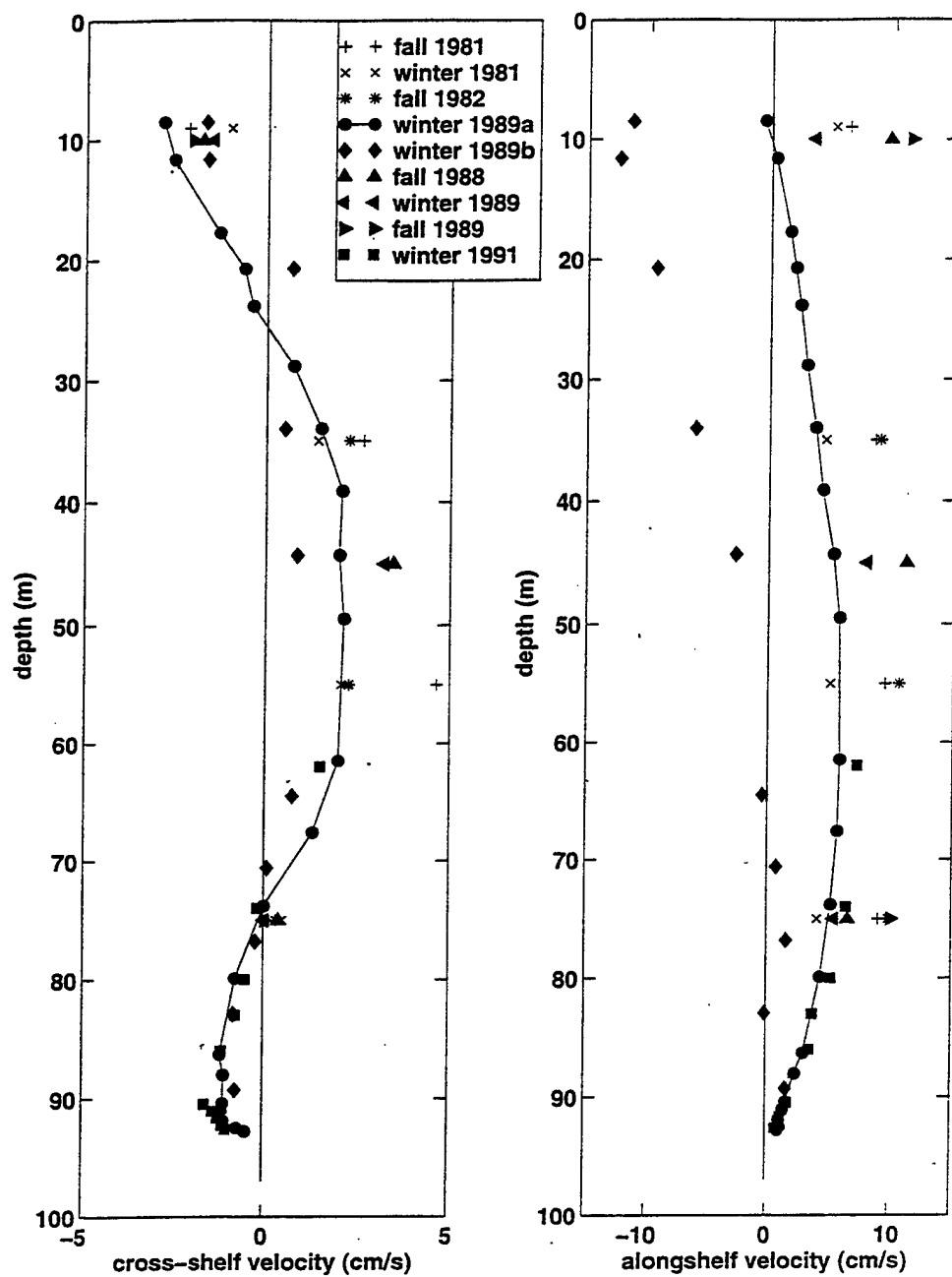
Figure 1. Mean cross-shelf and alongshelf currents at mid-shelf (C3) off northern California for the various fall and winter from various mooring deployments between 1981 and 1991.

To gain some insight into what process might be responsible for the persistent structure of the cross-shelf velocity profile the associated dynamical balances are investigated. Assuming the flow is hydrostatic and neglecting temporal accelerations and the non-linear advective terms, the momentum balances may be written as

$$f\mathbf{k} \times (\mathbf{u} - \mathbf{u}^i) = \int_{z^i}^{z} g\frac{\nabla\rho}{\rho_o} + \frac{1}{\rho_o}\frac{\partial\tau}{\partial z} \tag{1}$$

where f is the Coriolis parameter, $\mathbf{k}$ is the vertical unit vector, $\mathbf{u}$ is the velocity vector, $\mathbf{u}^i$ is the *interior* velocity at depth z^i, ρ_o is a reference density and τ is the stress vector. The interior flow is assumed to be geostrophic, *i.e.* $f\mathbf{k} \times \mathbf{u}^i = -\nabla P^i/\rho_o$. Based on (1) the Coriolis force associated with the mean velocity anomaly $\mathbf{u} - \mathbf{u}^i$, *i.e.* deviations from the interior velocity in Figure 1, is either balanced by the buoyancy anomaly (*i.e.* a geostrophic balance), the stress divergence (*i.e.* an Ekman balance), or some combination of the two.

In the upper half of the water column, estimates of the vertically integrated terms in (1) using observations from the fall and winter of 1988-89 indicate the mean cross-shelf wind stress is small and the alongshelf flow is in geostrophic balance, *i.e.* the vertical shear in the mean alongshelf flow in the upper half of the water column is in thermal wind balance with the cross-shelf density gradient. In contrast the cross-shelf velocity anomaly is primarily balanced by the mean alongshelf wind stress (*i.e.* an Ekman balance) and the mean alongshelf density gradient is typically small. However, there are periods when there is a substantial geostrophic component to the cross-shelf flow, possibly associated with mesoscale features impinging on the shelf from offshore (*Largier et al.*, 1993). Thus the mean alongshelf wind stress, though weak, drives an offshore Ekman transport which causes the isopycnals to slope upward toward the coast (upwelling) and the resulting cross-shelf density gradient is in thermal wind balance with vertical shear in the alongshelf flow.

In the lower half of the water column, estimates of the vertically integrated terms in (1) in a coordinate frame relative to the bottom indicate the mean cross-shelf bottom stress is small and the mean alongshelf flow is also in geostrophic balance. The mean cross-shelf density gradient tends to be vertically uniform in the lower 30 m of the water column and is in thermal wind balance with the vertical shear in the alongshelf velocity. The mean alongshelf bottom stress is small because the thermal wind balance in the lower water column brings the near bottom alongshelf velocity to nearly zero (Figure 1), as hypothesized in recent theoretical studies of the adjustment of the bottom boundary layer to a stratified flow over a sloping bottom (*Trowbridge and Lentz*, 1991; *Garrett et al.*, 1993). Hence the mean cross-shelf transport in the lower water column (relative to the interior velocity) is not balanced by the mean bottom stress which is about an order of magnitude smaller (*i.e.* this is not an Ekman balance). Limited observations suggest this transport is in geostrophic balance with an alongshelf density gradient, *i.e.* there is a thermal wind balance between the mean vertical shear in the cross-shelf velocity and the alongshelf density gradient. If true, this latter balance suggests this alongshelf density gradient is a persistent feature during the fall and winter. This raises the question of what the scales of this alongshelf density gradient are and how it is setup and maintained?

References

Chapman, D. C., and S. J. Lentz, Adjustment of stratified flow over a sloping bottom, *J. Phys. Oceanogr.*, *27*, 340–356, 1997.

Csanady, G. T., The arrested topographic wave, *J. Phys. Oceanogr.*, *8*, 47–62, 1978.

Dever, E. P., Wind-forced cross-shelf circulation on the northern California shelf, *J. Phys. Oceanogr.*, *27*, 1566–1580, 1997.

Garrett, C., P. MacCready, and P. Rhines, Boundary mixing and arrested Ekman layers: rotating stratified flow near a sloping boundary, *Ann. Rev. Fluid Mech.*, *25*, 291–323, 1993.

Largier, J. L., B. A. Magnell, and C. D. Winant, Subtidal circulation over the northern California shelf, *J. Geophys. Res.*, *98*, 18,147–18,179, 1993.

Lentz, S. J., and D. C. Chapman, Seasonal differences in the current and temperature variability over the northern California shelf during the Coastal Ocean Dynamics Experiment, *J. Geophys. Res.*, *94*, 12,571–12,592, 1989.

Smith, R. L., A comparison of the structure and variability of the flow field in three coastal upwelling regions: Oregon, Northwest Africa, and Peru, in *Coastal Upwelling*, edited by F. A. Richards, pp. 107–118, American Geophysical Union, 1981.

Trowbridge, J. H., and S. J. Lentz, Asymmetric behavior of an oceanic boundary layer above a sloping bottom, *J. Phys. Oceanogr.*, *21*, 1171–1185, 1991.

Trowbridge, J. H., and S. J. Lentz, Dynamics of the bottom boundary layer on the northern California shelf, *J. Phys. Oceanogr.*, *28*, 2075–2093, 1998.

Some thoughts on the advancement of acoustics methods for monitoring sediment transport since 1986

Jim Lynch, Jim Irish, and Peter Traykovski
WHOI AOP&E Department

Jim Lynch's remarks

It's interesting, when reminiscing on the life a good friend and respected scientific colleague like Bill Grant, to consider "what he would have thought" of the advances that have been made in his field in the ensuing years. I'd like to follow this whimsical thought for a few pages, concentrating on my own area of expertise, ocean acoustics, which certainly has had a role in sediment transport/boundary layer studies in the past two decades.

When I came to WHOI in 1982, my main focus was (and mostly still is) lower frequency acoustics, in the area of 10-1000 Hz. However, with the departure of Marshall Orr from WHOI (to do *many* good things in the years following, I am happy to say) just before my arrival, the high frequency (HF) acoustics program was without a "hero" on the WHOI scientific staff. Bill Grant and Marshall Orr had collaborated on the early uses of high frequency acoustics in oceanography, successfully imaging suspended sediments, breaking internal waves and other phenomena. But with Marshall's departure, the WHOI HF acoustics program was in strong danger of evaporation. After a series of discussions between Charley Hollister, Bill Grant, and I[1], I was inveigled into working in the HF arena part time, and in particular into doing some sediment transport measurements. This didn't seem like it would be a particularly challenging sideline – after all, Bill and Charley and their co-conspirators were just trying to measure diluted *mud*, for god's sake – how challenging could *that* be???? So I trotted off to meet engineer Frederick Roland (Fritz) Hess[2] and work a bit with the Acoustic Backscatter System (ABSS) that Marshall Orr and Fritz had cobbled up. I expected a fairly straightforward project to play with, which would have all the loose ends tied up quickly. In retrospect, it's not surprising that I was naïve – I still am – but, it's appalling just *how* naïve I was. About fifteen years worth of experience has given me a lot of respect for Mud. (I now even capitalize it occasionally!) Rather than the absolutely simple measurement I had envisioned, sediment transport is one of the most devilishly difficult measurements to make that I have ever encountered. However, to get back to the topic, we *have* made some progress in

---

[1] Just as a historical note, Bill touted the scientific interest and societal importance of sediment transport studies, inspiring me to try to stretch into a new area. Charley Hollister, on the other hand, asked what I planned to do if my Associate Scientist promotion fell through, and whether or not I had talent in "fast food merchandising." This is called the "high/low" approach, and it worked quite well.

[2] The old saying is that bad things come in threes. In the case of sediment transport, the WHOI HF acoustics effort not only lost Bill Grant in the 1980's, but also engineer Fritz Hess and electronics technician Rick Filyo. We dedicate this article to the memories of all three of these good friends and colleagues.

measuring sediment transport using acoustics means, which I think Bill would have immensely enjoyed seeing.

When I started working with the ABSS instrument, in about 1983, the biggest worry was calibration. Sure, the acoustic instrument seemed to make nice vertical profiles of backscattering, but what was it really seeing? Could this backscattering be converted to believable particle concentrations? And why did the acoustical instruments occasionally disagree with transmissometers, which were the "industry standard" concentration measurement at that time? Until these questions were answered, nobody was going to believe in the acoustics measurements, and particularly acoustic concentration estimates, a distressing state of affairs for the HF technique. Since then, *much* has been learned. Calibration is *still* an issue, but it has been realized that this is a universal issue for all instruments that estimate particulate concentrations in the ocean. The size dependence of the particulates, variations in their material properties, aggregation/disaggregation effects and the presence of other possible scatterers (biologics, bubbles, thermal microstructure, etc.) can all affect the calibration of *any* instrument measuring concentration in the ocean, not just acoustics. Acoustics was seen to have a greater sensitivity to the *larger* particles, as opposed to optics, which preferred the finer particles in suspension. This was quickly understood to be the simple difference between acoustics working (mostly) in the Rayleigh scattering regime, which meant it sensed the *volume squared* of a particle, as opposed to optics, which worked in the geometrical optics regime, meaning it saw the *cross sectional area* of the particles. Each technique selectively measured a certain part of the size distribution of the suspended sediments, which accounted for the occasional differences between the optics and acoustics measurements at the same spot. This difference turned out to be a rather useful thing, in that by having both acoustical and optical instruments co-located, one could distinguish between large and small particles. This behavior was exploited in several experiments to discriminate between advective events (where small, slow-to-settle particles drift from site to site, well after a local event) and local suspension events, where larger particles (as well as fines) are pulled off of the bottom by turbulent stresses. The large particles fall out much more quickly, so that when they are seen, the odds are that the event is a local one.

The difference between optics and acoustics measurements leads one right to the topic of particle size distribution estimation, which has to be done as part of the concentration estimation to get at mass flux. Our "optics/acoustics comparison" was really a crude multifrequency particle size distribution inverse, and we realized early on that the "Greenlaw-Johnson" [Johnson, 1987]. multifrequency inverse for particle sizes could in theory give vertical profiles of size distribution as well as concentration. Alex Hay, then of Memorial University in Newfoundland, showed that this type of inverse worked well for beach sand sized particles, and all we had to do at WHOI, where we were more interested in the shelf, slope, and even the abyss, was to translate Hay's work to

deeper water.[3] Unfortunately, that little transition was not as easy as it sounds. Beach sands are (roughly) in the 100-800 micron size range, whereas the muds, silts, and even sands further out to sea are more in the 1-200 micron size range. To get enough acoustic bandwidth to pull of the multifrequency trick for shelf, slope, and abyss sediments, we'd need to get up to about 50 MHz acoustic frequency. Unfortunately, going past about 10 MHz is nearly impossible in the ocean, due to seawater attenuation effects siphoning off all the acoustic energy at higher frequencies. Due to these problems, our hopes of vertically profiling the sediment size distribution using acoustics have been diminished; we get *some* vertical profiling size distribution information from acoustic multifrequency techniques on the shelf, but not all that we would want. I'm sure Yogi Agrawal will talk about how optical *multiangle* scattering instruments partially resolve this sizing problem, so let me end the size discussion with a plug for Yogi [Agrawal, 1983-98].

Another bugbear that has become increasingly famous in sediment transport studies is aggregation and disaggregation effects. Aggregation effects seem to be common and important, especially in shelf plume work [Hill, 1995]. If acoustics (or standard optics or x-rays or neutrinos, for that matter) have problems with getting the sizes of fairly regularly shaped particles, they have absolute *fits* trying to deal with aggregate sizes, shapes, and material properties. To get at aggregate properties with transmissometers or OBS's or acoustics is a state-of -the art worry at present. Given the difficulties encountered in measuring the scattering from these beasties (which is the first order thing we need to know to invert for their properties from backscatter measurements), I for one am not optimistic that we will really get at them with such measurements. Paul Hill's camera seems to be the best way to look at aggregates at present.

Another important part of the sediment transport problem that acoustics has been useful in addressing is the bottom roughness, and in particular it's evolution during storm events. Now, in 1985 or so, when I started with the HF acoustics work at WHOI, one couldn't even image the bottom during sediment transport events; to quote John Trowbridge (a respectable reference in this field), "as soon as the murder was being committed, the lights went out." Optical pictures, which were the state of the art, gave before and after looks at the bottom – but not "during." Bottom roughness during storms was, and often still is, inferred by it's hydrodynamic effects, with mixed results. However, a few years ago, Alex Hay started imaging bottom ripple migration in the nearshore with a rotary sector scanning sonar originally used for (ugh) sewer pipe work, and we again had the brilliant thought to take his ideas to deeper water. Rather startlingly, this time the "technology transition" (read theft) was pretty straightforward, and we have seen feature migration/ transformation/evolution in many different shelf environments. This acoustic technology is a real advance in understanding the "bottom roughness" part of sediment transport. (Thanks, Alex!)

---

[3] Our biggest source of technical inspiration through the years has been Alex Hay. We would watch carefully what he did in shallow water, cabled nearshore experiments, and than shamelessly transport the exact same measurement to deeper water with autonomous instruments, where we would then claim to have "pioneered the technique." Of course, the techniques generally would not work as well in deeper water, which provided Alex with great amusement.

The sediment transport problem really has two facets, the suspended load problem and the bedload problem. The suspended load, as difficult as it is to measure, seems to be the easier of the two to deal with. The bedload problem (how much muck slogs along the very-near-bottom) has yet to be cracked experimentally, as far as I know. Now, having the sector scanner technology to use, we thought to ask: can we relate the "feature migration" that we see to actual mass transport? Perversely, he two are not necessarily the same (features can move in the opposite sense to transport at times), and so we have to be careful. Just our sector scanner technology won't give all the answers here, and so something new is needed. At this point, I'd like to turn the story of our acoustic sediment transport group's work over to Jim Irish and Peter Traykovski, who have been our group's most important players in recent years. Their work on Doppler technology may just present a solution to the bedload problem, so they have some important things to say.

Before turning over the page, however, I'd like to get back to Bill Grant, without who's influence the acoustic sediment transport program at WHOI probably would not have continued. I think Bill would have loved to see what progress we have made in acoustically estimating particle sizes, making images of the bottom *during* storms, looking at the wave boundary layer, and beginning to look at bedload transport. Bill was a pro at pointing out good things to look at with new technologies, and we hope our list would be similar to his. All I can say in conclusion, is that I believe we honor lost friends and colleagues like Bill the best when we continue their work, and looking at the people who are participating in the Bill Grant Symposium, such honor is assured.

References:

1) R. Johnson, 1987. Bar room conversation at ASA meeting.

2) Y. Agrawal, 1983-98. Frequent bar room conversations, various sites.

3) P. Hill, 1995. Bar room conversation at AGU meeting.

Peter Traykovski's remarks

Although my time at WHOI began after Bill Grant's era the first thing I did when I found out that I was going to be doing my Ph.D. Thesis on sediment transport was to start looking at the literature. Needless to say, I quickly found Bill Grant's name everywhere. There is no doubt that Bill Grant's work has made a significant impact of the field of sediment transport, from the development of much used Grant-Madsen (GM) model, which became the Grant-Glenn-Madsen (GGM) model, and now with yet another Ph.D. thesis based on his model may become the Grant-Glenn-Madsen-Styles (GGMS) Model, to understanding how the bottom roughness interacts with the flow and transport immediately above it.

In my opinion, many of the recent advances in sediment transport have come from our increased ability to perform high spatial and temporal resolution field measurements, many of which have been based on acoustic and optical techniques as pursued by Jim Lynch and others. In particular the acoustic backscattering profiler (ABSS, and now the ABS) has allowed us to observed the detailed temporal evolution of vertical profiles of suspended sediment. In wave dominated sandy environments with large ripples this observational technique has revealed the presence of ejections of

sediment laden clouds from the ripples during each half phase of the wave phase. With non-linear asymmetric wave motions this can result in substantial offshore sediment transport due to waves alone. At the same time as these ejection are occurring above the ripples, another acoustic instrument, the rotary sidescan sonars, have imaged the migration of the ripples. Interestingly, under the wave conditions which caused the offshore suspended transport due to the ejections, the migration occurs in the opposite (onshore) direction.

This has led us to become increasingly interested in observing sediment transport in the few millimeters just above the stationary seabed. Since spatially resolving this motion from the stationary seabed itself is very difficult, as the transport occurs with grains jumping, sliding and rolling across the seafloor, we are hoping that Acoustic Doppler based instrument will be able to resolve this mode of transport. Acoustic Doppler based systems to measure vertical profiles of backscattered intensity (as the ABSS did) *and* 3-axis velocity have been recently developed by Alex Hay and Len Zedel. This provides an ideal tool to estimate suspended sediment flux since velocity and intensity are measured from the same grains. We are hoping to once again build on, or shall we say "borrow" Alex's work by extending the capabilities of this type of instrument to the range bin that contains the seafloor return, since this is where the bedload occurs.

While observations in sandy environments with the ABS have taught us that we need to look very carefully at what is happening just above the seafloor, in environments with large quantities of fine sediment such as the continental shelf off of the Eel River a similar lesson is being learned. Here the ABS has revealed the presence of fluid mud layers 10 to 20 cm thick, or a liquefied muddy seafloor. Transport in these layers may be an important mechanism for cross shelf sediment transport and the formation of flood deposits. Again the ABS has revealed the importance of velocity and concentration measurement very near the seafloor. Acoustic Doppler based measurements at an appropriate frequency could provide the necessary velocity profiles while other techniques should be pursued for an accurate concentration or density measurement.

While I did not have the privilege of working directly with Bill Grant, his work set up the foundations for which many younger scientists works is currently based on, and no doubt, will be based on in the future. In particular, the theoretical framework that is included in the GM, GGM, GGMS, ... models provides an important basis from which to interpret and compare our observations and thus ultimately improve our understanding of sediment transport..

Jim Irish's remarks

I became interested in ocean research through an interest in geomorphology and stream flow. I was considering studying stream flow, sand transport and beach processes. This interest was based on observing nature while canoeing around Michigan and enjoying the many lakes there. In the process of exploring oceanography and attending graduate school, I got "sidetracked" into deep-ocean tides and more basic physical oceanography. I was involved in the periphery of HEBBLE, and got involved in the optical detection of sediments with the U.S. Army Corps of Engineers in the New York Bight. But after coming to WHOI and starting to work with Jim Lynch, that I felt than I was really in the sediment transport business. We have expanded this research effort

127

utilizing new technologies and tools, and are now pushing forward toward new observational techniques that would have really excited Bill Grant.

I first met Bill in the early 1980's when he and Sandy Williams shared shiptime on the R/V WECOMA with Wendell Brown and myself during CODE (Coastal Ocean Dynamics Experiment) off the Northern California coast. Bill and Sandy were measuring bottom stress, sediment transport and bottom features from large tripods. Ten years later, as part of STRESS (Sediment Transport Events on Shelves and Slopes), Jim Lynch and I deployed the same tripods in the save area to further study sediment transport. The tripods now held a suite of new optical and acoustic instrumentation (acoustic and optical backscattering, Laser *in situ* scattering, and a sector scanning sonar) not available at the time of CODE. Scott Glenn (now at Rutgers University) was also a part of CODE working with Bill Grant. We are again working with him on the New Jersey shelf trying to understand sediment transport and bottom roughness physics, continuing and expanding the observational and modeling work started by Bill. Scott Glenn's BASS (Bottom Acoustic Stress Sensor developed by Sandy Williams) utilizes the same basic sensor design with updated controller and recorder that was used during CODE.

A major interest of mine is in utilizing new technology for observing the ocean. I keep looking for new sensors and techniques that improve our ability to observe and understand the ocean. I really became involved with sediment concentration observations when I started working with Henry Bokuniewicz (SUNY/ Stony Brook) and the New York Corp of Engineers. They were interested in a low-cost monitoring of suspended sediment at dredge disposal sites in the New York Bight to assure that the dredged sediment was being dumped in the proper place and that it remained on site. At that time I had a Masters student, Jeff Mather, (who now has his own company building optical oceanographic sensors) who developed a low-cost optical backscattering sensor to measure sediment concentrations. We had just purchased several of John Downings OBS sensors, and Jeff (a new student at that time) was exclaiming "$2,000 for that? With $50 in parts I could make a better sensor!" His thesis was just this development, but his cost estimate was up to $260. Today, his company is producing a lower power, more stable Optical Backscattering Sensor with programmable gain for $995, so I guess he did make a better sensor. I can also remember when I was just out of graduate school and starting at the University of Washington. Dick Sternberg had a student, John Downing, who was looking at the new nephalometer that Dick a just bought (which was the same as used by the USGS and Bill Grant in CODE) and was saying "$5,000 for that? Why I can build as good a sensor for less." And he also produced a better sensor for sediment transport work that has been accepted by the U.S. Army Corps of Engineers as standard.

This optical sensor development was the start of my awaking to asking what these sensors were really measuring. Manufacturers were calibrating them with Fomizan, since it was a standard. However, this was unrelated to what the sensors were "seeing" in the real world. Users were required to calibrate the sensors with the sediment they were observing during each deployment to obtain reasonable results. It was only after I started to work with Jim Lynch using an acoustic approach to sediment observations, that I really understand the problem. Basically, we don't have a sensor that measures sediment mass concentrations – we have sensors that measure various scattering returns from particles, and rely on pre- and post-cruise calibrations with sediment collected to connect our observations with reality.

When I started working with Jim Lynch, he handed over the ABSS (Acoustic BackScatter System) for calibrating and preparation for deployment. It was still using the first RCA CMOS microprocessor (long since discontinued) and complicated custom circuitry to digitize and store the acoustic profiles. With present day technology, we are utilizing a PC-104 format computer system with digitizer and hard disk. The system will sample under software control, and store several orders of magnitude more data than was possible during CODE. One could also utilize a small, low-powered Tattletale recording system, and have the same digitizing capability and large storage capacity as the old system for a fraction the cost and space. This is due to the microprocessor developments in the last twenty years. When Bill Grant was active, this technology was just beginning to be utilized in oceanographic instrumentation. Now most instrument systems are microprocessor controlled, and have the recording capability we didn't dream of in the early 80's. With the capability of making more detailed observations, and recording so much more data, I can imagine how Bill would be advancing our understanding of oceanic processes. He would really be excited about the capabilities and about what we should be able to do next.

The acoustic and optic sensor's return scattering that is a function of particle shape, not the volume and density required for mass transport. With the Yogi Agrawal's development of the LISST (Laser *In Situ* Scattering and Transmiossometry) sensor, that measures the particle size distribution by Mie scattering and then sums the observations to get concentration, we are beginning to get close to measuring what is needed. The approach that we are using now, that of multi-frequency acoustics and optics as a broadband excitation to resolve the size dependent scattering and doing the inverse to obtain estimates of particle size class distributions, is only marginally successful. We don't have the full range of excitation wavelengths required by the particle size distribution, and we are still not sure of the particle shape effects. The LISST helps understand the particle size distribution at one height, not the profiles required for sediment transport on a size by size class basis. Also, we are ignoring the whole problem of particulate aggregation altogether, it may be an important process that changes the scattering (hence our calibration) as a function of time. Paul Hill and his associates are now investigating this problem, and making progress.

Bill was interested in processes occurring at the sea floor, and would be excited by our new acoustic imaging techniques to look at the bottom features. We "borrowed" the concept from Alex Hay's pioneering work in the coastal zone and produced an autonomous rotating scanning sonar system for imaging the bottom during times of high suspended sediment transport on the shelf. Previous methods of optical camera pictures missed the processes of bottom feature movement because they occurred during sediment transport events when the high suspended sediment concentration obscured the bottom. The only times that the bottom could be seen was before and after storms. Therefore, the exact movement during the transport events was unknown. With the scanning sonar system, we now have records of the ripple movement and realignment during storms and can start quantifying what is really occurring and model the processes. I can imagine Bill's excitement about the possibilities of improving models of bedform movement.

Again, utilizing improved acoustic techniques, Peter Traykovski has done the initial tank tests which indicates that by using a broadband acoustic technique to look at the bottom few cm of the boundary layer, there is the possibility of measuring the

transport of sediment moving at the bottom. For the first time, we now are getting close to having the potential to measure the entire sediment transport process, and upgrade the existing models which were Bill's pioneering effort in this field.

In the coming few years, I believe that we will continue to be able to utilize more powerful microprocessor controlled systems with telemetry to measure more processes for longer duration than ever before. Then we will begin to have the capability to observe the extent of nature's variability and be able to begin to unscramble the processes occurring. Bill Grant would have loved the tools that we have now, and been excited about the data we will be able to collect over the next few years. I would have been honored to be working with Bill Grant now, but his memory of what he did, his encouragement of others will live on in our continuation of his work.

Review, Modification and Extension of
what
The Grant-Madsen Model for Wave-Current Interaction
can do for you.

"A Tribute to the W in W-C and the G in G-M"

by

**Ole Secher Madsen, Ralph M. Parsons Laboratory,
Department of Civil and Environmental Engineering,
Massachusetts Institute of Technology**

Introduction

I want to take this opportunity to thank the organizers of this Symposium on Coastal Ocean Processes in honor of Bill Grant for getting the idea, bringing it to fruition and for giving me the honor to deliver the Keynote Address at the opening session.

Some of you may wonder about the rationale behind the timing of this Symposium. It is just about twelve years ago that Bill so tragically and so very prematurely left us with fond memories. However, twelve years is usually not recognized as a significant milestone, e.g. it takes 12.5 years to get a copper wedding anniversary; besides, who wants to celebrate a tragic day? I know the organizers were grappling with this question, and not until I sat down to write this summary did it occur to me that I could offer a legitimate reason for the timing of this Symposium. Virtually to the day, *Bill handed in his first homework set in my course on "Coastal Engineering" 25 years ago.* Granted this reason may be somewhat personal, but I like to celebrate that particular day as the one marking Bill's entrance into the field of Coastal Engineering and Sciences. I cannot think of any better day or reason for celebration than that.

Let me move ahead to the fall of 1976 when Bill and I attended a NSF-sponsored workshop in Vail, CO. At the time, Bill was gearing up for the stretch run towards completion of his thesis. We were both looking for a rooftop to jump from when we heard Jim Smith's presentation of his model for wave-current boundary layer flows. Thank you, Jim, for not covering the case of waves and currents at an angle in your analysis and for making a couple of assumptions that differed from ours. Bill and I did not waste any more time looking for rooftops and proceeded, instead, to publish the Grant-Madsen version of a model for combined wave-current boundary layer flows over rough bottoms - the topic of my Keynote Address.

By the way, for those of you interested, *Bill received a grade of 98 on his first homework in "Coastal Engineering"*, and one can even get some significance out of that.

Review

The major difficulty in modeling turbulent flows is associated with the specification of a turbulent eddy viscosity that relates the dynamics (shear stresses) and kinematics (velocity gradients) of the mean flow. In physical terms, the eddy viscosity may be thought of as the product of a velocity and a length scale representing the turbulent velocity fluctuations and the mixing length, respectively. For turbulent shear flows over plane rough boundaries experimental observations have established that the velocity profile near the boundary is logarithmic - a feature predicted by adopting an eddy viscosity scaled by the shear velocity and the distance from the boundary. Physical arguments may be presented in support of this basic nature of the eddy viscosity in the immediate vicinity of the boundary for steady as well as unsteady flows, with the velocity scale being the instantaneous shear velocity. In fact, the boundary conditions imposed on the turbulence equations in elaborate turbulence closure models essentially reduce to a requirement that the eddy viscosity behave in this exact manner as the bottom is approached.

For combined wave-current boundary layer flows over a rough bottom the contribution of the waves to the generation of turbulence is limited to the thickness of the wave boundary layer. Above the wave boundary layer the appropriate velocity scale for the eddy viscosity is consequently based on the current shear velocity. Inside the wave boundary layer the instantaneous, i.e. time-varying, shear velocity should scale the eddy viscosity. However, if the time-varying shear velocity is split into a constant and a time-varying part, a representative constant value should capture the leading-order wave effect on turbulent wave-current boundary layer flows if it dominates the time-varying part. By choosing the constant value equal to the maximum shear velocity one is assured of its dominance except for brief periods around the times of shear reversal. Furthermore, choosing the maximum value suggests improved predictions for the presumably important periods of large bottom shear stress at the expense of the accuracy of predictions when the bottom shear stress is low. For completeness it should be noted that Bill, in his thesis, used a representative shear velocity based on its average value and changed to the maximum in response to a reviewer's comments when his thesis was published.

The preceding arguments, combined with a mixing length that varies linearly with distance from the bottom, lead to the eddy viscosity formulation employed in the GM-model for wave-current interaction. Its lack of time-dependency, while physically displeasing, has only minor effects on model predictions so long as the relative bottom roughness is small. For very rough bottoms the sensitivity of model predictions to choice of representative shear velocity suggests that modifications may be called for in order to extend the GM-model's validity to very rough bottoms. More than the lack of time-dependence, the discontinuous spatial behavior of the eddy viscosity appears physically unrealistic - and it is! Obviously, the waves' contribution to turbulence, while correctly represented in the immediate vicinity of the bottom, does not remain constant as implied by a linearly increasing eddy viscosity inside the wave boundary layer. It may, however, be shown that the velocity profile of simple turbulent shear flows depends very weakly on the spatial form of the eddy viscosity, so long as its near-bottom variation is "correct", i.e. linearly varying with distance from the boundary.

132

The near-bottom linear increase of the GM-model's eddy viscosity with distance from a rough bottom and its subsequent (admittedly overly abrupt) decrease at the edge of the wave boundary layer capture the most important features of far more elaborate turbulence closure models, and result in reasonably accurate predictions of the velocity profiles for combined wave-current boundary layer flows over rough bottoms. The only "fitting parameter" of the model is the scaling factor used to define the thickness of the wave boundary layer. For its general application, the GM-model requires specification of the waves (rms. near-bottom orbital velocity amplitude and mean period), the current (magnitude and direction at a chosen reference elevation or magnitude and direction of the current bottom shear stress), and the *bottom roughness*.

Modification

All models for turbulent shear flows over rough plane boundaries assume that the bottom roughness can be specified in terms of a single roughness length, the equivalent Nikuradse sand grain roughness. Given the similarity of turbulent boundary layer flows immediately above the bottom it seems reasonable to assume that the bottom roughness should be the same, whether the flow is steady or unsteady, so long as the individual bottom roughness elements resemble three-dimensional sand grains whose diameters are small compared with the scale of the wave boundary layer thickness. However, for waves propagating over movable beds, ripples may form and the bottom roughness can neither be regarded as three-dimensional or small. The drag forces exerted on the flow by individual roughness elements dominate the boundary resistance experienced by a flow over two-dimensional, large roughness elements. This form drag must be conceptualized as a uniformly distributed equivalent bottom shear stress to be treated within the framework of turbulent flows over plane rough boundaries. Since the drag force exerted on two-dimensional bodies, e.g. circular cylinders, depends on the nature of the flow, steady versus oscillatory, it is not at all clear that the flow resistance experienced by waves and currents, separately or combined, can be represented by a single bottom roughness scale.

Motivated by the concern expressed above, an extensive set of laboratory experiments on wave, current and combined co-directional wave-current boundary layer flows perpendicular to artificial two-dimensional ripples was recently completed in the Parsons Laboratory. Measured wave attenuation was used with the GM-model's predictions to determine the equivalent bottom roughness experienced by the waves in the presence and absence of currents. LDV measured velocity profiles were analyzed based on the GM-model to obtain bottom roughness values for currents with and without superimposed waves. In this manner we succeeded in demonstrating that waves, currents, and co-directional combined wave-current flows over the same two-dimensional bottom roughness configuration experience the same equivalent bottom roughness.

Whereas this result is very encouraging, the conclusion that a single roughness value can be used in conjunction with the GM-model to model combined *co-directional* wave-current boundary layer flows over a rippled bottom was reached only after artificially enhancing the wave boundary layer thickness "predicted" by the GM-model by a factor of 2 to 3. Consistent with the apparent increase in wave boundary layer

thickness for combined wave-current flows, the GM-model's prediction of wave orbital velocity profiles inside the wave boundary layer failed. However, a combination of a slight modification of the eddy viscosity and a correction of an unfortunate oversight in the interpretation of the wave boundary layer scale factor "predicted" in the original GM-model, resolves these problems.

The modification of the eddy viscosity is achieved by simply adding the value of the hydrodynamic bottom roughness to the "distance from the boundary" used in the original GM-model's definition of the mixing length scale. This modification improves the prediction of wave orbital velocities within the wave boundary layer for large values of the bottom roughness dramatically, whereas it has a negligible effect for small bottom roughness. It does not, however, improve the boundary layer thickness prediction.

When Bill and I developed the original GM-model we determined the velocity deficit predicted by our model for a relative roughness of 0.01, and adopted a criterion of this being about 5% of the free-stream velocity to obtain a scaling factor of roughly 2 in our expression for the wave boundary layer thickness. It is somewhat embarrassing to admit that this scaling factor's dependency on the relative roughness was overlooked by us (and I believe by others as well). Correction of this oversight leads to a significantly larger value of the boundary layer thickness scaling factor as the bottom roughness increases. Corresponding to the bottom roughness obtained from the experiments with artificial ripples, the correctly predicted wave boundary layer thickness is, in fact, in excellent agreement with observations. Thus, the modified GM-model's ability to predict the boundary layer structure for combined *co-directional* wave-current flows over a wave-rippled bed has been established.

Extension

In inner-shelf waters waves, and therefore wave-generated ripples, are oriented at a relatively small angle to the direction of the shoreline. Since currents in this region are expected to be primarily parallel to the coast, *co-directional waves and currents over a rippled bed are the exception* rather than the rule. The capabilities of the modified GM-model demonstrated in the preceding section therefore pertain to a special and less interesting case of the general problem of combined wave-current flows over a wave-rippled bottom. To deal with this problem, we need to consider currents at an angle to the direction of wave propagation.

To examine the physics of wave-current interaction over a wave-rippled bottom, let us for the moment remove the waves and consider the interaction of a current that is incident at an angle to the axes of two-dimensional bottom roughness elements, ripples. Since the bottom is rippled it is expected that the drag force from individual roughness elements dominate the flow resistance experienced by the current, at least if the current is not near-parallel to the ripple axes. By nature a drag force created by the pressure difference between front and back of the object is perpendicular to the axes of the ripples, i.e. not in the direction of the flow above for obliquely incident currents. Only the component of the drag force in the direction of the current will contribute to the flow resistance experienced by the primary flow. Thus, the current will experience a resistance and hence an equivalent bottom roughness that are expected to decrease as its

angle of incidence to the ripple axes increases. The component of the drag force in the direction perpendicular to the current will provide the forcing for a lateral flow. This forcing is limited to a near-bottom region scaled by the height of the ripples, and will set up a near-bottom lateral flow which will drag the overlying fluid along, thus creating a lateral flow component that is absent if the bottom roughness elements were three-dimensional. Corresponding to waves and currents at an angle over a wave-rippled bed, these simple physical arguments suggest that: (i) *bottom roughness* is a function of the flow characteristics as well as of the physical characteristics of the bottom itself and it can be expected to take on different vales for the waves and the current; and (ii) the current velocity will exhibit three-dimensional features and will turn in the direction of the ripple axes as the bottom is approached from above. Part of the former of these anticipated characteristics has been qualitatively supported by field observations.

Experimental results obtained in Parsons Laboratory for currents over artificial two-dimensional ripples placed along the bottom at angles of 0, 30, 45, and 60 degrees to the flume axis provide experimental confirmation of the anticipated flow features described above. Development of a theoretical model that captures these complex three-dimensional flow features is not an easy task. Some assistance may be obtained from the experimental data's suggestion that the flow resistance experienced by the velocity component perpendicular to the ripple axes appears to be independent of the primary flow's direction. Utilizing this concept a preliminary theoretical model has been developed. In this model the flow in the direction perpendicular to the ripple axes is treated based on the modified GM-model formulation of co-directional combined wave-current flows over a rippled bed, whereas the flow parallel to the ripple axes is treated based on the GM-model with an eddy viscosity that neglects the presence of ripple-generated turbulence, i.e. the axes-parallel flow is assumed to experience only a grain-size roughness. Despite the apparent ability of this model to predict most of the observed flow characteristics with reasonable quantitative agreement, in particular, it successfully reproduces experimental results obtained for the limiting case of currents parallel to the ripple axes, some of its physical underpinnings need to be carefully examined and improved.

Concluding Remarks

The existence of the lateral near-bottom ripple-induced flow is important for sediment transport processes in inner-shelf waters. Take, for example, the conditions corresponding to waves with a following wind, i.e. active wind-generated waves, in the inner shelf. The wind will, in addition to generating waves, induce a wind-driven shore-parallel current. With ripples on the bed, the shore-parallel current will near the bottom be turned towards the ripple axes, i.e. potentially cause a seaward transport of suspended sediments. Since the depth-averaged shore-normal current must be required to be vanishingly small, the ripple-induced seaward flow has to be balanced by a shoreward flow induced by mean sea level sloping downward towards shore.

Bill, we sure could use your help in dealing with the problem of extending your model to the case of combined wave-current interaction over a rippled bottom, and in a number of other problems for that matter, e.g. when does the current generate ripples that are superimposed on those generated by the waves and how does this complicate matters?

A Selection of Relevant References

Barrantes, A. I., Turbulent boundary layer flow over two-dimensional bottom roughness elements, ScD Thesis, Dept. Civil and Env. Engrng., MIT, Sept. 1996

Davies, A.G., R. L. Soulsby and H. L. King, A numerical model of the combined wave and current bottom boundary layer, *J. Geophys. Res., 93*(C1):491-508, 1988

Drake, D. E., D. A. Cacchione and W. D. Grant, Shear stress and bed roughness estimates for combined wave and current flows over rippled beds, *J. Geophys. Res., 97*(C2):2319-2326, 1992

Grant, W. D., Bottom friction under waves in the presence of a weak current: Its relationship to coastal sediment transport, ScD Thesis, Dept. Civil Engrng., MIT, Jan. 1977

Grant, W. D. and O. S. Madsen, Combined wave and current interaction with a rough bottom, *J. Geophys. Res., 84*(C4):1797-1808, 1979

Grant, W. D. and O. S. Madsen, The continental shelf boundary layer, *Ann. Rev. Fluid Mech.,18*:265-305, 1986

Hsu, T-W and C-D Jan, Calibration of Businger-Arya type of eddy viscosity model's parameters, *J. Waterway, Port, Coastal and Ocean Engrng.,ASCE,124*(5):281-284, 1998

Madsen, O. S., Spectral wave-current bottom boundary layer flows, *Proc. 24th Int. Conf. Coastal Engrng., ASCE, 1*:384-398, 1994

Madsen, O. S. and P. Salles, Drag law formulation of boundary resistance for flows over a rippled bottom, *Book of Abstracts 26th Int. Conf. Coastal Engrng., ASCE,* 322-323, 1998

Mathisen, P. P. and O. S. Madsen, Waves and currents over a fixed rippled bed: I & II, *J. Geophys. Res., 101*(C7):16533-16550, 1996

Ranasoma, K. I. M. and J. F. A. Sleath, Combined oscillatory and steady flow over ripples, *J. Waterways, Port, Coastal and Ocean Engrng., ASCE, 120*(4):331-346, 1994

Smith, J. D., Modeling of sediment transport on continental shelves, in *The Sea, 6, Marine Modeling,* ed. E. D. Goldberg et al., 538-577, 1977

Trowbridge, J. H. and Y. C. Agrawal, Glimpses of a wave boundary layer, *J. Geophys. Res., 100*(C10):20729-20743, 1995

Trowbridge, J. H. and O. S. Madsen, Turbulent wave boundary layers, 1 & 2, *J. Geophys. Res., 89*(C5):7989-8007, 1984

The Role of Bedform-induced Spatial Acceleration in Determining Bedform Evolution

S. R. McLean,*and J.M. Nelson[†]

For uni-directional flows where the threshold of sediment motion is exceeded, ripples and dunes are the rule rather than the exception. Generally these bedforms are asymmetrical with a fairly sharp crest that triggers flow separation. As Nelson, Mclean & Wolfe (1993) and Mclean, Nelson & Wolfe (1994) point out, the separation process produces a region of very high turbulence intensity above the trough and anomalous turbulence statistics near the bed, downstream of the reattachment zone. The correlation coefficient there is typically only about 0.2 to 0.3, significantly lower than is found in classical boundary layers. The lower correlation coefficient is indicative of more frequent occurrences of Quadrant 1 "events" in a joint probability distribution of the horizontal and vertical fluctuating velocity components (u' and w' respectively). Nelson, Shreve, McLean & Drake (1995) shows that these events, which are characterized by high streamwise velocity and upward vertical velocity, are highly efficient in transporting sediment. As a consequence, transport rates are higher than would otherwise be expected downstream of reattachment, where the mean velocity is quite small, but turbulent fluctuations are quite large.

Downstream of reattachment the mean flow near the bed increases with streamwise distance, thus the mean drag force on a sediment particle will increase as well. However, the turbulence intensity even near the bed is quite high. The high levels of turbulence decrease with distance downstream. Therefore two counteracting processes are acting over the stoss side of a ripple or dune. The transport capacity due to the mean flow increases, whereas the transport capacity due to the energetic events from Quadrant 1 decreases. The amplitude of the events is reduced as the turbulence decays and they become less frequent as the correlation coefficient increases toward the classical value of approximately 0.4. These two competing processes tend to produce a maximum in the local transport rate at a distance downstream of the reattachment zone that depends on the rates at which these two processes change.

As Nelson et al. (1993) point out, turbulence downstream of separation is strongly affected by the degree of acceleration that the flow experiences after reattachment. In a field of bedforms this is controlled by the steepness of the bedforms themselves. In order to investigate this process a series of experimental runs were conducted in the recirculating flume in the Ocean Engineering Laboratory at the University of

---
*Mechanical and Environmental Engineering Dept., University of California, Santa Barbara
[†]U.S. Geological Survey, Water Resources Division, Denver, Colorado

California, Santa Barbara. This facility is 23m long and 0.9m by 0.9m in cross-section. The common element in each run was an inclined ramp of length 0.8m and height $H = 0.037m$ on the downstream end. This ramp induced flow separation and mean flow and turbulence profile measurements were made at different distances downstream using a SonTek Acoustic Doppler velocimeter. Ramps of different steepness were placed downstream of the initial ramp. Five ramp steepnesses, having vertical rise to horizontal run ratios of 1:∞, 1:40, 1:20, 1:15, and 1:10 respectively, were investigated.
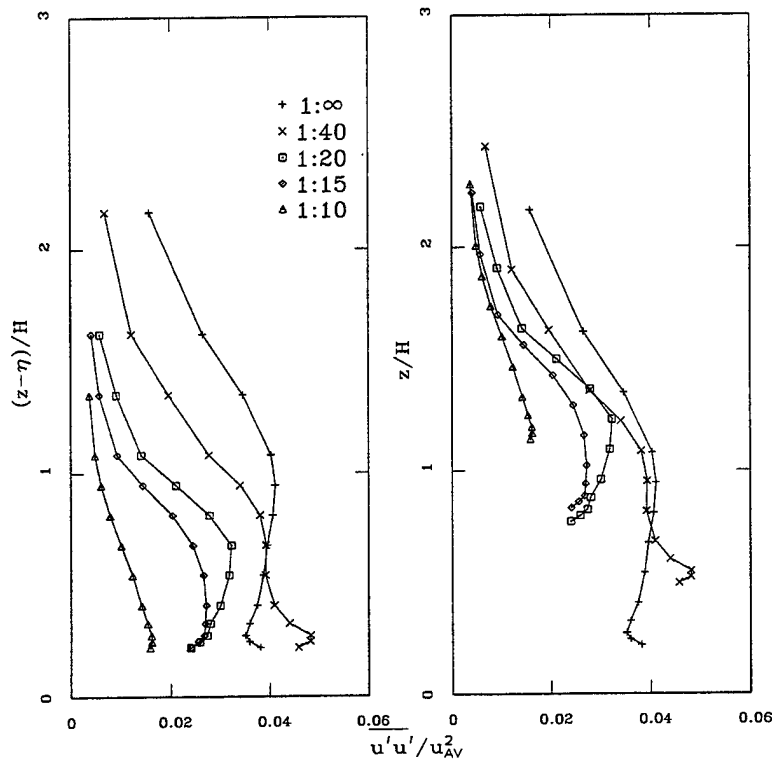
Figure 1: Vertical profiles of fluctuating streamwise velocity variance approximately $5H$ downstream of reattachment, normalized by the square of the vertically averaged local mean velocity. The left plot is relative to local bed elevation the right plot is relative to the trough elevation.

Presentation of the resulting data presents a challenge because of difficulties in isolating valid comparisons. For example all the flows separated at the same point but the zone of reattachment was more than $8H$ downstream for the flat bed case and only about $4H$ downstream for the 1:10 acceleration case. Therefore should profiles at equal distance from the point of separation be compared, or profiles at equal distance from the zone of reattachment? Should the vertical profiles be

plotted with respect to distance from the local bed or with elevation above an arbitrary datum? Should the turbulence quantities themselves be plotted or should they be normalized using a velocity scale like the local mean velocity?

Vertical profiles of $\overline{u'u'}$, measured approximately $5H$ downstream of the reattachment and normalized by the square of the local vertically averaged velocity, are shown in Figure 1. This can be thought of as a turbulence intensity. On the left the profiles are plotted relative to distance from the local boundary. On the right the profiles are plotted relative to z, the height above the trough elevation. It is clear from these plots that the fluctuating downstream velocity is significantly affected by the degree of acceleration experienced downstream of separation and reattachment. There is significantly less turbulence intensity when there is stronger acceleration.
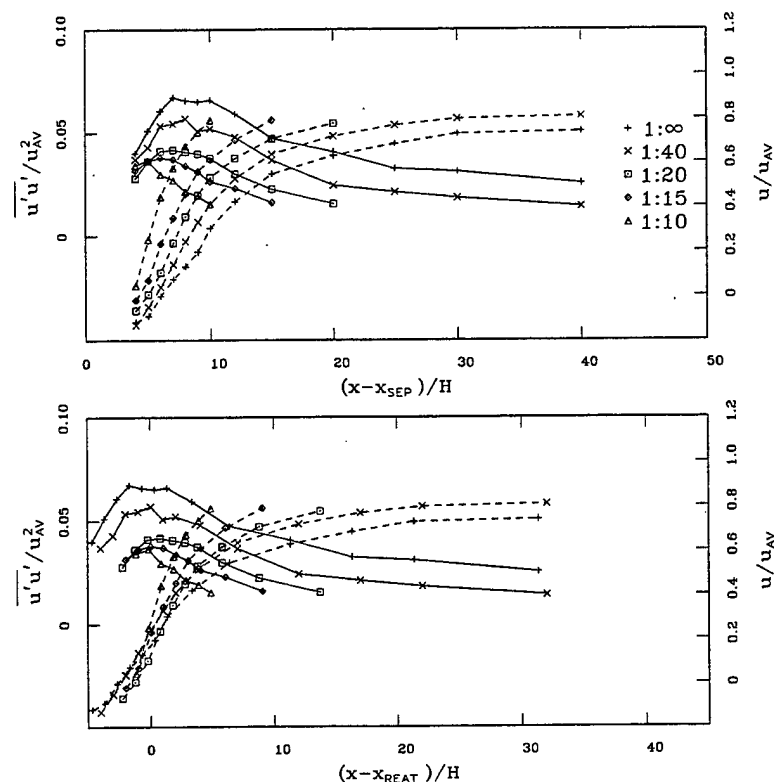
Figure 2: Plot of maximum turbulence intensity as a function of downstream distance. The top plot is relative to the point of separation, the bottom plot is relative to reattachment.

The effect that this might have on sediment transport is seen perhaps more clearly in Figure 2. Here the solid lines represent the maximum value of $\overline{u'u'}$ in a given profile, normalized using the mean velocity and plotted relative to distance downstream. The dashed lines represent the mean streamwise velocity at 7mm

above the bed. In the upper plot the abscissa is distance relative to the point of separation, in the lower plot the the abscissa is distance relative to the zone of reattachment, in both cases normalized by the height of the upstream ramp. It should be noted that there is no such thing as a *point* of reattachment in highly turbulent flows such as these. Eddy shedding from the upstream ramp crest is highly variable and reattachment can only be defined in a mean sense. The SonTek ADV could only measure to within about 7mm of the bed and does not give very accurate mean velocities near reattachment. Therefore, for this work the location of the center of the reattachment zone was estimated by dye insertion and also placement of a thin layer of fine sand in the vicinity of reattachment. The latter was done to locate the zone of maximum divergence.

Clearly acceleration dampens the overall level of the turbulence intensity and also causes more rapid decay with distance downstream. The local sediment transport rate is a complex, and as yet unknown, function of the mean velocity and the turbulence intensity (and perhaps other as yet unknown factors). One can imagine that qualitatively the transport may be reflected by a combination of the mean velocity and turbulence intensity curves as shown in Figure 2. This will produce a maximum somewhere downstream of the maximum in the turbulence intensity curves. This maximum represents the point at which the flow transitions from an erosional to depositional regime and thus the crest of any downstream bed feature must be located downstream of this transport maximum. It is clear that this maximum moves upstream as acceleration increases. This would lead to a shortening of the downstream bedform. But as the steepness increases, the near-bed velocity accelerates more and more strongly. This will increase the relative importance of the mean velocity in regard to transport. Eventually the maximum will occur where the velocity is maximum, which is at the crest. When that occurs the bedform will reach equilibrium. In a field of similar features, they would all propagate downstream with similar speed and without deformation. In natural flows such a situation may never become reality, but the tendency toward such a condition would be present under conditions that remain stationary for a reasonable length of time.

References

Mclean, S. R., Nelson, J. M. & Wolfe, S. R. (1994), 'Turbulence structure over two-dimensional bed forms', *J. Geophys. Res.* **99**(C6), 12729–12747.

Nelson, J. M., Mclean, S. R. & Wolfe, S. R. (1993), 'Mean flow and turbulence fields over two-dimensional bed forms', *Water Resources Res.* **29**(12), 3935–3953.

Nelson, J. M., Shreve, R. L., McLean, S. R. & Drake, T. G. (1995), 'Role of near-bed turbulence structure in bed load transport and bed form mechanics', *Water Resources Res.* **31**(8), 2071–2086.

AN EXAMINATION OF MUD SLURRY DISCHARGE THROUGH PIPES

Phinai Jinchai
Royal Thai Navy, Bangkok, Thailand

Ashish J. Mehta
University of Florida, Gainesville, FL 32611

SYNOPSIS: The dependence of the discharge of clayey mud slurries in pipes on cohesion and water content is examined by introducing a slurry cation exchange capacity, CEC_s. Based on tests in which forty-two clay-water slurries were pumped through a horizontal pipe viscometer, it is shown that CEC_s can serve as an approximate determinant of slurry discharge in the viscous flow range. This finding may be applied as a predictive tool for estimating the pumping requirements for transportation of dredged cohesive mud at *in situ* water content.

INTRODUCTION

Contamination of ambient waters during the dredging of bottom mud often occurs when the material to be removed is diluted in order to transport the resulting slurry by hydraulic means (Fig. 1). In order to minimize this source of contamination, technology for pumping mud through pipes at *in situ* density has been investigated in recent years. This approach has been shown to be useful for moderately dense mud slurries, which are characteristically transported in the viscous flow range (Parchure and Sturdivant, 1997). In that regard, an *a priori* assessment of the pumping requirements can be facilitated if an indication of the transportability of mud could be acquired by testing for its relevant properties as a precursor to dredging. Here we have examined an empirical approach as a basis for such testing by relating the pump-pressure driven pipe discharge of clayey mud slurries to an easily determinable parameter related to slurry cohesion and water content.

MUD SLURRY FLOW

Mud slurry considered here is non-settling and homogeneous, and one which flows steadily in the viscous range as a thick suspension. The rheology of such a slurry, which is characteristically non-Newtonian, can be simply described as a power-law fluid following the Sisko (1958) relation for the apparent viscosity η, which is

$$\eta = c\dot{\gamma}^{n-1} + \eta_\infty \qquad (1)$$

where c is a measure of the consistency of the slurry, and n characterizes its flow behavior. Thus, $n<1$ refers to a slurry which exhibits pseudoplasticity or shear-thinning, i.e., its viscosity decreases with increasing shear rate $\dot{\gamma}$. Conversely, $n>1$ denotes a dilatant or shear-thickening flow behavior, i.e., slurry viscosity increases with increasing $\dot{\gamma}$. When $n=1$ the slurry becomes Newtonian with a constant viscosity equal to η_∞, since in this case the consistency, c, is nil. At high, theoretically infinite, shear

141

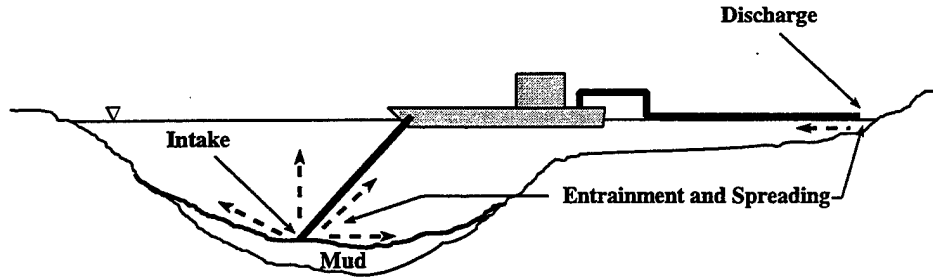rate a pseudoplastic also becomes Newtonian with viscosity η_∞.

Figure 1. Potential for entrainment and spreading of contaminated mud at intake and discharge points during dredging operation.

Knowing η, the steady discharge of a slurry can be readily calculated from the balance of pressure and shear forces in a pipe of radius R, which in turn amounts to a linear variation of the shear stress from zero at the pipe centerline to τ_w at the pipe wall according to

$$\eta\dot{\gamma} = -\frac{r}{R}\tau_w \qquad (2)$$

where r is the radial coordinate with origin at the centerline (Heywood, 1991). Combining (1) and (2) leads to

$$\left[\frac{c}{R^n}\left(\frac{\partial u}{\partial \zeta}\right)^{n-1} + \frac{\eta_\infty}{R}\right]\frac{\partial u}{\partial \zeta} + (\zeta-1)\tau_w = 0 \qquad (3)$$

where u is the local flow velocity such that $\dot{\gamma} = \partial u/\partial r$, and the coordinate $\zeta = 1 - (r/R)$. In (3), $\tau_w = R\Delta p/2L$, where the pressure drop Δp occurs over pipe length L. The corresponding discharge Q is then obtained from

$$Q = 2\pi R^2 \int_0^1 u(\zeta)(\zeta-1)d\zeta \qquad (4)$$

At high shear rates as the flow approaches Newtonian behavior, setting $c = 0$ in (3) one obtains the well-known Poiseuille formula for pipe discharge, $Q = \pi\Delta p R^4/8\eta_\infty L$ (Heywood, 1991). In general for a given pipe, provided the power-law coefficients c, n and η_∞ are known, the discharge can be calculated from (4). Further, if these coefficients can be empirically related to a representative property

of the slurry, then measuring this property can lead to a method for estimating the discharge. This development is described next.

When the slurry is composed of clay and water and is therefore cohesive, a candidate parameter characterizing slurry behavior is the cation exchange capacity (CEC) of the clay, a measure of cohesion. Inasmuch as cohesion has a strong influence on rheology, CEC can be expected to correlate with the power-law coefficients if not fully then at least to a significant extent. To examine this correlation, forty-two slurries of clay mixtures flocculated in tap water were tested. Three clays were chosen: a kaolinite (K), an attapulgite (A) and a bentonite (B), all with nominal median dispersed diameters on the order of 1 μm. For these mixtures a composite cation exchange capacity, CEC_s, can be defined as

$$CEC_s = f_K CEC_K + f_A CEC_A + f_B CEC_B \qquad (5)$$

where f is the weight fraction of the subscripted clays, and CEC symbols with subscript denote the corresponding cation exchange capacities. Note that given the water content f_w we have $f_K + f_A + f_B + f_w = 1$. The CEC values (in milliequivalents per 100 g of sediment) were: 6 for K, 28 for A and 105 for B. For the selected slurries the water content ranged from a relatively low 86% for a moderately dense slurry to a high 423% for a dilute slurry, and CEC_s from a very low 1.94 meq/100 g to 10.39 meq/100 g (Table 1). These parametric values were chosen to cover a reasonably representative range of slurry types.

EXPERIMENTAL RESULTS

The power-law coefficients were determined by measuring slurry viscosities over a range of shear rates (0.063 to 20.4 Hz) in a Brookfield (Model LVT) concentric cylinder viscometer. In order to cover a wider range, in each case an additional value of the viscosity at a shear rate that was an order of magnitude higher than that attainable in this viscometer was measured in a horizontal pipe viscometer (Fig. 2). This apparatus consisted of a 3.1 m long, 2.54 cm i.d. PVC pipe placed horizontally, with one end attached to a piston-diaphragm pump. Over the central 2.48 m length of the pipe the pressure drop was measured by two flush-diaphragm gage-pressure sensors. Each slurry was fed through a hopper at the pump end, and the discharge was measured at the other end. A correction to pressure gradient due to end-effects characteristic of this apparatus was applied following the procedure outlined in Heywood (1991).

Viscosity data for all slurries are given in Table 1. A typical example (slurry no. 15) is shown in Fig. 3. In this plot, the data point corresponding to $\dot{\gamma} = 981$ Hz was obtained in the horizontal pipe viscometer at a pressure drop $\Delta p = 95.4$ kPa. The best-fit line corresponding to (1) yields $c = 3.14$, $n = 0.22$ and $\eta_\infty = 0.234$ Pa. This value of n indicates that this slurry, as indeed all others tested, exhibited a shear thinning behavior. It remains to examine how these three coefficients vary with CEC_s. In Fig. 4 the consistency, c, is plotted against CEC_s for all slurries. Since CEC_s increases with increasing cohesion and decreasing water content, notwithstanding the evident smearing of data points, the observed mean trend of increasing consistency with CEC_s can be expected. Note that as CEC_s approaches zero, log$c$ tends to $-\infty$ as the flow becomes increasingly Newtonian. The mean line, a crude measure of the trend within the measured range of CEC_s, is given by:

$$\log c = 0.29 \mathrm{CEC_s} - 0.36 \tag{6}$$

Plots of n and η_∞ against $\mathrm{CEC_s}$ also show considerable data scatter; however, the respective mean trends are as follows (Jinchai, 1998):
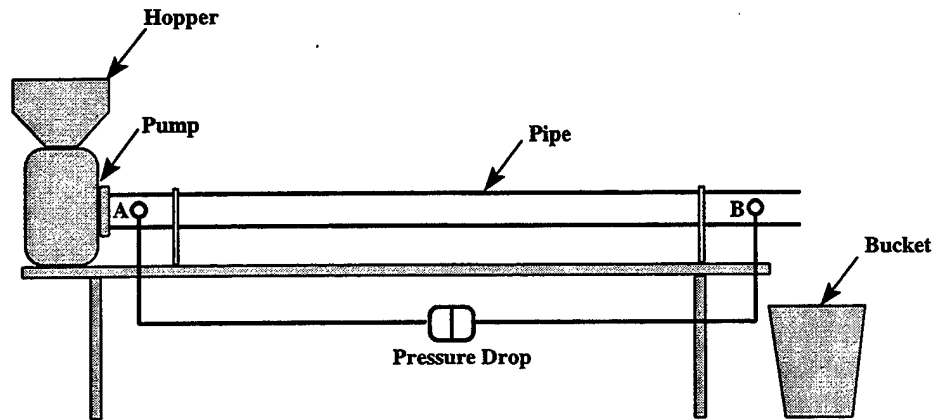

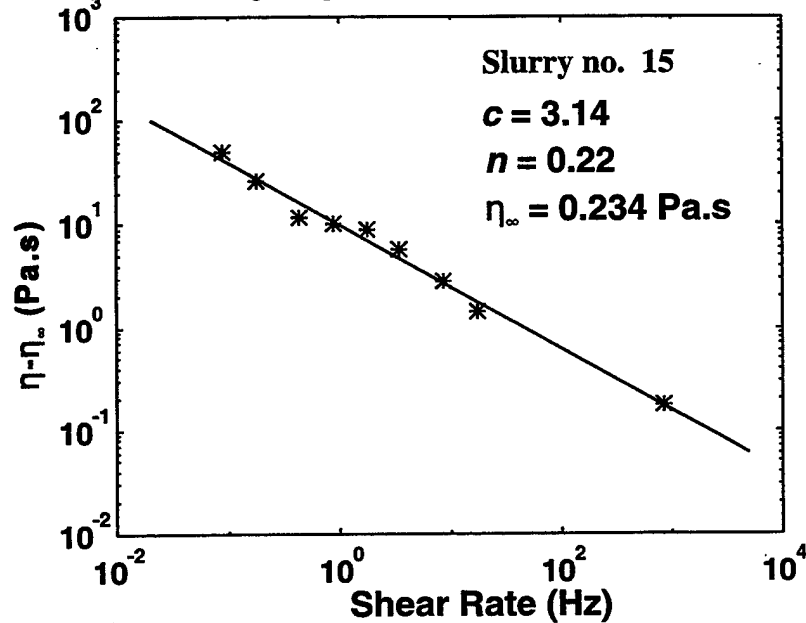Figure 2. Schematic drawing of experimental setup for the horizontal pipe viscometer.

Figure 3. Dependence of excess apparent viscosity, η-η_∞, on shear rate for slurry no. 15.

144

$$n = -0.033\,\mathrm{CEC_s} + 0.28 \tag{7}$$

and

$$\eta_\infty = 0.0015\,\mathrm{CEC_s} + 0.36 \tag{8}$$

As with (6), relations (7) and (8) are applicable only within the overall range of $\mathrm{CEC_s}$ for which they are determined. In any event, (7) implies that as $\mathrm{CEC_s}$ increased n decreased, which in turn means that the flow diverged from Newtonian response towards increasing pseudoplasticity. From (8) we observe that the η_∞ increased with increasing $\mathrm{CEC_s}$ along with consistency. As to data scatter, apart from experimental error we suspect that perhaps the most important reason is that $\mathrm{CEC_s}$, which describes the *state* of the slurry with respect to cohesion and water content, cannot fully capture the effects that arise during the *flow* of slurry. Thus, while $\mathrm{CEC_s}$ appears to be an important parameter correlating with the power-law coefficients, at best it can only be an approximate measure. Its utility lies in the comparative ease with which it can be determined using standard experimental methods and (5).

In order to demonstrate the significance of the method, slurry no. 1 was pumped at a pressure drop lower than that used to establish the power-law for that slurry. Accordingly, it was found that at $\Delta p = 68.5$ kPa the measured discharge was 0.00135 m³/s. The pipe Reynolds number was 450, which indicates that the flow was non-turbulent due to the high viscosity of the slurry (0.209 Pa.s at the prevailing mean shear rate of 836.6 Hz). In Fig. 5 this pressure drop and the power-law coefficients for the slurry (Table 1) have been used to solve (3) numerically using a finite difference scheme along with a no-slip boundary condition at the wall, i.e., $u(\zeta=0) = 0$ (Jinchai, 1998). Although the velocity profile was not measured, the corresponding calculated discharge was 0.00131 m³/s, which is lower than the measured value, but the two can be considered to be reasonably close. Also plotted in Fig. 5 for the purpose of comparison is the Newtonian discharge which would result at zero consistency. This discharge is only slightly higher (0.00134 m³/s) than that calculated for the power-law fluid, because at the high flow shear rate in the test the power-law behavior of the slurry was close to Newtonian.

CONCLUDING COMMENTS

If the relationships between the power-law parameters and $\mathrm{CEC_s}$ prove to be of general validity, the presented approach may be used as follows:

1) For sediment at the dredging site in question determine the $\mathrm{CEC_s}$ from (5),

2) calculate the power-law coefficients from the given mean trend line equations, and

3) knowing or setting the discharge requirements for pumping the dredged sediment, "back-calculate" the pressure drop required to achieve this discharge by iteratively solving for Δp from (3) and (4). Note that the required pump must deliver sufficient pressure to sustain this drop.

Table 1. Properties of slurries tested

Slurry No.	Slurry composition (%)	f_w (%)	CEC_s (meq/100 g)	c	n	η_∞ (Pa.s)
1	100%K	210	1.94	2.35	0.30	0.189
2	100%K	167	2.25	3.43	0.32	0.140
3	100%K	139	2.51	9.02	0.20	0.436
4	100%K	117	2.84	5.08	0.29	0.589
5	100%K	100	3.00	6.99	0.22	0.663
6	100%K	86	3.23	12.99	0.06	0.675
7	75%K+25%A	210	3.71	1.44	-0.07	0.338
8	75%K+25%A	169	4.28	7.69	0.17	0.547
9	75%K+25%A	139	4.80	9.98	-0.01	1.674
10	75%K+25%A	117	5.29	25.96	-0.28	0.904
11	50%K+50%A	210	5.48	4.30	0.22	0.238
12	50%K+50%A	169	6.33	13.21	-0.02	0.270
13	50%K+50%A	153	6.72	21.65	-0.12	0.295
14	50%K+50%A	139	7.10	76.08	-0.25	0.453
15	25%K+75%A	289	5.79	3.14	0.22	0.234
16	25%K+75%A	253	6.38	9.38	0.13	0.382
17	25%K+75%A	215	7.14	22.05	-0.13	0.560
18	25%K+75%A	189	7.77	34.08	-0.20	0.620
19	100%A	409	5.50	1.23	0.39	0.194
20	100%A	333	6.46	3.37	0.07	0.305
21	100%A	280	7.38	13.24	0.07	0.385
22	100%A	239	8.26	21.32	-0.24	0.557
23	90%K+10%B	273	4.26	2.98	-0.16	0.189
24	90%K+10%B	211	5.12	9.25	0.14	0.178
25	90%K+10%B	169	5.90	14.28	0.12	0.259
26	90%K+10%B	140	6.63	42.83	-0.04	0.380
27	65%K+25%A+10%B	231	6.47	9.04	0.18	0.218
28	65%K+25%A+10%B	204	7.04	17.50	0.09	0.277
29	65%K+25%A+10%B	182	7.59	21.05	0.06	0.308
30	65%K+25%A+10%B	163	8.12	57.83	-0.06	0.750
31	40%K+50%A+10%B	299	6.74	7.82	0.18	0.129
32	40%K+50%A+10%B	257	7.54	12.17	0.15	0.072
33	40%K+50%A+10%B	224	8.31	10.46	0.14	0.138
34	40%K+50%A+10%B	197	9.05	36.00	-0.02	0.284
35	15%K+75%A+10%B	423	6.20	1.82	0.21	0.177
36	15%K+75%A+10%B	345	7.28	6.17	0.24	0.145
37	15%K+75%A+10%B	290	8.31	8.71	0.16	0.126
38	15%K+75%A+10%B	248	9.30	22.13	0.03	0.362
39	90%A+10%B	415	6.93	4.12	0.25	0.199
40	90%A+10%B	339	8.13	14.83	0.05	0.107
41	90%A+10%B	284	9.29	17.32	0.03	0.373
42	90%A+10%B	244	10.39	89.59	-0.20	0.771
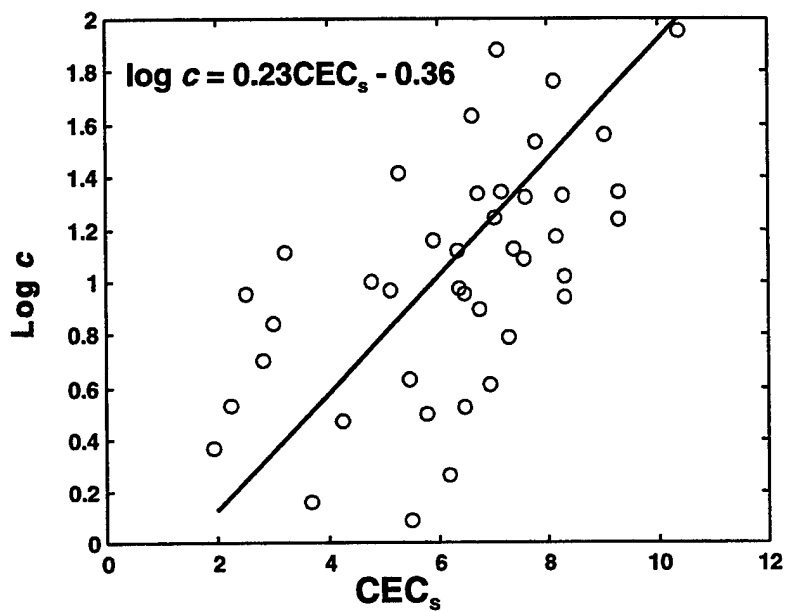
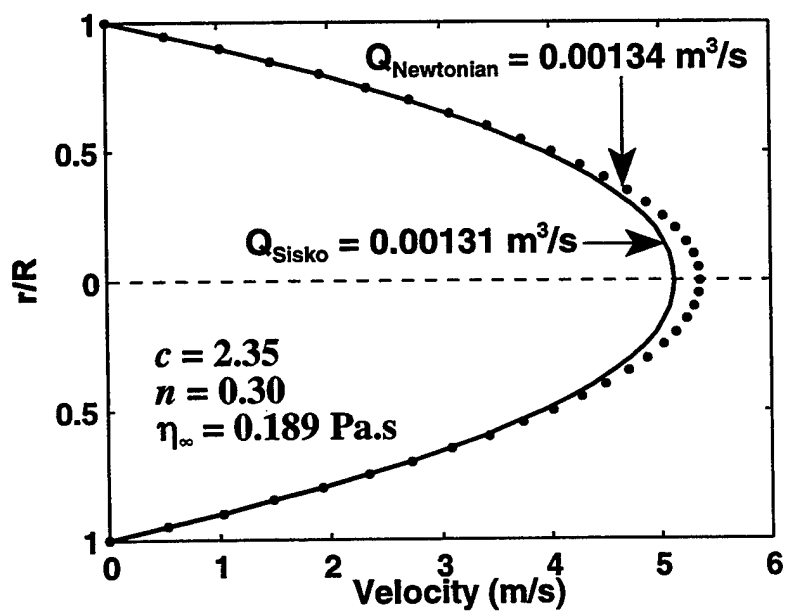Figure 4. Variation of the logarithm of consistency c on CEC_s.

Figure 5. Calculated Sisko power-law velocity profile and discharge for slurry no. 1, and comparison with the corresponding Newtonian flow values.

147

It is evident that the results of this method cannot be used under prototype conditions without rheometric re-calibration. Furthermore, where the mud is not predominantly clayey the use of CEC_s must be eschewed in favor of other parameters representative of slurry rheology. On the other hand, inasmuch as the flow behavior of most natural muds tends to be pseudoplastic within the range of water contents in the natural submerged environment, (3) and (4) should be applicable in these circumstances.

ACKNOWLEDGMENT

REFERENCES

Heywood, N. I. (1991). Rheological characterisation of non-settling slurries. *Slurry Handling Design of Solid-Liquid Systems*, N. P. Brown and N. I. Heywood eds., Elsevier, Amsterdam, The Netherlands, 53-87.

Jinchai, P. (1998). An experimental study of mud slurry flows in pipes, MS thesis, University of Florida, Gainesville, Fla.

Parchure, T. M., and Sturdivant, C. N. (1997). Development of a portable innovative contaminated sediment dredge. *Final Rept. CPAR-CHL-97-2*, U. S. Army Eng. Watwys. Expt. Sta., Vicksburg, Miss.

Sisko, A. W. (1958). The flow of lubricating greases. *Ind. Engrg. Chem.*, 50, 1,789-1,792.

THE SOUND OF THE SURF

W. Kendall Melville & Michael Ritter
Scripps Institution of Oceanography
University of California, San Diego
La Jolla, CA 92093-0213

Waves breaking at the coast, whether crashing on rocks in a storm or spilling gently as they approach a beach in fine weather, generate what is one of nature's most soothing sounds. It may be better to leave its description to the poets, but in recent years acoustical oceanographers have taken an interest as applications of acoustics in shallow water expand. Much of the interest relates to military applications but that does not detract from a more basic scientific interest in better understanding the acoustics of the surf zone. In the fall of 1996 the Marine Physical Laboratory at SIO conducted the Adaptive Beach Monitoring (ABM) experiment at Red Beach, Camp Pendleton, California. The ABM experiment was designed to use active and passive acoustics to monitor the surf zone and beach. As part of the ABM experiment, the authors measured the ambient sound across the surf zone along with supporting measurements of surface waves, currents and local meteorological conditions over a period of three weeks in November 1996. These measurements were supplemented by additional data from La Jolla Shores Beach at SIO during the fall of 1997. We present these measurements of ambient noise in the surf zone and relate them to local wind-generated waves, swell and the tides.

149

Which u* is it?

Douglas C. Miller
Graduate College of Marine Studies
University of Delaware
Lewes, DE 19958-1298
Dmiller@udel.edu

I knew of Bill Grant by reputation, of course, but I met him while a teaching assistant at Friday Harbor. It was in the spring of 1983, and he was a guest lecturer. He covered the basics of wave mechanics and unsteady flows. It was tough going, but in two whirlwind lectures he covered everything from basic wave mechanics to the recently published Grant and Madsen models. These lectures offered a level of insight that was impossible to glean from the published versions. I didn't get it all down, but I still have those notes.

A central issue in animal-sediment-flow interactions at that time was the critical shear velocity, u_{*cr}. Studies were well underway to investigate how this parameter affected benthic fauna and conversely how benthic fauna affected this parameter. It was also generally recognized that not all flows in the ocean match those used in laboratory flumes, especially in shallow places where sediment was most likely to move under the action of surface waves. My Ph.D. research was guided to get some first estimates of the relative magnitudes of biological and geophysical rates of sediment movement in this wave-dominated case. What I had absorbed of Bill's lectures gave me confidence to focus on this situation, although my attention was drawn eventually to feeding rates and behaviors in various wave-driven conditions.

Perhaps coincidentally, I have recently encountered a situation in which u_{*cr}, and wave-current boundary layers are, as before, central to the problem. Obviously, boundary-layer physic haven't changed in the interim, though the numerical models have advanced considerably, and even Kelvin functions are easily approximated in my desktop spreadsheet program. This real-life situation has some novel, complicating biological aspects to it. So it seems very much to be reminiscent of the early '80's, with ideas so far posed mainly as questions, such as "Which u_* is It'?"

The "coral beds" is the popular name for hard-bottoms located along the shallow western margins of Delaware Bay. This region is well known among local fishermen as a hot-spot for flounder, striped bass and red drum. Recreational fisherman and charter boat captains alike frequent it. I have heard many anecdotes about what species live there and how the beds are "not what they used to be." The Army Corps of Engineers has planned to use the area for spoils disposal and sand storage. So this situation is of considerable rable environmental as well as economic significance.

This summer, I obtained specimens from the coral beds using a dredge and by SCUBA divers. The coral beds are **not** a coral reef. These hard grounds appear to consist of patches and mounds of worm tubes among other benthic species. Worm tubes occur in limy nodules in clumps or relatively isolated on an otherwise sandy bottom. A bryozoan, *Schizoporella unicornis,* can also grow in clumps with a

leafy appearance, and this probably accounts for the local name "lettuce coral." To confuse things further, a true coral, the star coral *Astrangia danae* is a common member of the coral beds community. Whelks and spider crabs move amongst the coral beds', and are seen by the flow as additional roughness elements.

The polychaete worm tubes occur as nodules roughly egg- to fist-sized, up to 10 cm in their longest dimension, and half to one-quarter that in their flattest. To an engineer, they would be approximated as triaxial ellipsoids. They are reddish or orange in appearance, and overall look fairly smooth, but feel rough. The surface has scattered round openings and a fine-scale mesh-like pattern that requires close examination to see.

Tubes of two polychaete species form the mass of the nodules. White, calcareous tubes are secreted by the feather duster worm *Hydroides dianthus*. The sandbuilder worm, *Sabellari vulgaris,* cements sand-grain tubes. Most nodules examined had both tube types. It was common to find live specimens of both species on any single nodule, sometimes with abutting tube openings. Covering the worm tubes and accounting for the orange color is a monolayer crust of the bryozoan Schizoporella.

The nodules are a consortium of three epifaunal species, though each is found singly elsewhere in the region, and none is uncommon. *Hydroides* is a typical suspension feeder, and the bryozoan relies on fine suspended organic particles as well. In terms of its tentacle morphology and particle-handling behavior, *Sabellaria* is a deposit feeder. At the very least, it shows considerable dexterity in particle manipulation and preference when building its sand tubes. Attached to a firm substratum like large clam shells or pier pilings, *Hydroides* tubes grow into straight, spaghetti-like bundles. In the early '70's, *Sabellaria* tube masses formed large, low intertidal "worm rocks" all along the margin of the Bay. Today, the most predictable place to find the sandbuilder worm is on the carapace of horseshoe crabs. In my experience, and in the scant literature, it is uncommon to find these species together.

The coral beds cover the bottom in areas of strong tidal currents and are exposed to a considerable northeast fetch. My specimens came from the Broadkill Slough at a depth of 7 m or so, but the exact depth and areal distributions are poorly known. The conventional benthic sampling gear used in impact surveys would work poorly on these hard grounds, and this probably accounts for their lack of consideration in impact assessment studies.

I find it remarkable not only that the nodules are rounded but also that there are tube openings all around, on all sides. The bryozoan film, too. covers the entire surface of the nodule. The nodules feel light: inside they are onion-like, layered and porous. Worm tubes and bryozoan crust of all three species are commingled. Often at the center is a pebble or mussel shell, which appears to be the nucleus of nodule formation. Together these observations suggest the nodules are flipped over or rolled by some means. Presumably flipping and burial would be lethal for all three species. Do severe winter storms like nor'easters to which this coast is highly exposed flip the nodules? What is the u_{*cr} for the nodules? Is this value more or less than that of the pebble at the center? To what extent is the flow environment determining the intrinsic morphology of the coral beds" How does this influence their value as fish habitat and their susceptibility to spoils disposals nearby?

The shape and appearance of the nodules clearly suggest that they are rolled infrequently enough to allow colonization and appreciable tube growth, yet frequently enough that upwardly directed tube bundles are not formed. What is the critical u_* for the nodules, and does it change over time? Is this value reasonably exceeded by tidal currents, storm waves or both? Does the strength of this past winter's nor'easters account for the virtual lack of intertidal worm rocks this summer?

How does tube growth rate and composition (calcareous *versus* sandy) control nodule porosity and bulk density, and ultimately erodibility? To what extend do nodules contribute to bottom roughness, facilitating their rolling? While limiting local growth height, do storms re-distribute the nodules spreading the coral beds? Are there unexpected feedbacks here: would rapid tube growth by either species lead to substrata more likely to be moved or destroyed by storms? Is there a depth gradient in nodule form? What is the intrinsic, low-flow form? Does disturbance by nodule rolling, in fact, allow coexistence of this three-species consortium? Is the flow directly controlling the biological composition of the coral beds?

While requiring a hard substratum for settlement, *Sabellaria* requires fine sand particles for tube building and feeding. Is wave or tidal action enough to supply sand for these activities without burying or overturning the nodules? Conditions do appear vigorous enough to keep fine particles in suspension judging by diver's descriptions of limited visibility at the site. How would various flow scenarios affect the relative feeding and growth of the three species?

Despite the qualitative nature of the analysis taken so far, the means by which flows in the Bay affect, perhaps even control, the coral beds' physical and biological structure and distribution seem exceedingly complex. Several u_{*cr}'s are involved, for the nodules themselves, tube sand grains and fine food particles, and clearly the frequency distribution of such forces and seasonality are important too. Does reproduction and settlement coincide with predictably gentle summertime conditions?

This is not unlike an earlier time when the more direct interactions of flow and sediment and organisms seemed likewise complicated. Since physics always leads biology, flow and sediment transport model runs would go a long way towards answering these questions. How to parameterize the biological components and what to measure, much less model, are thornier issues. As I flip through my old lecture notes, I sense that Bill would listen and offer his remarkable insight. The depth of focus that is my lasting impression of Bill's lectures and papers won't come from such model calculations, but only from a thoughtful and precise analysis, a consideration of the important scales and magnitudes, like that so exemplified by his papers.

Biological influences on transport of postlarval soft-shell clams (*Mya arenaria*)

Lauren S. Mullineaux, Robert Dunn*, Susan W. Mills,
Heather L. Hunt and Lara K. Gulmann
Biology Department, Woods Hole Oceanographic Institution
Woods Hole, MA 02543 USA
*now at: Dept. of Ecology & Evolutionary Biology
U-43 University of Connecticut, Storrs, CT 06269-3042 USA

INTRODUCTION

Juveniles of the soft-shell clam *Mya arenaria* (L.) are subject to post-settlement transport, as reported in both field (Emerson and Grant, 1991) and laboratory (Roegner et al., 1995) studies. This transport may contribute to the high temporal and spatial variation in recruitment observed in many populations (e.g., Möller and Rosenberg, 1983). Suspension of juveniles and their subsequent translocation is due to boundary shear stress on the clams and the surrounding sediments. Susceptibility of juvenile clams to resuspension can be influenced by their burrowing and byssal-drifting behaviors. Small clams cannot burrow deeply and are restricted to the upper layer of sediment, making them the most susceptible to resuspension. Suspension also may be facilitated through local disturbance by benthic organisms and fish, as well as by more-intensive anthropogenic disturbances (i.e., Brown and Wilson, 1997).

The mud snail *Ilyanassa obsoleta* (Say) occurs commonly in high densities and may be an important disturber of soft-shell clams. This snail feeds on surface sediments and carrion (Feller, 1984) and is common in intertidal flats and shallow subtidal areas on both coasts of the continental USA. It has been shown to reduce the abundance of the nematode *Pseudotheristid nematodes* (Nichols and Robertson, 1979), and bivalves and other organisms (Hunt et al., 1987), and induce migration of the amphipod *Microdeutopus gryllotalpa* (DeWitt and Levinton, 1985) and the snail *Hydrobia totteni* (Levinton et al., 1985). In the presence of *I. obsoleta*, the larger species such as *M. gryllotalpa* and *H. totteni* emigrate actively, but the mechanism by which *I. obsoleta* excludes smaller infaunal species remains unclear.

Our objective in the present study was to examine the role of the mud snail in the disturbance and subsequent suspension of postlarval soft-shell clams. We used laboratory flume experiments to determine whether snails affect the boundary shear stress at which clams are suspended and the proportion of clams suspended in a particular flow environment. These experiments were intended to provide the ability to predict the range of boundary shear stresses in which snails may have an effect, and to estimate the probable magnitude of the effect. We then used manipulative field experiments to determine whether the presence or absence of snails affected suspension and transport of postlarval clams in field flows.

MATERIALS AND METHODS
Flume experiments

Flume experiments were conducted in a 17 m long, 60 cm wide, steady re-circulating flume located in the Rinehart Coastal Research Center (RCRC) at Woods Hole Oceanographic Institution. The flume was equipped with an impeller pump and a two-axis Laser Doppler Velocimeter (LDV) that provided simultaneous along-stream and vertical velocity measurements (described in Trowbridge et al., 1989). The water height was set at 12 cm during each trial run, and 4-minute velocity averages were measured at ten heights over the center of the channel. Calculations of boundary shear velocity (u_*) were made from the resulting velocity profile using the log profile technique (e.g., Jumars and Nowell, 1984). For all treatments, a removable bottom panel of the flume was fitted with a 20 x 20 x 2 cm deep recessed sediment tray.

Experiments were conducted with three different sizes of clams (1.3 mm, 1.8 mm, and 2.3 mm) corresponding to the size range of juvenile *Mya arenaria* through their first summer season in Barnstable Harbor, Massachusetts, USA. Sediment for all trials was collected in Barnstable Harbor, and had a median grain size in the 150 to 180 μm range after sieving. Adult snails (*Ilyanassa obsoleta*) roughly 1.2 to 2.0 cm in length were also collected from Barnstable Harbor.

Clams were introduced into the sediment tray while it was submerged in a running seawater table and allowed to burrow for 20 minutes. The tray then was moved from the seawater table into a recessed section of the flume, in a flow speed of less than 2 cm s^{-1}. The treatment flow speed was established, and a vertical velocity profile was measured for the 40-min experimental interval. At the end of the run, the flow speed was reduced to less than 2 cm s^{-1}, and the tray removed from the flume. The sediment was sieved through a 500 μm sieve, and the clams were counted under a dissecting microscope. A new set of clams was used for each flume run. For the snail treatments, 40 snails were placed on the sediment immediately following the placement of the clams, and allowed to move about and burrow.

To determine whether snails lowered the critical erosion velocity of juvenile clams (low velocity treatment), and whether they increased clam suspension during sediment transport (high velocity treatment) we conducted replicate flume runs for each clam size-group. These runs consisted of 3-4 replicate runs for each of two snail treatments (with and without snails) and each of two shear velocities. At the lower shear velocity, bulk sediment transport did not occur, and only clams exposed to the surface were susceptible to suspension. At the higher shear velocity, bulk sediment transport did occur, making buried clams also susceptible to suspension. Greater shear velocities were used for the larger clams because of their presumed deeper burial position. All shear velocities were within the range of those estimated from current velocities recorded through a tidal cycle by Ayers (1959) over a Barnstable Harbor tidal flat.

Two hundred clams were used in each flume run except for the low-velocity treatment of the experiment on the largest clams, for which 100 individuals were used per run. The proportion of clams retained in the flume runs (excluding unburied individuals) was arcsin transformed and analyzed for each clam size in a separate two-way ANOVA (Systat version 6.1) with snail presence (two levels: snail and no-snail) and velocity (two levels: fast and slow) as fixed factors.

Field experiments

To test for the effect of snails on juvenile clams in the field, a set of ten cages, five with snail-access holes and five without, were placed on plots of sediment in Barnstable Harbor. Snails were removed from all plots at the start of the experiment and were allowed to migrate back only onto plots with access holes. Each cage frame was 0.33 m tall and covered a 1 m² area plot with 1.25 cm plastic mesh netting. Cages that allowed entry of snails had four 2.5-cm diameter access holes on each side and 20 holes on the top.

Plots were arranged in a 2 x 5 rectangular array, separated from each other by 2 - 3 m. Snails were removed from all plots and cages were buried approximately 3 cm into the sediment on all sides of the plot. Sediment under the cages was sampled with 6.5 cm diameter cores to a depth of 4 cm at the beginning of the experiment (July 15) and at intervals of 12, 34 and 45 days. Five additional cores were collected in nearby ambient sediments to measure clam abundance in ambient sediments outside the cages. These nearby cores were taken 3 days before the experiment started (July 12; day -3), and on days 12, 34 and 45 as for the plots.

The initial core sampling was performed before cages were in place, but after all snails had been cleared from the plots. Subsequent samplings were done by temporarily opening the mesh and taking a single core near the center of the plot. The specific location of the sample within the plot was recorded and no location was sampled twice.

In the laboratory, samples were stained overnight in Rose Bengal, sieved onto a 300 μm sieve and juvenile *Mya arenaria* (0-year-class recruits) were counted under a dissecting microscope. Abundances of *M. arenaria* were compared between treatments (two levels; snails versus no-snails) and among days (three levels: day 12, day 34 and day 45) of the experiment using a two-way analysis of variance (Systat version 6.1). Abundances on day 0 were not included in that ANOVA, but were analyzed separately in a one-way ANOVA to determine whether initial mean abundances differed between the two snail treatments. Abundance of *M. arenaria* juveniles in the ambient sediments was compared among sampling days (four levels: day –3, day 12, day 34 and day 45 of the experiment) with a one-way ANOVA.

Wind velocities were recorded approximately 30 km from the field site at the Woods Hole Oceanographic Institution meteorological station in Woods Hole for the duration of the experiments. The measurements were used to document the timing of major wind events in the region.

RESULTS
Flume experiments

For all clam sizes and all shear velocities, the proportion of clams retained was greater in the no-snail than the snail treatments (Fig. 1), indicating that the snails enhanced clam suspension. Clam retention also was greater in the slow-flow than fast-flow treatments. As expected, most of the clams (>90% of the mid and late-season sizes) in the slow-flow treatments were not eroded from the sediments in the absence of snails. At the "slow" shear velocities used (0.7 - 1.3 cm s⁻¹), individual sediment grains were observed to move, but bulk sediment transport (erosion of 1 mm or more from the sediment surface) did not occur. With the addition of snails, however, over 40%
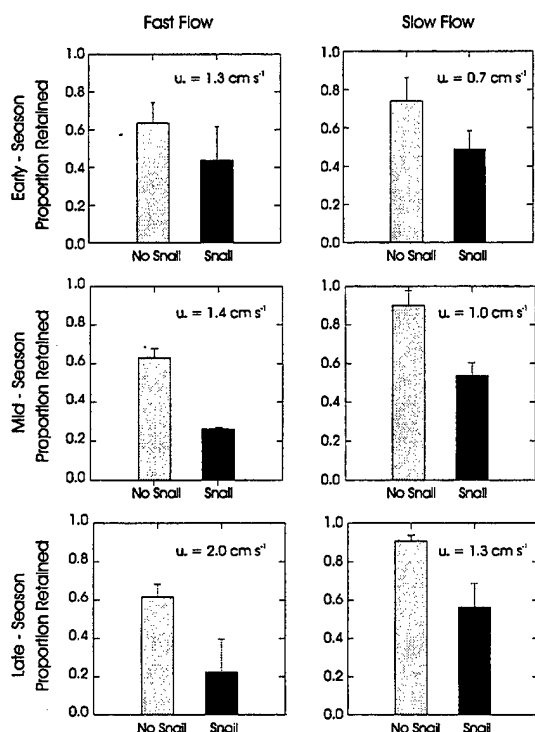
Fig. 1. Proportion of early- (1.3 mm), mid- (1.8 mm) and late-season (2.3 mm) *Mya arenaria* (mean and standard error; n = 4 for early and 3 for mid and late) retained in flume runs. Unburied clams were excluded from calculation of proportion retained. Snail treatment was exposed to disturbance by *Ilyanassa obsoleta*; No-snail treatment was left undisturbed. Shear velocity u_* shown for each set of runs. Two-way ANOVA showed the snail effect was significant for the mid- (F=36.7; P=0.001) and late-season (F=10.8; P=0.011), but not the early-season (F=2.9; P=0.11) clams. Similarly, the speed effect was significant for the mid- (F=21.9; P=0.002) and late- (F=8.7; P=0.018), but not early-season (F=0.35; P=0.56) clams.

of the clams were suspended. Erosion of the sediment was increased (data not shown) and visual observations showed that once the clams were exposed to the sediment surface they were unable to burrow back down. This result indicates that snails lower the shear velocity at which active, burrowing juvenile clams are suspended.

For the medium and large clam sizes, suspension in the fast-flow treatment without snails was similar to suspension in the slow-flow treatment with snails (Fig. 1), suggesting that the effect of snails in the field (at these densities) may be comparable to a substantial (0.6 to 0.7 cm s^{-1}) increase in boundary shear velocity. Bulk sediment transport occurred at the shear velocities used in the fast-flow treatments ($u_* >1.3$ cm s^{-1}).

As expected, the different clam sizes were not equally susceptible to suspension. For example, in the absence of snails, the proportion of mid-season (1.8 mm) clams retained at $u_* = 1.4$ cm s^{-1} was much lower than the proportion of late-season (2.3 mm) clams retained at $u_* = 1.3$ cm s^{-1}, but similar to the proportion of late-season clams retained at $u_* = 2.0$ cm s^{-1} (Fig. 1). This pattern of larger clams needing a higher shear velocity than smaller clams to suspend a specific proportion of individuals was consistent for all combinations of snail and flow treatments.

Field experiments

Abundance of *Mya arenaria* juveniles was significantly higher in the no-snail than the snail plots over the course of the 45-day field experiment (Fig. 2). At the start of the experiment (day 0), *M. arenaria* abundance was not significantly different between the plots intended for the no-snail cages and those intended for snail cages, but was significantly lower than abundances in ambient
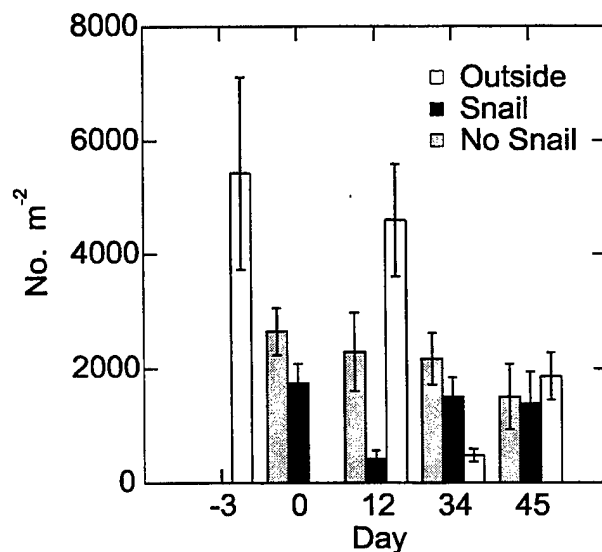
Fig. 2. Abundance of *Mya arenaria* in 6.5 cm diameter core samples collected in ambient sediments (Ambient), and under cages that permitted (Snail) or excluded (No Snail) immigration of *Ilyanassa obsoleta*. Values are means and standard errors of 5 samples. Ambient sediment samples were taken 3 days before experiment started (July 12, 1997). On day 0 (July 15), samples were taken in cleared plots before cages were put in place. On days 12, 34 and 45, samples were taken under cages and in ambient sediment. Two-way ANOVA with snail presence and sampling date as fixed factors showed a significant effect of snails $(F=4.3; P=0.049)$.

sediments collected 3 days before the initiation of the experiment (one-way ANOVA with post-hoc Bonferroni test; $df_{treat}=2$; $df_{error}=10$; $F = 6.005$; $P < 0.02$). This difference probably resulted from the disturbance caused by removing the snails from the experimental plots. High abundances in the ambient sediment persisted to day 12 (Fig. 2), but became significantly lower on days 34 and 45 (one-way ANOVA with post-hoc Bonferroni test: $df_{day}=3$; $df_{error}=14$; $F = 9.205$; $P < 0.001$). On day 45, numbers of *M. arenaria* juveniles in ambient sediments were slightly higher than on day 34, but their mean size (data not shown) was no smaller, as would have been expected for a late-season recruitment event.

The cages operated as intended, with no *Ilyanassa obsoleta* invading the no-snail treatment (except in cases when wind events eroded underlying sediments and provided access), and many invading the snail treatment, in numbers comparable to their natural abundances. No substantial difference in the abundance of potential predators was noted between the two cage treatments or between the caged plots and ambient sediments.

The magnitude of the difference in *Mya arenaria* abundance between no-snail and snail treatments varied notably through the course of the experiment (Fig. 2). Much of this variation corresponded with the unwanted invasion of snails into no-snail plots through pits eroded under the cages (these snails were removed and the pits refilled with sediment when detected). For instance, on day 12, snails had been excluded successfully from all no-snail plots except one, which harbored a few individuals. Mean *M. arenaria* abundance in the no-snail plots was more than 5 times that in snail plots. On day 34, snails had invaded three of the five no-snail plots (but in lower than natural densities), and the difference in *M. arenaria* abundance between the no-snail and snail plots was much reduced. On day 45, snails had invaded four of the no-snail plots (in near-natural densities), and *M. arenaria* abundance in the no-snail plots was only slightly higher than in the snail plots. The experiment was terminated on that day.
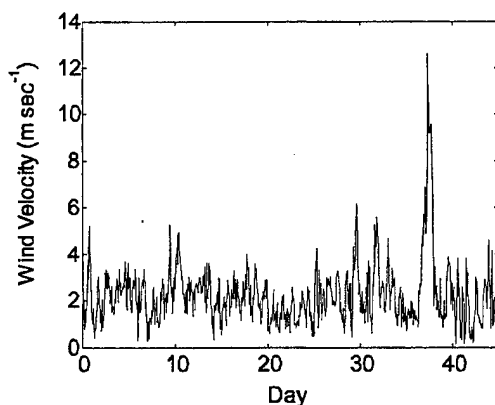
159

Fig. 3. Hourly averaged wind speeds recorded at the Woods Hole Oceanographic Institution meteorology station in Woods Hole, MA. Record starts on July 15, 1997 and covers the 45-day duration of the field experiment. Scour in the field experiments appeared to be caused by wind events on Days 29, 31 and 36-37.

Wind records from the WHOI meteorology station provided evidence of three substantial storms that we suspect were responsible for the observed sediment scour. The wind events on August 13 and 15 (days 29 and 31) were characterized by sustained gales of 5 to 6 m s^{-1} with strong gusts (Fig. 3). Because sediment transport on tidal flats can be greatly enhanced during such events, the scour observed in our experiments probably occurred on one or both of these dates. Thus, by day 34, the snails would have had access to the no-snail plots for only a few days. The storm that began on August 20 (day 36) was larger than any other during the experiment, and was characterized by sustained winds of >10 m s^{-1}. The snails probably gained entry to the no-snail plots at this time, and were thus present for most of the final interval.

DISCUSSION

Our flume experiments suggest that in natural field conditions disturbance by the snail *Ilyanassa obsoleta* is likely to cause juveniles of *Mya arenaria* to be suspended in flows slower than those needed to suspend undisturbed clams. Thus, the presence of snails is expected to expand the range of flow environments in which juvenile clams are susceptible to transport. These studies also indicate that disturbance is likely to increase the magnitude of hydrodynamic transport of clams during sediment transport events except during very energetic events when all clam juveniles are suspended regardless of the presence of snails. The mechanism of disturbance appears to be two-fold: the snails move laterally just below the sediment surface and expose clams to boundary shear stresses both by mixing them vertically and by causing the sediment above them to erode.

Our field observations on days 12 and 34 (for which storm disturbance was minimal) support the flume prediction that disturbance by *Ilyanassa obsoleta* enhances suspension of *Mya arenaria* juveniles and leads to a local decrease in clam abundance. The snail effect was not apparent on day 45 because a large storm on day 36 had allowed snails access to the no-snail cages. The mechanism of disturbance in our study was by the snail increasing the susceptibility of juvenile clams to passive erosion. We suggest that this mechanism also may have played a role in the reduction of nematodes (Nichols and Robertson, 1979) and other taxa (Hunt et al., 1987) observed in previous field manipulations of *I. obsoleta*.

We expect that *Mya arenaria* juveniles become less susceptible to suspension as they grow because they become heavier and capable of deeper burrowing. When they initially settle, and can be suspended in shear velocities as low as 1.0 cm s^{-1} (Roegner et al., 1995), they are likely to be transported in routine tidal flows (as measured in Ayers, 1959). At some size, they will no longer be suspended by tidal flows, but may be transported by energetic wind events. Also, at some size, they will burrow below the depth disturbed by the snail *I. obsoleta* (roughly 1 to 2 cm), and will attain a refuge from that disturbance. Investigation of these critical sizes is worth further research, as it will provide information about the relative influences of hydrodynamic transport and biological disturbance on *M. arenaria* juveniles as they grow through the first year.

Ilyanassa obsoleta is likely to play an important role in determining the adult distributions of *M. arenaria* because snails can increase the suspension of mid and late season clams during wind events, and potentially can suspend clams even in tidal currents. This process may operate on scales of a few meters, by moving juveniles to different tidal heights. Or it may operate on scales of kilometers, possibly transporting juveniles out of an entire habitat during an ebb-tide sediment transport event. Not enough is known about the costs and benefits of post-larval resuspension to speculate upon whether or not it may be advantageous to the clams. Potential advantages to resuspension include transport to a more suitable habitat. However, resuspension may expose clams to increased risk of predation, as well as to possible transport into a less hospitable area.

LITERATURE CITED

Ayers JC (1959) The hydrography of Barnstable harbor, Massachusetts. Limnol Oceanogr 4: 448-462

Brown B, Wilson WH (1997) The role of commercial digging of mudflats as an agent for change of infaunal intertidal populations. J Exp Mar Biol Ecol 218: 49-61

DeWitt T, Levinton J (1985) Disturbance, emigration, and refugia: How the mud snail, *Ilyanassa obsoleta* (Say), affects the habitat distribution of an epifaunal amphipod, *Microdeutopus gryllotalpa* (Costa). J Exp Mar Biol Ecol 92: 97-113

Emerson CW, Grant J (1991) The control of soft-shell clam (*Mya arenaria*) recruitment on intertidal sandflats by bedload sediment transport. Limnol Oceanogr 36: 1288-1300

Feller R (1984) Dietary immunoassay of *Ilyanassa obsoleta* , the eastern mud snail. Biol Bull 166: 96-102

Hunt J, Ambrose WJ, Peterson C (1987) Effects of the gastropod, *Ilyanassa obsoleta* (Say), and the bivalve, *Mercenaria mercenaria* (L.), on larval settlement and juvenile recruitment of infauna. J Exp Mar Biol Ecol 108: 229-240

Jumars PA, Nowell ARM (1984) Fluid and sediment dynamic effects on marine benthic community structure. Am Zool 24: 45-55

Levinton J, Stewart S, Dewitt T (1985) Field and laboratory experiments on interference between *Hydrobia totteni* and *Ilyanassa obsoleta* (Gastropoda) and its possible relation to seasonal shifts in vertical mudflat zonation. Mar Ecol Prog Ser 22: 53-58

Möller P, Rosenberg R (1983) Recruitment, abundance and production of *Mya arenaria* and *Cardium edule* in marine shallow waters, Western Sweden. Ophelia 22: 33-55

Nichols JA, Robertson JR (1979) Field evidence that the eastern mud snail, *Ilyanassa obsoleta*, influences nematode community structure. Nautilus 93: 44-46

Roegner C, André C, Lindegarth M, Eckman JE, Grant J (1995) Transport of recently settled soft-shell clams (*Mya arenaria* L.) in laboratory flume flow. J Exp Mar Biol Ecol 187: 13-26

Trowbridge JH, Geyer WR, Butman CA, Chapman RJ (1989) The 17-meter flume at the Coastal Research Laboratory. Part II: flow characteristics. Woods Hole Oceanographic Institution Technical Report 89-11: 1-37

Bedload Transport in Oscillatory Flows at Intermediate Wave Reynolds Numbers

Jonathan M. Nelson

US Geological Survey, Water Resources Division National Research Program,
MS-413, Box 25046, Lakewood, CO 80225 (jmn@usgs.gov)

Ronald L. Shreve
Department of Earth and Spaces Sciences, UCLA, Los Angeles CA 90095

Jørgen Fredsøe, Mutlu Sumer, and Carsten Lodahl
Institute of Hydrodynamics and Hydraulic Engineering,
Technical University of Denmark, DK-2800, Lyngby, Denmark

Predicting sediment transport in complex flows requires an understanding of the role of the near-bed turbulence structure in particle entrainment and movement. The mean flow and turbulence structure relevant to sediment transport traditionally is parameterized by bed shear stress, because mean flow and near-bed turbulence statistics in steady, uniform boundary-layer flows scale with this parameter. In complex (i.e., nonuniform or unsteady) flows, however, bed shear stress does not completely characterize the near-bed turbulence and so is not necessarily an accurate predictor of sediment-transport rate. For example, it is a poor predictor of local bedload sediment flux downstream of a typical bedform because turbulence produced in the free-shear layer downstream of the separation point markedly enhances sediment entrainment and transport with little, if any, effect on bed shear stress. Similarly, unsteady flows that have identical instantaneous bed shear stresses (in an ensemble-averaged sense) but different acceleration rates should have different turbulence structures and hence different sediment-transport rates.
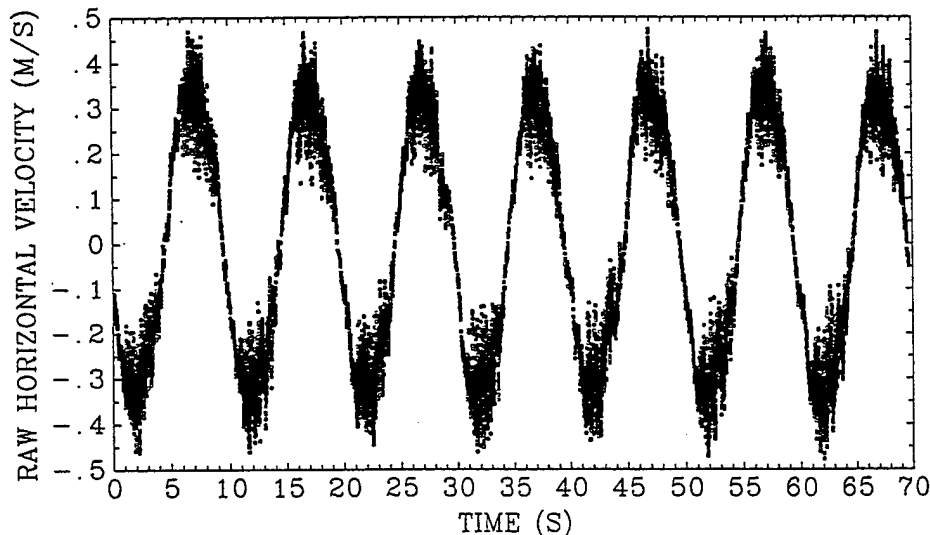
Figure 1. Laser-Doppler measurements of horizontal velocity 3mm from the bed.

As part of an investigation of the effect of flow nonuniformity and unsteadiness on sediment transport, we measured bedload transport and near-bed flow over a flat bed in an oscillatory flow duct. Sediment flux and velocity were determined at 100hz using synchronized high-speed cinematography and laser-Doppler velocimetry, respectively. We used 0.8 and 1.3 mm well-rounded particles, with Shields numbers of about 0.08 (based on maximum stress), corresponding to wave Reynolds numbers of about 2×10^5 and 3×10^5 for 10s waves. We chose this range of Reynolds number because it corresponds to the greatest variation in turbulence structure over the wave.

In Fig. 1, horizontal velocity time series measured 3mm from the bed (wave boundary-layer thickness was 2 cm) clearly show the effects of acceleration in modifying the turbulence field. Over much of the accelerating limb of the waves, turbulence is damped. As the acceleration wanes, the flow becomes turbulent, and remains so
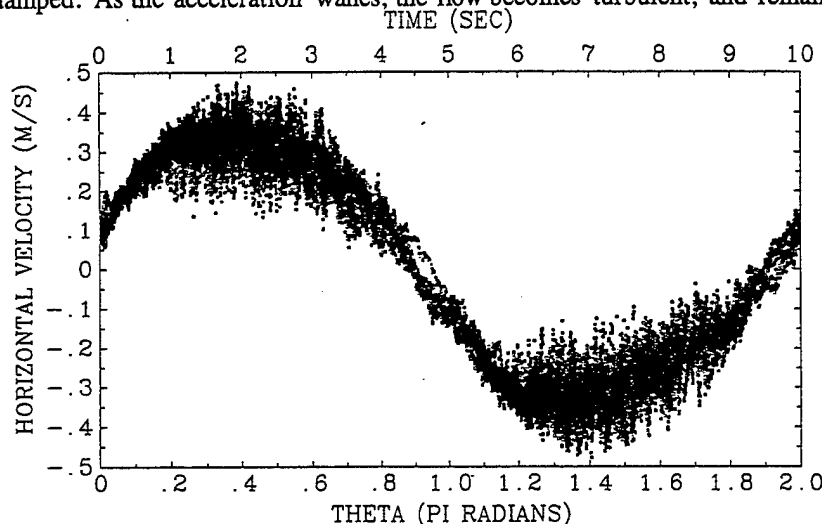
Figure 2. Data from Fig. 1 plotted versus the phase of the wave in the outer flow.
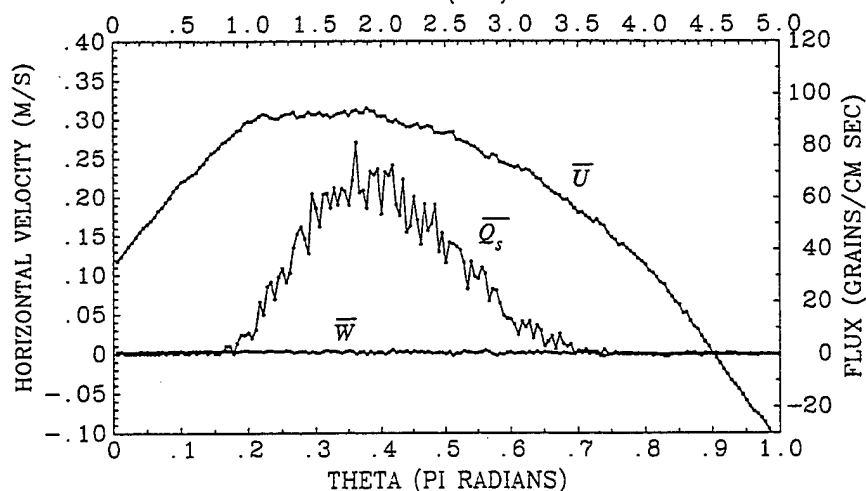
Figure 3. Ensemble-averaged velocity and sediment flux as a function of wave phase.

164

over much of the decelerating limb of the wave. Acceleration tends to inhibit turbulence, while deceleration enhances its development. In Fig. 2, the data in Fig. 1 are plotted as a function of wave phase; the near-bed flow leads the outer flow as expected. Interestingly, the near-bed flow exhibits variability over all phases of the wave, even though turbulence production is damped over much of the wave. Outside the wave boundary layer, measurements do not show this variability, the response is essentially perfectly harmonic. Apparently, turbulence generated during during and immediately after the peak velocity has a weak effect on flow behavior even after the flow appears to "relaminarize".

Computing ensemble averages in one degree bins over 60 waves shows that transport is not uniquely related to either mean velocity or Reynolds stress. Fig. 3 shows that ensemble-averaged transport tends to increase rapidly late in the accelerating limb of the wave, even though ensemble-averaged near-bed velocity is nearly constant. Near-bed velocity is almost constant during this period because the pressure gradient driving the flow is balanced by the increase in downward vertical momentum flux associated with the development of turbulence. Although the ensemble-averaged transport increases with stress, it drops off when stress continues to increase (Fig. 4; < > indicates smoothing of the data by averaging over five degree bins in one degree increments). Note that the maximum stress for this range of Reynolds number lags the wave, in agreement with the other measurements and direct numerical simulations.
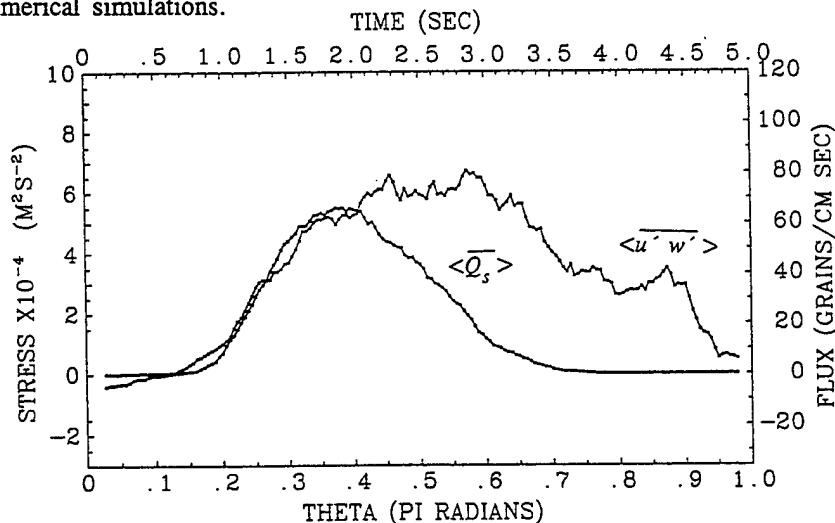
Figure 4. Ensemble-averaged momentum and sediment flux versus wave phase.

Sediment transport as a function of boundary shear stress shows dramatic hysteresis (Fig. 5), with a single value of stress yielding much different bedload fluxes depending on the sign of temporal acceleration. This behavior is explained by alteration of the turbulence statistics by acceleration. Near-bed deceleration promotes rapid boundary layer growth and changes in turbulence structure and sediment transport compared to the accelerating phase. Boundary shear stress is a very poor predictor of bedload transport in this flow; it does not fully characterize the flow variability as it does in a steady, uniform flow.
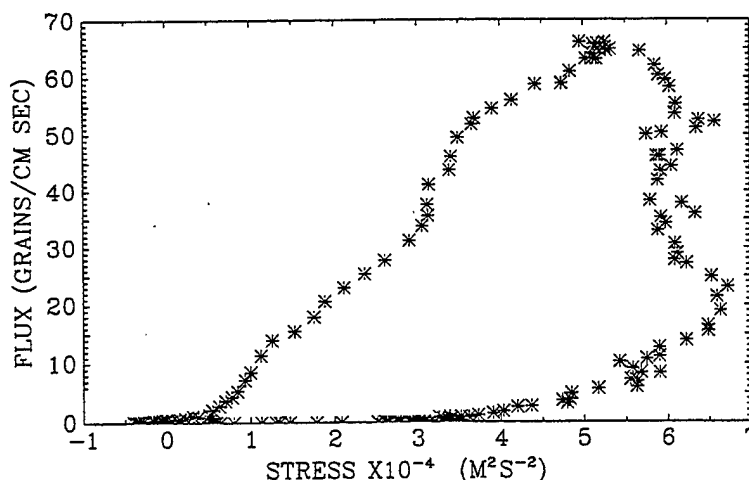
Figure 5. Ensemble-averaged stress versus sediment flux.

Sediment entrainment and transport is primarily a function of fluid drag on sediment particles on or near the bed, and those fluid drag forces are strongly dependent on the flow velocity near the sediment grains. On the accelerating limb of the wave, turbulence production along with vertical momentum exchange tend to be damped, so velocity near the bed increases without much increase in the variability of that velocity. As the near-bed velocity approaches a maximum, the rate of acceleration decreases, resulting in a rapid increase in turbulence production and associated growth of the boundary layer. Thus, the maximum instantaneous velocities near the bed occur after the maximum ensemble-averaged mean velocity (see Figs. 2 and 3). Sediment-transport rates are sensitive to higher moments of the velocity distribution, so transport increases even while the mean velocity does not. Relating bedload fluxes to ensemble-averaged values of some higher percentile (e.g., the 84th percentile) of the streamwise velocity distribution near the bed results in a very accurate predictor for sediment flux at all phases of the wave (Fig. 6).
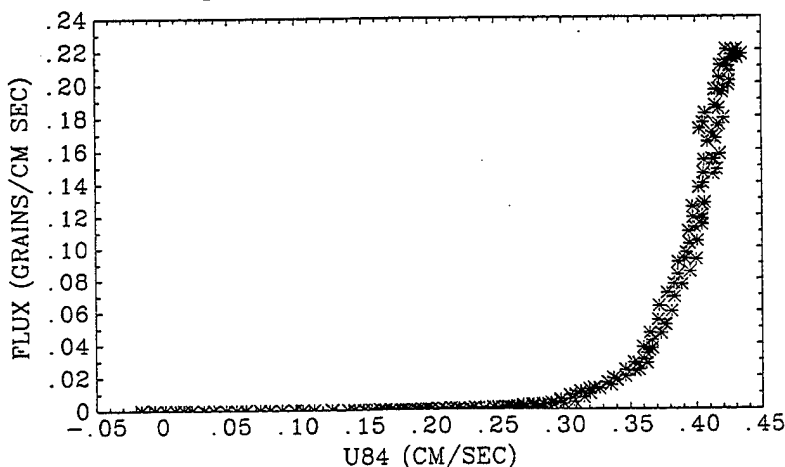
Figure 6. Ensemble-averaged sediment flux versus 84th percentile of U.

Evidence for Offshore Veering of the Undercurrent over the Central California Coast

Marlene A. Noble[1] and Steven R. Ramp[2]

[1]U. S. Geological Survey, Menlo Park CA
[2]Naval Postgraduate School, Monterey CA

In the last 2 decades, several programs have investigated subtidal circulation patterns on the central and northern California shelf and upper slope. These studies have shown that the poleward-flowing California undercurrent is the dominant feature in currents flowing over the upper and middle slope. This undercurrent is a strong eastern-boundary current that generally lies just seaward of the shelf break, inshore of the much broader California Current system that flows equatorward through the upper reaches of the eastern, central Pacific ocean. The undercurrent, which carries warm, salty water northwestward along the continental slope from Baja, California to Vancouver, Canada tends to follow the slope isobaths, though it is not known whether the undercurrent flows continuously along the western continental margin. Local oceanic and topographic features may perturb the flow in the undercurrent and either force it offshore or obscure its characteristic signal. The undercurrent is thought to be relatively narrow (with widths between 10 and 40 km), energetic (maximum speeds between 20 and 50 cm/s) and shallow (depths to 600 m). Over most of the year, the core of the undercurrent lies near 200 m, but tends to rise to the sea surface in winter.

In February, 1991, an array of 6 current-meter moorings was deployed for one year across the central California outer shelf and slope, in part to investigate the characteristics of the undercurrent in this region of the slope. The main line of the array, sites A-D, extended 40 km across a smooth, fairly gently-sloping section of the outer shelf and slope (Figure 1). Water depths ranged from 90 to 1400 m. The northern line of the array was shorter, 14 km, but because it cut across a much more steeply-sloping section of topography that has many small canyons and large gullies, it actually reached deeper water depths. The outermost mooring, site E, was deployed just inside a small canyon, with a rim near 1500 m and an axis depth of 2000 m. Each mooring had between 3 and 6 instruments. In order to highlight the undercurrent signal, all data from these instruments were low-pass filtered to remove fluctuations with periods less than 33 hours.
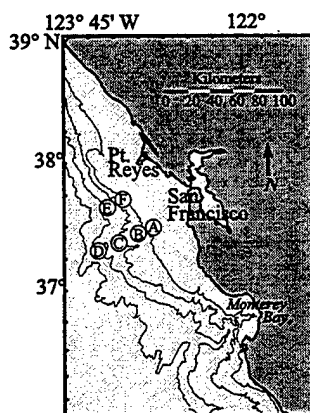

Figure 1. Locations of the moorings deployed on the shelf and slope. Ⓐ indicates mooring location.

The mean flow along the slope was predominately poleward (Figure 2). Mean current speeds were generally around 8 cm/s along the southern line, with the highest speeds near the ocean surface. The mean flow through the southern line was 1.2 Sv. The flow was still poleward, but reduced to 0.4 Sv across the shorter northern line, which is a 20% reduction of transport across an equal area of the southern line. Actual current speeds below the shelf break at site F were reduced significantly, with speeds of a few cm/s, compared to speeds of 20 - 30 cm/s at equivalent sites along the southern line. A similar pattern was seen in the first mode for alongslope currents; flows across the southern line were stronger and appeared at deeper depths. If one adds the fluctuating amplitude of the first modal currents to the mean flow field, transport over the year ranges from 0 to 2.5 Sv poleward along the southern line; 0 to 1 Sv poleward along the northern line. The actual poleward transport is probably greater than estimated by these measurements because both the mean and correlated alongshelf flow field obviously extended seaward of our measurement sites.
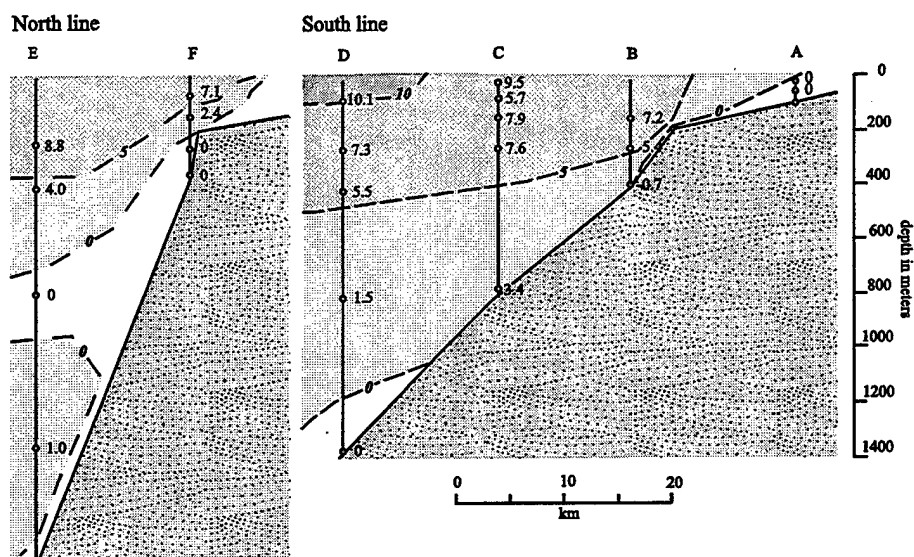
Figure 2. Alongslope mean flow across the southern and northern line of the array.

We suggest that the core of the undercurrent lay further offshore along the northern transect than the southern transect (and thus was not sampled by this array). This is somewhat surprising because it is well known that vorticity constraints tend to cause subtidal currents over sloping topography to flow along isobaths . Recent work, (Susan Allen, Personal Communication) has shown that steady, subtidal flow fields cannot remain parallel to isobaths when isobaths converge relatively quickly in space. The spatial acceleration forces, which result from the focusing of a broad, slow flow over gently sloping portion of the Farallon topography into a faster, narrower current over the steeper topography, override vorticity constraints. These accelerative, or inertial, forces, arise from the non-linear, advective terms in the alongshore equation of motion, $v \, \delta v/\delta y$. Essentially, because the current cannot turn rapidly enough to adiabatically follow the topography; it flows into deeper water.

Allen has derived a parameter ε, that shows the minimum distance that can exist between 2 contours and still have the flow follow isobaths. ε must be greater than

$$\left(\frac{U_0 \Delta x}{f}\right)^{1/2} \quad .$$

U_0 is the velocity over contours spaced Δx apart and f is the Coriolis parameter. Along the southern line, Δx is 25 km between 200 and 1000 m, 30 km between 200 and 1500 m. For typical flow values of 25 cm/s, ε is 8-9 km. This is much shorter than the actual distance between isobaths. The flow can follow topography along the southern line .

Along the northern line, the distance between the 200 and 1000 m (1500 m) isobaths is 5 (8) km, somewhat smaller than the maximum isobath convergence calculated above. Hence, for typical flow velocities, the undercurrent will tend to cross isobaths as it flows toward the northern line. Our measurements support this inference. Normally 1-2 Sv flows across the gently-sloping topography of the southern line. The abruptly-converging isobaths just north of the southern line force the current to veer offshore, into deeper water. Because of vorticity constraints, the undercurrent will turn counterclockwise and move even further offshore. Hence, the undercurrent is reduced in amplitude at site E relative to C, as is our estimate of the net transport across the northern line.

The isobaths bracketing sites B and F, 200 and 500 m, converge particularly rapidly. South of site B, they are about 10 km apart, then converge to 6 km at site B, less than 1 km at site F. For typical flow values, ε is about 5 km for site B, consistent with the large currents actually measured there. But ε is about 4 km northwest of B, much larger than the actual isobath separation at site F. This site seems to be permanently shadowed, consistent with the very small flows observed below the shelf break. Poleward currents at site B need to be less than a few cm/s to be able to follow these steeply converging isobaths.

The abrupt topographic convergences suggest that this region is a preferential site for generating undercurrent meanders. The meanders can close into clockwise eddies that have been seen to drift offshore in regions to the north of our site.. The eddies may interact with the offshore jet generated seasonally at Pt Reyes or they may enter the equatorward California Current System and be swept back across the array. The strong southward flow observed over the slope at the beginning of the measurement period may well have been such an eddy.

Mechanisms of sediment dispersal and the influence of floods on the northern California continental shelf

A.S. Ogston*, D.A. Cacchione*, R.W. Sternberg† and G.C.Kineke‡
*U.S. Geological Survey (MS-999), 345 Middlefield Road, Menlo Park CA 94025
†School of Oceanography, Box 357940, University of Washington, Seattle WA 98195
‡Department of Geology and Geophysics, Boston College, Chestnut Hill MA 02467

Introduction

As part of the sediment dynamics component of the STRATA FORmation on Margins project (STRATAFORM; Nittrouer & Kravitz, 1996), three tripods were deployed concurrently on the northern California continental shelf in an alongshelf array near the 60-m isobath. The G65 (Virginia Institute of Marine Science) location is directly offshore of the mouth of the Eel River, and the K63 (U.S. Geological Survey) and S60 (University of Washington) locations are approximately 13 and 28 km north of the river mouth, respectively (Figure 1). A 40-day time period during the winter of 1996-97 demonstrates the different mechanisms by which sediment moves on the continental shelf, and the influence of local circulation on the resulting sediment flux direction. Fortuitously, a 30-year flood occurred in the Eel River during which extremely high suspended sediment concentrations were observed at both the K63 and S60 locations. These high concentrations are located in the area of the flood deposit and not beneath the surface plume, are too large to be caused simply by wave resuspension. This raises the question, could thin lenses of fluid mud form on the continental shelf, and could these high concentrations of sediment be responsible for a significant portion of sediment movement across the shelf in regions of small mountainous rivers?

Field Experiment

The three tripods were deployed on the mid-shelf silt deposit which has been associated with floods on the Eel River. Figure 1 shows the approximate location of the 1997 flood event bed (Wheatcroft, unpublished). Instrumentation on all three tripods included vertical arrays of Optical Backscatter Sensors (OBS) and electromagnetic current meters, and a pressure sensor, amongst other more specialized instrumentation. The tripods were concurrently deployed over the period from 11 Nov 1996 to 21 Jan 1997. This study specifically examined events during the 40-day period between 1 Dec 1996 and 8 Jan 1997 when the Eel River was in its winter high-flow stage.

Sediment Transport Events – Integrated Flux

The different conditions under which sediment moves on the continental shelf are demonstrated in a 40-day period during which all three tripods were deployed. Table 1 shows the magnitude and direction of vertically-integrated sediment flux from six different events under varying conditions for the three different sites. For the larger events (A-E), there is an offshore component to the flux, but in the alongshelf direction
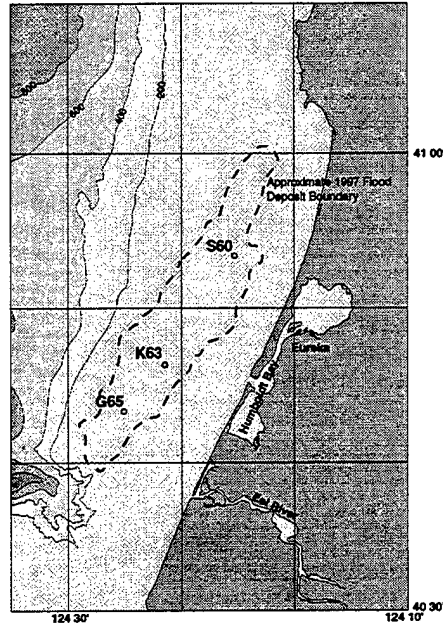
Figure 1. Site map

the flux is strongly dependent upon the local circulation during the time of the event. The largest event (E) is associated with the 30-year flood in January 1997.

During all events except the 30-year flood, the direction of flux was similar between sites, although there is a more southerly trend at S60 than at K63. During the 30-year flood event (E), the flux of sediment at K63 and S60 are substantially higher than at G65 and there appears to be a convergence of flux between the two locations, consistent with the depo-center of the flood deposit. The sediment flux summed over the time of the flood event accounts for 75% of the winter flood season flux.

Table 1. G65, K63 and S60 vertically integrated sediment flux events

	G65		K63		S60		
	Flux Integ. (g/cm/s)	Avg.Flux Direction (deg. N)	Flux Integ. (g/cm/s)	Avg.Flux Direction (deg. N)	Flux Integ. (g/cm/s)	Avg.Flux Direction (deg. N)	Conditions
A	0.082	236	0.095	213	0.43	217	Large waves
B	0.46	356	0.38	8	0.27	310	Large waves, small flood
C	0.26	264	0.14	272	0.15	254	Medium waves, small flood
D	0.15	353	0.21	14	0.15	331	Medium waves
E	0.40	200	11.4	283	6.03	254	Medium waves, large flood
F	0.43	239	0.046	48	0.44	168	Small waves

172

Eel River Flood Period Sediment Flux

The time averaged total, mean, and fluctuating components of sediment flux at 20 to 30 cm above the seabed (above the level of the extremely high concentration observations) were determined for two time periods; the two-month winter flood period, and the approximately 3-day period of the 30-year flood. These were compared to a previously analyzed year of record at S60 (1995-1996; Ogston & Sternberg, in press).

During the two-month winter flood period:
- in the across shelf direction, the net sediment flux was directed offshore at all locations. In the alongshelf direction, each location was different: slightly south at G65, north at K63, and south at S60. The flux magnitudes at K63 and at S60 were similar, and significantly larger than the flux at G65. The differences in both magnitude and direction of the sediment flux may be attributed to the circulation on the Eel shelf,
- the flux due to fluctuating components (periods less than 3 days) was significantly smaller than flux due to mean components, again emphasizing the importance of low frequency circulation.

During the 30-year flood period:
- the direction and magnitude of the mean component determined the net direction of the flux and was the same as for the two-month flood period. The alongshelf magnitude was 5 to 6 times larger at G65 and K63 and 11 times larger at S60 than for the flood period,
- the across shelf flux is an order of magnitude larger at K63 and S60 during the 30-year flood conditions. The increase in the across shelf magnitude is attributed to both the increase in suspended sediment concentration and the increase in mean currents, suggesting the importance of advection and gravity-driven processes.

In comparison with the year-long record that was analyzed previously at the S60 site:
- the net direction of flux was consistent with the two-month winter flood period, and the 3 days of the 30-year flood period,
- the flux was an order of magnitude smaller than during the two-month flood period, and two orders of magnitude smaller than during the 30-year flood period.

Fluid Mud?

The suspended sediment concentration time series at K63 shows evidence of extremely high concentrations between 2 Jan 1997 and 6 Jan 1997. OBS's have been found to exhibit a linearly increasing response at relatively low concentrations and a decreasing response at extremely high sediment concentrations depending on the gain settings (Kineke & Sternberg, 1992). During at least two 12 to 24-hour periods during the 30-year flood event, the lowest sensor at K63 appears to fall into the range of decreasing response, as displayed by larger apparent concentrations higher in the water

column when using only the linearly increasing calibration curve. A laboratory calibration with in-situ sediment of the complete response shows a span of 0 to 2 g/l in the linearly increasing response range and an approximate span of sediment concentrations of 160 to 600 g/l in the decreasing response range for the lowest sensor. Although the decreasing response calibration probably over-estimates sediment concentration because of density changes due to flocculation processes, it is apparent that sediments were in suspension at concentrations much greater than 10 g/l at 13 cm above the bed, and could be considered fluid mud.

Conclusions

The sediment-transport time-series from the three tripods demonstrate the various mechanisms by which sediment moves on the continental shelf, and the importance of local circulation on the direction of sediment flux. There is a high correlation between wave orbital velocity and suspension of sediment as has been previously documented, but the contribution due to sediment input by the Eel River is a more complicated and unaccounted for aspect in modeling of suspended sediment transport.

Specifically,
- There is considerable alongshelf variability in sediment flux. In order to understand the fate of Eel River sediments, circulation on the shelf must be considered.
- There is a persistent offshore flux of sediment. The alongshelf flux convergence between K63 and S60 during the 30-year flood might explain the bulls-eye shape of the flood deposit.
- Extremely high concentrations of sediment were observed at 13 cm above the bed (up to 100's of g/l) during Eel River flooding suggesting that fluid mud formation may be an active process on narrow shelves off small mountainous rivers, which may not have been observed previously due to instrument limitations.
- Sediment flux during one extreme flood event can account for 75% of the winter flood season sediment flux.

References

Kineke, G.C. & R.W. Sternberg. 1992. Measurements of high concentration suspended sediments using the optical backscatterance sensor. *Marine Geology 108*:253-258.

Nittrouer, C.A. & J.H. Kravitz. 1996. STRATAFORM: A program to study the creation and interpretation of sedimentary strata on continental margins. *Oceanography 9*, 146-152.

Ogston, A.S. & R.W. Sternberg, in press. Sediment transport events on the northern California continental shelf. *Marine Geology*.

PIV Measurements of Turbulence and Flow Structure in the Bottom Boundary Layer

L. Bertuccioli, P. Doron, J. Katz and T. Osborn
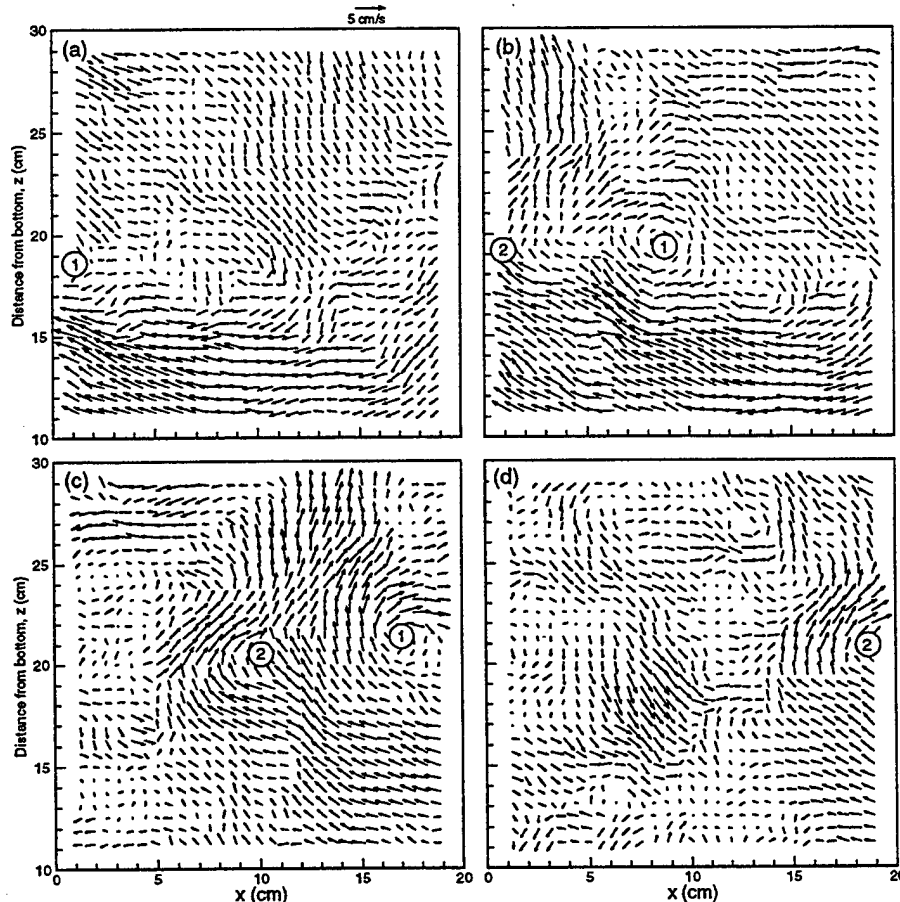The Johns Hopkins University

Figure 1: Sequence of velocity fluctuations vector maps measured in 14m deep water, at 1s intervals. u'(x,z)=u(x,z)-U(z), w'(x,z)=w(x,z)-W(z); u, w: Velocity components of a vector; U, W: Averages of u, w at constant z, over the entire data set. Note the structures designated "1" and "2" being convected across the sample area. Data from New York Bight, June 1998.

A submersible Particle Image Velocimetry (PIV) system for measuring the flow and turbulence characteristics in the bottom oceanic boundary layer has been developed and deployed. This device produces a 2-D array of 29x29 vectors of the instantaneous velocity distribution within a

20x20cm sample area (e.g., fluctuating velocity distributions shown in Figure 1). This data is then used to determine the velocity profiles, turbulence intensity and shear stress, vorticity distributions, dissipation and turbulent spectra. The submersible system also contains a CTD, a precision pressure transducer, optical transmission and dissolved oxygen content sensors, a tilt meter, a compass, and means to align the sample area with the mean flow. This instrument has been deployed off the WHOI dock during testing, and off Cape May, NJ and in the New York Bight for data acquisition near the bottom of the coastal ocean.

The data from the New York Bight was collected in 14m deep water, above a sandy bottom, at elevations ranging from about 10cm to 1.4m. Data for each elevation consists of 2 minutes of image pairs recorded at 1Hz. The data include the flow structure and Reynolds stress profiles within the inner layer. Figure 2 presents the measured turbulence parameter profiles. The results indicate, that the turbulence near the bottom is highly non-isotropic. For example, at an elevation of 15cm above the bottom, $|u'|/U=33\%$, $|w'|/U=12\%$ and $-u'w'/U^2=0.8\%$. An estimate of the external potential flow pressure gradient can also be computed from the vertical profile of U/W, and it indicates the existence of large scale phenomena, well beyond the time scale of our measurements. These trends will be resolved by analyzing longer data series with the upgraded data acquisition system.
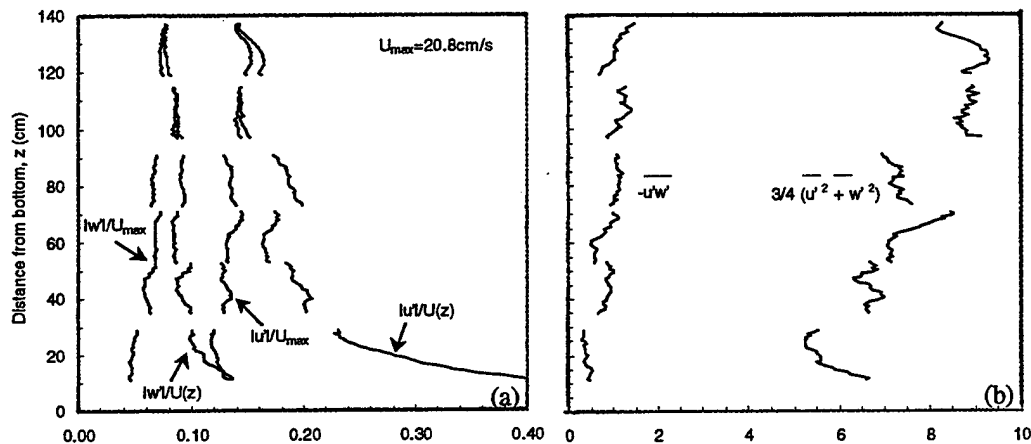
Figure 2: (a) Vertical profiles of RMS velocity fluctuations; (b) Vertical profiles of Reynolds stress and estimate for the Turbulent kinetic energy, assuming v'=0.5(u'+w'). U_{max} is the largest value of U(z); Averages of u'^2, w'^2, u'w' are at constant z, over the entire data set.

Another set of data was recorded off Cape May, NJ in 9m deep water, at an elevation of about 1.5m. In this case the wave induced motion has twice the amplitude of the mean current, and there are strong wave and beat effects on the turbulence. The small scale turbulence can be resolved by averaging data over individual vector maps, and it appears to be isotropic.

Circulation in a Hypersaline Lagoon

Clinton D. Winant
Center for Coastal Studies
Scripps Institution of Oceanography
La Jolla, CA, 92093-0209

Location and Physical Description

Laguna San Ignacio is one of several lagoons located along the western coast of the Baja California peninsula, about 500 miles south of the border between Mexico and the USA (Phleger and Ewing, 1962). The lagoon (Figure 1) which is about 28 km long and 4 km wide, is one of the calving grounds for the gray whale during the winter season. The entrance is composed of two distinct channels on either side of an extensive sand bar.
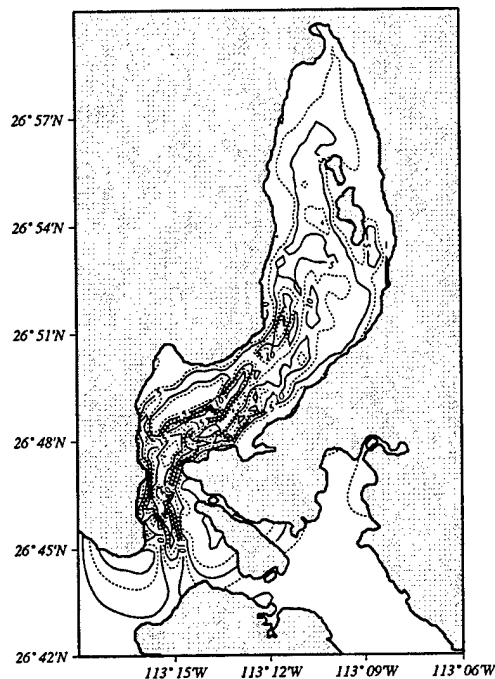
Figure 1: Laguna San Ignacio bathymetry

Behind the bar the two channels merge in the narrowest area, where maximum depths are about 20 m. Further north, most of the tidal flow is confined in three deep channels, surrounded by intertidal flats. The channels merge on the western side of the two islands, near the northern end of the lagoon. East of the islands the water is quite shallow. The central channel extends up to the northernmost extremity of the lagoon.

Climatology

During the late fall and winter (November through March), the weather is modulated by upper level synoptic activity, consisting of eastward propagating cyclones and anti-cyclones. Laguna San Ignacio is usually well to the south of winter storm tracks, and the atmospheric perturbations there are weaker than to the north, although there have been years when the winter storms were vigorous, resulting in relatively large rainfall. During the spring and summer the climate is arid, warm and given the strong winds, conducive to high levels of evaporation. During the late summer, tropical storm systems are frequently generated along the Pacific coast, in the vicinity of the Gulf of Tehuantepec. While these storm systems rarely propagate as far north as Laguna San Ignacio, the associated rainfall generates a second rainy period, in late summer.

Monthly averaged winds are from the northwest, with values near 5 m/s, except during spring when they reach 8 m/s. In the norther portion of the lagoon an intense localized wind system occurs with maximum velocities in excess of 10 m/s, oriented towards the opening. These winds are probably due to the temperature contrast between land and water, maximum intensities occur at night, and can persist over several days.

The daily averaged heat flux from the atmosphere to the lagoon varies between 150 and 300 W/m^2, depending on season. In combination with the persistent winds, this heatflux results in evaporation rates which always exceed rainfall, and vary between 3 mm/day in the winter and 10 mm/day during the summer.

Variation of Physical Properties

The evaporation acting over the surface of the lagoon results in higher salinities than in the neighboring Pacific, so the lagoon is hypersaline (Postma, 1965). A summertime profile of surface salinity along the central axis of the lagoon is illustrated in Figure 2. The excess salinity near the top of the lagoon varies between 3 psu in the winter and 6 psu in the summer.

Since the salinity does not continue to increase, some mechanism must exist which transports the salt left behind by evaporation back towards the ocean. The spatial gradient in salt is strong enough to influence the density so that the water near the top of the lagoon is generally heavier than near the entrance. This density variation
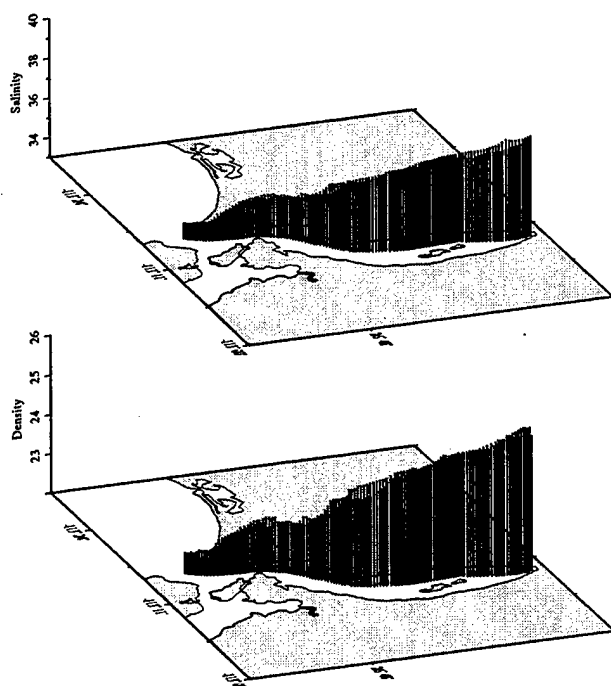
Figure 2: Surface salt and density in Laguna San Ignacio

is expected to drive a residual transport of heavier water towards the ocean, and could also be responsible for the flux of salt back towards the ocean (Largier et al.,1995).

Because of the confined entrance, and because the length of the lagoon is much greater than the depth, large tidal currents are required to keep the water level in the lagoon close to that of the open ocean. Vertical profiles of currents have been observed at four locations near the central axis, between the entrance and the top. The tidal currents are aligned with the axis of the lagoon and range between 1.2 m/s near the entrance and 0.1 m/s near the northern extremity. Tidal fluctuations in pressure and salinity lag currents by near 90 deg near the central axis. There exist significant spatial asymmetries in the tidal regime, comparable to those envisioned by Stommel and Farmer (1952) which can drive residual flows and provide a mechanism to transport salt back towards the ocean. Fischer et al. (1979) refer to this mechanism as tidal pumping.
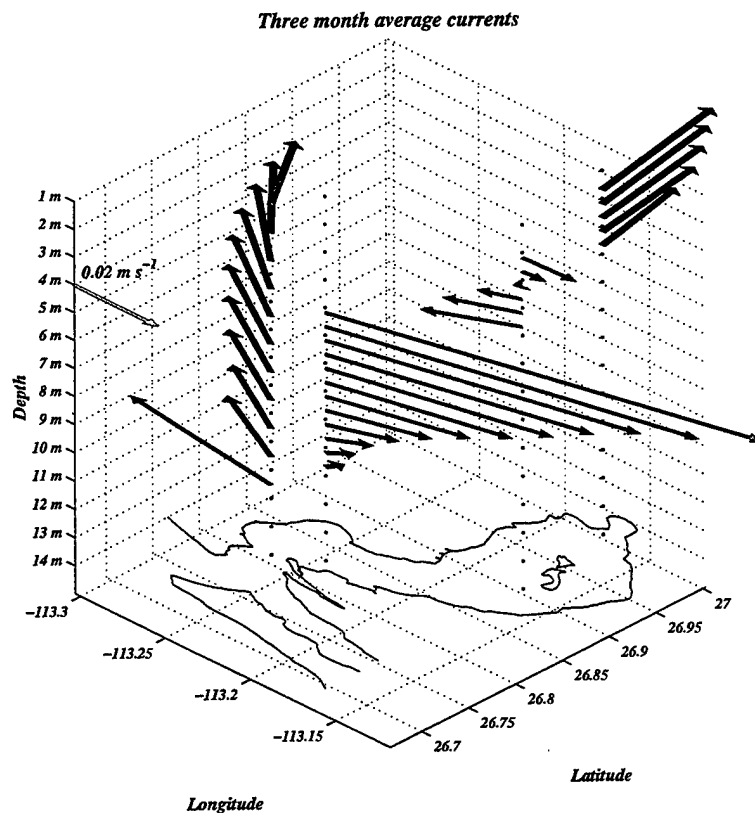
Figure 3: Three month average current profiles

The wind exerts a southward stress on the surface of the northern half of the lagoon. Because the lagoon is shallower east of the islands, the wind stress is expected to generate a clockwise residual circulation around the the islands, as suggested by Fischer et al. (1978). Drifting buoys support this result.

Three month long averages of currents measured at the locations noted above are illustrated in Figure 3. Currents at the two locations closest to the entrance are directed toward the top of the lagoon. Since there can be no net transport of water at any section, the residual circulation at locations on the sides of the lagoon must be directed towards the ocean, as in the inlet circulation suggested by Stommel and Farmer (1952). The vertical profile of currents measured south of the islands is consistent with buoyancy driven flow, with the time averaged velocity of the lower layer towards the ocean. Near the head of the lagoon the average velocities measured in the center of the channel are directed towards the north at all the measurement depths. This flow provides the water which is driven towards the ocean, at the surface and east of the islands, in response to the northerly wind stress.

Conclusions

The excess salt left by evaporation in the lagoon returns to the ocean by a variety of mechanisms acting in different areas. Near the top of the lagoon, where the depth is shallow and there is a lot of wind, the wind stress and the tides combine to produce a circulation which has a vertical structure in which bottom currents are directed towards the top of the lagoon, and a horizontal structure in which the circulation is clockwise around the islands. South of the islands, the vertical circulation is in the opposite direction and consistent with the density and salt distribution: the lower layer carries saltier water towards the ocean while the upper layer bring relatively fresh water from the Pacific into the lagoon. The tidal circulation in the lower lagoon is confined in three channels separated by shallow flats. The phase and amplitude of currents and salt varies in a section perpendicular to the axis, and these asymmetries result in a net transport of salt towards the ocean. In the entrance we expect that tidal pumping is responsible for the net transport of salt.

References

Fischer, H.B., E.J. List, R.C.Y. Koh, J. Imberger, and N.H. Brooks, Mixing in inland and coastal waters, Academic Press, Inc., San Diego, 483 p., 1979.

Largier, J.L, J.T. Hollibaugh and S.V. Smith, Seasonally hypersaline estuaries in Mediterranean-climate regions, *Estuarine, Coastal and Shelf Science*, 1995.

Phleger, F.B. and G.C. Ewing, Sedimentology and oceanography of coastal lagoons in Baja California, Mexico, *Bull. Geol. Soc. of America*, 73, 145-182, 1962.

Postma, H. Water circulation and suspended matter in Baja California lagoons, *Neth. J. Sea Res.*, 2(4), 566-604, 1965.

Stommel H. and H.G. Farmer, On the nature of estuarine circulation, *Woods Hole Oceanographic Inst. References*, Nos. 52-51, 52-63, 52-88, 1952.

EXPERIMENTAL AND THEORETICAL STUDY OF SHORELINE RESPONSE TO CHANGING BASE LEVEL

Chris Paola, John B. Swenson, and Gary Parker
St. Anthony Falls Laboratory
University of Minnesota
Minneapolis MN 55414

Introduction

The coupling between sea level and shoreline seems direct and straightforward. For example, high stands of sea level should correspond to times of maximum shoreline transgression, and the distance shoreline migrates per unit change in sea level should be set by the slope of the coastal plain. This simple geometric view is complicated by long-term coastal subsidence. *Pitman* [1978] constructed a geometric model of shoreline migration on a passive continental margin with subsidence rate linearly increasing in the mean transport direction. Assuming a long-term sea-level fall with shorter, but still very slow, cycles superimposed on it, Pitman made the counterintuitive prediction that shoreline would be in phase not with sea level but with the rate of change of sea level. Thus times of maximum regression would correspond to maxima in rate of fall, while times of maximum transgression would correspond to maxima in rate of rise. Thus shoreline position is phase-shifted by 90° from sea level. This phase shift is a limiting case of Pitman's model as the period of the sea-level cycles becomes long relative to a time constant that is characteristic of a particular basin. *Angevine* [1989] subsequently showed that in the high-frequency limit, shoreline and sea level are in phase. Comparable phase-shifting has since been observed in more sophisticated diffusion-based models of shoreline behavior [*Jordan and Flemings*, 1991], and a phase-shifted shoreline response has been applied to the interpretation of sea-level history on passive margins [*Miller et al.*, 1985; *Miller et al.*, 1993]. An equally important, though less widely known, prediction of the Pitman model is that the amplitude of sea-level response is much smaller for slow than for rapid sea-level changes. Thus basins could be thought of as high-pass filters for recording sea-level changes.

Experimental methods

The XS basin. Here we describe the results of an experiment designed to test some of these theoretical ideas on the relation between shoreline migration and base-level variation. The experiment was performed at St. Anthony Falls Laboratory (SAFL) in a prototype of the XS (Experimental Stratigraphy) basin, a new experimental basin that allows formation of physical stratigraphy in a system with a flexible subsiding floor. The prototype basin is 1.3 m long and 1 m wide, with up to 0.8 m of accommodation space for deposition. The floor uses a honeycomb design with 10 independent cells to produce spatially variable subsidence. Sediment and water can be fed from anywhere along the perimeter of the basin, and base level is independently controllable.

Experimental conditions. The experiment described here comprised two base-level cycles, a slow one followed by a rapid one. All other variables remained constant. We fed water and a 50:50 mixture (by volume) of quartz and coal sand from a single source point. The two sediment types have similar median sizes (120 μm), but the coal has a specific gravity of 1.3 while the quartz sand has a specific gravity of 2.65. Hence the coal sand is significantly more mobile than the quartz sand and serves as a proxy for fine sediments, whose behavior in a small-scale experiment such as this would not be

representative of the behavior of fines in the field. Base level was controlled from the end of the basin opposite the sediment-feed point using a float and siphon attached to a constant-head tank mounted on a vertical track. Subsidence was induced in a bowl-shaped pattern with a maximum in the center of the basin. The rates of subsidence and of water and sediment discharge were held constant throughout the run. The sediment discharge was set to balance the rate of production of volume by subsidence (the accommodation rate) in the basin.

First the basin was run with constant conditions for 10 hours to stabilize the shoreline (Fig. 1). Then the slow cycle of base-level fall and rise was begun. The slow cycle had an amplitude of 0.09 m and took a total of 30 hours, long enough that the rate of fall was never greater than the maximum subsidence rate. Thus the delta-front sediments were never exposed. The cycle time was also longer than the equilibrium time for the basin (3.4 hr [*Paola et al.*, 1992]). After base level had returned to its equilibrium position, the system was run with constant conditions for 6 hours to re-stabilize the shoreline. Then a rapid cycle of base-level fall and rise was begun. The amplitude of this cycle was 0.1 m, and the cycle time was reduced to 2 hours. After the rapid cycle the system was again subject to constant conditions until the end of the run.

Results

Slow base-level cycle. The slow fall and rise produced a nearly symmetric regression and transgression of the shoreline. Autocyclic incision intensified as the fluvial system lengthened—a scale effect due to the small size of the prototype basin—but otherwise the cycle was not accompanied by incision, and the sand body produced extended laterally over the entire width of the basin. In addition, because subaerial deposition continued throughout the regression, the base-level fall was not accompanied by any major increase in sediment transfer into deep water. Eventually, at the lowstand, the sandy fluvial system extended over the entire length of the basin.

Figure 1. Shoreline response (gray) along two transects to slow and rapid base-level forcing (black).

The temporal relationship between shoreline position and base level (Fig. 1) shows no indication of a strong phase shift between shoreline position and base level during the slow base-level fall. Maximum regression coincides directly with the low stand of base level. Indications of significant influences of subsidence on shoreline behavior appear during the transgression, however. Shoreline begins to transgress as soon as base level stabilizes at the bottom of the cycle, during the low stand. Shoreline continues to retreat in a series of back-stepping pulses and reaches maximum transgression just as the rate of

base-level rise begins to decrease. The experimental data do not show the theoretically predicted attentuation of shoreline response for the slow relative to rapid cycles. Rather, the amplitude of shoreline response is somewhat larger for the slow cycle than for the rapid one.

Rapid base-level cycle. The second base level event in the basin produced a markedly different response. During base level fall there was brief competition among the various major channels before one captured all of the flow. Restriction of flow to one channel yielded a laterally restricted incised valley that fed a low-stand fan in deeper water. The fan, although in this basin not composed of turbidites, represents the transferred coarse sediment derived from the sediment supply as well as reworked material from the incised valley. In natural systems, the fan deposits would be composed of turbidites and debris flows, instead of the grain flows found in the basin.

During the subsequent base level rise, all of the sediment supplied to the system was used to fill the incised valley, so the perched interfluve area remained starved of sediment. Stratigraphically, the entire rapid cycle is represented by a disconformity in these areas. As the valley was filled, bank erosion led to widening of the valley, resulting in a much broader disconformity than had formed during the previous base-level fall. This effect would also be present at natural scales, but is exaggerated in the basin because of the noncohesive, unconsolidated nature of the sediment fill. Highstand deposition across the entire fluvial surface did not resume until the maximum base level position was reached.

Deposition during the transgression is marked by a thickening and fining upwards sequence. This unusual sequence type results from a combination of two effects during valley filling. As the rapid rise moves shoreline landward, the sediment fed to the system is forced to deposit over a shorter distance, leading to a thickening upwards cycle. At the same time, the landward shoreline migration also leads to upward fining.

Rebound regressions. Both cycles show a tendency for the shoreline to overshoot its equilibrium position at the end of the base-level rise. This exaggerates the transgression, and the shoreline subsequently progrades back to its equilibrium position. These "rebound regressions" are not due to any imbalance between sediment supply and subsidence; neither of these was changed during the run. The overshoot and rebound regression are much more pronounced for the rapid cycle, where they resulted from starvation of much of the system as all supplied sediment was funneled into the incised valley.

Growth faults. Prominent sets of growth faults developed at the end of both base-level cycles. Those from the slow cycle are better developed than those from the rapid one. Observed stratigraphic relations suggest that the slow-cycle faults were initiated while the shoreline was prograding back after the overshoot at the end of the slow base-level cycle. Fault motion continued until sometime during the rapid fall. The volume of sand trapped in the faults is large enough to have significantly inhibited progradation of the shoreline.

A prominent failure of the delta front occurred during the falling limb of the rapid cycle, when the rate of fall was greatest. This collapse appears to have exploited the existing growth faults, and was probably enhanced by high pore-water pressures in the deltaic deposit, and gravitational instability of the relatively dense, well packed quartz sand on the lighter, more porous coal.

Theoretical Model

We investigated the shoreline response using a two-dimensional computational model that uses linear diffusion to represent the fluvial system and a constant angle of

repose to represent the submarine system. The problem is of "moving-boundary" form in that the positions of the shoreline and delta toe are unknown a priori and must therefore be determined as part of the solution to the governing equations for bed elevation. The position of the delta toe at any time is determined by the intersection of the angle-of-repose morphology with either basement or previously deposited sediments. The model does not allow submarine erosion, a condition that renders it fundamentally different from models that assume a diffusional governing equation for evolution of the submarine system. The depositional mechanics of this model of fluvio-deltaic sedimentation are analogous to a generalized form of the classical Stefan problem, which involves tracking the advance of a melting front into an isothermal solid. In this analogy, the fluvial system is analogous to the liquid phase, shoreline to the phase front, and sea level to a time-dependent melting temperature.

The model was used to simulate the stratigraphic response to variable-frequency base-level forcing using the known boundary conditions in the experimental basin. The model correctly predicts a frequency-independent in-phase relationship between shoreline position and base level. The model also captures the shoreline overshoot observed at the end of the rapid cycle of base-level rise. We also investigated whether changing the subsidence pattern could account for the absence of a strong phase shift for the slow cycle by repeating the calculations for a passive-margin geometry. The model does not predict a significant phase shift for this geometry either, even if the base level cycles are superimposed on a long-term eustatic fall as was done in Pitman's calculations. The absence of a phase shift between shoreline and base level seems to be a basic characteristic of systems with passive submarine transport such as that in the experiment, independent of the subsidence geometry.

References

Angevine, C.L., Relationship of eustatic oscillations to regressions and transgressions on passive continental margins, in *Origin and Evolution of Sedimentary Basins and Their Energy and Mineral Resources*, edited by R.A. Price, pp. 29-35, Amer. Geophys. Union, Washington DC, 1989.

Jordan, T.E., and P.B. Flemings, Large-scale stratigraphic architecture, eustatic variation, and unsteady tectonism: a theoretical examination, *J. geophys. Res., 96* (B4), 6681-6699, 1991.

Miller, K.G., G.S. Mountain, and B.E. Tucholke, Oligocene glacio-eustasy and erosion on the margins of the North Atlantic, *Geology, 13*, 10-13, 1985.

Miller, K.G., P.R. Thompson, and D.V. Kent, Integrated Late Eocene - Oligocene stratigraphy of the Alabama coastal plain: correlation of hiatuses and stratal surfaces to glacioeustatic lowerings, *Paleoceanography, 8* (2), 313-331, 1993.

Paola, C., P.L. Heller, and C.L. Angevine, The large-scale dynamics of grain-size variation in alluvial basins, 1: Theory, *Basin Res., 4*, 73-90, 1992.

Pitman, W.C., Relationship between eustacy and stratigraphic sequences on passive margins, *Geol. Soc. Amer. Bull., 89*, 1389-1403, 1978.

THE IMPORTANCE OF TECHNOLOGY IN BENTHIC RESEARCH AND MONITORING; LOOKING BACK TO SEE AHEAD

Donald C. Rhoads[1], Roger Ward[1], Josephine Aller[2], and Robert Aller[3]

"When the only tool you own is a hammer, every
problem begins to resemble a nail"

Abraham Maslow

Developmental Psychologist,
1908-1970

ABSTRACT

Benthic studies in the 1800's addressed zoological and natural history investigations requiring only direct observation of intertidal zonation ("marine sociology"). Exploration of the subtidal awaited development of dredges and grab samplers at the turn of the century. Diving observations followed in the early 1940's. These tools were sufficient to address both academic and fisheries questions of the day; Identification of marine organisms and their geographic/bathymetric distributions. These traditional techniques can be broadly classified as **mechanical samplers** which are still used today albeit in more sophisticated forms such as compartmentalized box cores, Van Veen and McIntyre quantitative grabs, and epibenthic sleds.

Classical mechanical samplers continue to be used and will always have a role to play in "ground truth" sampling. However, a technological revolution in seafloor investigations began after 1972 with passage of the Marine Protection, Research, and Sanctuaries Act (MPRSA, Public Law 92-532). Up to this time, benthic studies were focused on basic research or applied fisheries surveys. The MPRSA widened the scope of investigations to include benthic monitoring. Agencies such as the USEPA, USACOE, and NOAA faced a significant challenge in attempting to monitor numerous benthic impacts using solely classical mechanical samplers. Sampling and data work-up took too long and were too expensive. Subsequently, many **remote sensing/sampling technologies** have been developed or proposed to facilitate efficient habitat mapping and data collection. In large part, these technologies have been borrowed from the medical field (e.g. x-radiography and ultrasound imaging, immunosensors), military R&D developments (e.g. downward-looking sonar, side-scan sonar, laser line-scan imaging, multibeam, autonomous underwater vehicles (AUVs), manned submersibles, satellite/areal photography/spectroscopy), photonics (e.g. fiber optics, planar optrodes, laser imaging, sediment profile imaging, and digital imaging), and magnetics (biomagnetometry).

Benthic ecology is becoming increasingly interdisciplinary, including the complex interplay between organisms, solid phase and pore-water chemistry, nutrient fluxes, sediment transport, geotechnical properties, and the fate and effects of contaminants. We have reviewed the universe

of existing and potential sensors/samplers/techniques (and their deployment platforms), for the U.S. Army Corps of Engineers and Naval Research Laboratory. Fifty-four (54) candidates are identified and placed into one of three categories of maturity: 1.) Existing sensors/samplers that can fulfill future needs with no, or little, modification (n=14), 2.) Existing sensors that would require major modifications to address future needs (n=17), and 3.) New sensors/samplers that now exist only as prototypes or concepts (n=23). Examples of current and future applications are discussed.

[1] Science Applications International Corp (SAIC), [2] Marine Science Research Center, Univ. of New York at Stony Brook.

POSTER SESSION

REMOTS® UV-IMAGING SPECTROMETER

Donald Rhoads[1], Drew Carey[2], John Scott[3]

Science Applications International Corp. (SAIC)
Woods Hole, Mass[1], Newport R.I.[2] and Narragansett, R.I.[3]

ABSTRACT

The next generation of sediment profile imaging cameras will include the capability of relating organism-sediment relations to quantified gradients in geochemistry and contaminant distributions. The SAIC prototype system shown here is fully functional and has been deployed for field use. The new system contains an electrically cooled charged coupled device (CCD) camera. Spectrally-rich light is provided by a 1000W mercury vapor lamp. Light emitted from the lamp passes through a filter that defines the band width for excitation light (up to four bands can be programmed). Turning mirrors direct the light downward to the prism mirror and onto the sediment profile. Any red-shift light that is emitted from the sediment (from PAHs, phaeopigments, humics, etc), is reflected upward to another turning mirror and the light is passed through a blocking filter. The blocking filter excludes the excitation wave lengths and only allows passage of the red-shift (longer wave length) light. The red-shift light is then passed through a filter wheel containing 17 narrow band pass emission filters and the resulting spectral array is imaged by the CCD camera. Interpretation of spectral signatures is aided by placement of blanks and prepared (spiked) standards in cuvettes at the top of the imaging window.

Future development is planned including using half of the imaging window for planar optrodes. These thin-film optrodes are capable of imaging and quantifying pore water dissolved oxygen and pH when excited with the appropriate excitation light. This work will be done with Dr. Robert Aller at the Marine Science Research Center, SUNY, Stony Brook, L.I.

Results of this development promises to fulfill the need for rapid and cost-efficient large scale screening of sediment associated contaminants and overall benthic habitat quality.

INTERNAL WAVES IN MONTEREY CANYON

Leslie Rosenfeld
Oceanography Department, Naval Postgraduate School, Monterey, CA

Eric Kunze
School of Oceanography, University of Washington, Seattle, WA

It has been known for some time, both from theory (Wunsch, 1969) and observations (Shepard, 1979), that submarine canyons are sites of enhanced internal wave activity due to the focussing of energy in this frequency band by the topography. Unfortunately, submarine canyons are notoriously difficult to make measurements in, and most of the observations are severely limited in temporal resolution and duration. Several NSF and ONR-funded experiments aimed at characterizing the internal wave and turbulence fields in a submarine canyon and on a continental slope were carried out in conjunction with each other in the Monterey Bay area during August 1997. Moored (Rosenfeld), microstructure profiler (Gregg, Lien, and Miller), expendable (Kunze), and shipboard (ADCP - Gregg et al. and Rosenfeld; CTD - Rosenfeld; Biosonics - Gregg, et al.) platforms were used to make velocity, temperature, and salinity measurements. Only the moored velocity and temperature data, and the nearby shipboard-lowered CTD data, are discussed here.

Previous CTD and vessel-mounted ADCP measurements made at 1.5-2-h intervals in this area over 24-h periods in April and October of 1994 (Petruncio et al., 1998) indicated that the variance was dominated by the semidiurnal internal tide, and showed phase and energy propagation in remarkable agreement with linear theory, with a kinetic energy maximum in a 150-250-m band centered 150 m above the canyon floor. During April, semidiurnal internal tidal energy was propagating toward the canyon head along characteristics that matched the predominant slope of the canyon floor. During the latter observational period, the semidiurnal internal tide appeared to take the form of a standing wave (Figure 1). It was noted by Petruncio et al. that their velocity measurements did not extend close enough to the bottom to confirm a predicted near-bottom phase reversal in the along-canyon flow (Wunsch, 1968), nor to explore expected turbulence in the bottom boundary layer.

Two self-contained RDI Acoustic Doppler Current Profilers, one a 300 kHz narrowband version (NB), and the other a 300 kHz broadband Workhorse (BB) were moored 2.8 km apart on, or near, the floor of the canyon at depths of approximately 390 and 337 m, respectively, for the period 5 August 1997 - 9 September 1997 (Figure 2). The sampling intervals were 3 min and 1.5 min, respectively. Both were set to measure velocity in 4-m bins, with the deepest bin centered 12 m above the bottom. Each mooring also supported an Alpha Omega thermistor 4 m above the bottom, with a 1-min sampling interval. The close spacing of the instruments was primarily intended for redundancy in case one failed, but the complete records obtained by each instrument provides insight into the high degree of spatial variability in this tortuous topography. 12-h CTD time series with 30-min resolution were made about halfway between the two moorings on 9 August and 21 August (Figure 2).
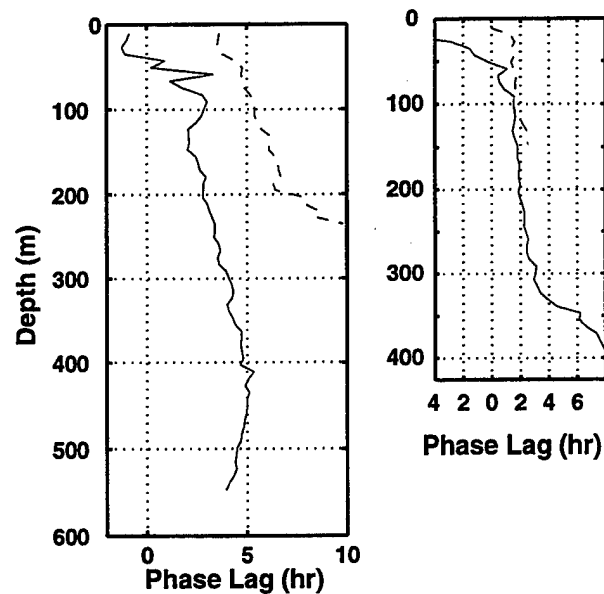
Figure 1. Phase of M_2 component of isopycnal displacement for two CTD time-series stations made over the Monterey Canyon axis in April (left) and October (right) 1994 (Petruncio et al. 1998).
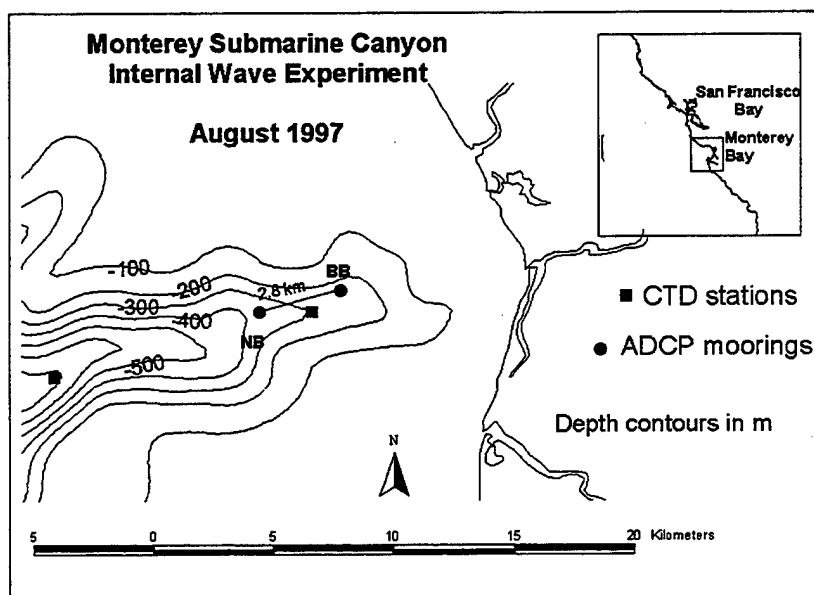

Figure 2. Relative positions of the ADCP moorings and CTD time series stations are shown. Depth contours relative to the measurement locations are not highly accurate due to the low resolution of the bathymetry available at the time of the experiment.

While analysis of these new data is just beginning, they clearly show that nonlinear effects become increasingly large as one approaches the bottom, as evidenced by changes in the kinetic energy spectra with depth (Figure 3). These spectra are compared to the Garrett-Munk spectrum calculated according to:

$$E_{GM} = \left[\frac{E_0 b^2}{2}\right]\frac{N_0}{N} f \frac{(N^2 - \omega^2)(\omega^2 + f^2)}{\omega^3 \sqrt{\omega^2 - f^2}}$$

using the canonical values (Munk, 1981) for b (1.3 km), N_0 (5.2 x 10^{-3} s^{-1}), E_0 (6.3 x 10^{-5}), the appropriate value of f for this latitude, and $N(z)$ calculated from the two 12-h averaged density profiles. Although G-M predicts slightly lower energy levels at 12 m above bottom relative to 112 m above bottom (based on the density profile), the opposite is observed. Throughout the internal wave band, energy levels in the lower part of the water column are elevated relative to G-M, but in general follow a ω^{-2} slope, except for the peaks associated with the tides and overtides.
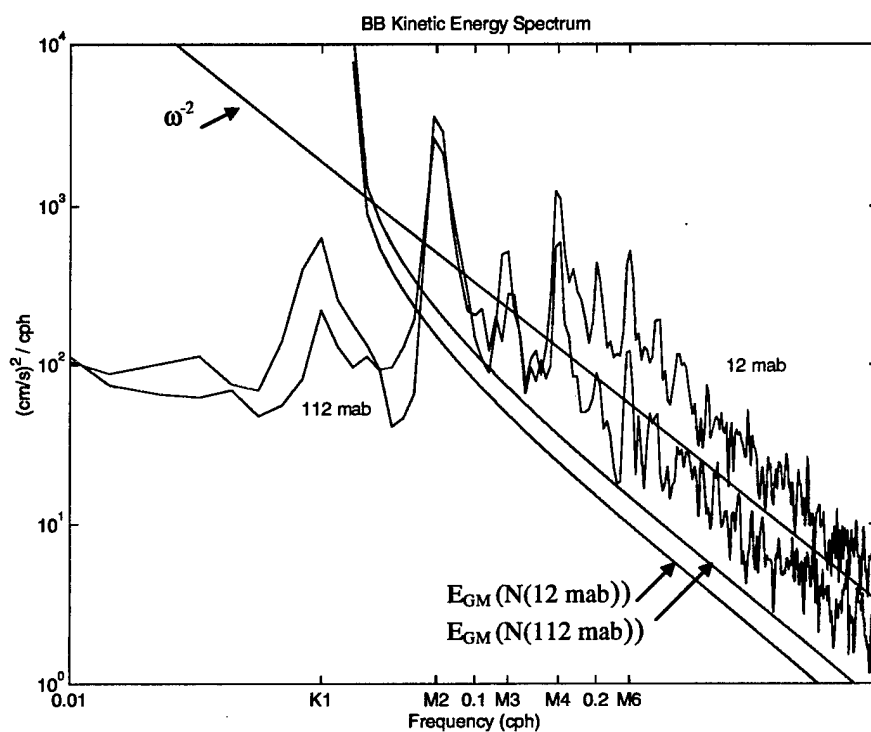
Figure 3. Kinetic energy spectra for the depth bins centered 12 and 112 m above the bottom at the BB mooring, together with the Garrett-Munk spectra calculated using values of N for these depths derived from the CTD time series.

193

The energy in the overtides (in addition to peaks at the diurnal and semidiurnal periods, there are significant peaks at the terdiurnal, quarterdiurnal and sixthdiurnal periods) and the bottom-trapped diurnal signal, also depend on the position of the mooring relative to the topography. This can be seen in the differences in the frequency dependence of the temperature variance (Figure 4) and kinetic energy at the same distances above the bottom at the two closely spaced moorings.
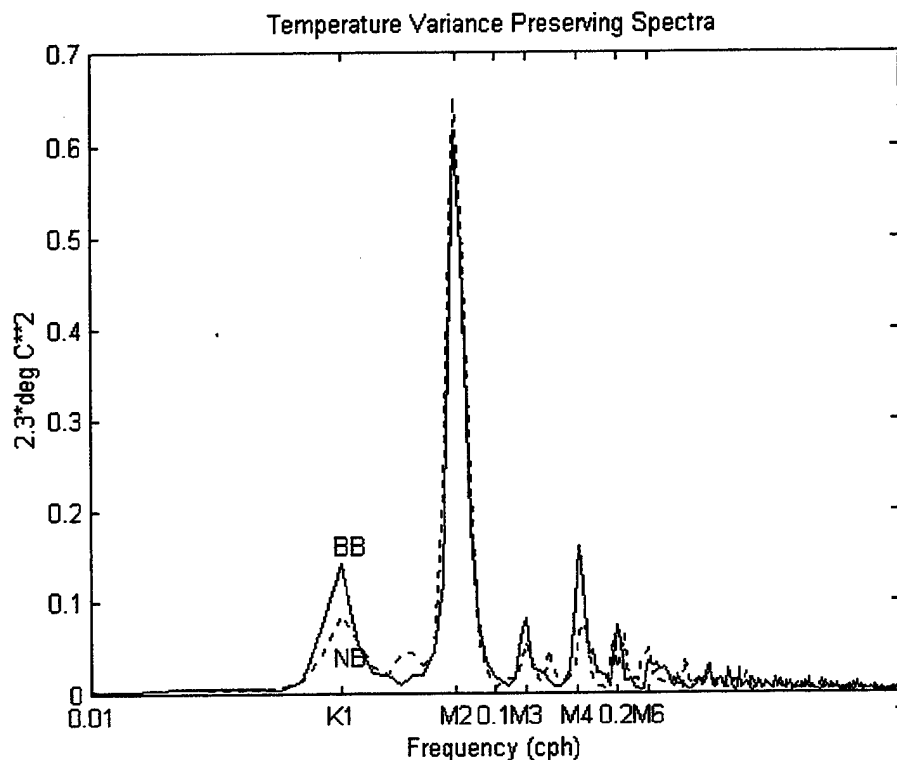

Figure 4. Temperature variance spectra 4 m above the bottom at moorings BB (solid) and NB (dashed).

While these findings are not in themselves surprising, the extremely nonlinear nature of the signal and the variation in the importance of the nonlinear terms over the duration of the measurements, which at first inspection is not linked to the spring-neap cycle, was not expected. Bore-like surges in velocity, with maximum speeds of ~ 70 cm s^{-1} and associated temperature changes, are seen on occasion. The sharp temperature drop after 0600 UTC on 9 August (Figure 5) occurred simultaneously with an increase in speed from 10 to 40 cm s^{-1} (in a 1.5 min interval) just after the current turned from downcanyon to upcanyon. While even during the 24-h period including this event, almost 90% of the near-bottom temperature variance can be accounted for by the sum of the K_1, M_2, M_3, M_4, and M_6 tidal constituents, the very rapid temperature drops are not well represented (Figure 5). Using the ratio of the amplitude of the M_4 to the M_2 constituent as a guide, it can be seen that the degree of nonlinearity varies greatly over time (Figure 5).
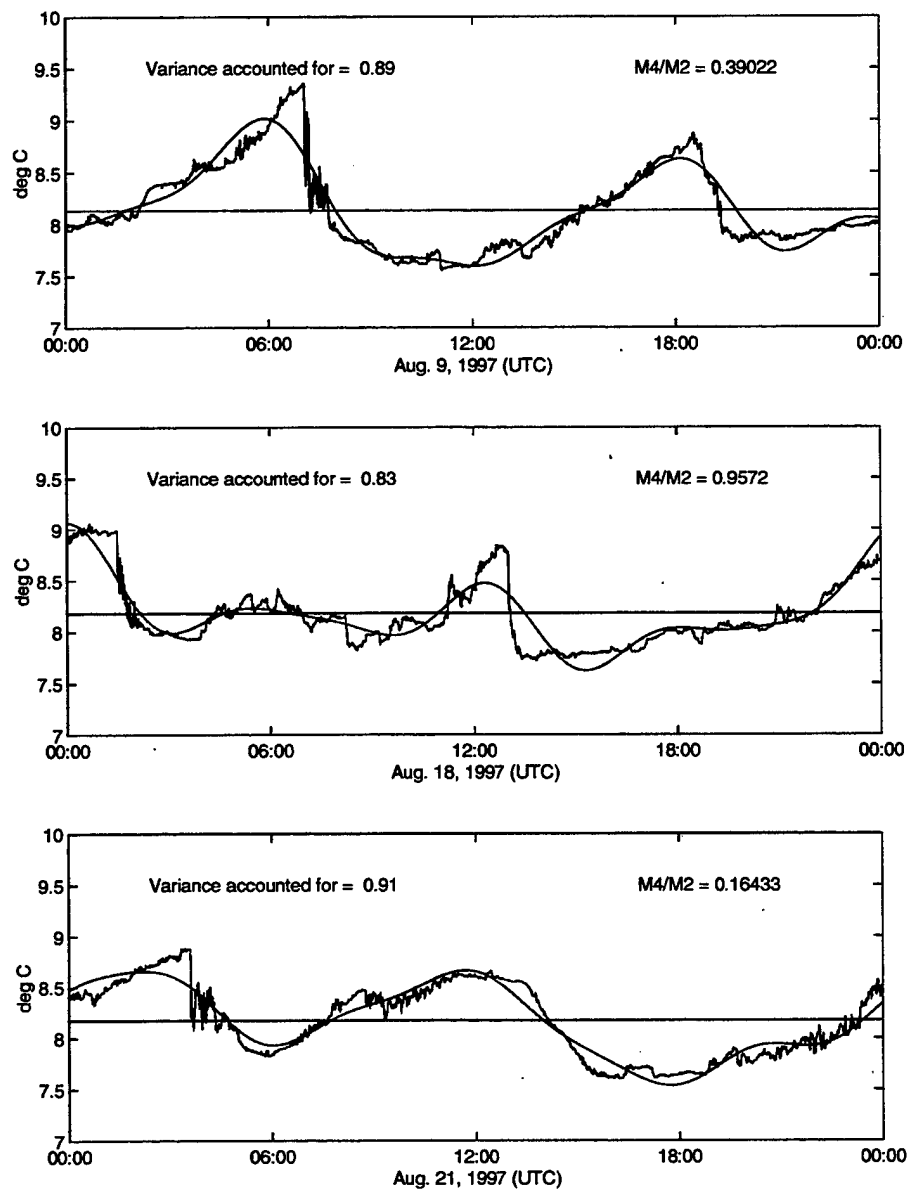
Figure 5. Temperature 4 m above the bottom at mooring BB is shown for three 24-h periods. The smooth lines represent least squares fits to the mean + K_1 + M_2 + M_3 + M_4 + M_6 constituents calculated over each of the 24-h periods. The variance accounted for by the smooth line and the ratio of the amplitudes of the M_4 to M_2 constituents are indicated.

The vertical structure also changes significantly with time, as seen in the isopycnal displacements derived from the two CTD time series (Figure 6). The 9 August time series, with vertical displacements in the lower water column exceeding 110 m in 390 m depth, shows a gentle phase progression over the lower 250 m of the water column, in the sense indicating downward energy propagation. The 21 August series shows a 180° phase reversal 150 to 200 m above the bottom, indicating a second mode type structure. Petruncio et al. (1998) speculated that the change from a propagating to a standing wave that occurred between their two experimental periods (Figure 1) was due to seasonal changes in the stratification modifying the characteristic paths and hence the reflection points; but these new data show similar kinds of changes over just 12 days. It has yet to be determined what caused this change in the stratification, which was particularly significant in the 50-250 m depth range. The complexity of the vertical structure is also seen in the deeper parts of the canyon in the expendable current profiler data, which show multiple current maxima in 100-300 m thick layers.
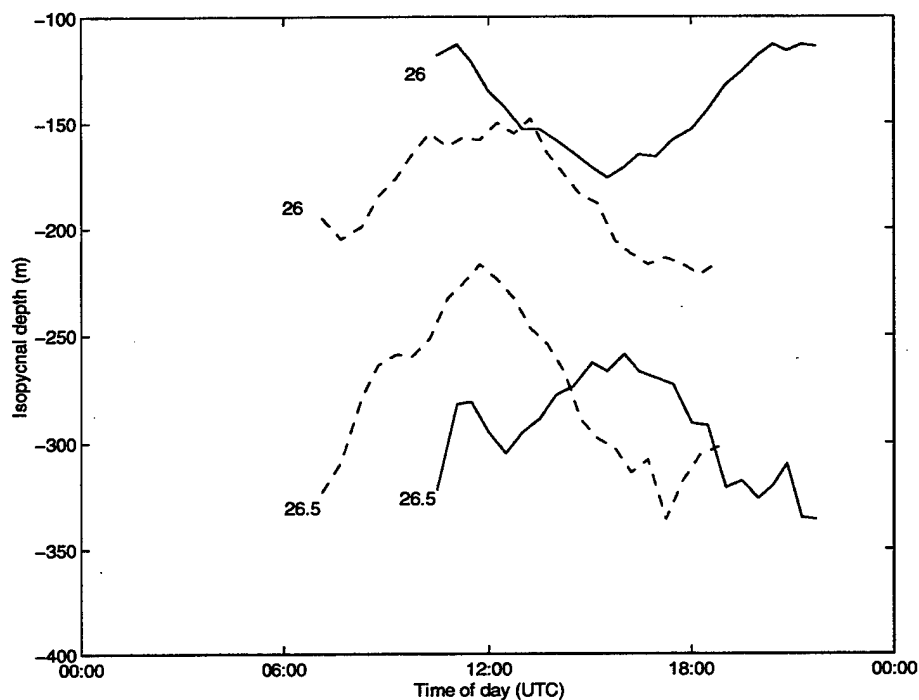
Figure 6. The σ_θ = 26.0 and 26.5 isopycnals are shown versus time of day for the 9 August (dashed) and 21 August (solid) CTD time series.

Inadequate bathymetry maps can make interpretation of canyon current records difficult. New high resolution data (vertical resolution of 0.1% of water depth and horizontal resolution of 2% of water depth) obtained by the Monterey Bay Aquarium Research Institute, explains the highly asymmetric flow measured in this experiment, and also observed at other locations (Shepard,

1979). The limited temporal resolution of most previous canyon current records has precluded determination of the energy spectrum over the full internal wave band, and has missed the highly nonlinear nature of events. Furthermore, the lack of good vertical resolution and near-bottom measurements have made the interpretation of vertical structure and phase propagation problematic and where it has been possible, it was only for brief snapshots in time. These ADCP data provide early indications that the near-bottom phase reversal in along-canyon current predicted by Wunsch (1968) exists at least some of the time. These data should allow significant progress to be made in addressing these issues - the results presented here being only very preliminary in nature. The moored data discussed here will also be integrated with expendable current, temperature, and dissipation profiles, as well as loosely-tethered microstructure profiles to obtain estimates of turbulence, mixing, and dissipation.

REFERENCES

Munk, W., 1981: Internal waves and small scale processes. *Evolution of Physical Oceanography*, B.A. Warren and C. Wunsch, eds., MIT press, 623pp.

Petruncio, E. T., L. K. Rosenfeld, and J. D. Paduan, 1998: Observations of the internal tide in Monterey Canyon. *J. Phys. Oceanogr.*, **28**, 1873-1903.

Shepard, F. P., N. F. Marshall, P. A. McLoughlin, and G. G. Sullivan, 1979: *Currents in Submarine Canyons and Other Sea Valleys*. AAPG Studies in Geology No. 8. American Assoc. of Petroleum Geologists, 173 pp.

Wunsch, C. H., 1968: On the propagation of internal waves up a slope. *Deep-Sea Res.*, **15**, 251-258.

Wunsch, C. H., 1969: Progressive internal waves on slopes. *J. Fluid Mech.*, **35**, 131-144.

A unified erosion formulation for cohesive sediments

Lawrence P. Sanford
University of Maryland Center for Environmental Science, Horn Point Laboratory

Jerome P.-Y. Maa
Virginia Institute of Marine Science

Introduction - Erosion or resuspension of bottom sediments is one of the most important factors controlling fine sediment transport in natural water bodies. Far from lateral sources and sinks of material, and in the absence of significant biological production, erosion is the major source for suspended particles in the water column. Erosion is also one of the most studied aspects of fine sediment transport. Researchers have employed theoretical approaches, laboratory flume studies, *in situ* flume studies, and field observations of suspended sediment variability to examine factors controlling the rate of erosion. There is general agreement that bottom shear stresses exerted by waves and currents are the dominant forces causing erosion and that site-specific sediment characteristics (including particle size distribution, particle density, cohesiveness, water content, and biological disturbance or binding) control resistance to erosion.

Unfortunately, there has been little agreement about the most appropriate mathematical formulation(s) for an erosion rate. Some advocate the use of a power law relationship between erosion rate and shear stress, others champion the use of an exponential form, and many opt for a simple linear relationship. Most models assume that there is some critical shear stress, τ_c, below which erosion does not occur, with erosion rate increasing as a function of the excess stress above this critical value. Much work has been done identifying factors that control the critical stress. However, others have argued that a critical stress is not necessary for practical modeling purposes. An important distinction can be made between cases in which τc increases with depth into the sediments and limits the extent of erosion, and cases in which there is no change in τ_c with depth. The former case is often called Type I erosion, and the latter Type II erosion. Both exponential and power law formulations have been used for Type I erosion, while a linear formulation is used most frequently for Type II erosion.

All of these erosion formulations have been used successfully to model fine sediment transport, with controlling parameters set empirically. However, the lack of consensus on a basic mathematical formulation for erosion betrays a lack of understanding of the underlying physics. It also inhibits intercomparison of data, since the results of studies assuming different erosion formulations frequently are reported in terms of incompatible parameters. The distinction between Type I and II erosion is useful, but the present lack of compatibility between erosion formulations appropriate to each Type is awkward and it does not allow for a smooth transition between Types. Finally, formulations with multiple empirical parameters (e.g., most of these formulations) require large amounts of data for calibration and are inherently error prone when extrapolated beyond their calibrated range.

In this paper, we present a simple extension of the linear erosion formulation that allows it

to be used to describe either Type I (depth-limited) or Type II (unlimited) erosion, and in so doing allows a unified approach to the entire suite of possible erosion behaviors. This formulation is tested by re-analyzing the data set presented by Maa, Sanford, and Halka (Marine Geology **146**, 1998, 137-145), hereafter referred to as MSH. In the remainder of the paper, we first summarize the relevant aspects of MSH, then present the model development and associated re-analysis of MSH's data, then compare model predictions to this re-analyzed data.

Background - *In situ* erosion rate measurements in Baltimore Harbor, MD -
MSH reported the results of *in situ* sediment stability tests carried out at four sites in Baltimore Harbor, MD during May, 1995. Tests were conducted using the Virginia Institute of Marine Sciences Sea Carousel, a submersible annular flume. Replicate experiments were performed at each site to determine both τ_c for incipient motion and the relationship between erosion rate E and excess shear stress. The Sea Carousel was lowered gently to the Harbor bottom and spun up to successively higher shear stress levels while continuously monitoring the suspended sediment concentration in the flume channel. Characteristics of the top 2 cm of sediment were determined from grab samples collected during a separate survey.

Bottom sediments were similar at all four sites, with mud (silt and clay) fractions ranging from 0.93-0.99 and porosities (ϕ = the volume fraction of water) ranging from 0.84-0.87. Benthic biota were negligible at all sites due to sediment contamination. The primary difference between sites was the level of regular exposure to physical disturbance from wind-generated waves, currents, and shipping traffic. Three of the sites were located along a transect into the Harbor near the edge of the dredged shipping channel, with the fourth in a shallow embayment partially protected by a submerged sand bar. In approximate order of increasing exposure, the sites were designated White Rocks (protected embayment), Ft. McHenry (innermost), Anchorage 5, and Paradise (outermost).

MSH found that the critical stress for incipient motion, τ_{ci}, tended to increase with increasing site exposure. The two sites with $\tau_{ci} \leq 0.05$ Pa were characterized by a thin, visible layer of flocculent surface material, which was much less apparent at the other sites with $\tau_{ci} \geq 0.1$ Pa. All sites exhibited Type I erosion behavior. τ_c increased rapidly with depth into the sediment; at each increased level of applied shear stress, all of the sediment that could be eroded by that stress was depleted over a typical time scale of 15 min. An equation of the form $E = E_o \exp(-\lambda t)$ fit the erosion data after each new shear stress step quite well, where E_o was the initial erosion rate and λ^{-1} was the time scale of sediment depletion. MSH related E_o to excess shear stress using a power law formulation, $E_o = m(\tau_b - \tau_c)^n$, where τ_b was the applied bottom shear stress. Both m and n tended to increase with increasing site exposure.

The results presented in MSH were valuable as an examination of differences in sediment stability between sites in an urban harbor, and as an illustration of the ubiquity of Type I erosion behavior in such an environment. However, they were limited in the sense that it was not possible to apply the information as presented for modeling sediment transport in Baltimore Harbor, and because changes in erosion parameters with depth into the

sediment were not derived. These limitations were starting points for the present investigation. Our goal in this study was to derive an erosion framework that would allow incorporation of MSH's results into a sediment transport model, specifically allowing for depth-dependence of erosion behavior.

Derivation of a new erosion formulation - We assume for simplicity's sake that both Type I and Type II erosion rate can be expressed through a simple modification of the standard linear erosion rate formulation:

$$E(m,z,t) = M(m)(\tau_b(t) - \tau_c(z)) \tag{1}$$

where M is the proportionality factor between erosion rate and excess shear stress. E may depend on total eroded sediment mass m, time t, and depth of erosion z. Differences between eq 1 and previous formulations are that both M and τ_c may vary during erosion and that the expression is written dimensionally rather than normalizing by τ_c. We further assume that $M(m) = \rho_s(1 - \phi(m))M'$, where ρ_s is the sediment density and M' is a constant. We thus collapse the eroded mass dependence of M into changes in porosity ϕ. Eq 1 then becomes:

$$E(m,z,t) = \rho_s(1 - \phi(m))M'(\tau_b(t) - \tau_c(z)) \tag{2}$$

Eq 2 is physically appealing because erosion rate is directly proportional to the sediment concentration at the sediment-water interface multiplied by the excess erosive force. Dividing both sides of eq 2 by $\rho_s(1 - \phi(m))$ yields

$$E'(z,t) = M'(\tau_b(t) - \tau_c(z)) \tag{3}$$

where E' is the erosion velocity, which no longer depends directly on m. Differentiation with respect to time yields

$$\frac{dE'}{dt} = M'(\frac{d\tau_b}{dt} - \frac{d\tau_c}{dz}\frac{dz}{dt}) \tag{4}$$

Defining $\alpha' = d\tau_c/dz$, and recognizing that $E' = dz/dt$, allows derivation of a governing equation for E':

$$\frac{dE'}{dt} + M'\alpha'E' = M'\frac{d\tau_b}{dt} \tag{5}$$

If we assume that α' is locally constant, then solution of eq 5 is quite straightforward. The solution for constant τ_b (the homogeneous solution) is

$$E' = M'(\tau_b - \tau_{co})\exp(-\alpha'M't) \tag{6}$$

where τ_{co} is the critical shear stress at time 0 and we have used the fact that eq 6 must reduce to eq 3 at time 0 to set the value of the integration constant. Converting eq 6 back to an expression for erosion rate in terms of sediment mass is straightforward, yielding

$$E = M(\tau_b - \tau_{co})\exp(-\alpha M t) \tag{7}$$

where $\alpha = d\tau_c/dm$. Eq 7 should be directly comparable to data from the MSH erosion tests, defining time 0 as the application time of each higher shear stress. Eq 7 is expressed in terms of m instead of z because eroded mass is much simpler to derive from the erosion test data.

In fact, eq 7 is precisely the form found by MSH for each step of their erosion tests if we set $E_o = M(\tau_b - \tau_{co})$ and $\lambda = \alpha M$. The difference between eq 7 and the MSH analysis is that E_o is linearly related to excess shear stress in eq 7, rather than the power law relationship found by MSH. Additional changes in E_o as erosion proceeds are attributed here to changes in ϕ, which can be quite rapid just below the sediment surface. We compare these predictions to re-analyzed MSH data below.

Re-analysis of the Baltimore Harbor erosion data - An unavoidable problem with the Sea Carousel is slow leakage of suspended solids through the gaps between the driving ring and the walls. This leakage is a function of both the suspended sediment concentration in the flume and the driving ring rotation rate, and it complicates attempts to account for the total mass of sediment eroded and/or the total depth of erosion. MSH derived an approximate value for leakage rate for each step of the erosion tests. We re-analyzed MSH's data to express leakage rate as a function of applied shear stress. Leakage rate was linearly related to shear stress as Q_L $(cm^3\ s^{-1}) = 113.7\ \tau_b$, where τ_b is expressed in Pa ($r^2 = 0.64$). Using this relationship, we corrected the time series of eroded mass from each erosion test to add back the lost sediment, resulting in estimates of the total eroded mass time series, $m(t)$.

The results of this analysis were used to derive profiles of τ_c v. m and profiles of M [$= E_o/(\tau_b - \tau_{co})$] v. m, using the values of E_o, τ_c, and τ_b reported by MSH. These profiles are presented in Figure 1. τ_c increases approximately as $m^{1/2}$. M increases rapidly at first, but then tends to level out or decrease. If we assume a decreasing exponential form for ϕ and a constant value of M' (hence an increasing exponential form for M) and fit this form to the data by least squares nonlinear regression, we get a curve given by $M = 68.3 \times 10^{-5}[1 - \exp(-0.027m)]$ g cm^{-2} s^{-1} Pa^{-1}; this is also shown in Figure 1. Unfortunately, the fit is not very good ($r^2 = 0.34$), indicating that additional sources of variability are present. One of these is probably inter-site variability. Another factor may be changing sediment composition as erosion proceeds (i.e., winnowing of fines). It is quite difficult to test these hypotheses directly, since the erosion depths were always quite small (< 1 cm).

A more robust test of our model is to compare values of λ estimated by MSH to values predicted by the model. This comparison is shown in Figure 2, with the model predictions based on the data shown in Figure 1. The agreement is in fact very good, lending credence to our formulation. More complete tests under more controlled conditions would provide a better test, with fine-scale measurements of ϕ and sediment composition included if possible.

Conclusions - A modified linear erosion formulation allowing for eroded mass (or depth) dependence of both the proportionality coefficient M and the critical shear stress τ_c offers a viable alternative to present formulations. It applies to both Type I and Type II erosion, allowing a seamless transition between the two behaviors. Assuming a locally constant τ_c depth gradient and attributing changes in M with depth to changes in porosity ϕ results in quite reasonable agreement between the model and *in situ* erosion test data. A significant issue that remains is to model the evolution of τ_c and M following deposition.

Figure 1 - Profiles of critical stress v. eroded mass (upper panel) and erosion proportionality factor v. eroded mass (lower panel), from reanalysis of MSH data. Best fit curves to all data also shown.

Paradise
White Rocks
Anchorage 5
Ft McHenry
tauc=0.02*m^0.53

Paradise
White Rocks
Anchorage 5
Ft McHenry
M=68.3[1-exp(-0.027m)]

Eroded mass, m (g)
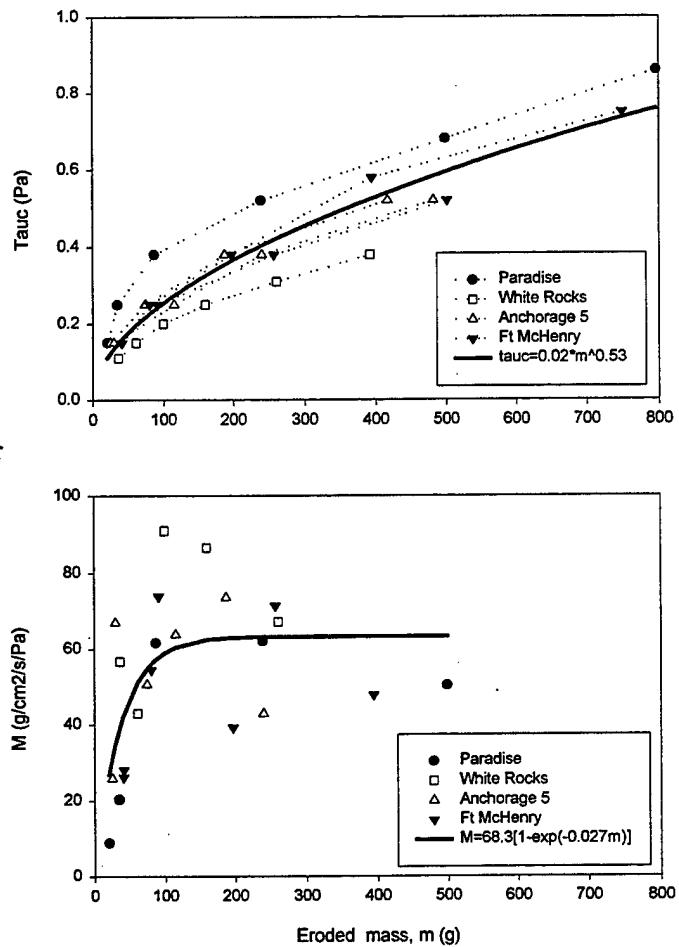
Figure 2 - Comparison between available sediment decay time estimates from MSH and available sediment decay time estimates from the present model.
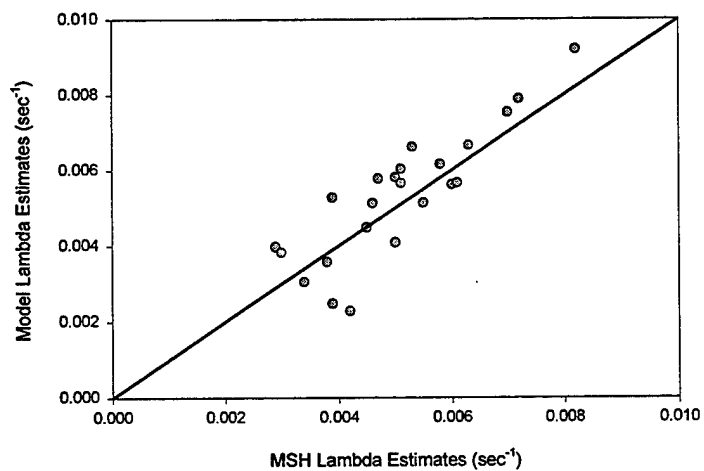
203

Tidal Resuspension of Protists in Buzzards Bay; Alterations of Community Structure and Implications for Food-Web Dynamics

Jeff Shimeta
Biology Department
Franklin & Marshall College
Lancaster, PA 17604-3003

ABSTRACT

Near-bottom currents and light transmittance, as well as profiles of protistan concentrations within surficial sediment and boundary-layer water, were monitored to determine the dynamics of resuspension at three stations in Buzzards Bay, MA. Tidal resuspension was indicated at all sites, where sediments ranged from silt to medium sand, and maximal bottom shear velocities were 0.82 - 2.2 cm s^{-1}. Typically, near-bottom light transmittance fell during weak flow as suspended material settled toward the bed, and transmittance increased during strong flow as material was mixed higher into the water column. Resuspension of protists was taxon specific, with heterotrophic nanoflagellates and certain ciliates displaying cycles of resuspension and deposition, whereas pigmented flagellates, diatoms, and other ciliates showed no variations of distribution. Resuspension links the sedimentary and boundary-layer communities of protists, and the taxon-specific dynamics cause periodic alteration of community structure. These effects, along with potential influences on feeding rates caused by boundary-layer shear, may have strong impacts on microbial food-web dynamics.

INTRODUCTION

Several studies of resuspension in Buzzards Bay have contributed to understanding tidal influences on nutrient cycling and organism-flow relationships (e.g., Rhoads et al., 1975; Roman & Tenore, 1978). Despite a substantial literature on resuspension of microalgae and bacteria, however, little is known about the impact of resuspension on protistan communities, particularly the heterotrophs, and on dynamics of the microbial food web. In fact, distributions and abundances of heterotrophic protists in subtidal fine sediments (other than of amoebae and forams), and especially in near-bottom water, are largely uncharacterized. Here I address links between the sedimentary and boundary-layer communities resulting from tidal currents and resuspension.

METHODS

Samples were collected at three widely separated sites in Buzzards Bay, MA (see Moore, 1963, for map): the Weepecket station (16 m depth, 41° 31.250' N, 70° 45.700' W), the Great Ledge station (16 m depth, 41° 31.959' N, 70° 54.171' W), and the Gifford Ledge station (14 m depth, 41° 35.250' N, 70° 42.750' W). At each site, an InterOcean Systems S4 current meter and a SeaTech transmissometer were moored 1 m.a.b. Samples of surficial sediment and near-bottom water were taken at several times throughout the tidal cycle to determine the resuspension of sediment and protists. Water samples from several heights within the bottom 1 m (as close as 0.5 cm above the bed) were pumped through a frame of intake nozzles (described in Shimeta & Sisson, in press) using a peristaltic pump or a McLane Research Labs Remote Access Sampler. Sediment cores were taken simultaneously by SCUBA divers and sectioned into depth intervals for analyses of grain size and cells. All samples were preserved with 1% glutaraldehyde and

examined by epifluorescence or transmitted-light microscopy. Cells were extracted from sediment by density-gradient centrifugation (Shimeta & Sisson, in press).

RESULTS AND DISCUSSION

The Weepecket station was predominantly silt, whereas the Great Ledge and Gifford Ledge stations were mostly sand >125 μm (Table 1), in agreement with Moore's (1963) survey of Buzzards Bay. Initial examination of protists indicated that community structure varied accordingly, with small flagellates predominant at the silty station and large ciliates relatively more abundant at the sandy stations. This correlation between grain size and community composition is common, and it is likely related to available pore space (Patterson et al., 1989).

Table 1. Grain-size distributions (% mass) at the three sampling stations.

Size Fraction (μm)	Weepecket	Great Ledge	Gifford Ledge
≥250	3.9	53.8	50.8
125-249	2.7	28.3	27.1
63-124	13.8	7.1	7.7
38-62	16.6	2.2	2.5
25-37	11.0	1.6	1.5
<25	52.0	7.0	10.4

The stations grouped differently with respect to maximal current speed measured 1 m.a.b. (Fig. 1). Current strength was similar at the Weepecket (silty) and Great Ledge (sandy) stations, whereas it was weaker at the Gifford Ledge (sandy) station. Maximal shear velocities (u_*, calculated assuming a bottom drag coefficient of 3×10^{-3}) were 2.2 cm s^{-1} at the Weepecket and Great Ledge stations, and only 0.82 cm s^{-1} at the Gifford Ledge station.

All three stations displayed tidal periodicity in near-bottom turbidity, apparently the result of tidal resuspension. At the Weepecket station, light transmittance at 1 m.a.b. fell toward the end of every slack tide (Fig. 1), suggesting that a cloud of seston settled toward the bottom during weak flow and was mixed upwards during tidal exchanges. At Great Ledge and Gifford Ledge stations, resuspension only appeared to occur during flooding tide, followed by steadily falling light transmittance as material settled throughout ebbing and slack low tides. Water-column profiles of light transmittance revealed that at all three sites the lutocline fell to deeper depths when near-bottom transmittance was lowest (Shimeta & Sisson, in press; unpublished data). The dynamics of near-bottom turbidity at the Great Ledge and Gifford Ledge stations were similar to that observed in Rhoads' (1973) and Rhoads et al.'s (1975) studies of resuspension in Buzzards Bay. In order for near-bottom light transmittance to increase during tidal exchange, erosion must be limited to a veneer of loose, flocculent material overlying sediment with a greater bed shear strength ("Type I" erosion; Amos et al., 1992). Thus, only a finite mass of sediment can resuspend, and the bed is not a continuous source of material during tidal exchange.

The differences in turbidity dynamics among stations appeared related to currents. Bottom flow at the Weepecket station was similar in strength during both flooding and ebbing tides, and it weakened at every slack tide, thus consistent with a cycle of resuspension and settling with every tide reversal. At the Great Ledge station the bottom current was stronger during flooding than during ebbing tide, and at the Gifford Ledge station the current weakened only immediately preceding slack low tide. Accordingly, at both stations material settled throughout the ebbing phase and only resuspended during the flooding phase.
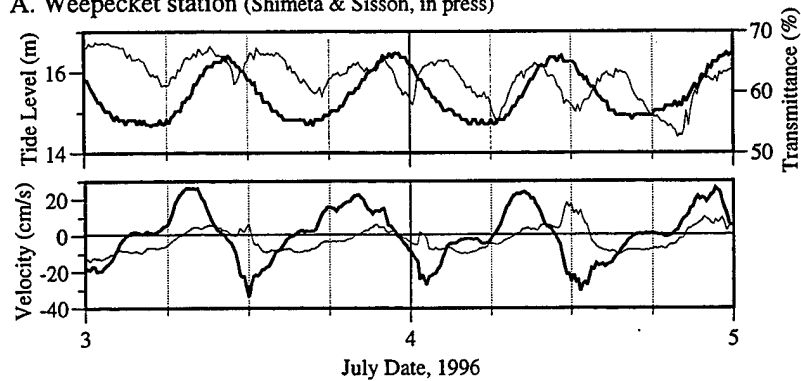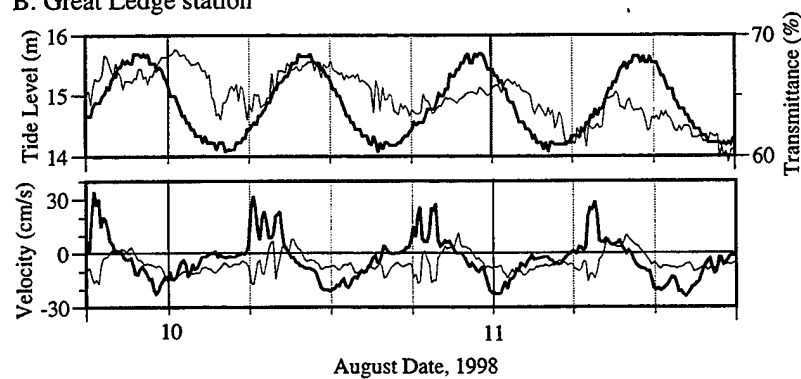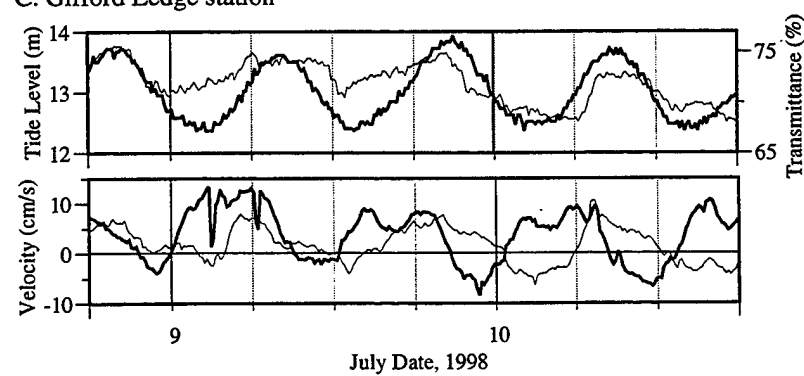
Fig. 1. Tide level (thick line), light transmittance (thin line), and velocity along the major axis (thick line) and minor axis (thin line) of flow at three stations in Buzzards Bay. A. Major axis = 20.0°. B. Major axis = 58.5°. C. Major axis = 50.6°. All minor axes = major axis - 90.0°.

Vertical profiles of cell concentrations throughout the bottom 1 m of the water column and the top 10 cm of sediment at the Weepecket station revealed taxon-specific resuspension of protists (Shimeta & Sisson, in press). (Results from the Great Ledge and Gifford Ledge stations are in prep.) Heterotrophic nanoflagellates and ciliates including scuticociliates, oligotrichs, and the hypotrichs *Euplotes* and *Urostrongylum* displayed cycles of resuspension and deposition corresponding to the tides. Typically, during tidal exchange cell concentrations were reduced in the top 2 mm of sediment and elevated in the bottom 1 m of the water column, compared to slack tide. Concentrations were elevated by as much as 4.6X near the bottom during strong flow, and some taxa, such as *Euplotes*, were found in the water column only during tidal exchange. Calculated maximal fluxes of cells across the sediment-water interface were of order 10^9 m^{-2} for nanoflagellates and 10^5 - 10^6 m^{-2} for ciliates (Table 2). In contrast, pigmented nanoflagellates, pennate diatoms, other ciliates showed no evidence of resuspension. The taxon specificity of responses to near-bottom flow may be due to behavioral adaptations or degree of association with particles.

Table 2. Maximal fluxes (cells m^{-2}) of protists across the sediment-water interface at the Weepecket station (Shimeta & Sisson, in press).

Heterotrophic Nanoflagellates	Scuticociliates	Oligotrichs	*Euplotes*	*Urostrongylum*
1.7×10^9	1.4×10^6	2.9×10^5	1.3×10^5	9.3×10^5

Resuspension of protists creates linkages between the sedimentary and water-column microbial communities that may be controlled to a large extent by flow in the benthic boundary layer. The taxon specificity of resuspension causes periodic alterations of community structure. Within the ciliate community in the bottom 1 m of the water column, tidal exchange altered the relative abundances of oligotrichs and tintinnids, as well as adding a significant fraction of scuticociliates to the community (Fig. 2). Furthermore, *Euplotes* was present in the water column only during tidal exchange. Within the top 2 mm of sediment, the relative abundances of oligotrichs, scuticociliates, *Urostrongylum*, and *Stichotricha* also varied greatly during the tidal cycle, with oligotrichs and *Stichotricha* being present in the sediment only at slack tide.

Resuspension and alterations of community structure may impact food-web interactions. As cells move between the sedimentary and water-column habitats they are exposed to differing types and amounts of food resources and predators, and alterations of community structure within functional groups (Fig. 2) changes the balance of competitors.

Bottom flow may also impact feeding rates directly by controlling the delivery of food particles to cells via microscale shear (Shimeta & Jumars, 1991; Shimeta et al., 1995). Cells feeding at the sediment-water interface experience strong laminar shear in the viscous sublayer, with a shear rate of $G = u_*^2/v$ (v = kinematic viscosity; Caldwell & Chriss, 1979). In the log layer, where the dissipation rate of turbulent kinetic energy is $\varepsilon = u_*^3/0.41z$ (z = height; Tennekes & Lumley, 1972), suspended cells experience a shear rate of $G = 0.365(\varepsilon/v)^{1/2}$ (Lazier & Mann, 1989). By these scaling equations, maximal G in the viscous sublayer was 67 - 480 s^{-1} at our three stations, and maximal G in the bottom 1 m of the boundary layer was 0.40 - 19 s^{-1}. For comparison, Shimeta et al. (1995) found that shear rates of only 0.1 - 10 s^{-1} were required to significantly enhance or suppress feeding rates of protozoans by as much as a factor of seven. Therefore, at all three of these stations, the strength of near-bottom flow and the

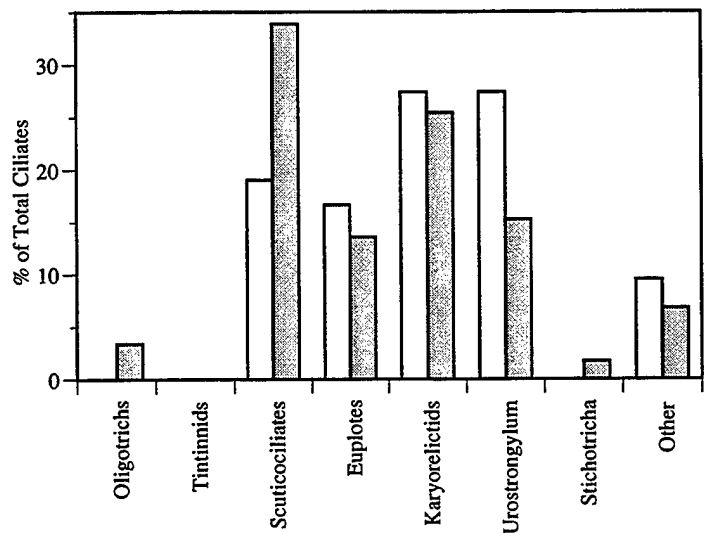A. Bottom 1 m of water column.
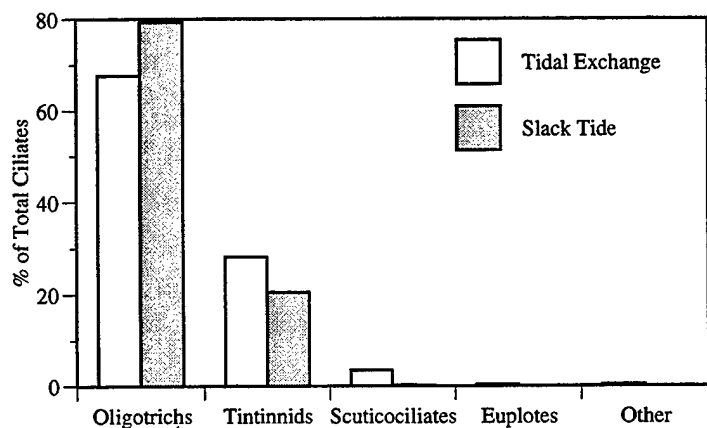
B. Top 2 mm of sediment.

Fig. 2. Tidally induced alterations of ciliate community structure in the bottom 1 m of the water column and the top 2 mm of the sediment at the Weepecket station on July 30, 1996.

resuspension/deposition of cells into regions of differing flow characteristics may strongly influence protozoan feeding rates and microbial food-web dynamics.

ACKNOWLEDGMENTS

REFERENCES

Amos, C.L., J. Grant, G.R. Daborn, & K. Black, 1992. Sea carousel - a benthic, annular flume. *Est. Coast. Shelf. Sci.* 34:557-577.

Caldwell, D.R. & T.M. Chriss, 1979. The viscous sublayer at the sea floor. *Science* 205:1131-1132.

Lazier, J.R.N. & K.H. Mann, 1989. Turbulence and the diffusive layers around small organisms. *Deep-sea Res.* 36:1721-1733.

Moore, J.R., 1963. Bottom sediment studies, Buzzards Bay, Massachusetts. *J. Sed. Petrol.* 33:511-558.

Patterson, D.J., J. Larsen, & J.O. Corliss, 1989. The ecology of heterotrophic flagellates and ciliates living in marine sediments. *Prog. Protistol.* 3:185-277.

Rhoads, D.C., 1973. The influence of deposit-feeding benthos on water turbidity and nutrient recycling. *Am. J. Sci.* 273:1-22.

Rhoads, D.C., K. Tenore, & M. Browne, 1975. The role of resuspended bottom mud in nutrient cycles of shallow embayments. In L.E. Cronin (ed.), *Estuarine Research*, Vol 1. Academic Press, New York, pp. 563-579.

Roman, M.R. & K.R. Tenore, 1978. Tidal resuspension in Buzzards Bay, Massachusetts. I. Seasonal changes in the resuspension of organic carbon and chlorophyll *a. Est. Coast. Mar. Sci.* 6:37-46.

Shimeta, J. & P.A. Jumars, 1991. Physical mechanisms and rates of particle capture by suspension feeders. *Oceanogr. Mar. Biol. Annu. Rev.* 29:191-257.

Shimeta, J., P.A. Jumars, & E.J. Lessard, 1995. Influences of turbulence on suspension feeding by planktonic protozoa; experiments in laminar shear fields. *Limnol. Oceanogr.* 40:845-859.

Shimeta, J. & J.D. Sisson, in press. Taxon-specific tidal resuspension of protists into the subtidal benthic boundary layer of a coastal embayment. *Mar. Ecol. Prog. Ser.*

Tennekes, H. & J.L. Lumley, 1972. *A first course in turbulence.* MIT Press, Cambridge.

Plugs and plumes

Dr. John Sleath
Department of Engineering, University of Cambridge, Cambridge U.K.

1. Plumes

Many investigators (see, for example, Hanes, 1990) have described site observations of isolated plumes of sediment in suspension. Possible generation mechanisms for these isolated suspension events include vortex shedding from bed forms, surface wave breaking and shear instabilities of the oscillatory boundary layer. The aim of the present paper is to put forward the suggestion that some of these suspension events are caused by spatially-limited plug formation of the sediment on the bed.

2. Plugs

We start by explaining what is meant by spatially-limited plug formation. Recent observations of velocity profiles within mobile beds of sediment in oscillatory flow show that sediment may be entrained in two different ways. Firstly, entrainment may be layer by layer as the flow speeds up after flow reversal, followed by progressive re-sedimentation as the flow decelerates at the end of the half cycle. This situation is illustrated by the measurements of Zala Flores and Sleath (1998) (referred to as ZFS) which are shown in Fig. 1. In this Figure y is distance measured vertically up from the initial bed level, t is time and ω is angular frequency.
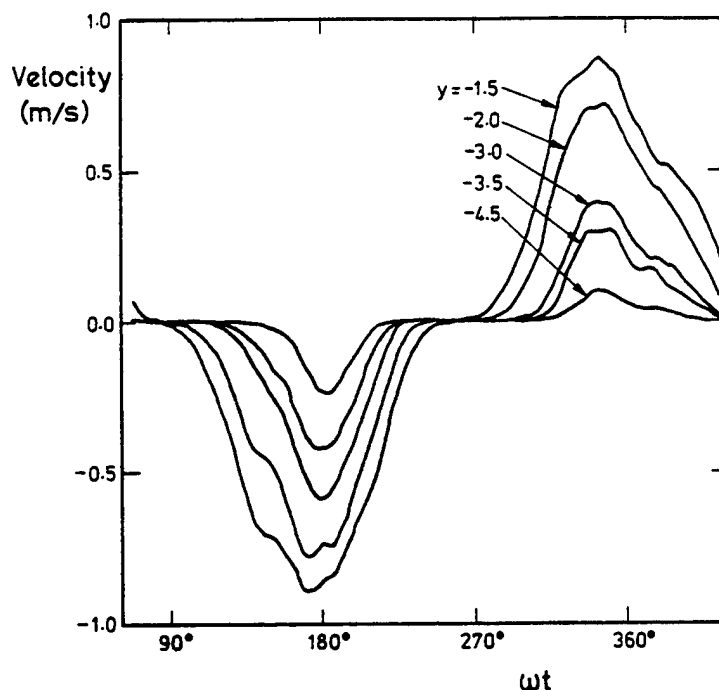

Fig. 1. Example of velocity records at various heights within a bed of sand. (ZFS Test no. S8)

Secondly, under certain circumstances, the sediment settles on the bed at the end of the half cycle but then starts to move as a single block when the flow reverses. This situation is illustrated in Fig. 2.
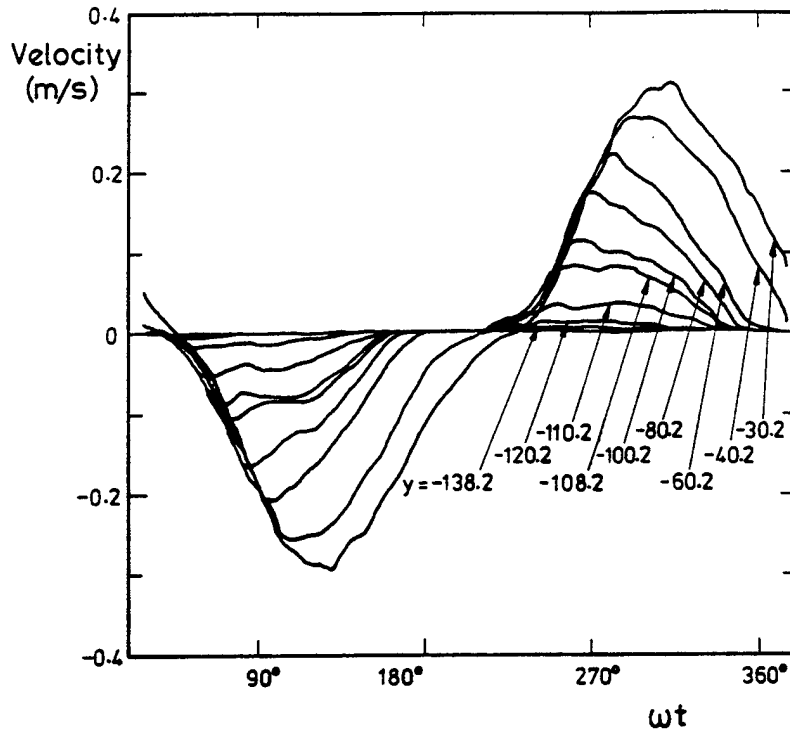

Fig. 2. Velocity records at various heights within a bed of sediment (ZFS Test no. A4)

The measurements of ZFS were made in an oscillatory water tunnel. In this situation the wave length is effectively infinite. Real surface waves are of finite length. If a plug of sediment forms on site it will be spatially-limited, i.e. of finite length in the direction of wave propagation.

3. How likely is plug formation on site?

Madsen (1974) derived a condition for movement of sediment as a solid block in oscillatory flow. The limiting condition may be written

$$\left| \frac{1}{(\rho_s - \rho)g} \frac{\partial p}{\partial x} \right| = C_* \tan \phi \tag{1}$$

where C_* is the limiting concentration of sediment in a stationary bed, ϕ is the angle of internal friction, p is pressure, x is distance in the direction of wave propagation, ρ_s and ρ are sediment and fluid density, respectively, and g is the acceleration due to gravity.

212

The analysis of Madsen (1974) does not account for the shear stress exerted by the flow on the surface of the bed. If the surface shear stress at the moment at which the sediment begins to move is in the same direction as the pressure gradient the bed will erode layer by layer from the top down. Thus, for plug formation to occur the shear stress on the surface must be in the opposite direction to the pressure gradient at the moment of initial motion. This is confirmed by analysis of ZFS's measurements. It is clear from an examination of the balance of forces acting on a segment of bed that the shear stress on the surface of the bed becomes less important, compared with the force due to the pressure gradient, as distance below the surface increases. It follows that for waves of infinite length the bed will always be less stable at large depths than at small depths if the shear stress is in the opposite direction to the pressure gradient. Thus, in ZFS's oscillatory water tunnel tests, for which wave length may be treated as infinite, the moving plug should always have extended to the bottom of the tunnel. In fact, the thickness of the moving plug was usually much smaller than this. The explanation appears to be that the vertical pressure gradient induced when the plug of sediment starts to move is important. Grains of sediment which are initially at rest in hollows between other grains force the plug upwards when sliding starts and this causes a downward flow of fluid through the plug. Taking account of the vertical pressure gradient induced by the downward flow, assuming Darcy's law to apply and making use of the Kozeny-Carman equation for permeability (Carman, 1937), the limiting condition for plug formation becomes

$$\left| \frac{1}{(\rho_s - \rho)g} \frac{\partial p}{\partial x} \right| \geq C_* \tan\phi \left(1 + \frac{180\nu\, C_* \alpha}{(1 - C_*)^3\, gD} \frac{\rho}{(\rho_s - \rho)t_*} \right) \tag{2}$$

where D is median grain diameter, αD is the distance the plug is forced upwards in time t_*, and ν is kinematic viscosity. This expression is for beds of infinite depth. The limiting value of pressure gradient is higher for beds of finite depth because of the need to allow for the shear stress exerted on the bed by the flow above.

By way of example, consider waves of period $T=12.5$s, sand of median diameter $D=0.1$mm, $C_*=0.64$ and $\phi=29°$. If, in addition, we assume $\alpha=0.13$, as for close packed spheres, and take $t_* = T/40$, Eq (2) reduces to

$$\left| \frac{1}{(\rho_s - \rho)g} \frac{\partial p}{\partial x} \right| \geq 0.60 \tag{3}$$

For loose sand the value of α would be close to zero. In that case Eq (2) would give

$$\left| \frac{1}{(\rho_s - \rho)g} \frac{\partial p}{\partial x} \right| \geq 0.35 \tag{4}$$

For naturally occurring waves the value of $1/(\rho_s - \rho)g\, \partial p/\partial x$ does not exceed about 0.4. Consequently, it is clear from Eqns (3) and (4) that plugs will only form under these conditions if the sand is loose ($\alpha \approx 0$). This was confirmed by ZFS's measurements which showed that plugs formed down to the depth at which sand had been disturbed during the preceding half-cycle.

This finding, that plugs are more likely to form in loose sand than in compacted sand, may explain why isolated suspension events are associated with groups of waves rather than individual very large waves: the leading waves in a group may be expected to loosen the bed whereas an isolated large wave following relatively small waves would be faced with a fully-compacted bed.

4. The effect of finite wave length

As pointed out earlier, the experiments of ZFS and Dick and Sleath (1991) and the quoted limits are for waves of infinite length. One effect of finite wave length, as shown by Madsen (1974), is to reduce the thickness of the mobile layer. Another important effect is that when the wave length is finite the sediment may be moving at one position on the bed and stationary, or even moving in the opposite direction, at another. In the case of a steep-fronted wave the transition from a situation in which the bed is stationary to one where sediment is in motion to a significant depth may be quite rapid.

In order to investigate this situation, we consider a step change in pressure gradient caused by a propagating wave. We assume that the pressure gradient ahead of this step is too low to cause the sediment to move. The sediment behind the step is mobile to a depth δ below the level of the undisturbed bed ahead of the step. We take the average velocity in the moving sediment to be u and the speed of the surface wave to be c. The situation is illustrated in Fig. 3
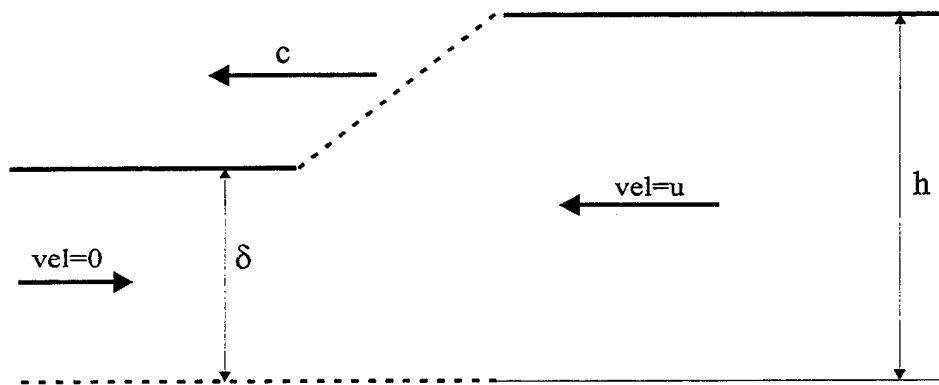

Fig 3. Definition sketch for segment of bed

We define

$$h = \frac{1}{C_*} \int_0^\infty C\, dy \qquad (5)$$

where C is the concentration at any height y. From continuity

$$c\delta = (c-u)h \qquad (6)$$

Thus, if c>>u,

$$h - \delta \approx \frac{u}{c}\delta \qquad (7)$$

Adopting typical values for the 50-year wave condition for the Southern North Sea we find

$$h - \delta \approx 6 \text{ cm}. \qquad (8)$$

In this calculation it has been assumed that the depth δ to which sand has been sufficiently loosened for plug formation to occur is 0.36m. Larger values than this are usually adopted for the

depth of disturbance in the surf zone. If δ were larger than 0.36m the value of h-δ would be larger. Also, since h and δ are defined in terms of the limiting concentration C_* the actual height to which sediment would be thrown up at the leading edge of the plug would be greater than the value given by Eq (8).

The situation shown in Fig. 3 is that at the leading edge of a wave. At the trailing edge the sediment could be moving in the opposite direction. A similar analysis leads to the conclusion that in this situation there would be a drop in bed level and, thus, no plume of sediment thrown up.

5. Conclusions

(1) The movement of sediment as a plug at the leading edge of a large wave causes a plume of sediment to be thrown up from the bed.

(2) Pressure gradients for naturally-occurring waves are not usually large enough for plug formation in sand which has not already been loosened. Consequently, plug formation is more likely to be observed with a group of waves, where the leading waves serve to loosen the sand, than with an isolated large wave.

(3) As pointed out by Bowen (1998), we would expect the plume produced by a group of waves to be intermittent. As the largest wave in a group decreases in size the plume disappears only to re-appear when the following wave has increased to a sufficient size.

References

Bowen, A.J., (1998) Private communication.

Carman, P.C., (1937) Fluid flow through granular beds. *Transactions Inst. Chem. Eng.*, **15**, 150-166.

Dick, J. E., and J. F. A. Sleath (1991) Velocities and concentrations in oscillatory flow over beds of sediment, *Journal of Fluid Mechanics*, **233**, 165-196.

Hanes, D.M., (1990) The structure of events of intermittent suspension of sand due to shoaling waves, in *The Sea*, **9**, B. Le Mehaute and D.M. Hanes (Eds), Wiley, New York.

Madsen, O.S., (1974) Stability of a sand bed under breaking waves, *Proc. 14th Conf. Coastal Engineering ASCE*, 776-794, New York.

Zala Flores, N. and J. F. A. Sleath (1998) The mobile layer in oscillatory sheet flow, *Journal of Geophysical Research*, **103**, C6, 12 783-12 793.

Flume Experiments on Larval Settlement of the soft-shell clam, *Mya arenaria* L.

P.V.R. Snelgrove

Fisheries Conservation Chair, Memorial University of Newfoundland, St. John's, Newfoundland, Canada A1C 5R3

J. Grant

Department of Oceanography, Dalhousie University, Halifax, Nova Scotia, Canada B3H 4J1

C.A. Pilditch

Department of Biological Sciences, University of Waikato, Hamilton, Private Bag 3105, New Zealand

Abstract

Like many benthic taxa, the soft-shell clam, *Mya arenaria*, is patchily distributed in nature. Near Halifax, Nova Scotia, Canada, *Polydora ligni, Pygospio elegans, Gemma gemma, Hydrobia* sp. and juvenile *M. arenaria* are very abundant at a sheltered site and virtually absent from an exposed site ~300 m away with similar sediment grain size composion. To evaluate whether larval settlement plays a role in establishing *M. arenaria* patterns, laboratory flume experiments were conducted with competent *M. arenaria* larvae. Natural cores from the sheltered and exposed sites with resident infauna intact, as well as cores from the same sites that had been defaunated by freezing, were inserted flush with the flume bottom. Highest settlement was observed in faunated cores from the sheltered site where *M. arenaria* are more abundant. Significantly lower settlement was observed in other treatments, including defaunated cores from the sheltered site. For corresponding treatments, settlement in sediment from the exposed site was less than that at the sheltered site. Of the abundant taxa in intact flume cores, only *Gemma gemma* densities were a significant predictor of *M. arenaria* settlement. These results suggest that *M. arenaria* larval settlement is greater in the presence of living *Gemma gemma*, though some selective capacity remains even where *G. gemma* are absent. We hypothesise that the sediment modification activity of *G. gemma* in relation to microbial filming may be the mechanism that determines suitability for settling *M. arenaria* larvae. A previously reported absence of *M. arenaria* spat at the sheltered site during intense field sampling by Emerson & Grant (1991) may be explained by annual variability in supply, or the observation that guts of some polychaetes in faunated cores were filled with *M. arenaria* larvae. If the latter is true, then selectivity may not help *M. arenaria* in this environment and soft-shell clam distributions at this site may be set primarily by post-settlement processes rather than at settlement.

Introduction

One of the most fundamental questions in benthic ecology is how pattern is maintained in benthic communities and the importance that larval settlement may play (Ólafsson et al. 1994; Snelgrove & Butman 1994). The soft-shell clam, *Mya arenaria,* occurs throughout shallow

northern boreal waters in muddy-sand areas and can often be patchy on multiple scales (e.g. Günther 1992). In Eastern Passage, Nova Scotia (Fig. 1), population dynamics of *M. arenaria* differ markedly between a sheltered and an exposed intertidal site located only hundreds of meters apart. Prior work indicates that despite the differences in wave exposure, the bulk grain size (~250 μm) and silt-clay content (~0.5%) of sediments are similar, although an organic mineral aggregate fluff layer is observed only at the sheltered

Fig.1 - Location of study sites within Halifax Harbour, Nova Scotia. Grey areas indicate intertidal areas and circles denote sampling sites. Eastern Passage is the channel in which both sampling sites are located.

site along with a reduced carbon:nitrogen ratio suggestive of more abundant microalgae (Grant & Emerson 1994). Several species occur at both sites (Emerson & Grant 1991), however, *Gemma gemma, Hydrobia* sp., and *Arenicola marina* occur only at the sheltered site and *Spisula* sp. occurs only at the exposed site (Emerson & Grant 1991). One other marked difference between the sites is that *M. arenaria* spat densities and transport were also found to be substantially higher at the exposed site seasonally (Emerson & Grant 1991).
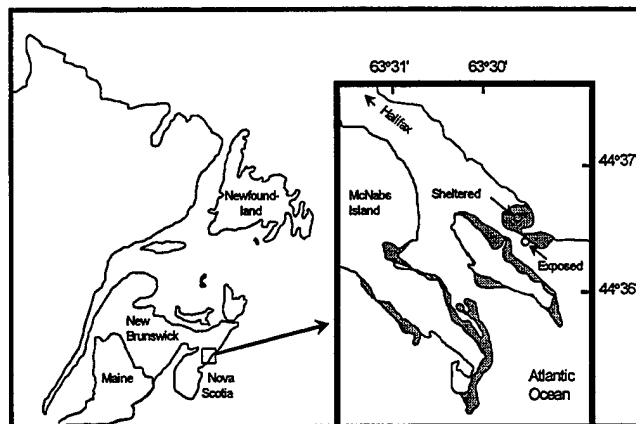
The goal of the present study was to use laboratory flume simulations to determine how differences in sediment composition and natural infaunal communities may influence habitat selection by settling *M. arenaria* larvae and thus contribute to *M. arenaria* population dynamics. To accomplish this goal we have expanded upon earlier flume studies that deliberately utilised simplified sediments (e.g. Butman et al. 1988) to test specific hypotheses on larval settlement. We have brought natural sediments with intact faunal communities into a flume to test whether fauna in sediments impacts larval settlement.

Methods

The study site was Eastern Passage, which is located in outer Halifax Harbour, Nova Scotia (Fig. 1). The Sheltered Site and Exposed Site that are the focus of this study are located approximately 300 m apart. Sediment grain size and organic content were similar but Sheltered sediment was fluffier with a slightly rougher, biogenically formed structure. In order to evaluate the fauna at the two sites, 4 replicate cores from each site were collected on July 19, 1996. Similar cores were collected on the two other dates when corresponding flume experiments were conducted but these cores were only spot checked to ensure they were not fundamentally different from the July 19 cores. Faunal cores served an additional function beyond evaluating the ambient fauna in that they ensured that any natural *Mya arenaria* settlement event would not confound the flume results described below.

The potential role that larval habitat selection may play in determining *Mya arenaria* patterns was tested in the flume at Dalhousie University (Fig. 2). Larvae were obtained by conditioning adults at 17°C and then spawning them by warming seawater to 22°C. Larvae were kept in aerated containers and fed daily a mixture of *Isochrysis galbana, Thalassiosira pseudonana* and/or *Chaetoceros muelleri*. When pediveligers were observed in the culture, larvae were deemed to be physiologically competent to settle and a flume experiment was initiated. The first step in a given experiment was to collect fresh faunal cores from the two sites in Eastern Passage and transport them to a seawater table at Dalhousie where they would be maintained in filtered, running seawater for the several days it took to complete a series of experiments. The experimental conditions for the flume experiments are given in Table 1.
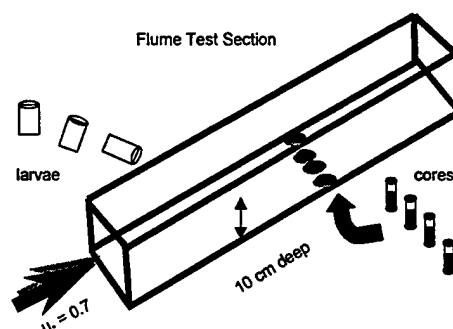

Figure 2 - Schematic representation of Dalhousie flume test section as it was configured for larval experiments. The flume was 7.32 m long and 50 cm wide. 37-cm diameter return pipe (not shown) provides return flow from beneath the flume and a low speed impeller within the pipe drives the flow. Cores were inserted from the underside of the flume as shown prior to filling the flume to 10 cm depth and setting the flow to achieve a shear velocity of 0.7 cm/s and then adding larvae.

Cores (4.36cm diameter) were inserted through the flume bottom so that the edge of the core itself and the sediment it contained were flush with the flume bottom. Treatments consisted of fresh cores from each site containing intact natural fauna, and cores from each site that had been defaunated by

Table 1 - Conditions During Experiments

Batch	Expt. Run	Length (h)	Larval Age (d)	Core Age (d)	Temp. Start (°C)	Temp. Finish (°C)
1	A	12	11	18	16.2	17.4
	B	12	12	34	16.8	17.6
	C	12	12.5	48	17.0	18.0
	D	12	13	62	17.6	18.1
2	A	12	11	12	17.9	19.2
	B	12	11.5	26	18.6	19.4
	C	12	12	40	18.9	19.8
	D	12	12.5	56	19.0	19.8
3	A	12	10.5	2	18.2	19.0
	B	12	11	17	18.6	19.3
	C	12	11.5	30	18.7	19.5
	D	12	12.5	48	18.9	19.5

freezing. One core of each treatment type was inserted to produce a 1 x 4 array (Fig. 2) that was oriented perpendicular to the flow direction. The flume was filled to 10-cm depth and flow set at a shear velocity of ~ 0.7 cm/s (representative of the natural environment) prior to adding 40,000 larvae per run. For each batch (=spawning) there were four sequential 12 hour runs with the 4 replicates of each treatment arranged in a Latin squares design. This methodology was repeated for three separate batches. At the end of each experimental run, the flume was drained and the sediments in each core removed and preserved in 10% formalin. Within days, samples were transferred to 80% ethanol with Rose Bengal and numbers of *Mya arenaria* larvae and all infaunal taxa were enumerated. A 106-μm sieve was always used for sample processing to ensure that recently settled *M. arenaria* would not be missed.

Results

Faunal cores collected from the two sites supported Emerson & Grant's (1991) finding of different faunal densities at the Exposed and Sheltered sites. Although a number of species were present at both sites, densities of all taxa were greatly reduced at the Exposed site compared to the

219

Sheltered site (Fig. 3). Among the taxa that were more abundant at the Sheltered Site was *Mya arenaria*, the focus of this study. Other abundant taxa included polychaetes (*Polydora ligni*, Pygospio elegans), molluscs (*Gemma gemma, Hydrobia* sp.) and oligochaete annelids. As was noted by Grant & Emerson (1994), the texture of the sediment differed markedly between the two sites. The sediment collected from the Sheltered site had a much fluffier appearance with fine material concentrated at the sediment-water interface. The material appeared to be partly biological in structure

Figure 3 - Densities of the most common taxa at the Sheltered and Exposed Sites. Bars denotes means and lines denote 1 se. Note differences in scale used to allow comparison between sites.

with biofilming and fine structure associated with polychaete tubes. By contrast, the Exposed site sediment looked very sandy, with little structure and no obvious fine material.

Flume experiments yielded relatively consistent results, with significantly higher *Mya arenaria* settlement in Sheltered Infauna cores than in all other treatments (Fig. 4). Settlement in Exposed No Fauna cores was significantly lower than in all treatments except Exposed Infauna cores. Thus, settlement was significantly higher in Sheltered Site cores for corresponding treatments. Similar patterns were observed in analysing the three sets of experiments (batches) separately, except that for two of the three batches, the Exposed Infauna and Exposed No Infauna cores were not significantly different from one another or from Sheltered No Fauna cores. In terms of temporal changes during a given series of experiments, peak settlement occurred during the second of the four experimental runs for all three batches, but selectivity seemed to remain consistent in that settlement was always highest in Sheltered Infauna cores regardless of larval or core age.
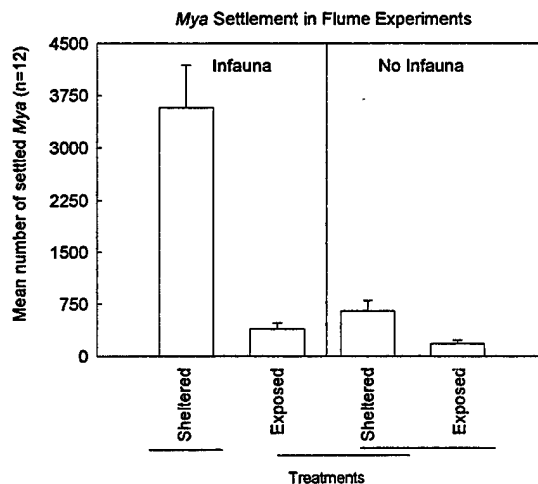

Figure 4 - Results of flume experiments on *Mya arenaria* settlement in intact Infaunal cores and corresponding No Infauna cores. Means are based on all 4 runs per batch x 3 batches for n = 12. Bars denote means and lines denote 1 se. Lines beneath treatments connect those that were not significantly different as determined by a Tukey's multiple comparisons test.

In order to test whether any infaunal taxa might have a positive or negative impact on larval settlement rates, we employed regression analyses to evaluate whether any of the abundant infaunal taxa in the cores that were placed in the flume were significant predictors of the amount of *Mya arenaria* settlement that occurred in those cores. Of the abundant

taxa shown in Figure 2, only *Gemma gemma* was a significant ($r^2 = 0.32$, n=12, p=0.03) predictor of *M. arenaria* settlement (Fig. 5).

Discussion

These experiments clearly demonstrate that settling *Mya arenaria* larvae are capable of habitat selection in realistic flows. The specific attribute of sediment that may increase or decrease larval response is unclear from these experiments, but we hypothesise that it may relate to biofilming of sediments. Because settlement was highest in both sheltered site treatments, there is some aspect of Sheltered site sediment that is more attractive to settling *M. arenaria* larvae than Exposed site sediment. Clearly, much of whatever made the Sheltered site sediment attractive was
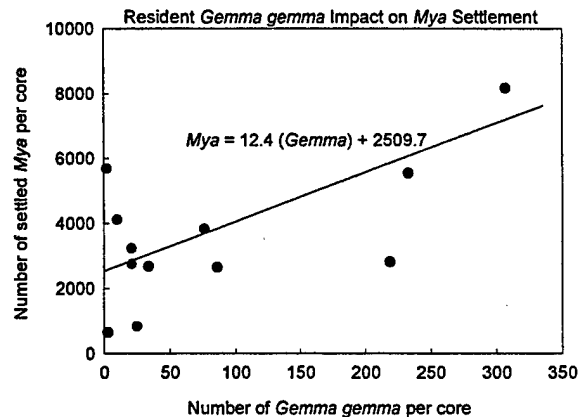

Figure 5 - The effect of *Gemma gemma* densities on settlement of *Mya arenaria* larvae. Only Sheltered Infauna cores were included in this analysis because *G. gemma* was effectively absent from other treatments.

lost in freezing/defaunation, given that settlement in No Infauna Sheltered cores was significantly lower than in Sheltered cores with infauna present. One explanation for this result is that some infaunal taxon had a positive (facilitation) or negative (inhibition) impact on *M. arenaria* settlement, but of all of the common species, only *Gemma gemma* was a significant predictor of *M. arenaria* settlement. Why *G. gemma* presence might increase *M. arenaria* settlement is unclear. Given the small size of *G. gemma* siphons it is unlikely that their siphoning activity enhanced larval flux to the bed. We hypothesize that *G. gemma* pumping enhances biofilming, which in turn enhances *M. arenaria* settlement. When Sheltered site sediments were frozen, this eliminated *G. gemma* and also destroyed much of the natural biofilm. This explanation of an indirect linkage between the two species would also explain the weakness of the relationship.

An obvious question with these results is whether the differences in *Mya arenaria* settlement are the result of active or passive processes. We believe that the latter is unlikely. It is true that biogenic modification of sediments in the Sheltered site sediments gave them a rougher texture, but these roughness elements were still much smaller than natural variability in core topography. In short, we believe that larger-scale variability in the topography of natural cores from both sites would have swamped any of the fine-scale roughness associated with the Sheltered site core bioroughness. A second possibility is that increased stickiness in Sheltered site cores might have enhanced larval retention. We believe this explanation to be unlikely because sediments would likely have retained some of their stickiness through freezing, but this explanation cannot be completely ruled out. Ahn et al. (1993) observed enhanced settlement of *Mercenaria mercenaria* larvae in the presence of *Gemma gemma* but fine-scale observations allowed them to rule out passive entrapment as an explanation.

It is tempting to conclude that these flume experiments provide clear evidence that habitat selection plays a major role in determining *Mya arenaria* patterns at Eastern Passage, but a more complex explanation is likely more appropriate. Emerson & Grant (1991) noted a complete

absence of *M. arenaria* spat at the Sheltered site in their study and very high abundances at the Exposed site during the fall. They concluded that post-settlement transport plays a major role in *M. arenaria* population dynamics. Reconciling their results with ours is not easy, but there are several reasonable explanations. First, broad-scale spat supply may have differed during the year of their study so that larvae never had the opportunity to "choose" Sheltered site sediments; habitat selection may play a greater role in some years relative to others. It is also possible that post-settlement predation may play a role, given that infauna are much more abundant at the Sheltered site and we noticed that some of the spionid polychaetes had guts that were full of *M. arenaria* larvae. Given the obvious capacity for habitat selection shown in our flume experiments, it is likely that both pre- and post-settlement processes play key roles in the population dynamics of *M. arenaria* at Eastern Passage and that the relative importance of each may vary over time.

Literature Cited

Ahn I-Y, Malouf R, Lopez G (1993) Enhanced larval settlement of the hard clam *Mercenaria mercenaria* by the gem clam *Gemma gemma*. *Mar. Ecol. Prog. Ser.* 99: 51-59.

Butman CA, Grassle JP, Webb CM (1988) Substrate choices made by marine larvae settling in still water and in a flume flow. *Nature* 333: 771-773.

Emerson CW, Grant J (1991) The control of soft-shell clam (*Mya arenaria*) recruitment on intertidal sandflats by bedload sediment transport. *Limnol. Oceanogr.* 36: 1288-1300.

Grant J, Emerson C (1994) Resuspension and stabilization of sediments with microbial biofilms: Implications for benthic-pelagic coupling. In: Krumbien WE, Paterson DM, Stal LJ (eds) *Biostabilization of Sediments*. Oldenburg: Bibliotheks ind Informationssystem der Universität Oldenburg, p. 121-134.

Günther C-P (1992) Settlement and recruitment of *Mya arenaria* L. in the Wadden Sea. *J. Exp. Mar. Biol. Ecol.* 159: 203-215.

Ólafsson EB, Peterson CH, Ambrose WG, Jr (1994) Does recruitment limitation structure populations and communities of macro-invertebrates in marine soft sediments: the relative significance of pre- and post-settlement processes. *Oceanogr. Mar. Biol. Ann. Rev.* 32: 65-109.

Snelgrove PVR, Butman CA (1994) Animal-sediment relationships revisited: Cause versus effect. *Oceanogr. Mar. Biol. Ann. Rev.* 32: 111-177.

Modes of sediment dispersal on continental shelves:
time for a reappraisal of methods and concepts?

Richard W. Sternberg
Andrea S. Ogston
University of Washington
School of Oceanography, Box 357940
Seattle, WA 98195-7940

David Cacchione
U.S. Geological Survey
345 Middlefield Road
Menlo Park, CA 94025

Over the past several decades, extensive observations of the sedimentology of continental shelves have provided considerable insights on sediment dispersal mechanisms, transport pathways, and depositional patterns. Two fundamentally different modes of sediment movement have been observed on continental shelves which can be described as *flow (or "storm") dominated* and *gravity dominated*. *Flow dominated* refers to grain movement forced by fluid turbulence which manifests itself as bedload and suspended load moving in response to waves, tides, and currents. Critical observations for flow dominated transport include time series of suspended sediment concentration profiles and associated velocity and pressure designed to elucidate boundary shear stress resulting from wave-current interactions, to identify net flow directions, and to compute sediment flux on varying time and spatial scales. *Gravity dominated* refers to extremely high concentrations of fine sediment maintained in nearbed suspensions on the continental shelf and manifested as fluid mud. Fluid mud layers can result from rivers with high suspended sediment loads that produce negatively buoyant underflows or are formed by some trapping mechanism (e.g., frontal zones). They are isolated from the overlying flows by sharp luticlines resulting from sediment induced stratification, do not sustain high levels of turbulence, and tend to move in the across-shelf direction under the influence of gravity. Fluid mud layers significantly reduce fluid drag over the seabed and thus can influence tidal propagation and dissipation on continental shelves.

Past studies have suggested that these two sediment transport modes tend to be associated with distinctly different shelf types. For example, continental shelves exhibiting flow dominated transport include all shelves except "muddy coasts", typically adjacent to small to moderate sized rivers (e.g., shelves off Washington; Palos Verdes and the Russian River, California; south coast of Australia; Great Britain; France). Fluid mud processes and gravity dominated transport are associated with shelves dominated by large sediment discharge from major rivers. Examples include the Gulf of Bohai off the Yellow River and the Brazilian shelf north of the Amazon River.

Recent advances in marine instrumentation and sampling experience derived from prior shelf studies have expanded the normal suite of observations carried out on continental shelves.

223

Examples include observations of flow velocity through the water column (ADCP), measurements of extremely high suspended sediment concentrations (OBS) and bed elevation changes (sonic altimeter), and profiles of the water column with multiple sensors from the sea surface directly to the seabed (e.g., sediment profiler). Results using these new methods in New Guinea, the Gulf of Mexico, and northern California suggest that our interpretation of shelf processes and resulting sediment transport have been too restrictive. Flow dominated and gravity dominated transport modes may not be limited to particular shelf types. In fact, moderate sized rivers have been shown to split into both hypopycnal and hyperpycnal (e.g., fluid mud) plumes and fluid muds have been documented on narrow, energetic shelves, receiving episodic discharge from a small river. These findings suggest that our past observations have been too limited in scope. Furthermore, these recent developments have broad implications regarding our observational methods and concepts of transport and deposition of shelf sediments, our ability to track materials entering the sea from terrestrial sources, and the complement of physics-based equations used to model shelf sediment transport.

Effect of Sediment Organic Content on Settlement and Growth of
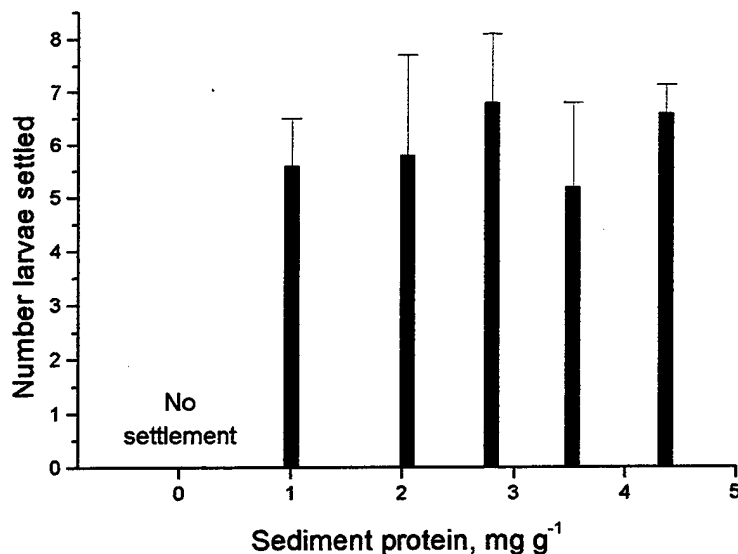## *Capitella* sp. I

Gary L. Taghon
Debra L. Linton
Rutgers University
Institute of Marine and Coastal Sciences
New Brunswick, New Jersey 08901-8521

The relative importance of larval settlement vs. post-settlement processes on the structure of benthic communities is a contentious topic in benthic oceanography. At least conceptually, it can be argued that settlement depends on fewer factors (e.g., boundary layer flow structure, larval behavior) than post-settlement processes (e.g., food limitation, competition, predation, physical disturbance). Both, however, have proven difficult to evaluate in the field, which has doubtlessly fueled the debate about their relative importance.

The polychaete worm *Capitella* sp. I has been the subject of several previous studies on larval settlement behavior, genetics, and population dynamics. Studies at the individual level show that growth and reproduction require high levels of sediment organic matter, consistent with the fact that large populations are only found in environments with high concentrations of organic matter. Previous studies on larval settlement show that larvae, when given a choice between sediments with very low and high organic contents, selectively settle in sediment with high organic content (Butman and Grassle 1992, Grassle et al. 1992, Snelgrove et al. 1993). Selective settlement takes place both in still water and at moderate flow speeds. The low sediment organic levels used in these experiments fall well below the minimal levels needed to support post-settlement growth, however, raising the question of whether larval selectivity has importance in the field. Accordingly, a series of experiments in still water and at moderate flows were conducted in order to investigate the effect of variable sediment organic matter content on settlement and growth of *Capitella* sp. I larvae.

Sediment treatments were set up by mixing different proportions of surface sediment collected from the intertidal zone of a *Spartina alterniflora* marsh on Delaware Bay (sieved to <1 mm) with the same sediment after it had been heated to 375°C for 24 h. The heating treatment oxidized all organic matter. Thus, the only differences in organic matter among treatments were quantitative, not qualitative, as the same type of organic matter was always present. Spontaneously hatched *Capitella* sp. I larvae were collected from cultures originating from Dr. J. P. Grassle. In the first series of still-water experiments, six sediments were prepared, ranging from 0.02 to 4.4 mg protein (g sediment)$^{-1}$. A small pile (2 cm diameter) of each sediment was placed around the perimeter of a dish. Thirty larvae were added one at a time to the center of the dish, and each was observed until it had settled into a pile. The experiment was replicated five times. No larvae settled in the lowest organic sediment, while there was no significant

difference in the numbers settling into the other five sediments (Fig. 1, p = 0.323, one-way ANOVA).

Figure 1. Number of *Capitella* sp. I larvae selecting sediments with different protein concentrations under still water conditions. Sediment protein measured with the method of Mayer et al. (1995). Bars are means plus 1 SD.

We have previously found that the concentration of bioavailable protein in sediment provides a better indicator of nutritional value to deposit feeders than the concentration of total organic carbon or total nitrogen (Taghon et al. 1990). Juvenile and adult *Capitella* sp. I require a sediment protein concentration greater than 1-2 mg protein g^{-1} in order to grow (Horng 1998). To determine whether newly settled larvae had a similar requirement, and also to examine settlement rate, an experiment was conducted in which larvae were given no choice of sediment in which to settle. Five newly hatched larvae were added to bottles containing each of the sediments used in the first experiment. Each treatment was replicated 20 times. Each bottle was censused immediately after the larvae were added, then every 5 min for the next 0.5 h, then daily until all larvae had settled. In addition, every 5 d for 3 weeks, the lengths of worms from five bottles from each treatment were measured. Settlement rate (Fig. 2) was significantly affected by sediment protein content (p < 0.00001, ANOVA), and was lower in the 1.0 mg protein g^{-1} treatment than in all sediments with greater protein contents (Tukey HSD comparison of means). The majority of larvae in all treatments settled within the first 0.5 h.
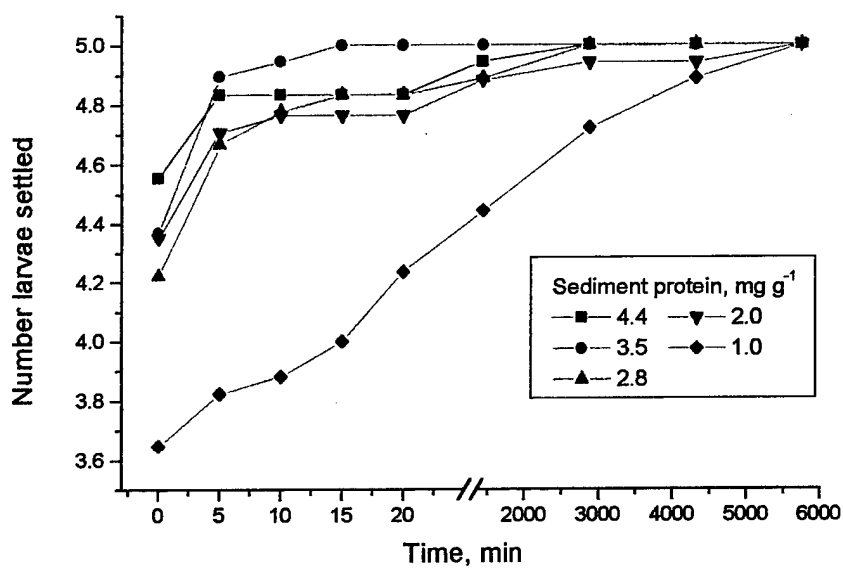
Figure 3. Settlement rate of *Capitella* sp. I larvae into sediments with different protein concentrations, under still water conditions. Note break in abscissa.
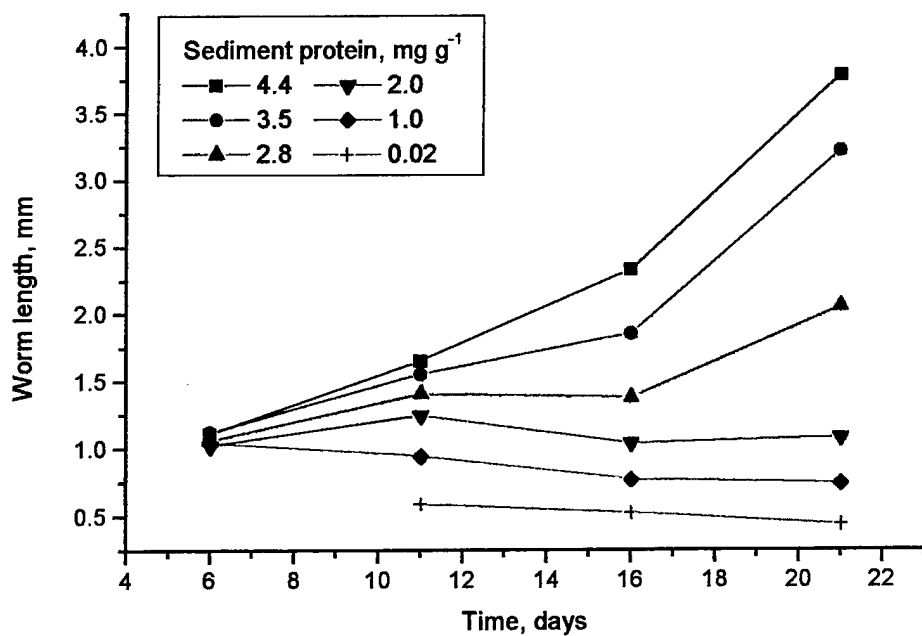

Figure 2. Worm size over time in sediments with different protein contents.

Growth of larvae was strongly affected by sediment protein content (Fig. 3). A one-way ANOVA of the length data on d 21 resulted in a highly significant treatment effect ($p < 0.00001$), and Tukey HSD multiple comparison of means showed that all treatments were significantly different from each other except for the two highest protein levels. Growth only took place when larvae settled into sediment with > 2 mg protein g^{-1}, similar to our previous results.

The results of these still water experiments indicate that, while *Capitella* sp. I larvae demonstrate selectivity while settling, the selectivity is best described as an "all or none" response. Larvae do not settle in protein-free sediment, but do not discriminate among sediments with widely varying concentrations of protein, even when the sediment is incapable of supporting growth of the worms. Thus, the importance of post-settlement processes, notably food availability, is implicated as being of great importance for this species. As argued by Butman and Grassle (1992), however, settlement must be evaluated under realistic flow conditions, as hydrodynamic conditions can markedly influence larval settlement. Accordingly, an experiment was performed to investigate substrate choice in flowing water. The flow experiments were conducted in a counter-rotating annular flume (refer to http://marine.rutgers.edu/flumes/flumes.html for details). The flume bottom was covered with a 1-cm-thick layer of medium grained, organic-free sand. Five sediment treatments were employed, each replicated 15 times: the same organic free sand used to cover the flume bottom, and four mud treatments of varying protein concentration, prepared as in the still-water experiments. Sediment was placed into shallow 4.7-cm diameter dishes, which were then inserted flush with the sand base on the centerline of the flume. Treatments were in random order with 10 cm-separation between adjacent dishes. Seawater (1-μm-filtered, 30‰, 15°C) was added, and flow set to achieve a u∗ of 0.29 cm s^{-1}. At the start of the experiment, ≈3900 *Capitella* sp. I larvae (< 48 h old) were added as the flume made one rotation past a fixed position. After 2 h, the flume was stopped, each dish was tightly capped before removal, and the contents were washed into bottles with 70% ethanol containing Rose Bengal. Samples were sorted with a stereomicroscope. Results for the four mud experiments are presented here (Fig. 4). A one-way ANOVA shows a highly significant treatment effect ($p < 0.00001$), and Tukey HSD comparison of the means showed that all were significantly different ($p < 0.05$).

Results of the flow experiment are not strictly comparable to the still water experiments for at least two reasons. First, different batches of larvae were used. Second, the sediment protein concentrations differ slightly. Nonetheless, the results indicate that the ability of the larvae to select among sediments was improved by moderate flows. In the still water experiments, larvae settled into sediments incapable of supporting their subsequent growth (i.e., sediment with less than 1-2 mg protein g^{-1}) as readily as into sediment with high food concentration. In flow, settlement was significantly lower into low-organic sediment. Previous experiments with this species also give some evidence that selection against sediment with inadequate (for growth) food concentrations is improved in moderate flows (Butman & Grassle 1992, Grassle et al. 1992).
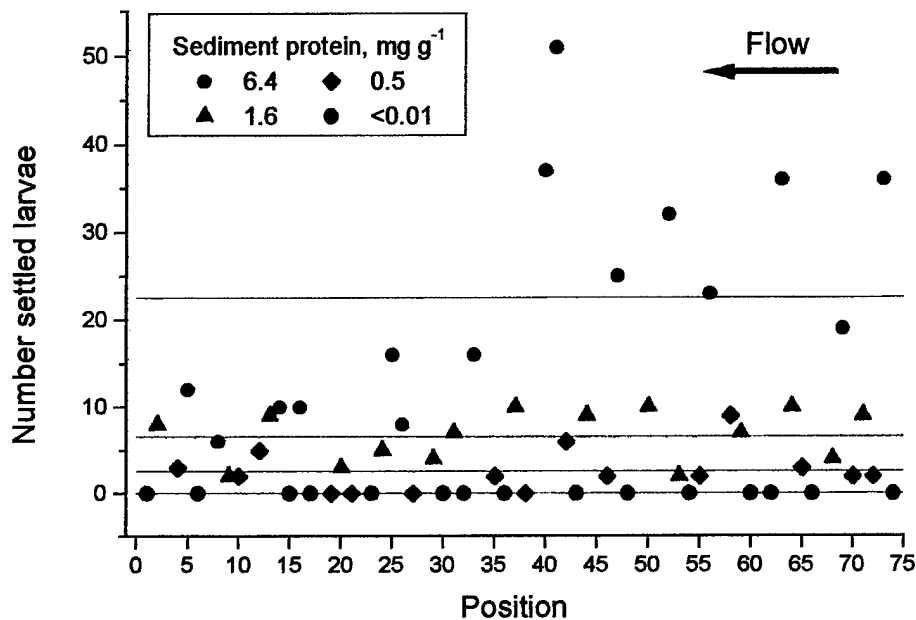
Figure 4. Settlement of *Capitella* sp. I in sediments with different protein concentrations, under flow (u* = 0.29 cm $^{-1}$). Position refers to placement of each treatment around the centerline of the annulus.

Further experiments are needed to reconcile these apparently disparate results. If species such as *Capitella* sp. I show significant settlement into sediments that may not support the subsequent survival of the animals, then the role of post-settlement processes in determining population dynamics takes on greater importance. If larval behavior is modified by flow, specifically, if the ability to settle in suitable habitats is actually enhanced by flow, then benthic oceanographers will need to acquire a much greater knowledge of benthic boundary layer conditions.

References

Butman, C.A., and J.P. Grassle. 1992. Active habitat selection by *Capitella* sp. I larvae. I. Two-choice experiments in still water and flume flows. Journal of Marine Research 50:669-715.

Grassle, J.P., C.A. Butman, and S.W. Mills. 1992. Active habitat selection by *Capitella* sp. I larvae. II. Multiple-choice experiments in still water and flume flows. Journal of Marine Research 50:717-743.

Horng, C.-Y. 1998. Influence of the marine polychaete, *Capitella* sp. I, on the fate of sediment-bound polycyclic aromatic hydrocarbons - the role of feeding activity. Ph.D. Dissertation, Rutgers University, New Brunswick.

Mayer, L.M., L.L. Schick, T. Sawyer, C.J. Plante, P.A. Jumars, and R.L. Self. 1995. Bioavailable amino acids in sediments: a biomimetic, kinetics-based approach. Limnology and Oceanography 40:511-520.

Snelgrove, P.V.R., C.A. Butman, and J.P. Grassle. 1993. Hydrodynamic enhancement of larval settlement in the bivalve *Mulinia lateralis* (Say) and the polychaete *Capitella* sp. I in microdepositional environments. Journal of Experimental Marine Biology and Ecology 168:71-109.

Taghon, G.L., R.R. Greene, and D. Bard. 1990. Effects of food value of artificial and natural sediments on functional response and net rate of energy gain by a deposit-feeding polychaete, p. 515-529. In: R.N. Hughes [ed.], Behavioural mechanisms of food selection. Springer-Verlag, Berlin.

Measuring Waves and Currents with an Upward-Looking ADCP

Eugene A. Terray
Dept. Applied Ocean Physics and Engineering
Woods Hole Oceanographic Institution
MS–11, 217 Bigelow
Woods Hole, MA 02543
(508) 289–2438
eterray@whoi.edu

R. Lee Gordon*
NortekUSA
San Diego, CA 92131
lgordon@nortekusa.com

Blair H. Brumley
RD Instruments, Inc.
9855 Business Park Avenue
San Diego, CA 92131
bbrumley@rdinstruments.com

Introduction

Bill Grant made seminal contributions to our understanding of the dynamics of continental shelf benthic boundary layers, particularly with respect to the role of surface waves in resuspending sediment, and in enhancing the mean stress via nonlinear wave–current interaction. His work drew attention to the necessity of knowing the relative direction between the waves and current in addition to the amplitude of the near-bed wave velocity.

Unfortunately, even today the technology for measuring waves and current profiles has remained distinct, typically requiring the experimenter to deploy different instruments. For example, in relatively shallow water (less than 10–20 meters) pressure gage/current meter triplets ('PUV gages') are routinely used to measure the near-bed wave intensity and direction, whereas in deeper water surface buoys are required (these are mostly of the 'pitch-roll-heave' or accelerometer type). Near-bed wave velocities are then inferred from linear theory. Neither of these approaches gives information on the current profile, knowledge of which is important both for the purpose of establishing the near-bed shear, and the direction of the advection at various depths.

---

* Work performed while employed by RD Instruments Inc.

Technique and Results

This contribution describes some of the results of our investigation into the possibility of estimating both wave height and direction as a function of frequency from a conventional bottom-mounted, upward-looking Acoustic Doppler Current Profiler (ADCP).

ADCPs differ from conventional wave sensors in several ways. Unlike 'single point' PUV triplets or buoys, they provide an array measurement, and a bottom-mounted instrument can measure from the near-bed to the near-surface. Close to the surface a variety of spatial lags are available for estimating wave direction (*i.e.* long lags between opposing beams, and short lags between bins along individual beams). However, since the beam separation is small close to the bed, wave orbital velocities (associated with the long waves) can be recovered in the same way as currents, so that the ADCP operates there much like a point sensor (Herbers *et al.*, 1991). It is also possible in many instances to follow the motion of the surface in the wave band using the interpolated backscatter intensity (Visbeck and Fischer, 1995). Hence a redundant estimate of height and direction is often possible over the energetic portion of the wave spectrum. Finally, bottom-mounted ADCPs avoid many of the hazards to which surface buoys are exposed. Furthermore, it is possible to bury most of an ADCP, permitting its use in shipping channels.

We have investigated the performance in the field of the standard four-beam "Janus" configuration, as well as a novel 3+1 arrangement consisting of a vertical plus three slant beams. The water depth, wave height and frequency-direction spectra are estimated from the ADCP measurements as follows:

- For ADCPs lacking a pressure transducer, water depth (and its variation over tidal time scales) is obtained using echo-ranging to the surface along the slant beams (in the case of the Janus configuration) or the vertical beam (in the 3+1 case).

- In the case of the Janus configuration, wave height spectra are recovered by combining velocity spectra from each of the four beams at various depths, and extrapolating the result to the surface. This procedure also yields an estimate of the spectral distribution of Doppler noise. In the case of the 3+1 configuration, the velocity along the vertical beam is sufficient to estimate the height spectrum (Zedel, 1994). As mentioned above, either the vertical beam in the 3+1 configuration or the Janus slant beams can be used in many cases to echo-locate the surface, thus providing a redundant estimate of the height spectrum.

- For both beam configurations, directional spectra are determined from the covariance between the various ADCP range cells (Terray *et al.*, 1990). Since the wave field is stationary, wave direction at different frequencies can be estimated independently. The covariance matrix at a particular frequency, $C(f)$, is related to the frequency-direction spectrum, $D(f, \theta)$ as

$$C(f) = \int d\theta \; \mathbf{H} \, D(f, \theta) \, \mathbf{H}^\dagger$$

where $\mathbf{H}(f, \theta)$ is the array response to a plane wave of frequency f propagating in the direction θ, and $\dagger$ denotes the complex conjugate transpose. We assume that linear theory is adequate to compute $\mathbf{H}$. Several techniques then are available to estimate the directional distribution at each frequency – we use the iterative maximum likelihood method (Krogstad et al., 1988) because of its robustness and simplicity. As a check we can also estimate the direction of the long waves from the range measurements along each of the slant beams by fitting a plane through the four measurements.

We have compared wave height and direction spectra obtained from ADCP velocity measurements in several field experiments to those obtained from a PUV triplet and a bottom-mounted pressure gage array in water depths of 8–12 m, and have found good agreement between the various methods. When available, the echo-ranging estimates of height and direction of the longer waves also agree well with those based purely on ADCP velocity measurements. We conclude that the ADCP-derived estimates of the directional properties of ocean waves in shallow water are competitive with those obtained by conventional techniques. Work is currently underway to validate the ADCP approach in deeper water.

References

Herbers, T.H.C., R.L. Lowe and R.T. Guza (1991): Field verification of acoustic Doppler surface gravity wave measurements. *J. Geophys. Res.* **96**(9), 17,023–17,035.

Krogstad, H.E., R.L. Gordon and M.C. Miller (1988): High resolution directional wave spectra from horizontally-mounted acoustic Doppler current meters. *J. Atmos. & Oceanic Phys.* **5**, 340–352.

Terray, E.A., H.E. Krogstad, R. Cabrera, R.L. Gordon and A. Lohrmann (1990): Measuring wave direction using upward-looking Doppler sonar. *Proc. of the IEEE 4th Working Conf. on Current Measurement*, G.F. Appell and T.B. Curtin eds., IEEE Press, 252–257.

Visbeck, M. and J. Fischer (1995): Sea surface conditions remotely sensed by upward-looking ADCPs. *J. Atmos. & Oceanic Phys.* **12**, 141–149.

Zedel, L. (1994): Deep ocean wave measurements using a vertically oriented sonar. *J. Atmos. & Oceanic Phys.* **11**(1) 182–191.

Acknowledgments

The effect of experimentally increased near-bottom flow on metazoan meiofauna at a deep-sea site

David Thistle[1] and Lisa A. Levin[2]

[1]Department of Oceanography, Florida State University, Tallahassee, FL 32306-4320, U.S.A

[2]Marine Life Research Group, Scripps Institution of Oceanography, La Jolla, CA 92093-0218, U.S.A.

It has been argued that strong near-bottom flows affect sediment-dwelling deep-sea animals, but the evidence comes largely from studies that compared sites separated geographically by 100's to 1000's of kilometers and in depth by 100's of meters. We present the results of the first experimental investigation of the effects of strong near-bottom flow on deep-sea metazoan meiofauna (small animals such as nematodes and harpacticoid copepods). At a site (32° 27.581' N, 127° 47.839' W) at 583 m depth on the Fieberling Guyot summit plain, the submersible Alvin placed three weirs designed to increase the near-bottom flow locally. After 6.5 weeks, sediments in the weirs and unmanipulated locations in the vicinity were sampled. The abundances of nematodes, harpacticoid copepods, ostracods, and kinorhynchs, considered collectively and as individual taxa, were significantly lower in the weir samples than in the background samples. The proportion of kinorhynchs in the fauna declined as well. These results suggest that strong near-bottom flow can reduce the abundance of meiofauna in the deep sea and alter assemblage composition. Such effects can be expected in other high-energy areas, e.g. the axes of submarine canyons and regions exposed to benthic storms. Several questions remain. For example, what is the balance between direct effects (e.g. erosion of animals from the deposit) and indirect effects (e.g. abrasion of animals by sediment particles) of strong flow? Also, does meiofaunal abundance always decrease with flow speed, or is the relationship more complex?

Nearshore Estimates of Turbulent Reynolds Shear Stress

John Trowbridge (Woods Hole Oceanographic Institution, Woods Hole, MA 02543)
George Voulgaris (University of South Carolina, Columbia, SC 29208)

Introduction

Turbulent Reynolds shear stresses are believed to play a dominant role (e.g., Allen, 1980; Battjes, 1988) in controlling the motion of water and sand in the shallow nearshore environment, defined here to be the coastal region with depths on the order of meters, where both winds and breaking waves force energetic alongshore flows. In spite of their importance, direct covariance measurements of turbulent Reynolds stresses have not been obtained in the nearshore environment, primarily because of large velocity variances produced by energetic waves, which irrevocably contaminate covariance estimates of turbulent stress obtained from individual sensors if there is even a small uncertainty in the orientation of either the sensor or the principal axes of the wave-induced velocity field (e.g., Grant and Madsen, 1986). Recently, Trowbridge (1998) developed and tested a technique to measure near-bottom turbulent Reynolds shear stress in the presence of energetic surface waves. This technique is based on the use of two velocity sensors, separated horizontally by a distance small in comparison with the surface wave length but larger than the scale of the energetic turbulent eddies (comparable to the height of the sensors above the bottom). With this scale separation, minus the density times half the covariance between horizontal and vertical velocity differences is a nearly wave-free estimate of the turbulent Reynolds shear stress. In the following, we describe a set of measurements and preliminary analysis designed to provide estimates of nearshore turbulent Reynolds shear stress based on the technique described above.

Measurements

As part of the SandyDuck field program conducted during late summer and early fall of 1997 at the U. S. Army Corps of Engineers Field Research Facility (FRF) in Duck, North Carolina, an array of five acoustic-Doppler velocimeters (ADVs), manufactured by Sontek, Incorporated, was deployed on a low-profile frame at a mean depth of approximately 4.5 m. The ADV array included three of the field version of Sontek's sensors (ADVF), and two of the more rugged ocean version (ADVO), one of which was fitted with pressure, temperature, pitch and roll sensors, as well as a compass. The relative positions of the ADVOs and two of the ADVFs were suitable for providing estimates of Reynolds stress by means of the differencing technique described in the Introduction, and the sensing volumes were at different heights, so that the measurements can provide estimates of the vertical gradient of Reynolds-averaged horizontal velocity.

The ADV measurements were designed to capitalize on other SandyDuck measurements, primarily for the purpose of testing a simplified alongshore momentum balance (wind stress plus cross-shore gradient of wave-induced radiation stress equals bottom stress). The frame was deployed between two alongshore arrays of sensors maintained by Steve Elgar, Tom Herbers, Bob Guza and Bill O'Reilly, so that an

estimate of cross-shore gradient of radiation stress can in principle be obtained by differencing measurements obtained along these lines. Jim Edson and Chuck Long obtained direct covariance measurements of wind stress at the end of the FRF pier.

The pair of ADVOs functioned well throughout the measurement period, except for an intermittent noise problem that affected one of the sensors. The ADVFs functioned for approximately six days, after which they were apparently damaged by a large object moving through the array.

Preliminary Results

Estimates of the alongshore component of turbulent Reynolds shear stress, obtained via the naive approach of computing covariances of horizontal and vertical velocities measured by individual sensors, produces four estimates (one each from two ADVOs and two ADVFs) that are poorly correlated, with little consistency in sign or magnitude (Figure 1a). In contrast, stress estimates obtained by differencing the pair of ADVO measurements and by differencing the pair of ADVF measurements agree in magnitude and sign and have much better correlation (Figure 1b).

Estimates of significant wave height (Figure 2a), obtained from ADVO pressure measurements and from ADVO velocity measurements via linear wave theory (e.g., Dean and Dalrymple, 1984), were small in comparison to the depth at the ADV frame during some periods and large enough to break (roughly 40 percent of the depth; see Guza and Thornton, 1980) during other events with strong alongshore flows (Figure 2b), indicating that the instrument frame experienced both unbroken and broken waves. Estimates of alongshore bottom stress are comparable to estimates of alongshore wind stress (Figure 2c).

Summary and concluding remarks

We have described nearshore measurements and analysis designed to determine turbulent Reynolds shear stress in the wind- and wave-driven nearshore environment. Preliminary analysis indicates that the technique of differencing velocity measurements from different sensors to produce stress estimates works reasonably well in this application. Future analysis will focus on filling in the gaps in the timeseries of stress estimates, on testing a simplified turbulence energy balance, and on testing a simplified alongshore momentum balance.

Acknowledgments

References

Allen, J. S. 1980. Annu. Rev. Fluid Mech. 12, 389-433.

Battjes, J. A. 1988. Annu. Rev. Fluid Mech. 20, 257-293.

Dean, R. G. and Dalrymple, R. A. 1984. Englewood Cliffs, NJ: Prentice-Hall.

Grant, W. D. and Madsen, O. S. 1986. Annu. Rev. Fluid Mech. 18, 265-305.

Guza, R. T. and Thornton, E. B. 1980. J. Geophys. Res. 85, 1524-1530.

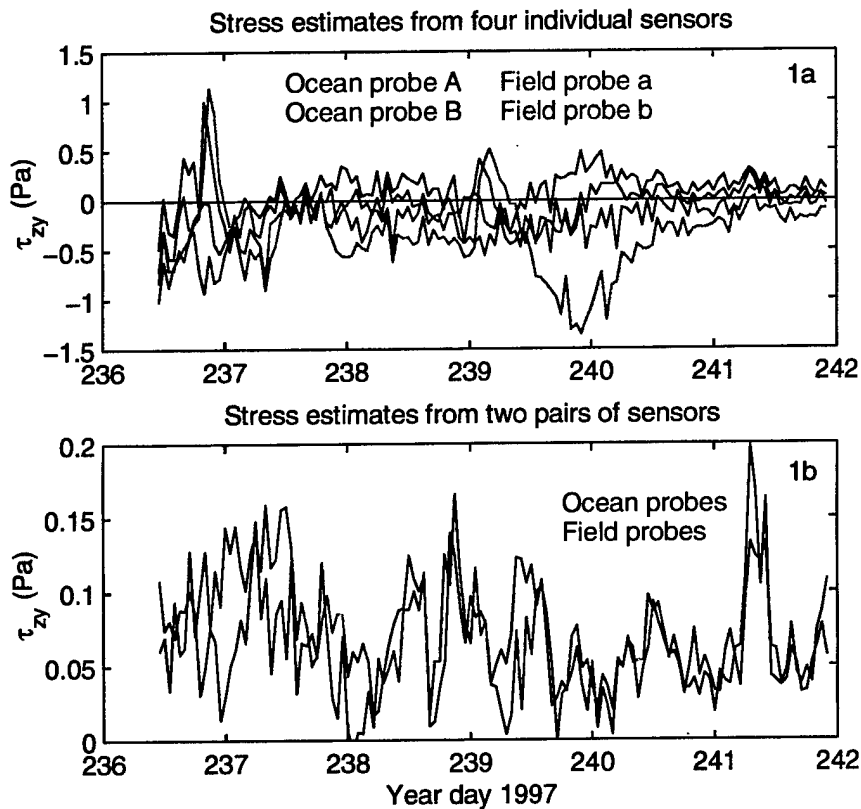Trowbridge, J. H. 1998. J. Atmos. Oceanic Technol. 15, 290-298.

Figure 1. Direct covariance estimates of alongshore stress obtained
(a) from individual sensors, and (b) from velocity differences measured
by pairs of sensors. Note the vertical scale change in panel (b).

239

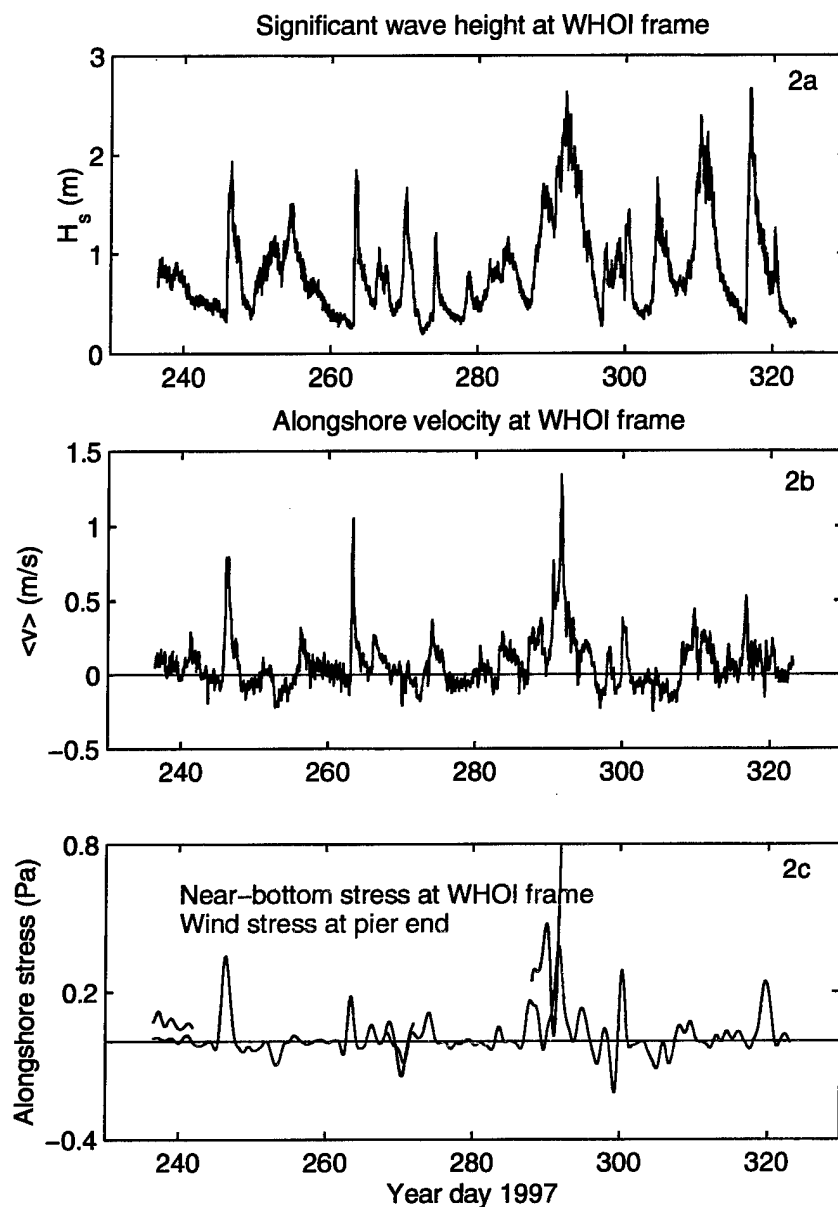Figure 2. Estimates of (a) significant wave height from pressure measurements at the ADV frame, (b) half–hour–averaged alongshore velocity at the ADV frame, and (c) low–pass–filtered alongshore wind stress (courtesy of Jim Edson) and alongshore bottom stress (from the ADVOs). Estimates of bottom stress correspond to periods when both ADVOs functioned well. Future work will be devoted in part to filling in gaps in this record.

Controls on the volume and distribution of resuspended fine sediment on the continental shelf

Patricia Wiberg, Environmental Sciences, University of Virginia, Charlottesville, VA 22903; pw3c@virginia.edu

During the past several decades considerable progress has been made in our ability to measure and to compute suspended sediment distributions in continental shelf bottom boundary layers. Measurements have advanced from single hourly measurements of near-bottom light transmission to vertical arrays of optical sensors to the detailed information about vertical and temporal structure available from recently developed acoustic backscatter profilers. Similarly, bottom boundary layer models have developed from the original wave-current interactions models of Smith (1977) and Grant and Madsen (1979) to account for a variety of processes such as stratification of the water, development of bed roughness, limits on sediment availability, and bed textural evolution.

There has been considerable synergy between the development of the models and the design and analysis of field measurement programs. It is difficult to analyze direct or indirect measurements of suspended sediment concentrations in the bottom boundary layer of the continental shelf without the aid of a model to characterize the velocity profile, bottom shear stress due to waves and currents, and turbulent mixing near the bed. At the same time, field measurements of velocity and suspended sediment concentration provide the data needed to test shelf sediment transport models. In particular, the availability of measurements of suspended sediment concentration at multiple elevations above the bed is essential for identifying the dominant processes responsible for the volume and distribution of sediment in the water column.

Quantitative formulations for suspended sediment in almost all cases begin with the premise that equilibrium concentration profiles represent a balance between upward turbulent diffusion and downward settling. This balance dictates the shape of the concentration profile; the volume in suspension depends on the concentration boundary condition, usually specified at a reference level close to the bed. Developing a general formulation for this boundary condition has been a major obstacle to progress on predictive models of suspended sediment transport. It is common in equilibrium calculations of suspension of noncohesive sediment to assume the reference concentration is proportional to excess shear stress. The coefficient of proportionality, however, has proven difficult to predict, with estimates ranging over several orders of magnitude when evaluated based on extrapolation of measurements in marine environments.

Sediment in many continental shelf settings, including most of the U.S. west coast, differs both in texture and sorting from the relatively well sorted sandy sediment that has historically been the focus of sediment transport studies. The presence of significant amounts of fine-grained sediment in the seabed introduces several additional considerations into suspended sediment calculations, including flocculation, cohesion, limits on availability, and consolidation; suspended-sediment-induced stratification of the water column can also be important in silt and silty-sand sites on the shelf.

A multi-year time series of near-bed currents, waves, and turbidity measured at a 60-m-deep sandy-silt site on the Eel River shelf, northern California provides an extensive set of data regarding fine-grained sediment resuspension for testing our conceptual and numerical models of this process. Sediment at this site is ~90% silt and 10% sand, with a mean size of roughly 30μm. Turbidity measurements indicate that sediment is resuspended frequently during fall and winter when bottom wave velocities exceed roughly 14 cm/s. Video camera images from the site reveal the presence of flocs in suspension with settling rates averaging about 1 mm/s (Sternberg et al., in press).

Under equilibrium conditions, the slope of suspended sediment concentration profiles depends on the ratio of particle settling velocity to fluid shear velocity. Fine-grained sediment with low settling rates would be expected to be distributed relatively uniformly in the vertical, with higher shear velocities producing more uniform profiles. Analysis of suspended sediment measurements 30 cm and 100 cm above the bed (cmab) at the 60-m site on the Eel shelf reveals a different picture. General trends in the slope of suspended sediment profiles were determined for a 5.5-month period during the winter of 1997-98 by averaging hourly suspended sediment concentrations associated with specified ranges of bottom wave velocity, u_0, and current shear velocity, $u*_c$ (Table 1). Several things are apparent. First, the concentration difference between 30 and 100 cmab is quite large; values 30 cmab are an average of 3 times the values 100 cmab. Second, concentrations 30 cmab are more strongly influenced by changing wave conditions than concentrations 100 cmab. Third, the difference in concentration between the two levels is the same or larger on average for higher values of $u*_c$.
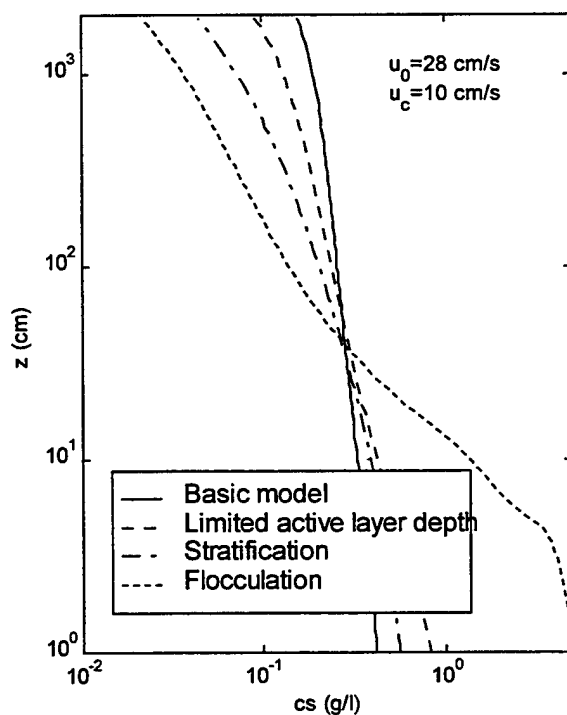
Table 1. Measured suspended sediment concentrations at a 60-m site on the Eel shelf

u_0 (cm/s)	$u*_c$ (cm/s)	c_s 30 cmab (g/l)	c_s 100 cmab (g/l)	c_s 30 - c_s 100	N
≤12	≤1.0	0.08±0.01 *	0.04±0.01	0.04	972
	>1.0	0.06±0.01	0.02±0.01	0.04	199
>12, ≤25	≤1.0	0.20±0.01	0.09±0.01	0.11	1220
	>1.0	0.32±0.03	0.16±0.02	0.16	388
>25	≤1.0	0.62±0.04	0.15±0.01	0.47	872
	>1.0	0.71±0.05	0.23±0.02	0.48	464

* 95% confidence intervals on means

Three possible mechanisms could be invoked to explain the observed trends in suspended concentrations on the Eel shelf. The fine-grained sediment in suspension may be present in a flocculated form, thereby increasing the settling rates of the particles by an order of magnitude. This would increase the ratio of settling velocity to shear velocity, consistent with a steeper concentration profile. The sediment in suspension might stratify the water column, particularly near the top of the wave boundary layer, inhibiting vertical mixing and producing a steeper concentration profile. Finally, if the availability of the finest fractions of the bed is limited, e.g. by armoring, such that they represent only a small to moderate percentage of the sediment in suspension, the relatively coarser composition of the sediment in suspension would also result in a steeper concentration profile (Figure 1). Studies of fine-grained marine sediment transport suggest that each of these mechanisms could be significant and, in all likelihood, act together to produce observed distributions of sediment in suspension.

Increasing the settling rate of the $<45\mu m$ fractions of the bed at the 60-m Eel shelf site to 1 mm/s, as though all of these fractions are present as flocculated particles when suspended, and neglecting for the moment any effects of stratification or availability, generally reproduces the observed concentration differences between 30 and 100 cmab for values of $u_{*c} \leq 1.0$ cm/s (solid curve and x, Figure 2; top row). These calculations are made using a shelf sediment transport model (Wiberg et al., 1994) that accounts for effects of waves, currents, and moveable bed roughness; the model is based on the original formulation of Smith (1977), but is similar to the models of Grant, Madsen and Glenn (Grant and Madsen, 1979, 1982; Glenn and Grant, 1987). Interestingly, calculations that include effects of both stratification and limited availability of fine sediment, but neglect the presence of flocs, produce very similar results (dashed curve and o, Figure 2; bottom row).

Figure 1. Comparison of calculated suspended sediment concentration profiles for a silt bed when effects of stratification, limited availability of fine sediment, and flocculation are included in the calculations; all of these effects are neglected in the "basic model" profile.

While both sets of model calculations shown in Figure 2 capture the observed increase in concentration with increasing u_0, they are inconsistent with the data in the manner in which concentration changes with increasing shear velocity. The data indicate a small but consistent increase in concentration 30 cmab with increased shear velocity for moderate to high wave

conditions. The calculated profiles instead show a decrease in concentration at that level as would be expected if an increase in turbulent mixing distributed sediment more uniformly through the water column. Including a correction for stratification in the flocculated calculations overestimates mean measured concentrations for $u_{*c} > 1.0$ cm/s under the highest wave conditions, while underestimating mean concentrations when $u_{*c} \leq 1.0$ cm/s. Taken together, these results support the idea that the fine-grained suspended sediment population comprises particles in both aggregated and disaggregated states. Extensive measurements available from this site and others provide data to constrain the relative abundance of flocs when combined with a suspended sediment model that accounts for effects related to both types of particles. Full incorporation of flocculation processes in suspended sediment calculations, however, requires characterization of floc formation time scales, floc breakup and changes in floc properties as flow conditions change.
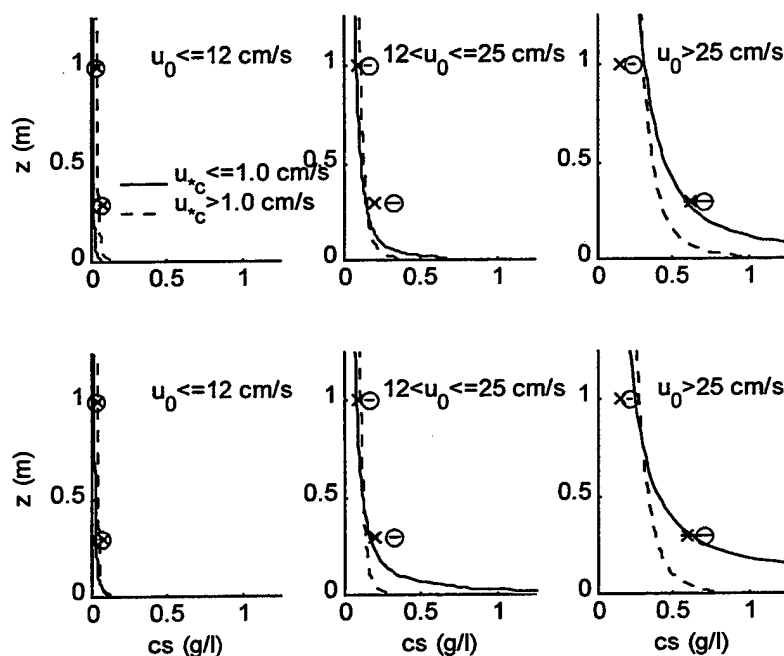
Figure 2. Measured (symbols) and calculated (curves) near-bed suspended sediment profiles for a range of bottom wave and current shear velocities; x,—: $u_{*c} \leq 1.0$ cm/s; o,---: $u_{*c} > 1.0$ cm/s. Top row: all sediment <45 mm is assumed to be flocculated, with no stratification or limit to availability. Bottom row: no flocculation, but effects of stratification and limited availability are included in the calculations.

In addition to flocculation processes that affect the distribution of fine sediment in suspension, consolidation processes can affect the volume in suspension. On the Eel shelf, fine-grained, flood-derived sediment is deposited with an initially high porosity. With time, the porosity of the surface sediment decreases and, at any time, the porosity tends to increase with

depth in the bed. Changes in porosity affect the critical shear stress for sediment entrainment. Decreasing porosity with depth may provide a physical basis for limiting sediment availability in primarily fine-grained beds. Temporal variations in consolidation are likely to explain somewhat higher than usual suspended concentrations for a several week period following a large flood event on the Eel shelf. Field measurements coupled with shelf sediment transport models and models of consolidation provide a basis for evaluating the effect of consolidation on transport.

References

Glenn, S.M. and W.D. Grant, 1987. A suspended sediment stratification correction for combined wave and current flows. *Journal of Geophysical Research*, **92**, 8244-8264.

Grant, W.D. and O.S. Madsen, 1979. Combined wave and current interaction with a rough bottom. *Journal of Geophysical Research*, **84**, 1797-1808.

Grant, W.D. and O.S. Madsen, 1982. Movable bed roughness in unsteady oscillatory flow. *Journal of Geophysical Research*, **87**, 469-481.

Smith, J.D., 1977. Modeling of sediment transport in continental shelves. In: *The Sea*, vol. 6, E.D. Goldberg, ed., Wiley Interscience, New York, pp. 539-577.

Sternberg, R.W., I. Berhane and A. Ogston, in press. Measurement of size and settling velocity of suspended aggregates on the northern California continental shelf. *Marine Geology*.

Wiberg, P.L., D.E. Drake and D.A. Cacchione, 1994. Sediment resuspension and bed armoring during high bottom stress events on the northern California inner continental shelf: measurements and predictions. *Continental Shelf Research*, **14**, 1191-1219.

CHEMICAL MEDIATION OF INTERACTIONS
BETWEEN ORGANISMS AND THEIR ENVIRONMENTS

Richard K. Zimmer
Department of Biology
University of California
Los Angeles, CA 90095-1606

Introduction and Overview

Mechanisms governing chemically-mediated interactions between marine organisms and their environments are largely unexplored. A mechanistic understanding of the role of chemical signals in the environment can lead to critical insights about natural selective forces driving ecological and evolutionary processes. Moreover, when chemicals affecting these phenomena are released into the environment, investigations must rigorously focus on principles of chemical production and transport. Once they have been determined, it becomes possible to ascertain the constraints of natural physicochemical processes on biological responses.

Chemistry indeed mediates a variety of critical biological interactions. Considerable information is now available on the many types of biological responses to environmental chemical stimuli. Sensory perception of chemical signals, for example, strongly influences predation, courtship and mating, kinship recognition and habitat selection. Although they are widely recognized as having critical importance, with few notable exceptions, mechanisms by which environmental chemical stimuli regulate marine ecological processes remain undescribed.

The study of chemical communication systems presents a particular challenge. To meet this task, my laboratory has developed new instrumentation and analytical techniques for identifying the structures and concentrations of bioactive molecules while measuring their distributions over time and space scales relevant to olfactory information processing. We examine how organisms use chemical signals to navigate successfully towards valuable resources within the ocean environment. Through field and laboratory studies, we are devising new theories on chemical communication systems and their roles in regulating ecological interactions among organisms.

Specific Research Contributions – Theory, Laboratory, and Field

Predation and animal navigation in turbulent odor plumes. Previous studies on taxonomically diverse marine animals have established the general existence, and importance, of the olfactory sense in a wide variety of behavioral processes. Evidence suggests that the sense of smell mediates search in many benthic organisms. Past investigations did not, however, link either the degree of successful olfactory-mediated search or guidance mechanisms with the hydrodynamic environment (shear stress and trubulence). To establish the interaction between hydrodynamics and chemoreception, we investigated in laboratory and field studies the predatory success and search strategies of estuarine crabs and snails. Water flow properties were found critical to the ability of animals to orient in odor plumes emanating from live prey and carrion. High flow speed or large sediment particle size increased boundary layer turbulence, thereby decreasing the success of chemo-orientation responses. In addition, high flow speeds also lessened the probability that animals contacted odor plumes. Thus, habitats with high flows can provide hydrodynamic refuges from olfactory-mediated predation.

Because animal navigation ability is contingent on the magnitude of boundary layer turbulence, olfactory-mediated search may also be ineffective in slow flows, if bottom roughness elements can generate sufficient turbulence. Further, search ability is extremely sensitive to small changes in benthic boundary layer structure. In estuaries, water flows are transitional between smooth- and rough-turbulent conditions (low and high turbulence, respectively). Accordingly, chemosensory systems appear geared primarily towards extracting information from hydrodynamically smooth flows. Our studies indicate that mechanisms governing the physical transport of odor signals can have profound influences, not only on the development of sensory and behavioral mechanisms, but also on biotic interactions such as predation, which in turn, can mediate community structure.

Hydrodynamic properties of chemical signal transmission. The hydrodynamic environment and constraints imposed by turbulence on chemical signal transmission have never before been investigated in ocean habitats. A fast, multichannel fluorometer with optical fiber probes, and a submersible electrochemical detection system with microelectrode sensors, have each been designed and fabricated by us to measure the distributions of chemicals following release in flowing water. These instruments sample the chemical environment on time and space scales relevant to signal processing by olfactory receptor neurons of marine animals. In our field experiments, chemicals that are constantly released quickly become patchily distributed due to turbulent mixing at sites downstream (and across-stream). The plumes thus consist of discrete odor (or chemical) patches separated by clean water. These patches have several properties, such as size, mean and maximum concentration, and rate of change in concentration, all potentially important in signal processing by nervous systems. We are currently conducting laboratory flume and field studies to establish those properties that provide the most reliable information to guide animals within turbulent odor plumes.

Chemical regulation of settlement in marine larvae. Habitat colonization by larvae is one of the most important factors structuring marine communities and we are investigating the interactions between waterborne chemical cues and hydrodynamic forces in establishing patterns of colonization on the seafloor. Our studies have provided the first experimental evidence that dissolved chemical cues mediate settlement by larvae under hydrodynamic conditions similar to those in natural benthic habitats. Small peptides (chains of amino acids) were isolated and identified as settlement and metamorphosis inducers using chromatographic and spectroscopic techniques. Mathematical models were employed to establish the quantitative structure/activity relationships between these peptide signal molecules, larval behavior, and development. Remarkably, the peptide cues are all structurally related to the carboxy-terminus sequence of mammalian C5a anaphylatoxin, a potent white blood cell chemoattractant. We propose an evolutionary link between more primitive external receptors functioning in chemical communication of marine organisms and internal receptors for mammalian neuro- and immunoreactive agents.

Summary: Past, Current and Future Research Directions

A mechanistic understanding of chemical signals in the environment can lead to important insights about the ecology of marine organisms. Recent advances in technology provide outstanding opportunities for new discoveries, thus allowing quantification of the associations between hydrodynamic, chemical and biological factors. Our past work on chemically-mediated interactions between organisms emphasized 1) predation, 2) chemical signal production and transmission, and 3) settlement by larvae. Current priorities include these same topics, as well as expanding

work on predation to remote deep sea and mountain stream habitats while beginning new projects on parasite/host interactions and sexual reproduction and gamete search behavior. By rigorously determining the effects of chemical signals on organisms under environmentally realistic conditions, and by integrating these findings within a larger ecological and evolutionary framework, we hope to contribute significant new theory and information on a wide range of topics in the ocean sciences. Such broad integrations are intellectually and technically challenging, and our future research will include interdisciplinary investigations on numerous spatial and temporal scales.

DOCUMENT LIBRARY
Distribution List for Technical Report Exchange – July 1998

University of California, San Diego
SIO Library 0175C
9500 Gilman Drive
La Jolla, CA 92093-0175

Hancock Library of Biology & Oceanography
Alan Hancock Laboratory
University of Southern California
University Park
Los Angeles, CA 90089-0371

Gifts & Exchanges
Library
Bedford Institute of Oceanography
P.O. Box 1006
Dartmouth, NS, B2Y 4A2, CANADA

NOAA/EDIS Miami Library Center
4301 Rickenbacker Causeway
Miami, FL 33149

Research Library
U.S. Army Corps of Engineers
Waterways Experiment Station
3909 Halls Ferry Road
Vicksburg, MS 39180-6199

Marine Resources Information Center
Building E38-320
MIT
Cambridge, MA 02139

Library
Lamont-Doherty Geological Observatory
Columbia University
Palisades, NY 10964

Library
Serials Department
Oregon State University
Corvallis, OR 97331

Pell Marine Science Library
University of Rhode Island
Narragansett Bay Campus
Narragansett, RI 02882

Working Collection
Texas A&M University
Dept. of Oceanography
College Station, TX 77843

Fisheries-Oceanography Library
151 Oceanography Teaching Bldg.
University of Washington
Seattle, WA 98195

Library
R.S.M.A.S.
University of Miami
4600 Rickenbacker Causeway
Miami, FL 33149

Maury Oceanographic Library
Naval Oceanographic Office
Building 1003 South
1002 Balch Blvd.
Stennis Space Center, MS, 39522-5001

Library
Institute of Ocean Sciences
P.O. Box 6000
Sidney, B.C. V8L 4B2
CANADA

National Oceanographic Library
Southampton Oceanography Centre
European Way
Southampton SO14 3ZH
UK

The Librarian
CSIRO Marine Laboratories
G.P.O. Box 1538
Hobart, Tasmania
AUSTRALIA 7001

Library
Proudman Oceanographic Laboratory
Bidston Observatory
Birkenhead
Merseyside L43 7 RA
UNITED KINGDOM

IFREMER
Centre de Brest
Service Documentation - Publications
BP 70 29280 PLOUZANE
FRANCE

50272-101

REPORT DOCUMENTATION PAGE	1. REPORT NO. WHOI-99-04	2.	3. Recipient's Accession No.

4. Title and Subtitle Coastal Ocean Processes Symposium: A Tribute to William D. Grant	5. Report Date May 1999
	6.

7. Author(s)	8. Performing Organization Rept. No. WHOI-99-04

9. Performing Organization Name and Address Woods Hole Oceanographic Institution Woods Hole, Massachusetts 02543	10. Project/Task/Work Unit No.
	11. Contract(C) or Grant(G) No. (C) N00014-98-1-0596 (G)

12. Sponsoring Organization Name and Address Office of Naval Research Rinehart Coastal Research Center United States Geological Survey	13. Type of Report & Period Covered Technical Report
	14.

15. Supplementary Notes
This report should be cited as: Woods Hole Oceanog. Inst. Tech. Rept., WHOI-99-04.

16. Abstract (Limit: 200 words)

This report is a compilation of abstracts distributed at the Coastal Ocean Processes Symposium: A Tribute to William D. Grant at the Woods Hole Oceanographic Institution from September 27 - September 30, 1998.

17. Document Analysis   a. Descriptors
coastal ocean processes
Benthic boundary layer
wave-current interactions

b. Identifiers/Open-Ended Terms

c. COSATI Field/Group

18. Availability Statement Approved for public release; distribution unlimited.	19. Security Class (This Report) UNCLASSIFIED	21. No. of Pages 266
	20. Security Class (This Page)	22. Price

(See ANSI-Z39.18)	See Instructions on Reverse	OPTIONAL FORM 272 (4-77) (Formerly NTIS-35) Department of Commerce